Investigating voltage-gated sodium channel expression in rat spiral ganglion neurons following noise induced hearing loss

Thesis submitted for the degree of

Doctor of Philosophy

at the University of Leicester

By

Alistair Gordon Fryatt BSc

Department of Cell Physiology and Pharmacology

University of Leicester

January 2010

Investigating voltage-gated sodium channel expression in rat spiral ganglion neurons following noise induced hearing loss

Alistair Gordon Fryatt

Abstract

Noise exposure has been shown to elevate hearing thresholds by damaging the cochlea through hair cell damage and the excitotoxic, excessive release of glutamate at the hair cell afferent spiral ganglion neuron (SGN) synapse. This excitotoxicity results in the loss of synaptic innervation of the neuron from the hair cell. In somatosensory neurons a similar axotomy results in altered voltage-gated sodium channel (Na_V) expression. This study investigates whether similar changes in Na_V expression occur in rat SGN following noise exposure. This study has shown the expression of $Na_V1.1$, 1.6 and 1.7 in normal rat SGN using RT-PCR and immunohistochemistry. The noise exposure protocol, 2 sessions presenting a single tone (14.8kHz) at a modest 110dB SPL for 2 hours with 48 hours between each session, resulted with elevated hearing thresholds of the sound-exposed rats of 18±4dB and 24±3dB at 24kHz and 30kHz respectively, with insignificant elevation at frequencies below 16kHz. RT-PCR showed no additional Na_V isoforms present in the sound-exposed cochlea. Quantitative PCR showed a significant decrease in $Na_V1.6$ mRNA expression level, reduced by 56% compared to normal hearing animals. $Na_V1.1$ mRNA was significantly reduced by 29% and $Na_V1.7$ mRNA was elevated by 20% when compared to control cochleae. Immunohistochemistry of sound-exposed cochleae showed increased $Na_V1.1$ staining along the peripheral processes of the SGN. Also, staining for $Na_V1.7$ in the SGN was altered in sound-exposed rats compared to control animals, with the majority of sound-exposed animals showing an increase in darker stained neurons. $Na_V1.6$ SGN cell body staining was not altered between sound-exposed and control neurons using immunohistochemistry. SGN cell body counting showed no decrease in neuronal number following sound exposure compared to control cochleae. These results show that Na_V expression in rat SGN alters following sound exposure, which may modify neuronal function in deafened animals.

Acknowledgements

I would like to especially thank the following people who have been instrumental in the production of this thesis. First, to my supervisorial 'dream team' of Dr Blair Grubb and Dr Mike Mulheran, for their scientific knowledge, infectious enthusiasm, commitment to this project, shocking yet highly amusing sense of humour (especially when in meetings) and for keeping their heads when all around them are losing theirs. Also to Dr Martine Hamann for sitting on my thesis committee.

To all the staff in BMS for taking care of the patients of my small auditory clinic, especially Ken White, Jenny Schofield and Debbie Burnsall for their anaesthetic and post-op care.

To Dr Catherine Vial, Dr Amit Prasai, Matt Barker and Susan Giblett for their help and invaluable technical expertise throughout the conduction of the experiments, as well as Diane Everitt for her morning 'special deliveries' when developing the cochlea extraction technique.

Thanks also to GSK for sponsoring this project, specifically to Dr Steve Etheridge and to Dr Martin Gunthorpe and Dr Julie Egerton for making my visit to Harlow very enjoyable and productive.

Lastly, I would like to thank my family and friends, specifically to my parents for all their support; Nadia and Ria for being excellent office-mates; the ever 'interesting' Jon, Rob and Emma; and my long suffering girlfriend Helen, for being my inspiration, support and helping make sense of my half-baked theories.

List of abbreviations

6-FAM	6-carboxyfluorescein
ABR	Auditory brainstem response
ACh	Acetylcholine
AHL	Age-related hearing loss
AMPA	α-amino-3-hydroxyl-5-methyl-4-isoxazole-propionate
AQ	Absolute quantification
ATP	Adenosine triphosphate
BDNF	Brain derived neurotrophic factor
Ca^{2+}	Calcium ion
Ca_V	Voltage-gated calcium channel
CAP	Compound action potential
CCD	Charge-coupled device
cDNA	Complimentary DNA
CNS	Central nervous system
C_T	Threshold cycle
Da	Dalton
DAB	3,3' diaminobenzidine
dB	Decibel
dB att	Decibel attenuation
dB SPL	Decibel sound pressure level
DCN	Dorsal cochlear nucleus
DNA	Deoxyribonucleic acid
DPX	Di-n-butyl phthalate xylene
DRG	Dorsal root ganglion
dUTP	Deoxyuridine triphosphate
EDTA	Ethylenediaminetetraacetic acid
E_{ion}	Ionic equilibrium potential
FCA	Freund's complete adjuvant
FITC	Fluorescein isothiocyanate
GABA	Gamma-aminobutyric acid
GAPDH	Glyceraldehyde-3-phosphate dehydrogenase
GITC	Guanidinium isothiocyanate
GLAST	Glutamate aspartate transporter
GPCR	G protein-coupled receptor
HRP	Horseradish peroxidase
IgG	Immunoglobulin G
IHC	Inner hair cell
IMS	Industrial methylated spirit
IP	Intraperitoneal
K^+	Potassium ion
K_{2P}	Tandem pore potassium channel
K_{Ca}	Calcium-activated potassium channel
K_{ir}	Inward rectifying potassium channel
K_V	Voltage-gated potassium channel
KA	Kainic acid
MET	Mechanoelectrical transduction
MNTB	Medial nucleus of the trapezoid body
mRNA	Messenger RNA
Na^+	Sodium ion
Na_V	Voltage-gated sodium channel
NIHL	Noise-induced hearing loss

NMDA N-methyl-D-aspartic acid

NT-3 Neurotrophin 3

NTC No template control

NTP Nucleoside triphosphate

OAE Otoacoustic emission

OCT Optimal cutting temperature

OHC Outer hair cell

OSL Osseous spiral lamina

P0 Postnatal day zero

PBS Phosphate buffered saline

PCR Polymerase chain reaction

PFA Paraformaldehyde

PNS Peripheral nervous system

PTS Permanent threshold shift

qPCR Quantitative polymerase chain reaction

RMP Resting membrane potential

RNA Ribonucleic acid

RNID Royal National Institute for Deaf people

ROS Reactive oxygen species

RT-PCR Real time polymerase chain reaction

SEM Standard error of the mean

SGN Spiral ganglion neuron

SOC Superior olivary complex

TAMRA Tetramethylrhodamine

TdT Terminal deoxynucleotidyl transferase

TMS Transcranial magnetic stimulation

TRP Transient receptor potential

TRT Tinnitus retraining therapy

TTS Temporary threshold shift

TTX Tetrodotoxin

TUNEL TdT-mediated dUTP-biotin nick end labelling

VCN Ventral cochlear nucleus

VGSC Voltage-gated sodium channel

WHO World Health Organisation

Table of contents

Table of figures

Chapter 1. Introduction

General introduction and rational for the study

It is estimated that 278 million people worldwide suffer from moderate to profound hearing loss (figures from the World Health Organisation, 2005), while the Royal National Institute for Deaf People (RNID) estimates that there are almost 9 million people suffering from hearing loss and deafness in the UK. Tinnitus can also accompany hearing impairment and is defined as the perception of sound in the absence of an appropriate acoustic stimulus. Hearing loss and tinnitus have a multitude of different causes, including exposure to noise (Schmuziger *et al.* 2006) and the result of aging (age-related hearing loss or presbyacusis).

One of the hypotheses regarding noise-induced hearing loss is the damage of the inner hair cells and afferent spiral ganglion neurons by the excitotoxic effect of excessive glutamate release (Puel 1995). This results in a deafferentation of the spiral ganglion neurons and damage to the peripheral processes, followed by a plastic re-innervation of the hair cells by the neurons. Physical damage to the preganglionic fibres of sensory neurons in the somatosensory system can cause alterations in voltage-gated sodium channel expression, which is thought to underlie neuronal hyperexcitability and the sensation of neuropathic pain (Novakovic *et al.* 1998, Hains *et al.* 2003, Rogers *et al.* 2006).

Our hypothesis is that these changes in the ion channel phenotype in the sensory system are part of a generalised response to neuronal damage/deafferentation. This study will investigate whether voltage-gated sodium channel expression changes, seen

in somatic sensory neurons, also occur in spiral ganglion neurons following noise-induced hearing loss. The work reported in this study will first characterise voltage-gated sodium channel expression in normal hearing Wistar rats, followed by the establishment of a noise-induced hearing loss model. The expression of voltage-gated sodium channels in the noise-exposed rats will then be analysed and compared to the spiral ganglion of unexposed animals.

Thesis layout and contents

This first chapter is concerned with reviewing the anatomy and physiology of the cochlea. Additionally, hearing and hearing loss will be reviewed and neuronal excitability will be discussed, particularly with reference to voltage-gated sodium channels. Chapter 2 is a description of the methods common to all experiments, in particular animal anaesthesia and tissue extraction. Chapter 3 describes the reverse transcription polymerase chain reaction (RT-PCR) and immunohistochemistry methods as well as voltage-gated sodium channel expression in spiral ganglion neurons in normal hearing rats. Chapter 4 details the sound-exposure protocol, audiometric measurements and the effects of noise-exposure on the hearing thresholds of rats. Chapter 5 covers the quantitative polymerase chain reaction (qPCR) method as well as the RT-PCR, qPCR and immunohistochemistry results from sound-exposed rats compared to unexposed rats. Chapter 6 reviews the conclusions of the previous chapters and details future experiments.

The sensation of hearing

Hearing is the ability to perceive and distinguish the different sounds in the environment so that an appropriate response can be performed. Sounds are created by vibrations that travel through the air as waves of alternating pressure. Hearing in humans is achieved by a complex process that starts with the detection of sounds by the ear. The transduction of the sound pressure waves into electrical signals is accomplished by the cochlea, a spiral shaped organ of the inner ear which contains the auditory hair cells. These hair cells are the receptor cells that transduce mechanical inputs that are created by sounds into an electrical response that is conducted to the brain for interpretation. A pair of human cochleae contains around 30,000 hair cells (Gelfand 2001) and the damage or loss of these receptor cells results in hearing loss and deafness (Gelfand 2001, Geisler 1998).

The auditory neural pathway begins with the ear where the hair cells release neurotransmitters that activate afferent nerve fibres, producing action potentials in the auditory nerve. This neuronal information projects first to the cochlear nuclei and then ascends to nuclei in the auditory brain stem. The brain stem nuclei are important for the processing of the auditory signals, including localizing the origin of the sounds (Forsythe 2002). The neuronal information is ultimately projected to the auditory regions of the cerebral cortex, where further analysis is done such as the integration and interpretation of complex sound patterns like human speech.

The mammalian ear

The mammalian ear is divided into three regions, the external or outer ear, middle ear and internal or inner ear that are responsible for the capturing of the sound pressure

waves, transmission of the sound energy to the cochlea and transduction of the sound energy into electrical signals respectively (Fig. 1.1). This organisation is conserved across all mammals, the only gross differences being in the number of cochlear turns and the range of sound frequencies that can be detected.

The external ear consists of the auricle, the external auditory canal and the tympanic membrane or eardrum. The auricle is a fold of cartilage supported skin that acts to capture the sound waves and focus them into the external auditory canal. The external auditory canal ends at the tympanic membrane, a thin diaphragm that vibrates in response to the sound pressure wave.

The middle ear is an air filled cavity that connects the tympanic membrane to the cochlear via a chain of three ossicles, or bones: the malleus, or hammer; the incus, or anvil; and the stapes, or stirrup. The malleus is connected to the tympanic membrane at one end and to the incus, which in turn is connected to the stapes. The stapes has a flattened terminal, called the footplate, which is inserted into an opening in the cochlea called the oval window.

The inner ear is a bony, fluid filled labyrinth that has two functional parts: the vestibular apparatus, the organ of balance; and the cochlea. Both organs utilize hair cells to transduce mechanical energy into electrical responses and both send projections to the brain in the form of the auditory nerve.

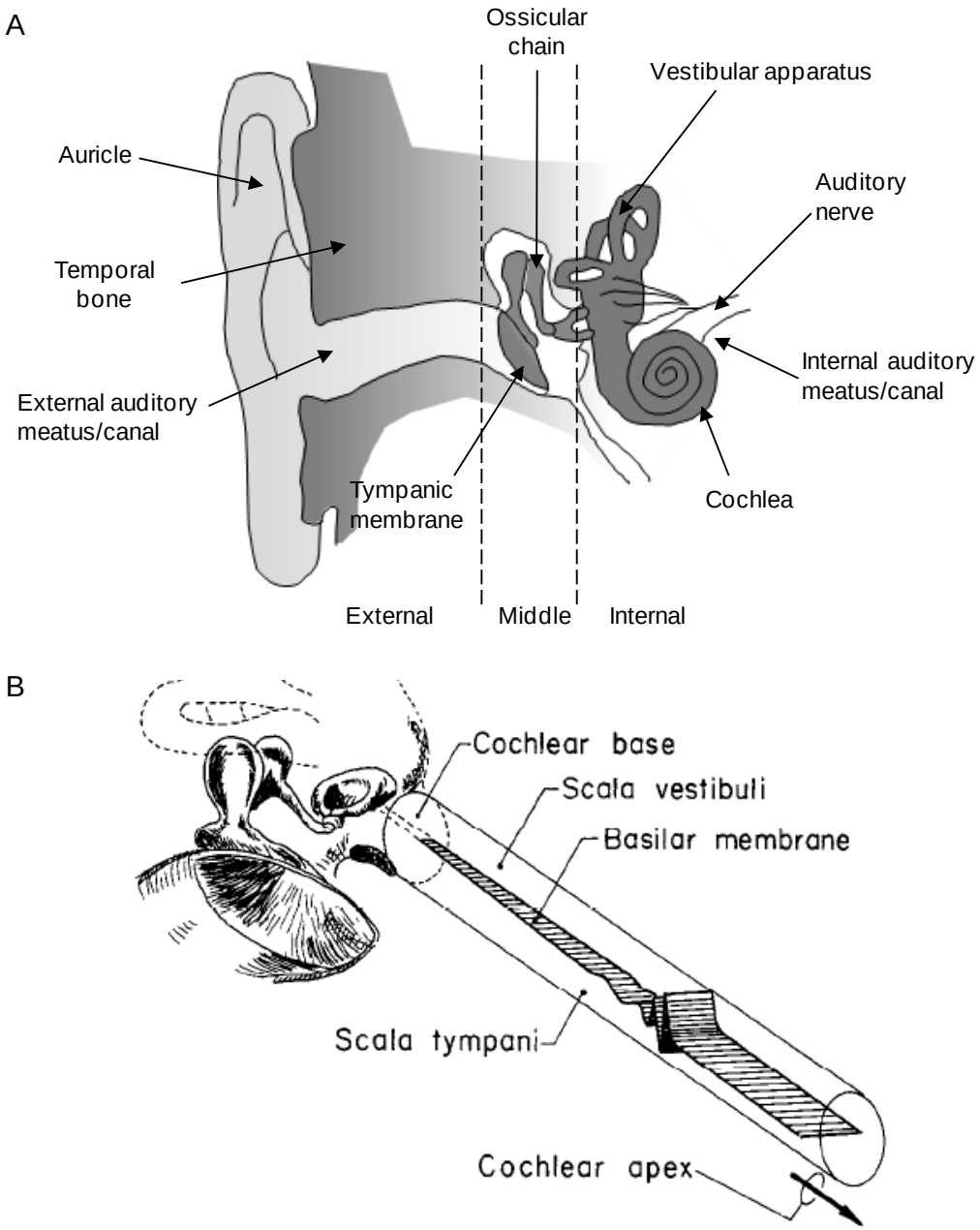

Fig. 1.1. Diagram of the mammalian ear. A) Representation of the human ear showing the external, middle and inner ear portions. This overall organisation is conserved in mammals, with the only differences in the number of cochlear turns. The auricle is responsible for collecting and directing sounds into the external auditory meatus. The tympanic membrane vibrates in response to the sounds causing the ossicular chain (malleus, incus and stapes) to move back and forth. The ossicular chain is connected to the cochlea, via the oval window, where the movement of the stapes is transduced into electrical signals by the organ of Corti and transmitted to the brain via the auditory nerve. B) Representation of the mammalian middle and inner ear, showing the cochlea uncoiled. The basilar membrane, tapered from the base to the apex of the cochlea and upon which the organ of Corti rests, is shown mid-oscillation in response to a pure tone delivered from the tympanic membrane and ossicular chain. The amplitude of the basilar membrane oscillation is not to scale with the rest of the diagram. Diagram in (B) is taken from Dallos 1992.

The anatomy of the mammalian cochlea

Overview: The mammalian cochlea is a coiled structure, tapered towards the apex, which is surrounded by a thin layer of bone, know as the otic capsule, and is embedded in the denser temporal bone of the skull. During embryogenic development, the central nervous system develops from the envaginated neural plate region of ectoderm to form the neural tube and the peripheral nervous system develops from neural crest cells that migrate from the dorsal region of the neural tube (Jessell and Sanes 2000). In contrast, the cochlea and vestibular apparatus develop from a completely distinct region of neural ectoderm known as the otic placode (Fekete 1996, Fekete and Wu 2002, Holley 2005). It is from this separate region of ectoderm that the cell types found in the cochlear and vestibular systems, including the neuronal components, are derived (Fekete 1996, Fekete and Wu 2002).

The core of the cochlea is termed the modiolus and contains both the cell bodies of the neurons that innervate the sensory cells, the spiral ganglion neurons, and the cochlear nerve formed from the spiral ganglion neuron axons. The cochlear nerve exits the cochlea through the internal auditory meatus and projects to the cochlear nucleus. The dendrites of the neurons are carried in a ridge of bone called the osseous spiral lamina (OSL), from which the basilar membrane projects towards the outer edge of the cochlea. Reissner's membrane also runs from the OSL to the outer edge of the cochlea, resulting in the cochlea being divided into three chambers. These canals are filled with fluid and run the entire length of the coil: the scala vestibuli, the upper chamber; scala tympani, the lower chamber; and the scala media (Fig. 1.2).

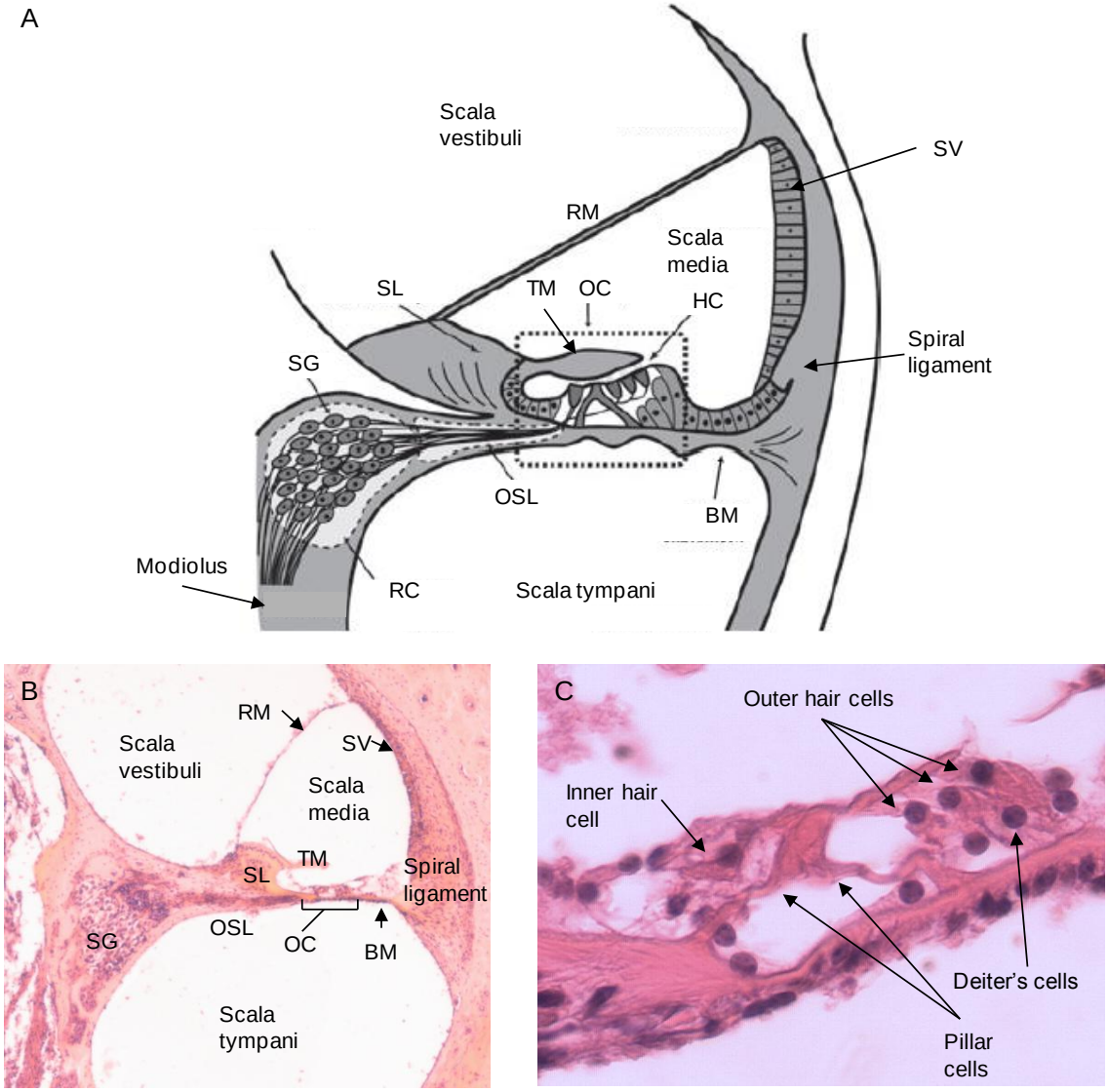

Fig. 1.2. Cross section through a turn of a mammalian cochlea. (A) Diagram representing the morphology of the membranous labyrinth. The scala media is lined by the stria vascularis (SV), Reissner's membrane (RM) and the basilar membrane (BM). The basilar membrane supports the organ of Corti (OC), which contains the hair cells (HC), with the tectorial membrane (TM) resting above, projected from the spiral limbus (SL). The cell bodies of the neurons that innervate the hair cells within the organ of Corti are located in the spiral ganglion (SG) inside Rosenthal's canal (RC) within the modiolus. The SG peripheral processes pass along the osseous spiral lamina (OSL) to innervate the OC. (B,C) Longitudinal section of an adult guinea pig cochlea showing (B) the morphology of the membranous labyrinth and (C) the structure of the Organ of Corti. (C) The organ of Corti with a single row of inner hair cells and three rows of outer hair cells. The outer hair cells are supported at their base by Deiter's cells and the inner and outer hair cells are separated by pillar cells. Diagram in (A) taken from Hurley *et al*. 2007

The cochlea is connected to the ossicular chain via the oval window located at the base of the scala vestibuli, whereas the round window allows transmission of the sound wave and the release of pressure at the scala tympani. The scala media runs for most of the length of the scala tympani and vestibuli, however the scala vestibuli and tympani are connected at the apex of the cochlea in a region called the Helicotrema. The scala media is bordered by the basilar membrane and Reissner's membrane and is also lined by the stria vascularis, a cell layer that is an ion transport epithelium and a vascular bed. The scala vestibuli and tympani are filled with perilymph, a filtrate of cerebrospinal fluid, while the scala media is filled with endolymph, a fluid with a high concentration of potassium ions (K^+) created by the expression of ion channels and pumps in the cells of the stria vascularis (Thalmann *et al.* 1981) and a low concentration of sodium ions (Na^+) thought to be created by Reissner's membrane (Lee and Marcus 2003). As the endolymph has a higher concentration of K^+ than the perilymph, there is a large electrochemical gradient between the endolymph and the perilymph, with a potential between +80 to +100mV with respect to the perilymph (Dallos 1992).

Organ of Corti: The hair cells are found in the organ of Corti (Fig. 1.2), on the medial side of the basilar membrane and are arranged in a single row of inner hair cells (IHC) and at least three rows of outer hair cells (OHC). The hair cells project stereocilia from their apical surface into the scala media, with the IHC stereocilia bundles arranged linearly and the OHC forming a V shape. The IHCs are flask shaped and are the cells responsible for the transduction of sounds resulting in the sensation of hearing while

the OHCs are rod shaped and create electromechanical feedback to amplify the auditory stimulus (Fettiplace and Hackney 2006).

The OHCs are supported at their base by Deiter's cells while the IHCs are surrounded by phalangeal cells (Geisler 1998). The arch between the row of IHCs and the first row of OHCs is created and supported by inner and outer pillar cells. The supporting cells form tight junctions around the organ of Corti and along the basilar membrane, electrically isolating the scala media from the perilymph inside the scala tympani (Gelfand 2001). While Reissner's membrane is considered to be a cellular barrier that separates the scala vestibuli and media, the basilar membrane allows the entry of perilymph into the spaces inside the organ of Corti. This means that the cell bodies of the hair cells are surrounded by perilymph but their apex and stereocilia are bathed in high [K^+] endolymph. Infiltration of the scala media by the perilymph is prevented by the tight junctions formed by the supporting cells at the organ of Corti and along the basilar membrane.

Tectorial membrane: On the medial side of the OSL there is an epithelial ridge known as the spiral limbus, which gives rise to the tectorial membrane. The tectorial membrane is an acellular, gelatinous extracellular matrix containing three types of collagen and three non-collagenous glycoproteins that are highly expressed exclusively in the inner ear. The membrane is hinged at the spiral limbus and runs the entire length of the basilar membrane. The tectorial membrane rests on top of the organ of Corti, forming a physical connection between the tips of the longest stereocilia projected from the OHCs and the lower surface of the tectorial membrane.

Spiral ligament: The spiral ligament forms the lateral wall of the scala media and contains the stria vascularis. Reissner's membrane is anchored at the spiral ligament, extending the ligament into the stria vascularis.

Basilar membrane: The basilar membrane is elastic in nature and, if uncoiled and flattened from the cochlea, forms a wedge shape with the narrow yet thick tip at the base of the cochlea, nearest the oval window, and broadening and thinning towards the apex (Geisler 1998). This increase in width and decrease in thickness results in a decrease in membrane stiffness from base to apex, the stiffness maintained by dense strands of collagen fibres that run at right angles to the length of the membrane. This allows different parts of the basilar membrane to resonate at different acoustic frequencies (Geisler 1998).

Central auditory pathway

The auditory nerve projects to the cochlear nucleus in the brain stem (Fig. 1.3). The cochlear nucleus is divided into the dorsal (DCN) and ventral (VCN) portions. The ascending neurons from the auditory nerve bifurcate into an ascending branch that innervates the anterior VCN (aVCN) and a descending branch that innervates the DCN via the posterior VCN (pVCN) (Forsythe 2002). The output from the DCN projects to the inferior colliculus. The axons from the aVCN project to the superior olivary complex on the contralateral side (cross to the opposite side) of the brain stem, via the medial nucleus of the trapezoid body (MNTB), while the remainder synapse with the superior olivary complex on the ipsilateral side (the same side) of the brain stem. The

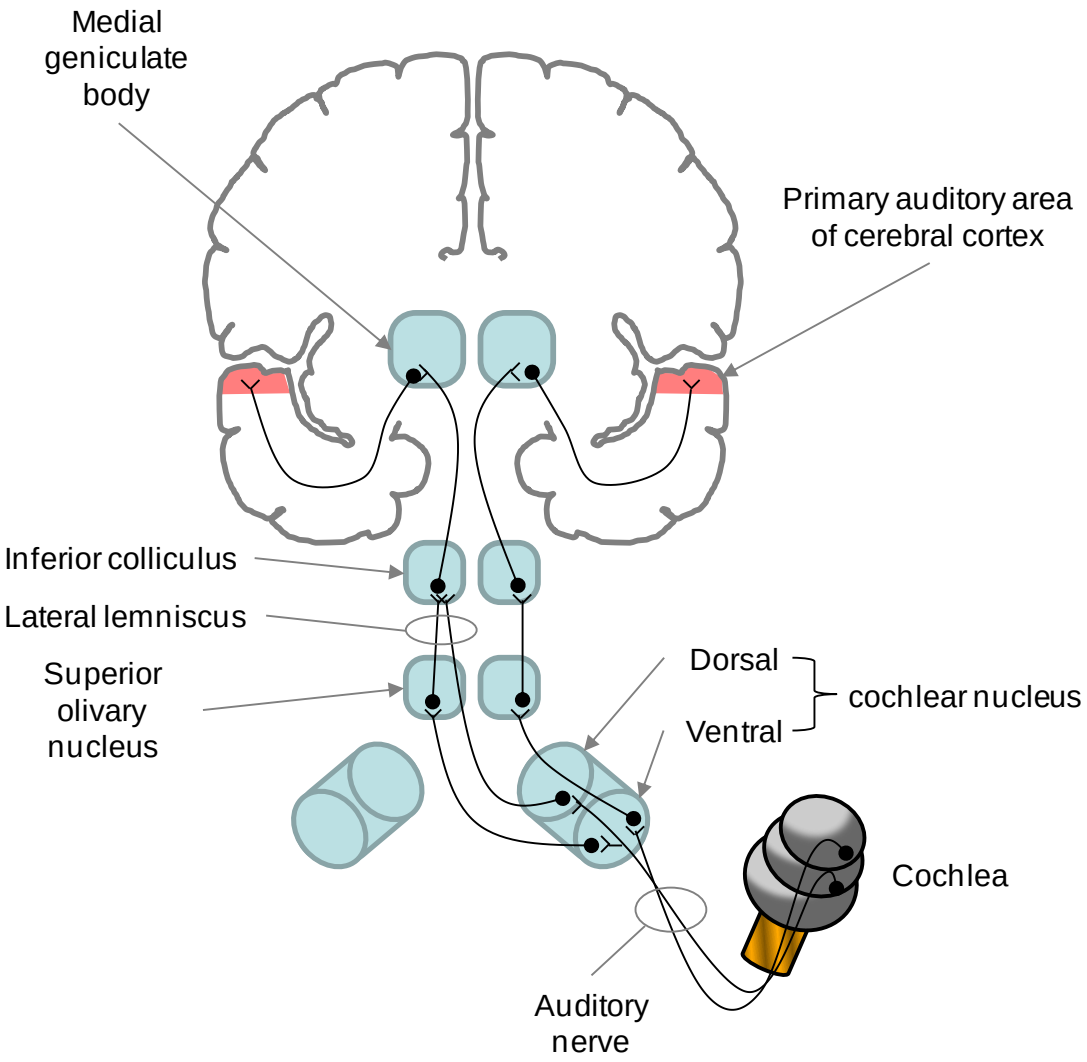

Fig. 1.3. Diagram of the human auditory pathway. Representation of the auditory pathway from the cochlea, through the brainstem to the primary auditory area of the cerebral cortex (shaded area). Diagram is not to scale.

fibres that decussate (cross to the other side) will either synapse with the superior olivary complex on that side or ascend directly to the lateral lemniscus. This means that each superior olivary complex receives information from both cochlear nuclei, resulting in bilateral representation at the level of the brain stem. Axons exit from the superior olivary complex and project towards the cerebral cortex via the lateral lemniscus. The neurons ascend from the lateral lemniscus and either synapse with or bypass the inferior colliculus and terminate at the medial geniculate body of the

thalamus by way of the brachium of the inferior colliculus. The medial geniculate body receives synapses from all the ascending neurons before axons project to the auditory cortex, located in the transverse temporal gyrus via the auditory radiations (Gelfand 2001).

The two sides of the auditory pathway are interconnected at each level by neurons that connect the auditory nuclei. In addition to the superior olivary complex receiving projections from both cochlear nuclei, the commissural tracts interconnect the nuclei of the inferior colliculus (the commissure of the inferior colliculus) as well as the nuclei of the lateral lemniscus (the commissure of the lateral lemniscus). Both sides of the auditory cortex are connected by the corpus callosum however there is no interconnection between the nuclei of the medial geniculate body found in the thalamus. The interconnectivity between the auditory nuclei means that if there was a disruption to the nerve fibres then the loss of hearing sensitivity would be minimal as the auditory information would still be represented via an alternative route (Gelfand 2001).

Physiology of hearing

Nature of sound waves

Sounds are waves of alternating pressure generated through mechanical vibrations that are transmitted through a medium, such as a gas or liquid. The properties of the pressure wave, such as frequency and amplitude, are proportional to the frequency and amplitude of the original mechanical vibrations. It must be noted that a pressure

wave can only be perceived as sound if it falls within the hearing frequency range of the subject, which is between 20Hz and 20kHz in humans.

Sound pressure is defined as the difference between the pressure found within the sound wave and the average local pressure of the medium outside of the sound wave in which it is travelling through. The decibel (dB) scale is used to measure sound pressure level (dB SPL), as the decibel is a logarithmic unit of measurement that expresses the magnitude of a quantity compared to a reference level. The logarithmic nature of decibels also encompasses the ability of the human ear to detect sounds across a wide range of amplitudes. The sound pressure level is defined as:

$$L_P = 10\ Log_{10}\left(\frac{p^2}{{p_{ref}}^2}\right) = 20\ Log_{10}\left(\frac{p}{p_{ref}}\right)$$

Where L_P is the sound pressure level, p is the root mean square sound pressure and p_{ref} is a reference sound pressure, commonly 20µPa in air and 1µPa in water. Thus an increase from 0dB SPL, the acoustic threshold of hearing, to over 120dB SPL, above the threshold of hearing induced pain, represents more than a million fold increase in sound pressure level.

Transduction of sound

The first step in hearing is the conversion of mechanical energy generated by vibrations into electrical signals that can be interpreted by the nervous system.

Outer and middle ear: The changes in air pressure are collected and directed to the tympanic membrane by the external ear. The tympanic membrane then vibrates in

response to the local changes in air pressure which in turn causes the vibration of the three bones in the ossicular chain. The stapes footplate then moves like a piston in the oval window of the cochlea.

Movements within the cochlea: As the scala vestibuli is filled with perilymph and is uncompressible, the stapes movement causes waves of alternating pressure in the perilymph which in turn causes the scala media to be displaced. As the basilar membrane is fixed at the osseous spiral lamina, the movement of the lymph causes the basilar membrane to oscillate, causing the hair cells to follow the motion of the basilar membrane. As the tectorial membrane pivots from the spiral limbus and not the spiral lamina, the tectorial membrane moves relative to the basilar membrane (Fig. 1.4). As mentioned previously, the hair cells project stereocilia from their apical surface to form bundles in the space between the basilar and tectorial membrane. The OHC stereocilia project into the tectorial membrane and thus are deflected by the movement of the membranes. The IHC stereocilia are not embedded in the tectorial membrane and so the stereocilia deflection is due to the movement of the endolymph under the tectorial membrane during the basilar membrane oscillations.

Stereocilia displacement: The hair bundle is the site of transduction of the hair cell and is an array of stereocilia arranged in rows of increasing height. The base of each stereocilia is tapered so that the stereocilia can move from side to side. The stereocilia are connected to each other by a series of interciliary links. The shafts of the stereocilia are connected along their length by side links while the apexes are attached to the side of the next tallest by a filamentous tip link (Fettiplace and Hackney 2006) so

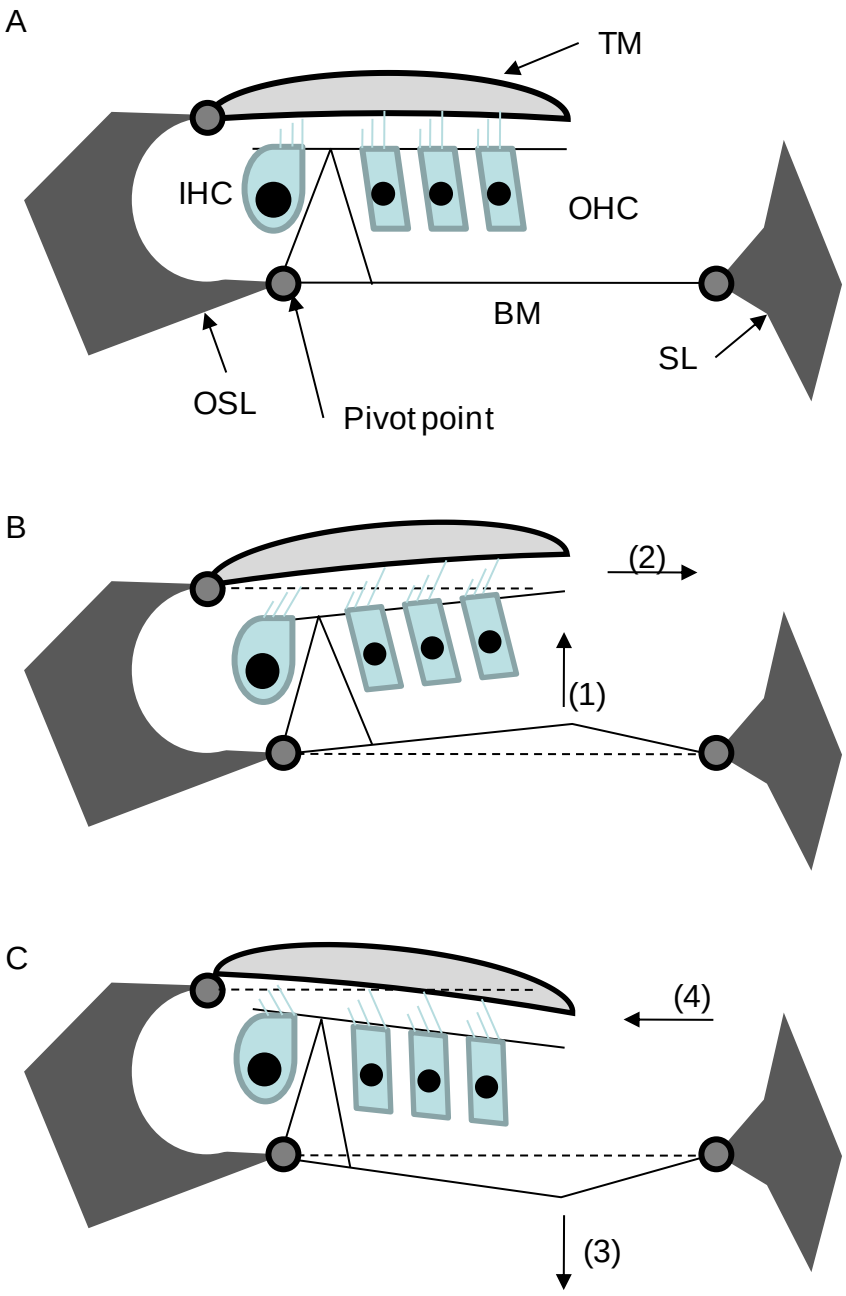

Fig. 1.4. The mechanism for generating shearing forces at the stereocilia within the organ of Corti. Diagram representing the organ of Corti when the hair cells are (A) at rest, (B) active, i.e. increased neurotransmitter release, and (C) inactive, decreased neurotransmitter release. The longest stereocilia of the outer hair cells (OHC) are connected to tectorial membrane (TM) where as the inner hair cells (IHC) are not. (1) The upward deflection of the basilar membrane (BM) towards the scala vestibuli results in the generation of the shearing force exerted upon the cilia, towards the longest cilia (2). (3) The downward deflection of the BM, towards the scala tympani, results in the shearing force exerted upon the cilia to cause the cilia to move in the opposite direction. Additional abbreviations: OSL, osseous spiral lamina; SL, spiral ligament. Adapted from Henderson and Hamernik 1995

that movement of the tallest stereocilia will cause the connected stereocilia to move in the same direction (Fig. 1.5). At the tip of the stereocilia the tip link is connected to a mechanoelectrical transduction (MET) ion channel (Dallos 1992, Fettiplace and Hackney 2006). The MET channel is a non-selective cation channel (Ohmori 1985, Corey 2006) that experimentally shows a particular permeability to potassium (K^+) and calcium ions (Ca^{2+}) (Lumpkin *et al.* 1997). The molecular identity of the MET channel is currently unknown, although many candidate ion channels have been proposed, including TRPA1 (for a detailed review see (Corey 2006)).

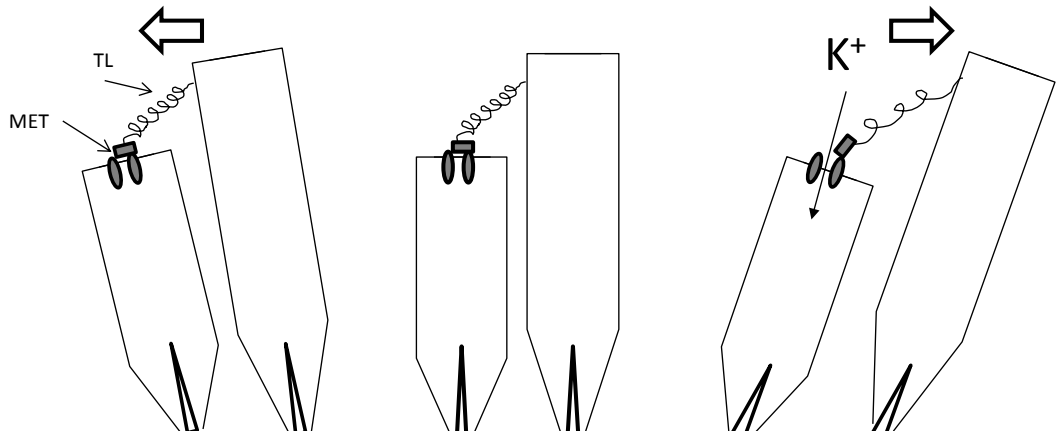

Fig. 1.5. Displacement of the stereocilia leads to ion channel opening. Simplified diagram representing the movement of cochlear hair cell stereocilia. The tips of the cilia are connected to the next tallest by filamentous tip links (TL). When the cilia move in the direction of the tallest cilia, the tip links are pulled tight and the non-selective cation channel mechanoelectrical transduction (MET) channel opens, allowing the entry of potassium (K^+) ions from the scala media. Diagram is not to scale.

The movement of the basilar membrane relative to the tectorial membrane causes shearing forces to be exerted on the stereocilia. The OHC stereocilia deflect because the longest stereocilia project into the tectorial membrane, leading to a direct manipulation of the OHC stereocilia. As the IHC stereocilia are not connected to the tectorial membrane, the deflection of the stereocilia is caused by the motion of the

surrounding endolymph that is displaced by the differential motion of the tectorial membrane and the reticular lamina (Legan *et al.* 2005). The shearing forces cause the stereocilia to bend away from the modiolus when the scala media is deflected upwards.

The deflection of the stereocilia away from the modiolus results in the opening of cation selective MET ion channels by the movement of the tip links, allowing K^+ to enter the hair cell (Fig. 1.6). The ions flow into the hair cells due to the relative positive charge of the endolymph. The influx of cations causes the hair cells to depolarise, activates voltage-gated Ca^{2+} channels and causes an increase in neurotransmitter release from the basal region of the hair cell. As the IHCs depolarise, the neurotransmitter glutamate is released into the synaptic cleft around the region of neuronal innervation (the synapse), resulting in the depolarisation of the afferent neurons. It must be noted that spontaneous glutamate release has also been observed (Glowatzki and Fuchs 2002). The OHCs express voltage-gated Ca^{2+} channels and Ca^{2+}-activated potassium channels that open following the depolarisation of the hair cells, resulting in the activation of the OHC motile mechanism (Dallos 1992, Fettiplace and Hackney 2006), shortening the cell body of the OHCs and delivering mechanical feedback to the movement of the basilar membrane (Fettiplace and Hackney 2006). The OHCs also express voltage-gated K^+ channels that allow K^+ efflux to repolarise the hair cell.

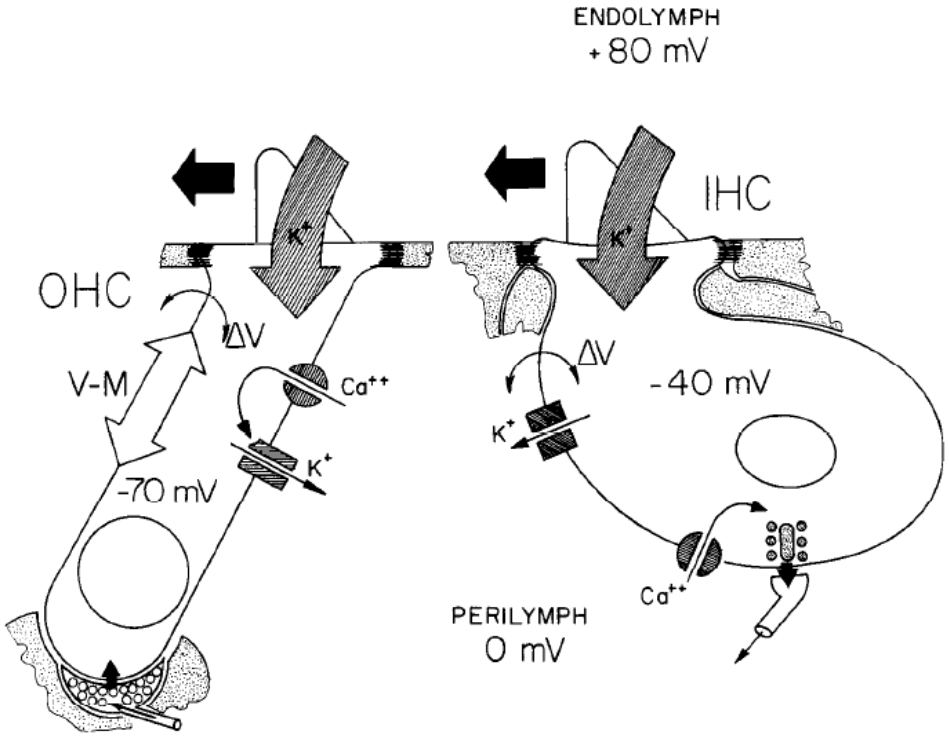

Fig. 1.6. Activation of the OHCs and IHCs. Deflection of the stereocilia in the excitatory direction, towards the longest stereocilia (solid arrows) results in the opening of transducer (MET) channels at the apex of the cilia. MET channel opening results in K^+ flow from endolymph into the hair cells down the electrical gradient (hatched arrows). OHCs and IHCs have different resting potentials. OHC basolateral membranes contain voltage-gated Ca^{2+} channels and Calcium-activated K^+ channels. Depolarizations (ΔV) due to the K^+ flux (receptor current) and subsequent calcium and potassium fluxes produce the ultimate receptor potential. In OHCs, the receptor potential activates the motile mechanism (V-M converter) that produces cellular shape changes, through comformational changes in the protein prestin, and delivers mechanical feedback to the basilar membrane oscillations. The dominant innervation of OHC is efferent, at the base of the OHC. IHC basolateral membranes contain voltage-gated K^+ channels and Ca^{2+} channels in the synaptic region. IHCs are almost exclusively innervated by afferents. Depolarisation leads to the activation of Ca^{2+} channels and the release of glutamate into the synaptic cleft. Taken from Dallos 1992.

Frequency selectivity of the cochlea

Basilar membrane: Due to the change in mechanical properties of the basilar membrane, increased width and decreasing stiffness from base to apex, different regions of the basilar membrane will oscillate and resonate at different frequencies.

The short and stiff basilar part of the basilar membrane resonates at high frequencies while the long and flexible apex resonates at lower frequencies. This means that, in response to a particular frequency of sound, a specific region of the basilar membrane will resonate, deflecting the stereocilia of the IHCs located at that region and stimulating the innervating SGN to generate action potentials, ultimately conveying the sensory information to the auditory cortex. This provides the cochlea with the ability to mechanically analyse components of sound based on their frequency and provides a structural basis for tonotopy.

Cochlear amplification: In addition to the mechanical properties of the basilar membrane, active processes occur to amplify or dampen the oscillations of the basilar membrane. This allows vibrations caused by low intensity sounds to be amplified, granting the ability to hear sounds at low volume. The active amplification was noted when comparing basilar membrane movements between dead and alive cochleae (Dallos 1992). This amplification is believed to be generated by the OHCs, as OHC loss has been shown to result in significant hearing loss (Dallos and Harris 1978). *In vitro* studies showed that OHCs could be stimulated to change the length of their cell bodies by changing their membrane potential (Brownell *et al.* 1985), indicating that the amplification arises from changes in cell shape (Dallos 1992, Patuzzi and Robertson 1988). While the contraction of muscle tissue though the interaction of actin and myosin filaments has been documented, OHCs were found not to express these proteins (Knipper *et al.* 1995), indicating a different method of cellular contraction. Indeed, OHCs were found to express the protein prestin (Dallos and Fakler 2002), which has been shown to be essential in generating OHC length changes in response

to acoustic stimulation (Liberman *et al.* 2002). The stereocilia have also been indicated in generating mechanical forces within the cochlea (Kennedy *et al.* 2005).

Otoacoustic emissions (OAEs) are faint sounds that are believed to be generated by OHCs in response to sound stimulation, and can be measured using sensitive microphones positioned in the external ear canal (Starr *et al.* 2001). OAEs are generated when the amplification of the basilar membrane oscillation, provided by the OHCs, causes a slight reversal of the travelling wave from the oval window to the helicotrema (Kemp 2002). This causes in a secondary oscillations of the ossicular chain and tympanic membrane, resulting in vibration and sound (Kemp 2002). OAEs are used as a measure of OHC function, as a reduction or absence of OAEs can be interpreted as loss or damage to the OHC population of the cochlea (Starr *et al.* 2001, Kemp 2002, Kujawa and Liberman 2009).

Spiral ganglion neurons

Overview: The hair cells are innervated by the primary auditory neurons, also known as the spiral ganglion neurons (SGN), which are contained within the modiolus. Humans have between 25,000 and 30,000 SGN while rats have about 16,000 SGN per cochlea (Gelfand 2001). The peripheral processes of the SGN (technically the dendrites) pass inside the osseous spiral lamina to innervate the hair cells. The cell bodies of the SGN run inside a hollow in the modiolar bone known as Rosenthal's canal. There are two types of SGN, Type I that innervate the IHCs and Type II that innervate the OHCs (Fig. 1.7). The axons from both types of SGN form the auditory nerve, which runs through the internal auditory meatus to the cochlear nucleus.

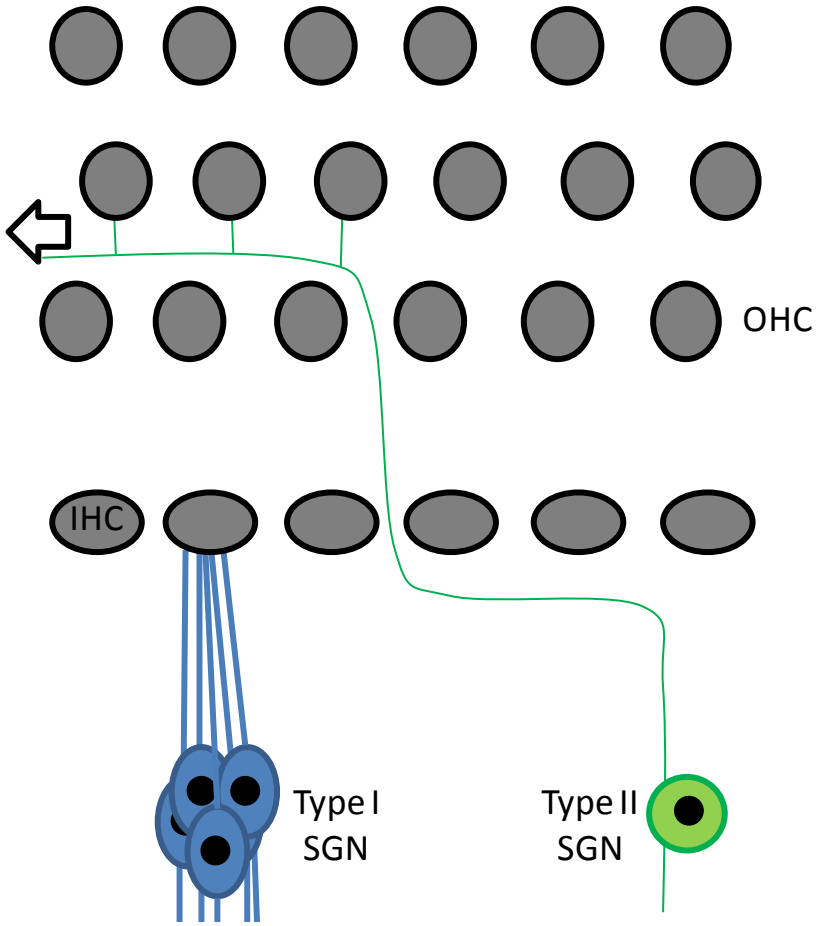

Fig. 1.7. Synaptic targets of the spiral ganglion neurons. A schematic representation showing the synaptic innervation of the inner hair cells (IHC, arranged in a single row) and outer hair cells (OHC, arranged in three rows) by the spiral ganglion neurons (SGN). A single IHC receives afferent innervation from between 10 and 30 Type I SGN, while many OHCs receive an afferent synapse from a single Type II SGN. The process from the Type II SGN will continue along the organ of Corti to innervate more OHCs (arrow). Diagram is not to scale.

There are morphological differences between the Type I and II SGN in addition to their innervation targets. Type I SGN have a cell body diameter of between 15 and 20µm, with a large round nucleus and myelinated axons. Type II SGN have a smaller cell body than the Type I, between 10 and 15µm in diameter, with an erratically shaped, lobular nucleus and their axons are unmyelinated (Geisler 1998). In the spiral ganglion, Type I SGN account for 90-95% of the neuronal population with the dendrites of several neurons innervating a single IHC, while each Type II SGN innervates many OHCs with a

lengthy bifurcated process (Geisler 1998, Dallos 1992). Even though there are many morphological differences between the two types of SGN it is very difficult to tell them apart by microscopy. Fortunately it has been reported that Type II SGN can be preferentially labelled by immunocytochemistry using antibodies specific to the 200-kDa neurofilament subunit (Berglund and Ryugo 1991) as well as another neurofilament protein peripherin (Hafidi 1998, Reid *et al.* 2004, Mou *et al.* 1998), which is also present in the unmyelinated somatosensory C-fibres (Goldstein *et al.* 1991, Amaya *et al.* 2000).

Function in hearing: As mentioned previously, the IHCs are considered to transduce sounds while the OHCs provide amplification of the basilar membrane oscillations. The IHCs release glutamate upon depolarisation, which results in the depolarisation of the Type I SGN and the generation action potentials. These action potentials are conducted along the SGN axons which form the auditory nerve, and towards the cochlear nucleus in the brainstem. Indeed it is believed that the Type I SGN respond to sound stimulation and are spontaneously active (Robertson 1984), although this spontaneous activity may be due to the spontaneous release of neurotransmitter from the hair cells (Glowatzki and Fuchs 2002). In contrast, Type II SGN are believed to be unresponsive to sound stimulation and do not generate action potentials spontaneously (Robertson *et al.* 1999).

Action potential generation properties: *In vitro* recordings have shown differences in action potential firing properties between the Type I and Type II neurons (Reid *et al.* 2004). Type II neurons are believed to generate multiple action potentials (slowly

adapting or accommodating) and show longer latencies (time between stimulus and the peak of the action potential) than Type I neurons which generate a single response (rapidly adapting or accommodating) and have short latencies (Reid *et al.* 2004, Mo and Davis 1997). It should also be noted that there is an apparent variation in Type I SGN action potential firing properties between apical and basal neurons when tested *in vitro* (Adamson *et al.* 2002a). While the basal SGN display short latencies and are rapidly adapting, some apical neurons show longer latencies and slow adaptation (Adamson *et al.* 2002a), although not to the same extent as the Type II neurons (Reid *et al.* 2004). These *in vitro* experiments where performed with cultured SGN from mice between 1 and 8 days old (Reid *et al.* 2004, Mo and Davis 1997, Adamson *et al.* 2002a), and it was reported that the differences could be due to the cell culture method or the differences could disappear during maturation of the animal, although similar K^+ channel expression between cultured and adult mouse SGN was seen using immunohistochemistry (Adamson *et al.* 2002a).

The resonating properties of the basilar membrane produce a tonotopic gradient along the length of the cochlea. This tonotopic gradient is continued in the SGN, with neurons at the base of the cochlea generating action potentials correlating to high frequency sounds and neurons at the apex generating action potentials correlating to low frequency sounds. The tonotopy is also continued at the cochlear nucleus and throughout the auditory pathway, as the neurons project to discrete regions within the nuclei.

Synaptic transmission within the cochlea

Synaptic innervation of the organ of Corti: Synapses are junctions between cells at which chemicals, or neurotransmitters, are released from the pre-synaptic cell to evoke an electrical response in the post-synaptic cell. This response is generated by the neurotransmitter binding to receptors located along the post-synaptic membrane. Broadly, there are two forms of neurotransmitter receptor, ionotropic receptors, which upon neurotransmitter binding open an ion channel to allow the passage of ions across the membrane, and metabotropic receptors, which indirectly mediate their action by the activation of an associated G protein (also known as G protein-coupled receptors or GPCRs).

Within the organ of Corti there are two forms of synaptic innervation, classified by which way information is transmitted (Fig. 1.8). The ascending or afferent connection of the hair cells is by the SGN innervating the hair cells. The descending or efferent connection is created by the innervation of the hair cells by neurons located in the superior olivary complex, located in the auditory brainstem (reviewed in (Puel 1995, Eybalin 1993)).

Inner hair cell innervation

Afferent innervation: The IHCs are afferently innervated by the Type I SGN, with between 10 and 30 neurons forming ribbon synapses with a single hair cell (Liberman *et al.* 1990). This large number of synaptic contacts would allow the sensory information to be conveyed at a high resolution. The IHC has a specialised structure along the pre-synaptic membrane termed the synaptic ribbon, as shown in Fig. 1.9 (Fuchs *et al.* 2003). This ribbon allows the fast release of neurotransmitter from the

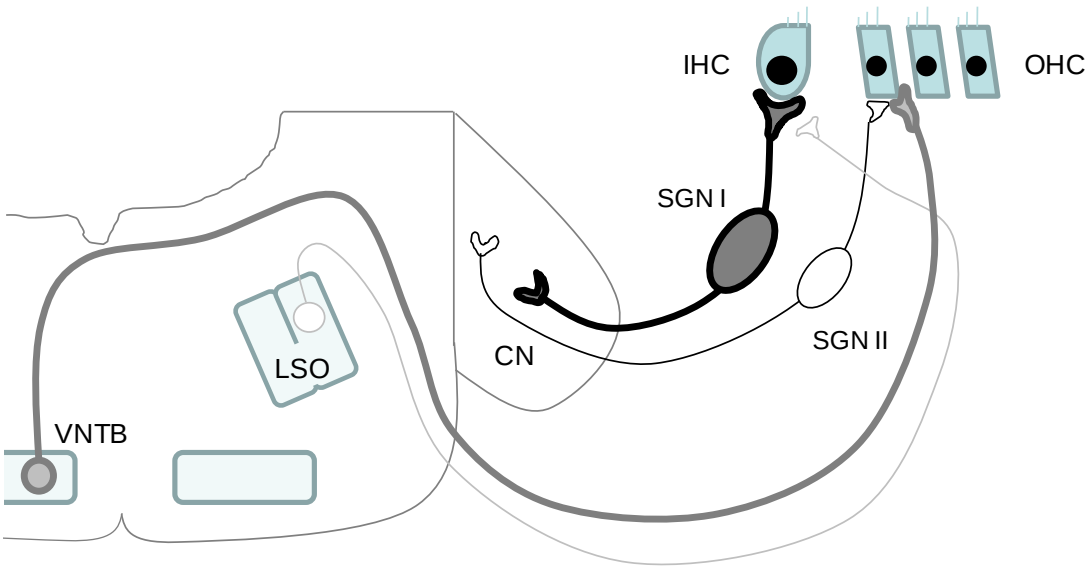

Fig. 1.8. Diagram of the synaptic innervation of the organ of Corti. Representation of the afferent and efferent connections to the hair cells in the organ of Corti. Inner hair cells (IHC) receive afferent innervation from the Type I spiral ganglion neurons (SGN I) while the outer hair cells (OHC) are afferently innervated by the Type II SGN (SGN II), with their axons projecting to the cochlear nucleus (CN). The OHCs receive efferent innervation from neurons in the contralateral ventral nucleus of the trapezoid body (VNTB) while the IHC/SGN I synapse is innervated by descending fibres from the lateral superior olive (LSO). Myelinated axons are indicated by thick lines where as unmyelinated axons are represented by thin lines. Diagram is not to scale. Adapted from Puel, 1995.

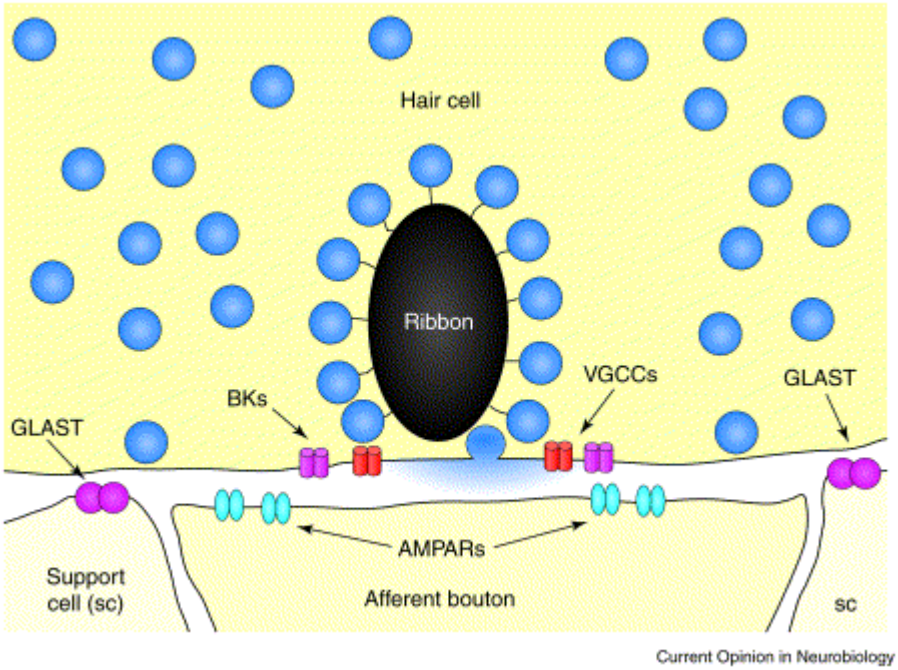

Fig. 1.9. Diagram of the IHC ribbon synapse. The inner hair cell's afferent synapse is contains an electron-dense synaptic body, or ribbon, to which small synaptic vesicles are connected. The ribbon is around 0.2 microns in diameter, and the synaptic vesicles are 35–40 nm in the mammalian cochlea. Voltage-gated calcium channels (VGCCs) and large conductance calcium-sensitive voltage-gated potassium (BK) channels are clustered near the synaptic ribbons. AMPA receptors are found on the postsynaptic afferent membrane, glutamate transporters (GLAST) are expressed by supporting cells that surround the inner hair cell and its afferent contacts. Taken from Fuchs *et al.* 2003.

anchored synaptic vesicles into the synaptic cleft upon depolarisation of the IHC (Glowatzki and Fuchs 2002). The neurotransmitter released from the IHC into the synaptic cleft has been identified as the excitatory amino acid, glutamate (Nordang *et al.* 2000).

There are two classes of glutamate receptors, ionotropic and metabotropic as described above (for detailed review see (Ozawa *et al.* 1998)). Of the ionotropic glutamate receptors, there are three classes all of which allow the passage of Na^+, K^+ and Ca^{2+}. All three classes consist of five subunits to form a functional receptor. The receptors are defined by the exogenous ligands that can activate them, NMDA (N-

methyl-D-aspartic acid) receptors, and the non-NMDA receptors AMPA (α-amino-3-hydroxyl-5-methyl-4-isoxazole-propionate) and Kainate (KA) receptors. To date several subunit isoforms have been identified, with NMDA receptor subunits (NR1 and $NR2_{A-D}$), AMPA receptor subunits ($GluR_{1-4}$) and KA receptor subunits ($GluR_{5-7}$, KA1 and KA2) found to be expressed. Both NMDA and non-NMDA currents have been identified in the cochlea (Puel 1995), although the rapid component of the post-synaptic excitatory current is believed to be mediated by AMPA receptors (Glowatzki and Fuchs 2002). Specifically, $GluR_{2-4}$, $GluR_{5-6}$, NR1, $NR2_{B-D}$, KA1 and KA2 subunits have been identified in the SGN (Niedzielski and Wenthold 1995, Ruel *et al.* 2008). While the activation of the glutamate receptors results in the depolarisation of the post-synaptic cell and action potential generation, excessive stimulation from glutamate release can lead to neural degeneration, termed excitotoxicity.

Glutamate excitotoxicity is due to the increased influx of ions, particularly Ca^{2+} as well as water, through the glutamate receptors resulting in swelling and degeneration of the neuronal processes (Lipton and Rosenberg 1994). The influx of Na^{+} will further depolarise the cell and ultimately lead to further Na^{+} entry (Taylor and Meldrum 1995), as described in Fig. 1.10. Additionally, the excess influx of Ca^{2+} results in the disruption of the Ca^{2+} homeostasis and activation of cellular pathways, as shown in Fig. 1.11, that can lead to apoptosis and cell death (Sattler and Tymianski 2000). While this excitotoxicity has been seen in the CNS (Rothman and Olney 1986, Choi and Rothman 1990) it has also been noted following the application of glutamate and noise exposure in the cochlea (Pujol *et al.* 1990, Puel *et al.* 1998). Upon the application of AMPA to the cochlea, degeneration of the IHC-Type I SGN synapse and withdrawal of

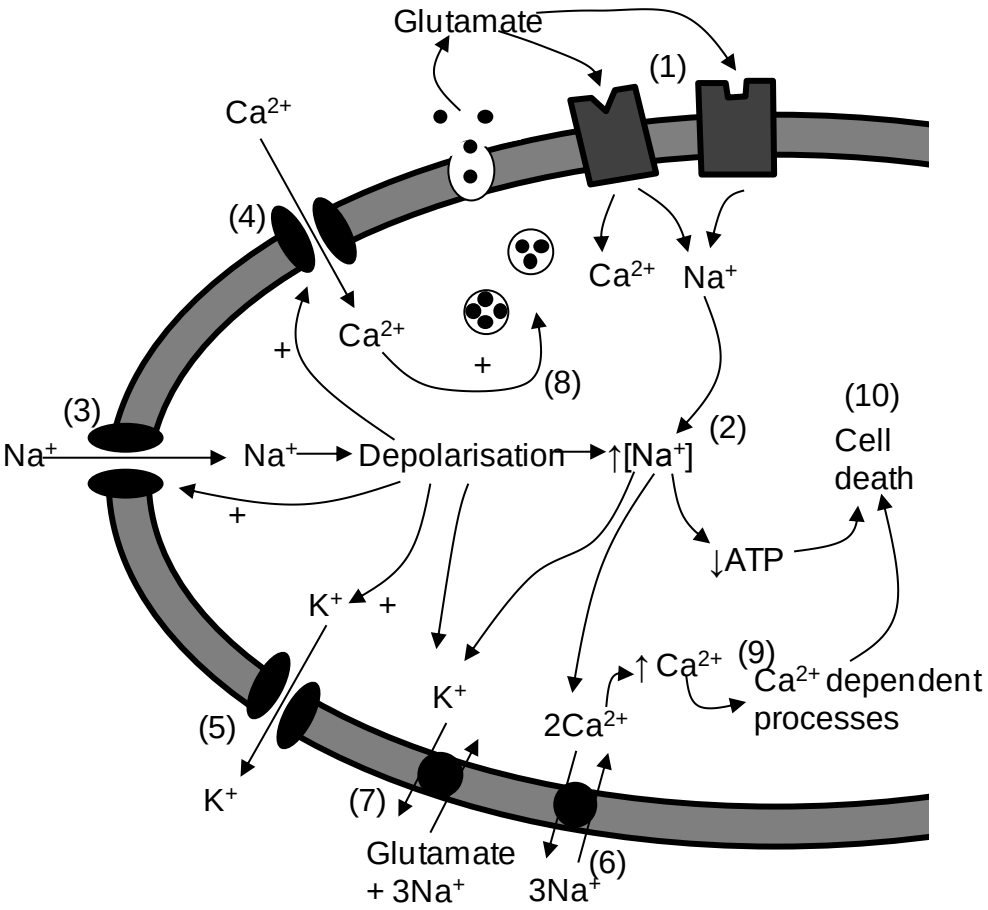

Fig. 1.10. Cellular events resulting from glutamate excitotoxicity. Glutamate binds to glutamate receptors (1), allowing the influx of Na^+ and Ca^{2+}, depolarizing the neuron (2) and activating other voltage-gated mechanisms, such as voltage-gated Na^+ channels (3), voltage-gated Ca^{2+} channels (4), voltage-gated K^+ channels (5). Na^+ influx increases Na^+ concentration, depleting ATP stores and causing influx of Ca^{2+} via reversed Na^+-Ca^{2+} exchange (6). With depleted ATP and ionic gradients, glutamate release continues via reversed glutamate transport (7). Ca^{2+} influx causes the vesicular release of glutamate (8) and the activation of Ca^{2+} dependent processes (9), eventually leading to neurotoxicity and cell death (10). Adapted from Taylor and Meldrum 1995.

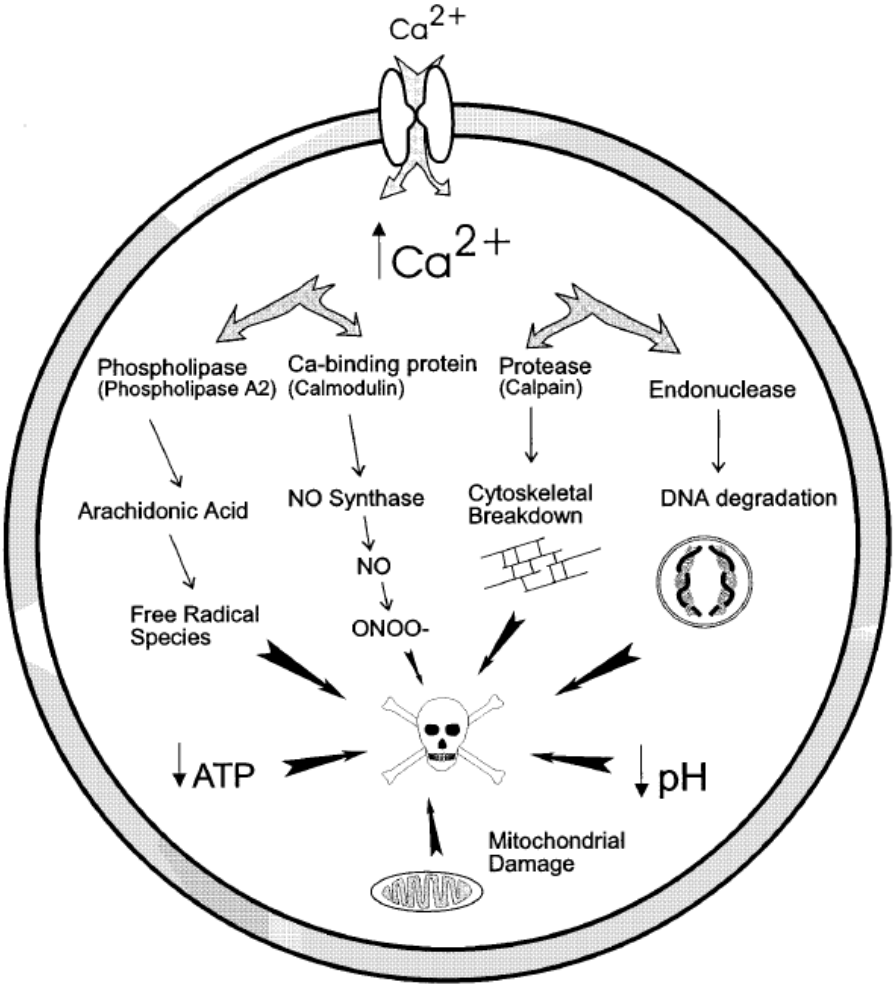

Fig. 1.11. A schematic of Ca^{2+} induced cell death. Descriptive diagram of proposed mechanisms by which intracellular Ca^{2+} elevation (↑-Ca^{2+}) may trigger secondary Ca^{2+}-dependent processes, which result in neurotoxicity and cell death (☠). NO, Nitric oxide; ONOO, peroxynitrite; ATP, adenosine triphosphate; ADP, adenosinse diphosphate; DNA, desoxyribonucleic acid. Taken from Sattler and Tymianski 2000.

the SGN dendrite was detected (Fig. 1.12). After one day of recovery the dendrite was observed to reconnect the IHC and resembled normal innervation five days after AMPA application (Puel 1995). This indicates that, following an excitotoxic episode, the SGN can loose their afferent synaptic connection and that the synapse can regenerate suggesting some degree of synaptic plasticity. However, it must be noted that a recent study has shown a decrease in synaptic ribbons and SGN number following prolonged

recovery from noise exposure despite the restoration of hearing thresholds (Kujawa and Liberman 2009).

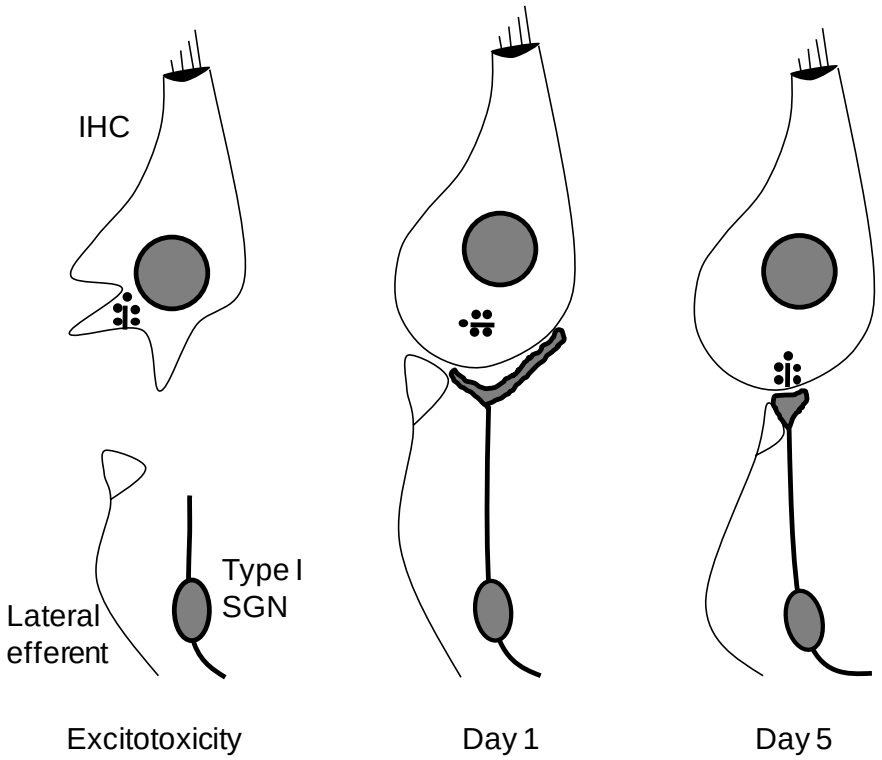

Fig. 1.12. Synaptic plasticity after excitotoxic injury. Schematic representation of the base of an IHC immediately (excitotoxicity, A), 1 day (B) and 5 days (C) after a perfusion of 200 µM AMPA into the cochlea. For simplicity only one synaptic complex is represented. A) Excitotoxicity injury results in destruction of the Type I dendrite of the spiral ganglion neuron (SGN) innervating the IHC. Hearing is lost at this point. B) One day after, the IHC is connected by filopodes from the regenerating neurite from the Type I SGN (which are sometimes branching), accounting for the beginning of recovery of hearing. Also the IHC at the stage is often directly contacted by efferent endings. C) Five days after AMPA a normal pattern of IHC innervation is observed, with the efferent neuron contacting the afferent synapse and hearing has also recovered. Adapted from Puel 1995.

Efferent innervation: The IHCs do not directly receive efferent innervation. Instead an axo-dendritic synapse is formed between the descending neuron from the lateral superior olivary complex and the post-synaptic membrane of the afferent Type I SGN, termed the lateral efferent pathway. While there are many candidate neurotransmitters for this synapse, the neurotransmitters that have drawn the most

attention are dopamine, acetylcholine (ACh) and gamma-aminobutyric acid (GABA). Application of dopamine has been shown to reduce auditory nerve activity by tonic inhibition and may protect against excitotoxicity (Ruel *et al.* 2001), while ACh application has been shown to increase the spontaneous and glutamate-induced firing activity of these fibres (Puel 1995, Felix and Ehrenberger 1992). GABA application did not affect the spontaneous firing rate but did reduce the activity induced by glutamate (Puel 1995, Felix and Ehrenberger 1992).

Outer hair cell innervation

Afferent innervation: The OHCs are directly innervated by the Type II SGN, with one neuron making synaptic connections with around 10 OHCs in the cochlear base and up to 50 OHCs at the apex (Dallos 1992). However, unlike the Type I SGN, there is debate as to whether the synapses formed are functional, as the Type II SGN are not spontaneously active nor do they respond to acoustic stimulation (Puel 1995, Robertson 1984, Robertson *et al.* 1999). While the neurotransmitter for this synapse has not been identified, the glutamate transporter GLAST has been identified in the Deiter's cells surrounding the basal region of the OHCs (Furness *et al.* 2002), suggesting that glutamate is the neurotransmitter between the OHC and the Type II SGN.

Efferent innervation: The majority of the OHC synaptic innervation comes from the efferent neurons, which send myelinated axons from the contralateral ventral nucleus of the trapezoid body in the auditory brainstem, termed the medial efferent pathway (Dallos 1992). The neurotransmitter released by the efferent neurons is believed to be

ACh, application of which has been shown to reduce OHC length *in vitro* (Brownell *et al.* 1985) and reduce OHC motility as noted by reduction in OAEs (Kujawa *et al.* 1992), which also occurs when the efferent pathway is stimulated (Siegel and Kim 1982). Of the two types of ACh receptors, the ionotropic nicotinic receptors and metabotropic muscarinic receptors (Bonner *et al.* 1987, Sargent 1993), nicotinic ACh receptors consisting of α9 and α10 subunits have been identified in the OHCs (Elgoyhen *et al.* 1994, Elgoyhen *et al.* 2001).

Hearing loss

Hearing loss can be broadly divided into two categories, conductive and sensorineural, although both can be present simultaneously. Conductive hearing loss is due to sound not reaching the inner ear, due to blockage or damage of the outer or middle ear. Causes include the build-up of ear wax or fluid from ear infections, ruptured ear drum or otosclerosis, abnormal bone growth that prevents the ossicles in the middle ear from moving properly. Sensorineural hearing loss is a result of damage to the cochlea hair cells and/or the auditory nerve, which is permanent as the hair cells are not replaced in the adult mammalian cochlea (Daudet *et al.* 1998, Yamasoba *et al.* 2003). While the decline in hearing is a natural part of aging (age-related hearing loss (AHL) or presbyacusis), noise exposure, ototoxic drugs, infectious diseases and head injuries can also result in permanent sensorineural hearing loss.

Drug induced hearing loss

Prescribed drugs have been shown to produce hearing loss, known as ototoxicity. The more common prescribed ototoxic drugs are aminoglycoside antibiotics, such as

gentamycin (Holley 2005), and drugs prescribed for chemotherapy, such as cisplatin (Panici *et al.* 1993). These drugs are believed to be ototoxic by producing reactive oxygen species (ROS) that induce apoptosis in the cochlear hair cells, particularly the OHCs (Rybak and Whitworth 2005).

Noise-induced hearing loss

Noise-induced hearing loss (NIHL) is considered to be a major cause of avoidable, permanent hearing loss. Noise can be divided into two categories: impulse noise, where the noise is of high intensity but lasts for a short period of time such as explosions; and continuous, where the noise is of lower intensity but lasts for a longer duration, such as exposure to loud music or machinery. In some cases noise exposure is unavoidable, such as military personnel and workers in the construction industry, although ear plugs or ear defenders can be used to lessen the exposure. However NIHL can also be generated from completely avoidable sources, such as the use of personal music devices at high volume and socialising in noisy environments.

The cellular consequences resulting in NIHL are difficult to define. Very loud noise is believed to damage the cochlea through mechanical means, with the force of the vibrations of the cochlear partitions resulting in structural damage of the hair cell stereocilia (Spoendlin and Brun 1973). This results in hearing loss due to a loss or non-functioning hair cells. At lower noise intensities, the overstimulation of the hair cells causes the excessive glutamate release into the synaptic cleft, resulting in excitotoxic degeneration of the sensory nerve terminals and hair cell membranes (Puel *et al.* 1998). Ultimately, apoptosis is initiated in the hair cells after noise exposure and the

dead cells are removed from the organ of Corti. The surrounding support cells form tight seals to prevent the infiltration on the scala media endolymph (Holley 2005), producing an epithelium scar along the basilar membrane (Leonova and Raphael 1997, Abrashkin *et al.* 2006). SGN loss follows as a consequence of hair cell death, as the hair cells provide neurotrophins to support the SGN (McFadden *et al.* 2004).

Age related hearing loss

Age-related hearing loss (AHL), also known as presbyacusis, occurs due to the irreversible degeneration of specific cell types within the cochlea (Holley 2005), which can be further classified by the cell types lost. 'Sensory AHL' is due to degeneration of the hair cells, 'neural AHL' relates to loss of SGN number, 'strial AHL' results from a decline in the cells within the stria vascularis, while 'mixed AHL' is a combination of cell type losses. However it must be noted that the numbers of these cells decline naturally with age, so AHL is referred to as an accelerated loss of a particular cell type (Ohlemiller and Gagnon 2004). The more common cause of AHL is sensory AHL, predominately seen with a greater loss of OHC compared to IHC, and progressively spreading from the high-frequency basal regions of the cochlea towards the apex (Holley 2005, Daudet *et al.* 1998). Hearing can be restored with the use of a hearing aid but this does not prevent further hearing loss. The only treatment to restore hearing would be to replace the lost cells, however this would be unhelpful if the underlying cause of the original cell loss is unresolved (Holley 2005).

Tinnitus

Overview: Tinnitus is defined as the perception of sound in the absence of an appropriate acoustic stimulus. Tinnitus is also sometimes accompanied by hearing impairment. A distinction can be made between objective tinnitus and subjective tinnitus. Objective tinnitus is audible to the patient and the examiner while subjective tinnitus is perceived by the patient only, and can be further divided into a peripheral form (sound conduction tinnitus and neurosensory tinnitus) and a central form (tinnitus arising from a region of the neuronal auditory pathway). Tinnitus can be caused by a multitude of different effects, including exposure to loud noise (Schmuziger *et al.* 2006), drugs such as Quinine (Marcus 2005), diseases like Ménière's disease (Rask-Andersen *et al.* 2005) but can also occur spontaneously in healthy individuals or in conjunction with other disease processes.

Possible neural correlates for tinnitus generation

The neurological site of the generation of tinnitus is unknown as yet but there are many theories and candidate locations along the auditory pathway that could be responsible for the perception of tinnitus. These sites are broadly divided into generation from within the cochlea, termed peripheral generation, and the nuclei within the auditory pathway, termed central generation.

Peripheral generation of tinnitus: The perception of tinnitus is usually accompanied by a degree of hearing loss (Simpson and Davies 1999) and it is accepted that 70-80% of deaf people have tinnitus (Levine 1999). As hearing loss is associated with the damage and death of hair cells, it is logical to assume that tinnitus generation is caused by damage to the cochlea and the sound transduction mechanism outside of the central

processing centres. Ototoxic drugs and noise exposure have shown to cause structural changes to the hair cells, such as the fusion of the stereocilia (Kössl *et al.* 1990). This fusion could cause an increase in ionic conductance through the stereocilia, resulting in an increase in neurotransmitter release from the hair cells (Simpson and Davies 1999). Additionally, noise exposure has been reported to alter the SGN in the damaged region, which would alter the responsiveness to stimulation by the hair cells (Simpson and Davies 1999). The SGNs have a spontaneous level of activity (Robertson 1984, Robertson *et al.* 1999), which has been shown to decrease following prolonged noise exposure (Chen *et al.* 1996) believed to be due to hair cell damage (Liberman and Dodds 1984). Any change in this spontaneous activity following modest noise exposure could lead to the generation of tinnitus.

Tinnitus is also a symptom of Ménière's disease, thought to arise from the disruption of the scala media, endolymphatic hydrops, thus disrupting the normal function of the hair cells (Hamid 2009). Tinnitus associated with Ménière's disease has been shown to be treatable using aminoglycoside antibiotics (Sala 1997) and osmotic-stabilizing drugs (Filipo *et al.* 1997) in some cases. The activity of these drugs is restricted to the cochlea, indicating a peripheral site for tinnitus generation.

Central generation of tinnitus: The central generation of tinnitus is thought to arise from the nuclei from the central auditory pathway becoming sensitised as a result of a lesion, resulting in neuronal hyperactivity which is perceived as sound (Møller 1997). This is supported by evidence that quinine, which generates the perception of tinnitus in humans, can alter the spontaneous firing rate in areas of the cat primary auditory

cortex (Simpson and Davies 1999). Additionally, an increase in the spontaneous activity of the dorsal cochlear nucleus has been identified following noise exposure (Zhang and Kaltenbach 1998, Kaltenbach *et al.* 2004, Finlayson and Kaltenbach 2009), as well as increase in the activity of the inferior colliculus after salicylate (Chen and Jastreboff 1995), cisplatin or noise exposure (Bauer *et al.* 2008), in animal models. This increase in activity is thought to generate the sensation of tinnitus, with a positive correlation between increased DCN activity and detection of tinnitus behaviour identified in animal models (Kaltenbach *et al.* 2004).

In conclusion, the debate over the neural site for the generation of tinnitus is on-going, with a distinct possibility that the sensation of tinnitus can arise from several auditory areas simultaneously and not just a single, discrete region. It must also be noted that the generation of tinnitus may not be uniform and that the site of tinnitogenesis may vary between individuals. A good example is the reported incidence of tinnitus following auditory nerve sectioning, where between 45-65% of patients report relief from their tinnitus sensation following surgery (House and Brackmann 1981, Pulec 1995). This suggests that both peripheral and central tinnitus generation can exist.

Treatment of tinnitus

Pharmacological agents to treat tinnitus: To date there is no universally accepted pharmacological treatment for tinnitus. The most commonly prescribed drugs are antidepressants, sedatives and anxiolytics, such as nortriptyline and alprazolam (Simpson and Davies 1999) however it is unsure if these drugs are treating tinnitus or the depression and anxiety often experienced by tinnitus sufferers (Davies 2004).

Intravenous administration of lignocaine, a local anaesthetic, has proved to be the most effective pharmacological treatment for tinnitus, with the symptoms ameliorated in approximately 60-80% of sufferers (Simpson and Davies 1999, Davies 2004). However, lignocaine is not used as a viable treatment for tinnitus due to its short duration of action and cardiac side effects (Simpson and Davies 1999, Davies 2004). Anticonvulsants, such as carbamazepine and lamotrigine, have also been used to treat tinnitus as their mode of action is to reduce neuronal excitation (Simpson and Davies 1999). However, drug trials have been difficult to conduct and ratify the effectiveness of any pharmacological agent due to the varying nature of tinnitus and the perceptual aspect of the condition, resulting in a large placebo response (Dobie 1999). Dietary suppliments have been reported to relieve tinnitus, such as *Ginkgo biloba* (Birks and Grimley Evans 2009), although further examination did not support their effectiveness as tinnitolytics (Drew and Davies 2001).

Pharmacological alternatives: Non-pharmacological treatments for tinnitus include the use of transcranial magnetic stimulation (TMS) to the temporoparietal cortex. Low frequency TMS has been shown to decrease cortical excitability and modify the symptoms of auditory hallucinations with some evidence of suppressing tinnitus for a short period of time (Pridmore *et al.* 2006, Fregni *et al.* 2006, Richter *et al.* 2006).

Tinnitus retraining therapy (TRT) can also be employed. Based around the neurophysiological model of tinnitus developed by Jastreboff (reviewed in (Baguley 2002)), TRT aims to reduce the perception of the sufferers tinnitus by a combination of counselling and increasing background sounds through hearing aids and white noise

generators. While TRT does not treat the underlying cause of tinnitus, it does address the emotional aspect of experiencing chronic tinnitus, i.e. fear and depression, and has been shown to be effective in reducing the perception of tinnitus in some cases (Henry *et al.* 2007).

Tinnitus and pain

Many parallels have been drawn between tinnitus and the sensation of chronic pain (Møller 1997). Both conditions are ameliorated by antidepressants, anticonvulsants and the local anaesthetic lignocaine (Simpson and Davies 1999). Lignocaine acts by inhibiting voltage-gated Na^+ channels expressed by neurons by blocking the ionic pore through binding to the S6 region that binds the vestibule (Catterall 2000), thus blocking the pore and stopping the flow of Na^+ (Catterall 2000, Palmer and Carter 2002). This means that Na^+ cannot cross the neuronal membrane and thus action potentials cannot be generated. This results in a reduction in neuronal activity and sensory perception. As lignocaine can reduce the sensation of tinnitus it is conceivable that voltage-gated Na^+ channels contribute to the perception of tinnitus in a similar way to the excessive voltage-gated Na^+ channel activity in damaged peripheral nerves that leads to the perception of chronic neuropathic pain (Devor 2006).

Neuronal excitability

Generation of the resting membrane potential: The contents of a cell are contained within a plasma membrane, which provides a hydrophobic barrier to prevent the entry of hydrophilic ions. The membrane of a neuron is permeable to charged ions, such as Na^+, K^+, Ca^{2+} and chloride ions (Cl^-), crossing through ion channels and membrane

pumps, with the intracellular concentrations of these ions strictly controlled (Table 1.1). The general movement of the ions across the membrane is determined by two forces: diffusion, with ions moving from regions of high concentration to low concentration, and the electrical charge, with ions attracted to regions of opposite charge. Membrane pumps however use active transport to move ions against their concentration gradients, using energy released from the hydrolysis of ATP. The movement of the ions generates a potential difference across the membrane and when the two forces are balanced this potential is referred to as the equilibrium potential, as defined by the Nernst equation:

$$E_{ion} = 2.303\ \frac{RT}{zF}\ Log_{10}\ \frac{[ion]_o}{[ion]_i}$$

Where E_{ion} is the ionic equilibrium potential, R is the gas constant, T is the absolute temperature, z is the charge of the ion, F is Faradays constant, $[ion]_o$ is the extracellular concentration of the ion and $[ion]_i$ is the intracellular concentration of the

Ion	Concentration (mM)		Equilibrium potential at 37°C (mV)
	Extracellular	Intracellular	
K^+	5	100	-80
Na^+	120	15	62
Ca^{2+}	2	0.0002	123
Cl^-	150	13	-65

Table 1.1. Ionic concentrations for a typical neuron. Table detailing the intracellular and extracellular, as well as the equilibrium potentials, for potassium (K^+), sodium (Na^+), calcium (Ca^{2+}) and chloride (Cl^-) ions for a typical neuron at 37°C.

ion. Thus E_{ion} is proportional to temperature, as an increase in temperature would cause an increase in diffusion, and inversely proportional to ionic charge, as an increase in charge would reduce the potential difference to balance diffusion. Applying the Nernst equation to the K^+ concentrations from Table 1.1, where:

$$E_K = 61.54\ Log_{10}\ \frac{5}{100}$$

$$E_K = 61.54 \times -1.3$$

$$E_K = -80mV$$

Thus E_K is -80mV at 37°C. If neurons where only permeable to K^+ then the resting membrane potential (RMP) would equal E_K. However, the neuronal membrane is also permeable to Na^+, which means that the RMP will reside between E_K and E_{Na}. What determines the RMP is the relative permeability of the membrane to potassium and Na^+, as defined in the Goldman equation where:

$$V_m = 61.54\ Log_{10}\ \frac{P_K[K^+]_o + P_{Na}[Na^+]_o}{P_K[K^+]_i + P_{Na}[Na^+]_i}$$

Where V_m is the membrane potential and P_{ion} is the relative permeability of the membrane for that particular ion. As the membrane permeability to K^+ is between 40 to 100 times greater than that to Na^+, applying this data to the Goldman equation where:

$$V_m = 61.54\ Log_{10}\frac{40(5) + 1(150)}{40(100) + 1(15)}$$

$$V_m = 61.54\ Log_{10}\frac{350}{4015}$$

$$V_m = -65mV$$

Thus the RMP for this neuron is -65mV, with typical RMP of between -60mV and -80mV depending on the neuronal type (Koester and Siegelbaum 2000b). This example

has ignored the contribution of Cl^- to the RMP, as neurons generally do not actively transport Cl^- and thus the movement of Cl^- across the membrane reaches equilibrium at RMP.

Action potential generation: Action potentials are generated when the permeability of the membrane to K^+ and Na^+ is altered (as described by (Hodgkin and Huxley 1952)). Action potentials are the unit of neuronal information and result from depolarisation of the membrane above the threshold for activation, meaning that action potentials are all or nothing events. At rest the net flux of charge is null, maintaining the constant RMP. When the membrane becomes depolarised past the threshold for action potential generation (at around -55mV), normally due to influx of Na^+ or Ca^{2+} through activation of ionotropic neurotransmitter receptors, voltage-gated Na^+ channels rapidly open, increasing the permeability of the membrane to Na^+ (Koester and Siegelbaum 2000c). This allows greater influx of Na^+ into the neuron, causing further depolarisation, pushing the membrane potential closer to the E_{Na} and resulting in the upstroke of the action potential (Fig. 1.13). The repolarisation is generated by the inactivation of the Na^+ channels, halting the influx of Na^+, and the activation of voltage-gated K^+ channels, resulting in increased K^+ permeability and an increase of K^+ efflux, hyperpolarising the membrane and pushing the membrane potential towards E_K. A brief after hyperpolarisation can also be seen, where the membrane potential falls below the previous resting level due to the combined conductance of K^+ through voltage-gated K^+ channels and leak K^+ channels. The membrane potential then returns to RMP when the voltage-gated K^+ channels inactivate. This sequence of

depolarisation and voltage-gated ion channel activation is repeated along the axon of the neuron, resulting in action potential propagation.

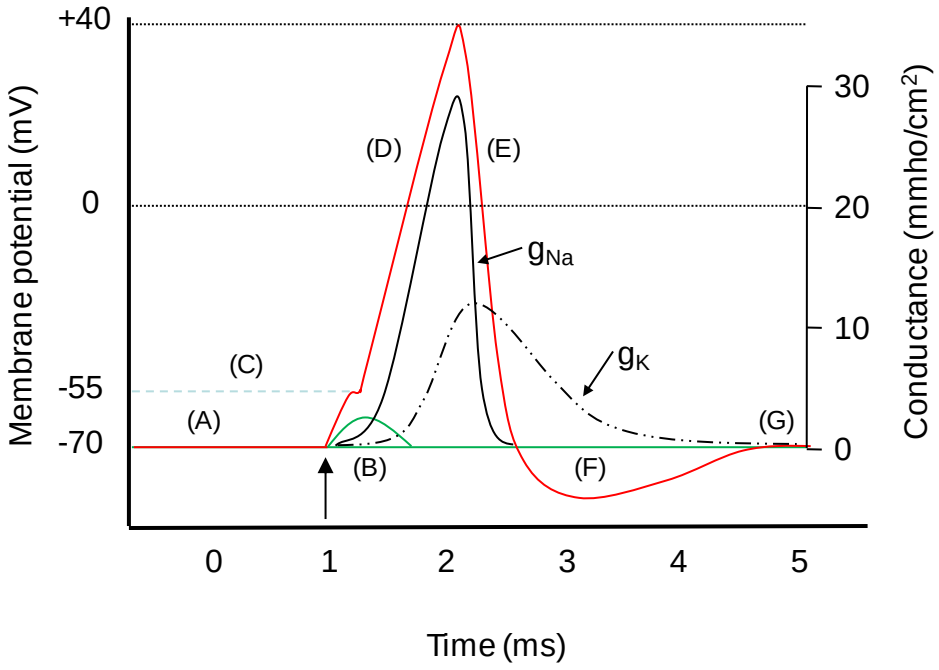

Fig. 1.13. Representation of an action potential. Diagram representing the membrane potential changes during an action potential and the associated changes in the conductance of the membrane to Na^+ (g_{Na}) and K^+ (g_K). At rest, the membrane potential of the neuron remains constant, in this case at -70mV (A). When stimulated (arrow), the neuron is depolarised and the membrane voltage becomes less negative. When a small depolarising stimulus is given the action potential fails to initiate (B) as the membrane is not elevated above the action potential generation threshold, in this instance -55mV (C). When the stimulus depolarises the membrane above the threshold, the action potential is initiated (red line), characterised by a rapid increase in membrane voltage, also known as the upstroke (D), generated by the activation of voltage-gated Na^+ channels (Na_V) and the rapid influx of Na^+ into the neuron. The down stroke or falling phase of the action potential (E) is caused by the inactivation of Na_V, halting the Na^+ influx, and the activation of voltage-gated K^+ channels (K_V), causing an efflux of K^+ from the neuron. A brief undershoot can sometimes be observed (F) caused by the increased K^+ efflux from K_V channels and leak channels. As the K_V channels begin to inactivate, the balance of K^+ efflux and Na^+ influx is restored, returning the membrane to the resting potential (G). Adapted from Hodgkin and Huxley, 1952.

Action potential propagation: Action potentials are propagated along axons in one of two ways depending on whether the axon is myelinated (Reviewed in (Koester and

Siegelbaum 2000a)). Unmyelinated axons propagate their action potentials through local-circuit current flow, where depolarisation spreads along the axon activating voltage-gated Na^+ channels and propagating the action potential. The action potential is propagated in one direction due to the voltage-gated Na^+ channels entering a state of inactivation after opening.

Axons that have a myelin sheath, from the wrapping of Schwann cells in the PNS or oligodendrocytes in the CNS, propagate action potentials through saltatory conduction. The myelin wraps around the axon in discrete regions with gaps of bare axon between each region, the gaps known as nodes of Ranvier. The action potential spreads quickly along the axon regions covered in myelin, known as internodes, due to the low capacitance and high membrane resistance the myelin sheath produces. The nodes of Ranvier regenerate the action potential due to the dense clustering of voltage-gated ion channels at these nodes, thus the action potential is considered to jump from node to node.

Voltage-gated Sodium Channels

Voltage-gated sodium channel structure: Na^+ channels are large transmembrane proteins that allow the influx of Na^+ through the hydrophobic plasma membrane. Voltage-gated Na^+ channels (Na_V) consist of a single 260kDa α-subunit and are sometimes associated with one or more 33-36kDa β-subunits (Catterall 2000, Yu and Catterall 2003). The α-subunit consists of four homologous regions of six transmembrane domains while the β-subunits are single transmembrane proteins that can modulate the channel gating properties (Fig. 1.14). Of the six transmembrane

domains of each section of the α-subunit, the fourth domain (S4) is the voltage sensing region. The ionic pore is formed by domains S5 and S6 as well as the extracellular loop that links them.

Voltage-gated Na^+ channels are critically important because they regulate the influx of Na^+ into the neuron that causes the depolarisation of the neuronal membrane potential, resulting in the rising phase of action potentials. There are three activation states of voltage-gated Na^+ channels: closed or resting, where the pore is closed and there is no flow of ions; open or active, where a conformational change in the voltage sensing S4 regions reorganises the pore forming regions to allow the influx of Na^+; and

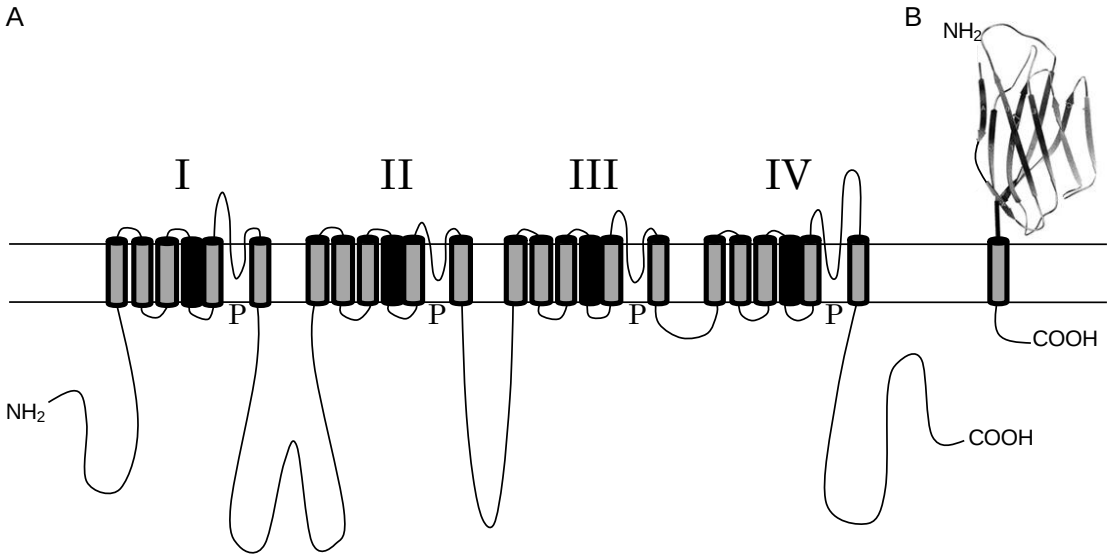

Fig. 1.14. Structure of the voltage-gated sodium channels. The voltage-gated sodium channel (Na_V) consists of an α-subunit (A) with accessory β-subunits (B). The α-subunit is a single polypeptide chain, proposed to consist of four repeating motifs (I-IV). Each domain contains six α-helical membrane spanning domains, represented by cylinders. Transmembrane domain 4 in each repeat is believed to be the voltage-sensitive region, indicated by the darker cylinder. Bold lines represent the polypeptide chains of each subunit. The loop between transmembrane domains 5 and 6 lines the Na^+ selective pore (P). B) The β-subunit consists of a single transmembrane domain with a globular N-terminal region, made from β-pleated sheets. Image adapted from Catterall et al. 2005a.

inactivated, where an intercellular loop, the link between the third and fourth regions, undergoes a conformational change to close the pore, stopping the flow of Na^+ and as an inactivation gate (Catterall 2000, Yu and Catterall 2003, Tombola *et al.* 2006). Voltage-gated Na^+ channels enter an inactive state upon sustained depolarisation and can only open again once returned to the closed conformation (Catterall 2000, Catterall *et al.* 2005a).

Voltage-gated sodium channel tissue expression: There are ten genes that encode for mammalian voltage-gated Na^+ channel α-subunits, of which nine have been expressed in exogenous systems. The nine isoforms are classified as $Na_V1.1$-$Na_V1.9$ and have differential expression throughout the mammalian nervous system, as summarised in Table 1.2. Neurons forming the brain and spinal cord (CNS) have been shown to predominantly express $Na_V1.1$, $Na_V1.2$, $Na_V1.6$ (Whitaker *et al.* 2000, Whitaker *et al.* 2001, Krzemien *et al.* 2000). $Na_V1.3$ has also been shown to be expressed in adult human CNS neurons (Whitaker *et al.* 2000, Whitaker *et al.* 2001), but there is clear evidence that this isoform is predominantly expressed during embryogenesis (Beckh *et al.* 1989, Beckh 1990, Felts *et al.* 1997). The expression of $Na_V1.7$, $Na_V1.8$ and $Na_V1.9$ are restricted to the PNS (Toledo-Aral *et al.* 1997, Dib-Hajj *et al.* 1998, Dib-Hajj *et al.* 1998), although $Na_V1.6$ has also been identified in DRG neurons (Beckh 1990, Black *et al.* 1996). $Na_V1.8$ and $Na_V1.9$ are particularly identified in subpopulations of the medium and small diameter sensory neurons of DRG, respectively (Amaya *et al.* 2000), which are known to transmit nociceptive information (Dib-Hajj *et al.* 1998, Dib-Hajj *et al.* 1998, Fang *et al.* 2002, Djouhri *et al.* 2003). The isoforms $Na_V1.4$ and $Na_V1.5$ have

been shown to be expressed at high levels in rat skeletal muscle (Trimmer *et al.* 1989) and cardiac muscle (Rogart *et al.* 1989) respectively.

Na_V α-subunit (Former classification)	**Channel Expression**	**TTX Sensitivity**
1.1 (Brain type I)	Central neurons; cardiac myocytes	6nM
1.2 (Brain type II)	Central neurons	12nM
1.3 (Brain type III)	Central neurons; expressed in embryonic life	4nM
1.4 (SkM1)	Adult skeletal muscle	5nM
1.5 (h1, skmII)	Cardiac myocytes; central neurons	1-2mM
1.6 (PN4, NaCh6)	DRG neurons; Nodes of Ranvier of sensory and motor neurons	1nM
1.7 (PN1)	All DRG neurons; Schwann cells; neuroendocrine cells	4nM
1.8 (PN3, SNS)	Small and medium sized DRG neurons and their axons	60mM
1.9 (NaN, SNS-2)	C-type DRG neurons, preferentially expressed in nociceptive DRG neurons	40mM

Table 1.2 Distribution of mammalian voltage-gated Na^+ channel α-subunits. Table shows the typical tissue expression of the mammalian voltage-gated Na^+ channel α-subunits, indicating former classification and sensitivity to tetrodotoxin (TTX). (Catterall,W.A. *et al*. 2005a).

Voltage-gated sodium channel properties and pharmacology: The voltage-gated Na^+ channel isoforms, in addition to their distinct expression patterns, also display subtle differences in their electrophysiological properties that convey altered excitability characteristics in diverse neuronal tissues (Palmer and Carter 2002, Catterall *et al.*

2005b). $Na_V1.6$ has been shown to produce a persistent current after depolarisation (Rush *et al.* 2005) as well as a resurgent current in cerebellar Purkinje neurons (Raman and Bean 1997) and large diameter DRG neurons (Cummins *et al.* 2005). In these cases the cell bodies are depolarised and the Na^+ currents activate and inactivate in a normal fashion, but when the cell is repolarised to voltages around −50 or −60mV where voltage-gated Na^+ channels would usually be in the inactive state, a flow of Na^+ current flows briefly, promoting the firing of a second action potential. However, $Na_V1.6$ null mutant neurons have been show to still produce resurgent currents (Do and Bean 2004) indicating that resurgent currents may not be unique property of $Na_V1.6$ channels. $Na_V1.7$ has been shown to have slow repriming kinetics, which allows these channels to be activated by small depolarising steps that would not usually activate the channel (Cummins *et al.* 1998). $Na_V1.3$ has been shown to display fast activation and inactivation kinetics with a rapid recovery from inactivation, allowing rapid action potential generation (Cummins and Waxman 1997, Chen *et al.* 2000). Of the two isoforms expressed also exclusively in nociceptive DRG neurons, $Na_V1.8$ has been shown to have a high threshold of activation and slowly inactivate (Rush *et al.* 1998, Akopian *et al.* 1999), while $Na_V1.9$ has a low threshold of activation and produces a persistent current (Cummins *et al.* 1999). As the threshold of activation of $Na_V1.9$ is close to the resting membrane potential of the DRG neurons (-70mV), this subunit is believed to contribute to setting the threshold or action potential generation in these neurons (Baker and Bostock 1997)

There are few pharmacological agents that can specifically block the ionic pore of the different voltage-gated Na^+ channel subtypes. Tetrodotoxin (TTX) is known to

selectively block all voltage-gated Na^+ channel subtypes at nano-molar concentrations, except for $Na_V1.5$, $Na_V1.8$ and $Na_V1.9$ (Catterall *et al.* 2005b). However, recent studies have revealed agents that have been reported to be more selective for particular voltage-gated Na^+ channel isoforms. The tarantula venom peptide ProTx-II has shown to selectively inhibit $Na_V1.7$ (Schmalhofer *et al.* 2008) while a TTX metabolite, 4,9-anhydro-TTX, has been shown to specifically block $Na_V1.6$ (Rosker *et al.* 2007). Both these compounds are at least 100 fold more selective for $Na_V1.7$ and $Na_V1.6$, respectively, compared to the other voltage-gated Na^+ channel isoforms.

Voltage-gated sodium channel expression in SGN: At present, the expression of voltage-gated Na^+ channels in the mammalian spiral ganglion has been poorly characterised, with the published discovery of the expression of $Na_V1.6$ in mouse SGN (Hossain *et al.* 2005). $Na_V1.6$ has been shown to be expressed at nodes of Ranvier along peripheral neuronal axons and in the dendrites of neurons in the central nervous system (Caldwell *et al.* 2000) as well as neurons of the peripheral nervous system (Krzemien *et al.* 2000, Tzoumaka *et al.* 2000, Dietrich *et al.* 1998, Goldin 2001). Additionally, $Na_V1.2$ was also identified in the organ of Corti using immunohistochemistry and was localised to the efferent processes innervating the IHCs and OHCs, but not in the SGN (Hossain *et al.* 2005).

Voltage-gated sodium channel expression following nerve damage: There are many examples of altered voltage-gated Na^+ channel subunit expression in neurons, particularly in somatosensory neurons in animal models of neuropathic and inflammatory pain. Neuropathic pain is thought to be generated from an increase in

spontaneous activity of the sensory neurons, resulting in facilitation of central synapses in the spinal cord and/or the brain (Rogers *et al.* 2006). Axotomy of the sensory nerves can result in the formation of a neuroma, a region of nerve growth that becomes hypersensitive to mechanical stimuli (Millan 1999). These neuromas have been shown to develop ectopic firing, believed to arise from the accumulation of voltage-gated Na^+ channels at the neuroma site (England *et al.* 1996, Kretschmer *et al.* 2002). In a rat model of nerve injury, the increase in the spontaneous activity of the sensory neurons increases through a decrease in the threshold for action potential generation, resulting in an increase in spontaneous membrane potential oscillations mediated through voltage-gated Na^+ channel conductance (Amir *et al.* 1999). These conductances have been shown to be modified through changes in voltage-gated Na^+ channel gene expression, protein phosphorylation (Hong *et al.* 2004) and changes in protein trafficking, as seen in painful neuromas (England *et al.* 1996, Kretschmer *et al.* 2002). Examples of how voltage-gated Na^+ channel gene expression can be altered in painful states are detailed below. These models are generated by damaging peripheral or central nerves by axotomy, through nerve ligation or entrapment, or injection of inflammatory compounds and further reveal that alteration of the voltage-gated Na^+ channel isoform cohort can result in altered neuronal activity (Rush *et al.* 2006).

It has been shown that $Na_V1.3$, an isoform that is expressed primarily in embryological development (Felts *et al.* 1997), is re-expressed following nerve injury that results in pain behaviour (Waxman *et al.* 1994). This has been shown in the sciatic nerve following chronic constriction injury (Hains *et al.* 2004), in the DRG following sciatic nerve axotomy (Black *et al.* 1999) and in the dorsal horn of the spinal cord, through

direct spinal cord injury (Hains *et al.* 2003). $Na_V1.3$ is thought to increase action potential generation due to this channel's fast recovery from inactivation, as discussed previously (Cummins and Waxman 1997, Chen *et al.* 2000). This shows that injury in both the peripheral and central nervous systems can result in aberrant expression of voltage-gated Na^+ channel isoforms that are not normally expressed in the affected tissue.

In addition to the re-expression of embryonic voltage-gated Na^+ channel isoforms, many studies have shown changes in endogenously expressed voltage-gated Na^+ channel isoforms following nerve damage. $Na_V1.8$ and $Na_V1.9$ are expressed in separate populations of the smaller diameter, nociceptive DRG neurons. Studies have shown that following lesioning of the sciatic nerve, there is a decrease in $Na_V1.8$ expression in the DRG cell bodies and an increase in $Na_V1.8$ staining at the site of injury due to the axonal transport of pre-synthesised protein stored in the Golgi apparatus (Novakovic *et al.* 1998, Thakor *et al.* 2009). Similarly, altered expression of $Na_V1.8$ and $Na_V1.9$ has been shown in injured human DRG neurons (Yiangou *et al.* 2000, Coward *et al.* 2000). This shows that the reorganisation of these channels occurs in both human and animal DRG neurons. Injection of inflammatory agents, such as Freund's complete adjuvant (FCA), has also resulted in an altered pattern of $Na_V1.7$, $Na_V1.8$ and $Na_V1.9$ expression in these neurons (Strickland *et al.* 2008). Evidence of altered endogenous voltage-gated Na^+ channel expression has additionally been shown outside of animal models of pain, with increased expression of $Na_V1.7$, $Na_V1.8$ and $Na_V1.9$ seen in human patients suffering from dental pain (Luo *et al.* 2008) and inflammatory rhinitis (Keh *et al.* 2008).

This shows that the voltage-gated Na^+ channel phenotype of these neurons is dynamic and can be plastically altered following damage. This also suggests that, following injury, the voltage-gated Na^+ channel expression in somatosensory neurons is re-organised to yield a hypersensitive/hyperactive phenotype resulting in the increased perception of painful sensations.

Other ion channels

While voltage-gated Na^+ channels are crucial for the initiation and propagation of action potentials, other ion channels are essential for the maintenance of the excitability of the neuronal membrane. The channels that allow the passage of K^+ and Ca^{2+} across the membrane are discussed presently.

Potassium channels

Potassium channels are transmembrane proteins that allow the passage of K^+ across the membrane. There are at least 70 genes in mammals that encode for K^+ channels, making them the largest and most diverse family of ion channels. Unlike the voltage-gated Na^+ channels, members of the K^+ channel superfamily are not a single protein, with a functional ion channel made up of subunits. Each subunit contains a region of amino acids that acts as a selectivity filter for K^+ known as the pore domain (Jenkinson 2006), with a total of four pore domains needed from the subunits to form a functional K^+ channel.

Inward rectifying potassium channels: The different types of K^+ channels can be broadly defined by the number of transmembrane domains of each subunit. Subunits with two transmembrane domains form inward rectifying potassium channels, K_{IR}, with the four subunits required to form a functional channel. K_{ir} channels are important in buffering cytoplasmic [K^+], setting the RMP and in the regulation of cell excitability. These channels are open around E_K, but the open probability declines under depolarization (Dart *et al.* 1998), as they become blocked by magnesium ions and spermine at the resting membrane potential (Butt and Kalsi 2006).

Tandem pore channels: The subunits of tandem pore channels (K_{2P}) have four transmembrane domains and are thought to contribute to the passive "leak" conductance of neurons which are active at resting membrane potentials, stabilise the membrane potential below the threshold for action potential generation and accelerate repolarisation (Jenkinson 2006, Goldstein *et al.* 2005). Each of these subunits contains two pore domains so to form a functional channel only two subunits are required.

Voltage-gated potassium channels: The voltage-gated K^+ channels (K_V) as well as the Ca^{2+} activated K^+ channels (K_{Ca}), consist of subunits with six transmembrane domains, although the $K_{Ca}1.1$ channel subunit has seven transmembrane domains. Each subunit has one pore forming domain, thus four subunits are required to form a functional channel. The pore forming domain of these channels is between transmembrane domains five and six and the voltage sensing region in transmembrane domain four. There are 40 genes that encode for human voltage-gated K^+ channel subunits with the

genes divided into families, K_V1 through K_V12. The functional voltage-gated K^+ channel can consist of one type of subunit to form a homotetramer, such as four $K_V1.1$ subunits, or as a heterotetramer, where one or more subunits are replaced by subunits from the same family, such as the $K_V1.1/K_V1.2$ heteromers observed in rat MNTB neurons (Dodson *et al.* 2002). This adds to the diversity of the voltage-gated K^+ channels as each subunit confers different properties to the functional channel.

Calcium-activated potassium channels: K_{Ca} channels form two distinct groups; the small-intermediate conductance and the large conductance channels. The small conductance (SK, $K_{Ca}2.1$-2.3) and intermediate conductance (IK, $K_{Ca}3.1$) channels are voltage insensitive and are activated by low concentrations of internal Ca^{2+}. The second group contains the big conductance (BK, $K_{Ca}1.1$) channel which is activated by internal Ca^{2+} as well as voltage. The other members of this group ($K_{Ca}4.1$, 4.2, 5.1) are not activated by Ca^{2+} but by internal Na^+ and Cl^- ($K_{Ca}4.1$, 4.2) and hydroxide groups ($K_{Ca}5.1$) (Wei *et al.* 2005).

Potassium channel expression in the SGN: It has been shown that $K_V1.1$, $K_V1.2$, $K_V3.1$, $K_V4.2$, as well as the large conductance K_{Ca} (Adamson *et al.* 2002a, Hafidi *et al.* 2005, Skinner *et al.* 2003, Davis 2003) and small conductance K_{Ca} SK2 (Dulon *et al.* 1998), are expressed in the mammalian cochlear spiral ganglion through immunocytochemistry. It has also been shown that staining for K_{Ca}, $K_V1.1$, $K_V1.2$ and $K_V3.1$ is more intense in the basal spiral ganglion neurons than the apical neurons and that there is intense staining for $K_V4.2$ in the apical neurons rather than the basal neurons (Adamson *et al.* 2002a).

Voltage-gated Calcium channels

Voltage-gated calcium channels (Ca_V) allow the passage of Ca^{2+} across the membrane upon depolarisation. In mammals there are 10 members identified in the voltage-gated Ca^{2+} channel family, each providing different roles in transducing the depolarisation at the cell membrane to changes in intracellular Ca^{2+} and, ultimately, the activation of cellular processes. The channels are distributed throughout the nervous system, with channel expression identified in neurons of the CNS and PNS as well as skeletal, smooth and cardiac muscle and endocrine cells (Catterall *et al.* 2005b).

Voltage-gated calcium channel structure: The functional channel consists primarily of the α_1 subunit, which has a similar structure to the voltage-gated Na^+ channel α-subunit. The α_1 subunit is a single polypeptide chain containing 4 homologous repeated domains, each consisting of 6 transmembrane domains, with the fourth domain sensitive to voltage changes and the loop between domains 5 and 6 forming the ion selective pore in each repeat. Auxiliary subunits include an intracellular beta subunit, a transmembrane $\alpha_2\delta$ subunit, connected to the α_1 subunit through disulphide bonds, and a γ subunit, identified to date in skeletal muscle only. While the auxiliary subunits modulate the properties of the channel, the pharmacological and electrophysiological diversity of the voltage-gated Ca^{2+} channel channels is due to the existence of the multiple α_1 subunits (Catterall *et al.* 2005b).

Voltage-gated calcium channel nomenclature: Ca^{2+} channels were originally named after the type of current the channel produced. L-type currents are long lasting,

require a large depolarisation for activation and are blocked by organic antagonists, such as dihydropyridines, phenylalkylamines and benzothiazepines. N-type, P/Q-type and R-type currents are similar to L-type currents but are blocked by the polypeptide toxins ω-conotoxin GVIA (Olivera *et al.* 1991), ω-agatoxin IVA (Mintz *et al.* 1992) and SNX-482 (Newcomb *et al.* 1998) respectively. T-type currents are different from the other currents in that they require less depolarisation, produce a transient current upon opening and are not blocked by the antagonists of the other current types (Catterall *et al.* 2005b). Previously the Ca^{2+} channels were identified by the currents they produced and which gene encoded the α_1 subunit. Following the formal reclassification of voltage-gated K^+ channels into K_V, a similar nomenclencture was adopted for voltage-gated Ca^{2+} channels, terming them Ca_V (Ertel *et al.* 2000), as summarised in Table 1.3 (Catterall *et al.* 2005b).

Channel	Current	Localisation	Specific agonists	Cellular function
$Ca_V1.1$	L	Skeletal muscle; transverse tubules	Dihydropyridines; phenylalkylamines; benzothiazepines	Excitation-contraction coupling
$Ca_V1.2$	L	Cardiac myocytes; smooth muscle myocytes; endocrine cells; neuronal cell bodies; proximal dendrites	Dihydropyridines; phenylalkylamines; benzothiazepines	Excitation-contraction coupling; hormone release; regulation of transcription; synaptic integration
$Ca_V1.3$	L	Endocrine cells; neuronal cell bodies and dendrites; cardiac atrial myocytes and pacemaker cells; cochlear hair cells	Dihydropyridines; phenylalkylamines; benzothiazepines	Hormone release; regulation of transcription; synaptic regulation; cardiac pacemaking; hearing; neurotransmitter release from sensory cells
$Ca_V1.4$	L	Retinal rod and bipolar cells; spinal cord; adrenal gland; mast cells	Dihydropyridines; phenylalkylamines; benzothiazepines	Neurotransmitter release from photoreceptors
$Ca_V2.1$	P/Q	Nerve terminals and dendrites; neuroendocrine cells	ω-Agatoxin IVA	Neurotransmitter release; dendritic Ca^{2+} transients; hormone release
$Ca_V2.2$	N	Nerve terminals and dendrites; neuroendocrine cells	ω-Conotoxin-GVIA	Neurotransmitter release; dendritic Ca^{2+} transients; hormone release
$Ca_V2.3$	R	Neuronal cell bodies and dendrites	SNX-482	Repetitive firing; dendritic calcium transients
$Ca_V3.1$	T	Neuronal cell bodies and dendrites; cardiac and smooth muscle myocytes	None	Pacemaking; repetitive firing
$Ca_V3.2$	T	Neuronal cell bodies and dendrites; cardiac and smooth muscle myocytes	None	Pacemaking; repetitive firing
$Ca_V3.3$	T	Neuronal cell bodies and dendrites	None	Pacemaking; repetitive firing

Table 1.3. Summary of tissue expression, pharmacology and function of voltage-gated calcium channels. Adapted from Catterall *et al*. 2005b.

Expression of voltage-gated calcium channels in the SGN: Reverse transcriptase-polymerase chain reaction (RT-PCR) analysis of RNA isolated from murine cochlea identified $Ca_V1.2$, $Ca_V1.3$ and $Ca_V2.3$, as well as β_1, β_3, β_4 and $\alpha_2\delta$ subunit RNA

expression (Green *et al.* 1996). A more recent study using isolated SGN, instead of whole cochlea homogenates, only identified $Ca_V1.3$ and $Ca_V2.3$, in addition to β_1, β_3 and $\alpha_2\delta$ subunits (Xie *et al.* 2007). These studies indicate that both L-type and R-type currents could be produced by SGN, currents that have been shown to repetitively generate action potentials. However, these studies do not show if the voltage-gated Ca^{2+} channel proteins are expressed in the SGN. Additionally, neurotransmitter release from IHC is believed to be mediated by Ca^{2+} influx through $Ca_V1.3$ channels (Platzer *et al.* 2000, Brandt *et al.* 2003), while $Ca_V3.1$ expression has been identified in rat OHC (Inagaki *et al.* 2008).

Transient receptor potential channels

While voltage-gated Na^+, K^+ and Ca^{2+} channels specifically allow the passage of a single species of ion, other ion channels exist that are not selective and which allow cations to pass though them, which are gated by changes in membrane potential. The transient receptor potential (TRP) channels are an example of such channels. The TRP channel consists of four polypeptide subunits, forming a tetrameric channel, with each subunit consisting of 6 transmembrane domains with the loop domain between transmembrane domains 5 and 6 lining the ion pore (Kedei *et al.* 2001, Clapham 2003). The mammalian TRP channel superfamily are encoded by at least 28 subunit genes, divided into six families based on sequence homology rather than ion selectivity or function, as the functions of the channels can be very unrelated (Clapham 2003). These families are: the classic TRPs (TRPCs); the vanilloid receptor TRPs (TRPVs); the melastatin or long TRPs (TRPMs); the mucolipins (TRPMLs); the polycystins (TRPPs); and ankyrin transmembrane protein 1 (ANKTM1, TRPA1) (Clapham *et al.* 2005). To

discuss all six families is beyond the scope of this chapter, instead the TRPV and TRPA1 families will be discussed (more detailed reviews can be found in (Clapham 2003, Clapham *et al.* 2005, Huang 2004)).

Vanilloid receptor TRP channels: TRPV channels are so called due to the activation of TRPV1, the first member of the family to be cloned, by the application of the vanilloid, capsaicin, the pungent component of hot chilli peppers (Jordt *et al.* 2003). The TRPV family consists of 6 members that share homology with TRPV1 and can be divided into two groups, TRPV1-4 which are sensitive to temperature, between 27^{o}C to 43^{o}C (Jordt *et al.* 2003), and TRPV5-6 which are believed to be responsible for Ca^{2+} absorption in the kidney (Clapham *et al.* 2005, Huang 2004). In addition to capsaicin and temperature, TRPV1 has also been shown to be sensitised to heat stimuli by protons (Clapham *et al.* 2005) and inflammatory mediators (Huang 2004), indicating that the channels are readily modulated following tissue damage. This is particularly pertinent when considering the tissues in which the expression of these channels has been identified. TRPV1-4 have been identified in sensory neurons as well as the bladder, spleen and lungs (Clapham 2003, Clapham *et al.* 2005, Jordt *et al.* 2003, Dhaka *et al.* 2006). TRPV1 and TRPV4 expression has been reported in the SGN and cochlea (Balaban *et al.* 2003, Zheng *et al.* 2003, Takumida *et al.* 2005). Additionally, mRNA and protein expression for TRPV1 was up-regulated while TRPV4 mRNA and protein expression was down-regulated following the application of kanamycin (Kitahara *et al.* 2005) or gentamicin (Ishibashi *et al.* 2009). Also, TRPV4 deficient mice show elevated hearing thresholds contributed to both age-related and noise-induced (4kHz pure tone

at 128dB SPL for 4 hours) hearing loss when compared to normal mice of the same age (Tabuchi *et al.* 2005).

TRPA: The TRPA family contains one member, TRPA1 also known as ANKTM1. TRPA1 was first thought to be responsible for sensing very cold temperatures (Jordt *et al.* 2003), but was also found to be sensitive to allyl isothiocyanate, the pungent ingredient in mustard, indicating a role in nociception (Jordt *et al.* 2004). TRPA1 is also a candidate for the MET channel found on the apex of hair cell stereocilia, although TRPA1 deficient mice were not found to be congenitally deaf (Kwan *et al.* 2006).

Aims of the project

This project addresses the question of whether the re-organisation of voltage-gated Na^+ channels seen in somatic nerves following injury occurs in SGN following modest ototrauma. As stated previously, the reorganisation of voltage-gated Na^+ channel expression has been shown in models when the sensory neurons have been lesioned, resulting in the loss of innervation of their sensory targets. This raises the question of whether the altered voltage-gated Na^+ channel expression is a response unique to the somatosensory neurons or if altered voltage-gated Na^+ channel expression is seen in all sensory neurons that are deafferented. Given the reported damage caused to the SGN following noise exposure, it seems that noise exposure can result in a loss of afferent synapses from the SGN in a similar fashion to the lesioning of the somatosensory nerves. Thus noise exposure will be used to investigate whether voltage-gated Na^+ channel expression is altered in SGN of deafened rats.

To this end, first the voltage-gated Na^+ channel isoforms expressed by normal rat SGN must be identified and anatomically defined. Then, following exposure to a novel sound protocol, shown to produce a moderate level of deafness, the voltage-gated Na^+ channel isoforms expressed by the SGN from deafened animals will be compared and contrasted to unexposed animals.

Expression of voltage-gated sodium channels in the cochlear spiral ganglion

The first section determined the expression of voltage-gated Na^+ channel α-subunit isoforms in the spiral ganglion neurons of adult Wistar rats with normal hearing. The expression was investigated by RT-PCR, to identify the mRNA expressed by the SGN, and immunohistochemistry, using antibodies raised against the voltage-gated Na^+ channel α-subunits to identify the expression of the proteins, their neuroanatomical distribution and their subcellular localization.

The specificity of the PCR primers and antibodies was determined by using control tissue from the CNS and PNS with already well characterized voltage-gated Na^+ channel expression, specifically the cerebral cortex, cerebellum and DRG.

Expression of voltage-gated sodium channels in the cochlear spiral ganglion following otoacoustic trauma

Wistar rats were exposed to a noise stimulus to observe any upregulation or downregulation of voltage-gated Na^+ channel subunits following acoustic trauma. This model of acoustic trauma was devised to expose the rats to a modest level of noise

(110dB SPL compared to 120dB SPL and above used in other studies) to generate hearing loss without complete disruption of the cochlea.

Previously conducted RT-PCR and immunohistochemistry was repeated using cochleae from rats that have been subjected to noise as well as control rats that have normal hearing. In addition, quantitative PCR allowed the measurement of the voltage-gated Na^+ channel mRNA copies in modiolar samples taken from rats that have undergone noise exposure and allow the comparison with the expression in unexposed individuals.

As stated previously, many parallels have been drawn between pain and tinnitus. This part of the thesis will investigate whether a similar re-organisation of voltage-gated Na^+ channel that occurs in pain models occurs following ototrauma.

Chapter 2. Experimental methods and materials

This chapter will cover the experimental details that are common to the following chapters, including the tissue extraction techniques and the details of experimental procedures carried out in the animal experiments.

Animal procurement and care

Adult male Wistar rats (150-200g) were purchased from Charles River UK (Charles River UK Ltd, Margate, UK). Animals were allowed a seven day acclimatization period before experimental use. Animals were kept in a 12 hour light/dark cycle, with minimum natural light, and were given water and food *ad libitum*.

Anaesthesia protocols

The experimental animals were anaesthetised to facilitate the recording of accurate auditory brainstem responses (ABR). The anaesthesia served several functions including, the placement of subdermal recording electrodes, ensuring the animal remained in the correct position for delivery of the tone pips and to reduce skeletal muscle contraction that would interfere with the ABR measurements. Three anaesthetic approaches were tested.

Isofluorane inhalation: Isofluorane (2-chloro-2-(difluoromethoxy)-1,1,1-trifluoro-ethane) is a volatile ether used to produce anaesthesia via inhalation. It has been shown to diminish excitatory synaptic transmission by reducing the release of glutamate and increasing glutamate uptake at synapses within the CNS (Larsen *et al.* 1994, Larsen and Langmoen 1998)

Isofluorane (IsoFlo, Abbott Laboratories, Maidenhead, UK), delivered with pure oxygen at a flow rate of 2l.minute^{-1}, was used in combination with injected anaesthetics to provide a manageable level of anaesthesia that required less manipulation and restraint of the animal compared to an injected anaesthetic alone. An initial concentration of 3% isofluorane was used to initially anaesthetise the animal, which was reduced to 0.5% isofluorane to maintain anaesthesia. While isofluorane induced adequate anaesthesia, repeatable ABR recordings could not be obtained. This was because the prolonged exposure to the anaesthetic gas caused a decrease in ABR waveform amplitude until the waveform could no longer be recorded. Isofluorane has been reported to affect the ABR measurement in rats, producing an increase in waveform latency (Santarelli *et al.* 2003). These preliminary experiments demonstrated conclusively that isofluorane gas is not a suitable anaesthetic for this study.

Ketamine with xylazine: Many studies in which ABRs have been measured used a combination of ketamine and xylazine to give a suitable level of anaesthesia using both mice (Kwan *et al.* 2006, Ou *et al.* 2000) and rats (Kojima *et al.* 2007, Tan *et al.* 2007). Ketamine injection produces dissociative anaesthesia by blocking postsynaptic NMDA receptors for glutamate (Kohrs and Durieux 1998) resulting in analgesia and deep sedation (Green 1975). The co-application of xylazine results in muscle relaxation and sedation (Green 1975) through the action of xylazine on the α_2-adrenoceptors (Hsu 1981).

A mixture of 100mg.kg^{-1} ketamine (Vetalar, Pfizer Ltd, Sandwich, UK) and 10 mg.kg^{-1} xylazine (Rompun, Bayer PLC, Newbury, UK) was given via intrapertioneal injection (IP) and trialled in five rats. This anaesthetic protocol gave a suitable level of anaesthesia that allowed the recording of repeatable ABRs. However following the conclusion of the experiment, three rats did not recover well from the anaesthesia. Additionally, studies have shown that ketamine and xylazine administration can increase the ABR thresholds (van Looij *et al.* 2004) and waveform latencies (Church and Gritzke 1987). This was an undesirable outcome and so a different anaesthetic protocol was investigated.

Hypnorm with midazolam: Previous ABR studies using guinea pigs as the experimental animal (Etheridge 2002, Fergie 2005) have used a combination of fentanyl citrate and fluanisone (Hypnorm, VetaPharma Ltd, Leeds, UK) with midazolam (Hypnovel, Roche Products Ltd, Welwyn Garden City, UK) to generate anaesthesia through neuroleptanalgesia. Neuroleptanalgesia is generated by the application of a sedative analgesic with a potent tranquilliser that provides depression of local reflexes (Reed *et al.* 1971) and voluntary motor activity while leaving cortical functions as unaffected as possible (Aubry *et al.* 1966). Fentanyl is a synthetic derivative of the opiate morphine and thus has similar properties but is a much more potent analgesic, with an analgesic effect between 20 and 100 times greater than morphine (Green 1975). Fluanisone, a butyrophenone derivative, acts as a tranquillizer and potentiates the analgesia provided by fentanyl. While fentanyl can also cause profound respiratory depression, the co-application of fluanisone partially antagonises this respiratory depression

(Green 1975). Additionally, the combination of fluanisone with fentanyl has been shown to produce a prolonged anaesthetic state in rats (Inoue *et al.* 1994).

Midazolam is a benzodiazepine derivative that, unlike other benzodiazepines such as diazepam, is water soluble and so can be delivered with Hypnorm in the same injection. The sole application of midazolam has been shown not to produce anaesthesia (Pieri *et al.* 1981). However, the combination of midazolam with Hypnorm in rodents produces suitable anaesthesia with muscle relaxation (Flecknell and Mitchell 1984).

The anaesthetic was prepared by diluting equal volumes of Hypnorm and midazolam in an equivalent volume of sterile water and mixing together (i.e. one part Hypnorm to one part midazolam and diluted with two parts water). The resulting solution contained 0.08mg.kg^{-1} fentanyl and 2.5mg.kg^{-1} fluanisone with 1.25mg.kg^{-1} midazolam in a single injection. The solution was administered at 2.7ml.kg^{-1} and was delivered via IP injection. This regimen gave a desirable level of anaesthesia and allowed repeatable ABRs to be recorded. Supplementary top-up injections could also be given if the anaesthesia became too light without having an adverse effect on the recovery of the animal.

As a result the Hypnorm with midazolam regimen was used as the anaesthetising protocol in the current study.

Pre-anaesthetic preparation: Ten minutes prior to the administration of the anaesthetic, the rats were given 40 $\mu g.kg^{-1}$ atropine (atropine sulphate, Antigen Pharmaceuticals, Croyden, UK) subcutaneously to reduce salivary and bronchial secretions and thus help the animal breathe. Additionally, during the anaesthesia oxygen was delivered to the rat via a face mask (500ml flow rate). The body temperature of the rat was measured by rectal probe thermometer (K-type ATK-1319 thermometer with stainless steel probe, ATP Instrumentation Ltd, Ashby-de-la-Zouch, UK) and maintained between 35.9 and 37.5^{o}C by laying the rat on a heat pad. Ocular lubricating ointment (Lacri-lube, Allergan Ltd, Marlow, UK) was applied to the eyes of the animal to ensure that they remained moist. The rat was also supplemented with normal saline, given subcutaneously at hourly intervals, to maintain the fluid balance and prevent dehydration. The depth of anaesthesia was tested by monitoring the pedal withdrawal reflex when a hind paw was pinched. ABR and sound exposure experiments would only begin if the pedal withdrawal reflex was absent, indicating that the animal was deeply anaesthetised.

Recovery: During recovery from anaesthesia, the normal solid diet pellets were replaced with a liquid alternative (Complan; Complan Foods Ltd, London, UK) to avoid inhalation of solid food particles. Normal bedding in the recovery cage was replaced with a blanket of vetbed (Petlife International Ltd, Bury St Edmunds, UK), with the cage placed on a heat pad and under a heat lamp to maintain body temperature.

Tissue dissection

All animals were sacrificed using an IP injection of pentobarbital (20% pentobarbital sodium solution for euthanasia, J.M.Loveridge Ltd, Andover, UK) in accordance with UK Home Office Animals Act 1986 (schedule 1).

Cerebral cortex and cerebellum: The rats were decapitated and the skin on the back of the head was cut away revealing the cranium. The bone was carefully removed from the back of the skull, starting at the foramen magnum, i.e. where the spinal cord leaves the skull, to expose the cerebellum and cerebral cortex. An incision was made at the front of the temporal lobes, removing the meninges, detaching the olfactory bulb and optic nerves. The brain was carefully removed from the skull, cutting the cranial nerves as they became visible, and placed in a petri dish.

Dorsal root ganglion: An incision was made along the spine of the rat to reveal the spinal vertebrae. The vertebral bone and surrounding musculature were removed to reveal the spinal cord and dorsal root ganglia. The DRG were gently teased away to remove connective tissue, cut from the sensory nerves and removed from the carcass.

Cochlea: The rats were decapitated and the brain was removed as above. The temporal bones, containing the bulla, were removed. The thin bone of the bulla was carefully removed to expose the cochlea (Fig. 2.1). The stapes bone was removed from the oval window and, using a sharp pair of forceps, the membranes covering the oval and round windows were pierced. For removal of the modiolus, the bone forming the otic capsule was gently removed with either a sharp pair of forceps or a sterile hypodermic needle. Starting at the round and oval windows, the otic capsule was

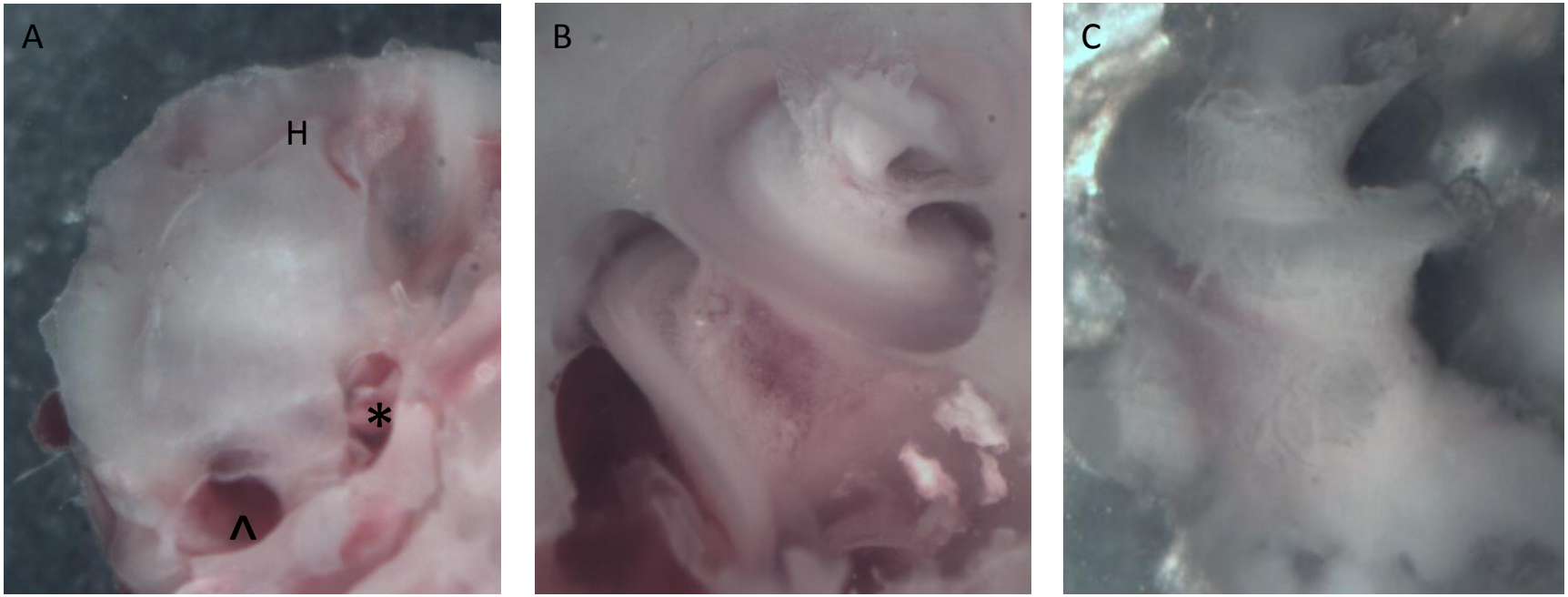

Fig. 2.1. Dissection of the modiolus. A) The bone forming the bulla was removed to reveal the cochlea, identified by the helicotrema (H), the oval window (*) and round window (^). B) The bone forming the otic capsule was carefully removed to reveal the modiolus. C) The modiolus was carefully removed from the remaining bone, ensuring that any remaining stria vascularis, basilar membrane, organ of Corti and auditory nerve was dissected away to limit contamination of the modiolar sample.

removed following the curve of the cochlea to the helicotrema, taking great care not to damage the modiolus. Once completely exposed, the modiolus was carefully removed from the remaining bone. Any residual stria vascularis, basilar membrane, auditory nerve or bone fragments were carefully removed to prevent contamination of modiolar sample by additional structures, such as the auditory hair cells.

Solutions for Immunohistochemistry

Unless otherwise stated, all chemicals and reagents were purchased from Sigma Aldrich (Gillingham, UK).

Phosphate buffered saline: Phosphate buffered saline (PBS) was used to wash the tissue sections between incubation steps. A stock solution of PBS was created using the following reagents in distilled water: 1.4M NaCl; 80mM Na_2HPO_4; 15mM KH_2PO_4; 27mM KCl. Before use this stock was diluted ten times, i.e. 100ml in a total volume of 1l, and the pH modified to 7.4 using 1M NaOH and 3M HCl, measured using a Jenway pH meter model 3310 (Bibby Scientific Limited, Stone, UK).

For the dilution of antibodies, both primary and secondary, PBS was supplemented with host specific sera. For example, when using secondary antibodies generated in goats, normal goat serum was added to PBS at a final volume of 10%. Similarly for permeabilization of the sections, the detergent Triton X-100 was added to the 10% goat serum PBS at a final volume of 0.5%.

Tissue fixation: To ensure that the morphology and antigenicity of the tissue sections was retained, the tissues were fixed in a preserving solution containing 2% paraformaldehyde (PFA). To create 400ml of 2% PFA solution the following method was used: add 8g PFA to 160ml of 0.2M Na_2HPO_4 solution and heat until dissolved; once dissolved, allow the solution to cool to room temperature; add 40ml of 0.2M NaH_2PO_4 followed by 200ml of distilled water.

Chapter 3. Characterisation of voltage-gated sodium channel expression of spiral ganglion neurons from normal animals

Introduction

As considered previously, voltage-gated Na^+ channels are essential for rapid depolarization of neuronal membranes and the generation and propagation of action potentials. In comparison to other sensory systems, relatively little is known about the voltage-gated Na^+ channel isoforms present in the SGN. Only one recent study has investigated the voltage-gated Na^+ channel expression in mouse SGN, identifying $Na_V1.6$ expression in the SGN and $Na_V1.2$ in the efferent processes innervating the inner and outer hair cells using immunocytochemical methods (Hossain *et al.* 2005). However, it was unclear whether the presence of all subtypes was analysed by these authors.

This chapter investigated the voltage-gated Na^+ channel expression in rat SGN at the RNA expression level, using RT-PCR and a panel of voltage-gated Na^+ channel isoform specific primer pairs. Identification of the voltage-gated Na^+ channel proteins will then be investigated using immunohistochemical methods and subtype specific voltage-gated Na^+ channel antibodies tagged with fluorescent and non-fluorescent markers. This allowed both the expression and the cellular localization of the voltage-gated Na^+ channel proteins along the SGN to be characterised.

Experimental methods

Unless otherwise stated, all chemicals and reagents were purchased from Sigma Aldrich (Gillingham, UK).

RT-PCR

RT-PCR general description: The reverse transcription polymerase chain reaction (RT-PCR) is a technique that enables the identification of mRNA expressed in individual specimens. This is accomplished by first isolating the RNA and reverse transcribing it into complimentary (c)DNA using a reverse transcriptase enzyme. This ensures that only the genes that have been transcribed into RNA, and hence those most likely to be translated into proteins, will be investigated instead of the entire genomic DNA of the specimen. The cDNA is probed using oligonucleotide primers and amplified using a thermal cycler machine and polymerase enzymes. The primers are designed to bind complimentarily to a unique nucleotide sequence of the target gene, to ensure the amplification of the gene of interest. As DNA is double stranded, the primers are designed to work in pairs that bind to specific complimentary nucleotide sequences on the forward and reverse oriented DNA strands.

The double stranded cDNA is first denatured and split into single strands by exposure to high temperature (Fig. 3.1). The reaction is cooled to allow the primers to anneal to the single stranded cDNA, forming a short region of double stranded DNA. The reaction temperature is then raised to allow this short region to be extended by a DNA polymerase enzyme (Kubista *et al.* 2006). This sequence of denaturing, annealing and extension is repeated to ensure that the PCR products can be detected, with around

35 cycles typically required for this purpose. The PCR products are then identified by size through electrophoresis. The PCR products and DNA standards ladder are loaded into an agarose gel containing ethidium bromide. Ethidium bromide allows for the identification of the PCR products as bands in the gel as it fluoresces orange when bound with DNA and exposed to ultraviolet illumination. The size of the PCR products is dependent on the number of nucleotide bases between the forward and reverse primer, and is calculated during the primer pair design.

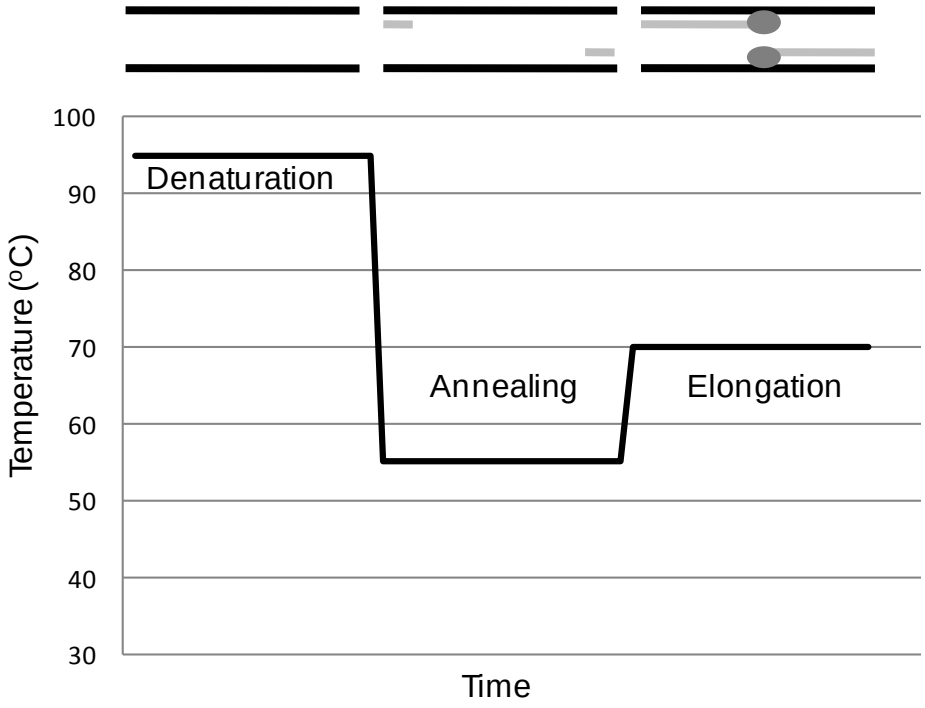

Fig. 3.1. Graphical representation of the PCR temperature cycle. 1) The temperature is raised to around 95°C to separate the double stranded DNA (top row, black lines), (2) the temperature is lowered to allow the primers to anneal (gray lines), (3) the temperature is raised to let the polymerase extend the primers (gray ovals). Adapted from Kubista *et al*. (2006).

Preparation: Several precautions were taken to ensure that the samples were not contaminated by exogenous RNase. All dissection equipment was rinsed in RNase AWAY™ (Invitrogen, Paisley, UK) before being autoclaved. Sterile scalpel blades and

petri dishes were also used. Bench top surfaces were cleaned using ethanol followed by RNase AWAY^{TM}.

Tissue extraction: Male Wistar rats (250-400g) were sacrificed using an IP injection of pentobarbital (20% pentobarbital sodium solution for euthanasia, J.M.Loveridge Ltd, Andover, UK) in accordance with UK Home Office Animals Act (1986) Schedule 1. The dorsal root ganglia (DRG) and cerebral cortex were rapidly excised and frozen over dry ice in a sterile RNase/DNase free tube. The temporal bones were extracted and excess bone was removed to leave the bony inner ear segment that contained the cochlea. The otic capsule of the cochlea was removed to reveal the modiolus, which was then carefully removed from the remaining bone and frozen over dry ice as above. For more details on the tissue extraction techniques please refer to Chapter 2.

RNA isolation and cDNA synthesis: Two modioli, from the left and right ear of one animal, six DRGs and 35 mg of cerebral cortex were pooled for each tissue sample. The total RNA was isolated from the samples using the RNeasy mini kit (QIAGEN, Crawley, UK). First, the tissues were homogenised separately in lysis buffer (Buffer RLT), containing guanidinium isothiocyanate (GITC) and β-mercaptoethanol, using a pestle and mortar and then centrifuged in a QIAshredder (QIAGEN). The GITC containing buffer was used to secure the purification of intact RNA by denaturing any residual RNase enzymes in the sample. Ethanol was added to the sample to provide appropriate binding conditions before applying the sample to an RNeasy mini spin column, where the total RNA bound to the membrane and contaminants were washed away (Buffer RW1, containing GITC and ethanol; Buffer RPE, containing ethanol). The

RNA was eluted in RNase free water and any remaining DNA was removed using DNase I (Invitrogen). The total RNA was reverse transcribed to cDNA using SuperScript^{TM} III Reverse Transcriptase (Invitrogen) The cDNA was stored at -80^{o}C until use.

PCR reaction: The PCR reaction was performed using BIOTAQ DNA polymerase (Bioline, London, UK), custom designed sense and antisense primers at a final concentration of 0.5µM (Sigma Genosys, Cambridge, UK) and 1µl of cDNA using a T-Gradient Biometra thermocycler (Biotron, Göttingen, Germany). The temperature was raised to 94^{o}C for 5 minutes to denature the sample, followed by thirty-five PCR cycles where the temperature was held at 94^{o}C for 45 seconds, then reduced to between 54 and 59^{o}C for 45 seconds to anneal the primers and cDNA followed by an increase to 72^{o}C for 1 minute for elongation (Fig. 3.1). The PCR products were sorted by electrophoresis using a 1% agarose gel with ethidium bromide and a 100 base pair DNA ladder (Promega, Southampton, UK) at 110V. The gel was photographed under ultraviolet illumination using a digital camera and Kodak digital science 1D software (Kodak). The RNA isolation, cDNA synthesis and PCR reaction was repeated four times, using tissue from a different rat each time.

Primer design: Primer pairs specific to the voltage-gated Na^{+} channel α-subunits under investigation and to β-actin used were either designed specifically or adapted from other published studies (Dib-Hajj *et al.* 1998, Dib-Hajj *et al.* 1998, Raff *et al.* 1997, Wooltorton *et al.* 2007) and are summarised in Table 3.1. The primer pairs were designed to cross intron-exon boundaries as determined from the rat sequences. This

Gene	Subunit	Forward primer 5'-3'	Reverse primer 5'-3'	Predicted band size (bp)	Annealing temperature (°C)
Scn1a	$Na_V1.1$	GCGTGCTGCCGGGAAAACATAC	ACGTCCTTCGCTCGCCCTCTGA	576	59
Scn2a	$Na_V1.2$	CGTCCGCAGAATCCAGAGA	CTTGAAGGGTCTTCCAACAAGTC	705	58
Scn3a	$Na_V1.3$	AGGGAAGGATTGACTTGCC	TGGACCTCTCCTTAGAGTCCA	295	58
Scn8a	$Na_V1.6$	AAGTGGACAGCCTACGGC	TTGTTGACAATATCGATTTCGAACCG	364	58
Scn9a	$Na_V1.7$	GACGACAGCGGCACGACTAAT	AGCTGCGAAGATCCCTGTAAAGA	402	54
Scn10a	$Na_V1.8$	GATCCGTGGAACTGGCTGGA	GAGGAATGCCCACGCAAAGGAATC	482	58
Scn11a	$Na_V1.9$	CCCTGCTGCGCTCGGTGAAGAA	GACAAAGTAGATCCCAGAGG	395	58
Actb	B-actin	TACAACCTCCTTGCAGCTCC	GGATCTTCATGAGGTAGTCTGTC	630	59

Table 3.1. PCR Primers. Primers were either designed or modified from others previously published. $Na_V1.2$, $Na_V1.3$, $Na_V1.6$ (Wooltorton *et al.*, 2007); $Na_V1.8$ (Dib-Hajj *et al.*, 1998a); $Na_V1.9$ (Dib-Hajj *et al.*, 1998b); β- actin (Raff *et al.*, 1997).

would show any genomic DNA contamination of the PCR products as a higher base pair size band than the calculated band. The identity of PCR products was confirmed by sequencing.

Immunohistochemistry

Immunohistochemistry general description: Immunohistochemistry allows the expression and cellular distribution of proteins to be characterised in prepared tissue sections. This is accomplished by using primary antibodies that specifically recognise epitopes on the target protein and the subsequent detection of the bound antibody-antigen complex. Detection is achieved through the use of secondary antibodies that are either conjugated with a fluorescent marker or an enzyme label, the latter of which produces an insoluble reaction product at the site of antibody-antigen interaction. The fluorescent tags or insoluble reaction products are observed using microscopy.

Cochlea extraction: Adult male Wistar rats (250-400g) were sacrificed using Euthanal® (20% pentobarbital sodium solution for euthanasia, J.M.Loveridge Ltd) (IP) in accordance with UK Home Office Animals Act (1986), under Schedule 1. The temporal bones were dissected and excess bone was removed to leave the bony inner ear segment that contained the cochlea. The cochleae were placed in 2% paraformaldehyde solution for 30 minutes. The cochleae were washed (1x15 minutes) in PBS then demineralised in 8% EDTA in PBS until soft enough to be cut by the cryostat blade (4 to 10 days at 4^{o}C). To ensure the morphology of the cochleae was preserved during sectioning, the cochleae were placed in PBS with 30% sucrose

overnight at 4^{o}C followed by Tissue Tek optimal cutting temperature (OCT) compound (Bayer diagnostics, Newbury, UK) overnight at 4^{o}C (Cho *et al.* 2004). The fixed, demineralised cochleae were quickly frozen in Tissue Tek OCT over dry ice/hexane and stored at -20^{o}C. Frozen 10μm sections were cut from the tissue blocks using a cryostat (Bright Instrument Company Ltd, Huntingdon, UK) and melted onto Polysine^{TM} slides (VWR International, Lutterworth, UK). The sections were circumscribed with an ImmEdge pen (Vector Laboratories, Burlingame, CA, USA), providing a hydrophobic barrier that contained the reagents within a defined area thus reducing the volume required. Tissue sections were air dried and either stored at -20^{o}C until use or used directly for immunohistochemistry. Slides were washed in PBS for 15 minutes prior to pre-incubation in blocking solution.

Brain extraction and preparation: Adult male Wistar rats (250-400g) were sacrificed as above, decapitated and the whole brain removed as described in Chapter 2. A disposable mould (Peel-a-way plastic embedding mould, Polysciences Inc, Warrington, PA, USA) was half filled with Tissue Tek OCT before the whole brain was placed in the mould and filled with enough Tissue Tek OCT to cover the brain completely. The filled mould was then placed in dry ice with hexane to quickly freeze the tissue and stored at -20^{o}C. Frozen 20μm sections were cut from the tissue blocks and melted onto Polysine^{TM} slides. The sections were circumscribed with an ImmEdge pen and prepared as above. Prior to the first incubation step, the sections were fixed in 2% paraformaldehyde for 10 minutes and washed in PBS (1x15 minutes).

DRG extraction and preparation: DRG from adult male Wistar rats (250-400g) were dissected as described in Chapter 2. Each extracted DRG was placed in a suitable mould containing Tissue Tek OCT and frozen over dry ice with hexane. Frozen 10µm sections were cut from the tissue blocks, melted onto Polysine^{TM} slides and prepared in an identical manner as the brain sections.

Antibody information: Information about the primary and secondary antibodies used in this study is presented in Table 3.2.

Antibody	Host	Dilution	Supplier	Product code
Anti-$Na_V1.1$	Rabbit	1:200	Alomone labs	ASC-001
Anti-$Na_V1.2$	Rabbit	1:200	Alomone labs	ASC-002
Anti-$Na_V1.6$	Rabbit	1:200	Alomone labs	ASC-009
Anti-$Na_V1.7$	Rabbit	1:200	Alomone labs	ASC-008
Anti-$Na_V1.8$	Rabbit	1:200	GSK	K109
Anti-$Na_V1.9$	Rabbit	1:200	GSK	R186
Anti-Peripherin	Mouse	1:100	Millipore	MAB1527
Anti-rabbit/FITC	Goat	1:400	Jackson ImmunoResearch	111-095-144
Anti-mouse/Texas red	Goat	1:400	Jackson ImmunoResearch	115-075-146
Anti-rabbit/Biotin	Swine	1:350	DAKO	E0353

Table 3.2. Immunohistochemistry antibodies. Details of the antibodies used in the study. Entries with / indicates a conjugation, i.e. anti-rabbit/biotin means anti-rabbit conjugated with biotin. Antibodies diluted in either 10% goat serum PBS for fluorescence immunohistochemistry or 10% swine serum PBS for non-fluorescence immunohistochemistry.

Fluorescent probe staining: For detection of Na^+ channel subtypes, the slides were incubated in the following: (1) blocking solution of PBS containing 10% goat serum, supplemented with 0.5% Triton X-100 for 30 minutes at room temperature; (2) sodium channel subtype specific primary polyclonal antibodies raised in rabbit diluted in blocking solution and incubated overnight at 4^oC; (3) goat anti-rabbit IgG conjugated with fluorescein isothiocyanate (FITC) for 2 hours at room temperature. The incubations were performed in a humidified incubation box to ensure that the sections did not dry out. Between each incubation step, the sections were thoroughly washed with PBS. Sections were then mounted with Citifluor AF1 mountant (UKC Chem. Lab, Kent, UK).

Control experiments were carried out to determine the amount of non-specific binding by omitting the primary antiserum from the incubation media. Where control peptides were available, pre-incubation of primary antibody with the control peptide overnight reduced the labelling to background levels (data not shown). Control peptides for the antibodies against $Na_V1.8$ and $Na_V1.9$ were not available.

For identification of Type II SG neurons, experiments were carried out using an anti-peripherin monoclonal antibody MAB 1527 raised in mouse (Millipore, Watford, UK) as this protein is known to be selectively expressed in Type II SG neurons (Hafidi 1998, Reid *et al.* 2004, Mou *et al.* 1998). Immunostaining was visualised with goat anti-mouse secondary antibodies conjugated with Texas Red (Jackson ImmunoResearch).

The sections were viewed using a Nikon Labophot 2A microscope equipped for epifluorescense imaging and photography, with a monochromatic CCD camera, frame grabber card and software (Scion Image^{TM}). Photography of tissue sections was carried out with the appropriate filters for FITC or Texas Red.

Scion ImageTM (Scion Corporation, Frederick, Maryland USA) was used to measure the cell body area and average fluorescence of the neurons from the epifluorescent images. Only neurons that showed an unlabelled nucleus and an intact cell body were measured. The fluorescence scale ranged from: 0= black; 255= white. Unless otherwise stated, this scale is used throughout the results and discussion sections.

Non-fluorescence DAB/HRP staining: For non-fluorescence detection of Na^+ channel subtypes, the tissue sections were incubated sequentially in the following solutions: (1) 0.2% hydrogen peroxide in methanol for 15 minutes; (2) blocking solution of PBS containing 10% swine serum, supplemented with 0.5% Triton X-100 for 30 minutes at room temperature; (3) anti-rabbit polyclonal antibodies as described above, overnight at 4^{o}C; (5) swine anti-rabbit biotin conjugated IgG, diluted with 10% swine serum in PBS for 35 minutes at room temperature (DAKO, Ely, UK); (6) streptavidin-horseradish peroxidase (HRP) conjugate prediluted for 30 minutes at room temperature (DAKO); (7) 3, 3'-diaminobenzidine solution (DAB substrate kit, DAKO) for 4 minutes at room temperature; (8) 70% IMS for 5 minutes followed by 100% IMS for 5 minutes and 100% xylene twice for 5 minutes. Steps 2 to 6 were performed in a humidified incubation box to ensure that the sections did not dry out. Between steps 1 and 8 the

tissue sections were thoroughly washed with PBS. Sections were mounted using DPX (RA Lamb, Eastbourne, UK).

The slides were examined using a light microscope (PriorLux, Prior Scientific Instruments Ltd, Cambridge, UK) equipped with a Moticam 2300 digital camera (Motic Instruments, Richmond, Canada) and images were captured using Motic Images Plus 2.0 (Motic Instruments). ImageJ (National Institute of Mental Health, Maryland, USA) was used to measure the cell body area and mean grey value of the neurons from the non-fluorescence images, with the grey value scale defined as: 0= black; 255= white.

Data analysis

Statistical analysis was carried out with data entered into a Microsoft Office Excel 2007 spreadsheet. Comparison of different data groups was performed using the two-tailed Students t-test. Results are expressed as means ± SEM and the significance level was set at $p \leq 0.05$ in all experiments.

Results

Voltage-gated Na^+ channel alpha subunit expression using RT-PCR

Validation of primer specificity in rat cerebral cortex and DRG: To confirm the specificity of the primers used, tissues with previously documented voltage-gated Na^+ channel α-subunit expression were utilised. Strong bands at the correct predicted sizes were observed for $Na_V1.1$, $Na_V1.2$, $Na_V1.3$ and $Na_V1.6$ in the cerebral cortex, with weak bands present for $Na_V1.7$ and $Na_V1.9$ (Fig. 3.2A). Using RNA isolated from rat DRG, intense bands were seen for $Na_V1.1$, $Na_V1.7$, $Na_V1.8$ and $Na_V1.9$ while a weak band was observed for $Na_V1.6$ (Fig. 3.2B).

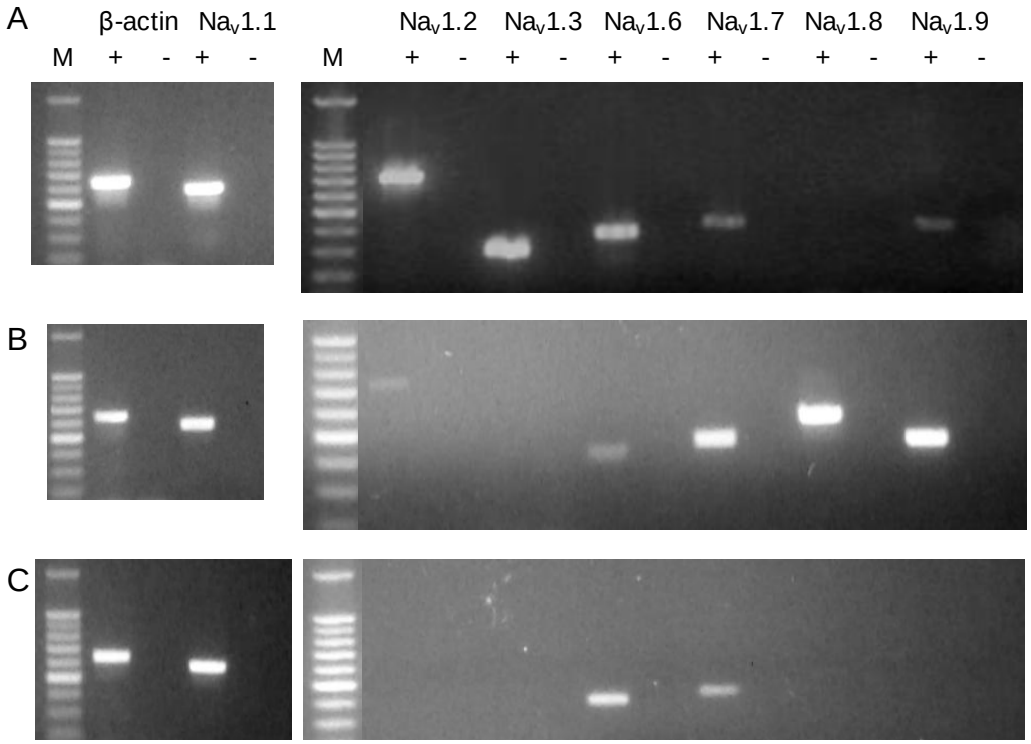

Fig. 3.2. Voltage-gated Na^+ channel mRNA expression in adult rat nervous tissues. PCR products were separated by electrophoresis on a 1% agarose gel stained with ethidium bromide. (A) PCR products were detected for $Na_V1.1$, $Na_V1.2$, $Na_V1.3$ and $Na_V1.6$ in the rat cerebral cortex, with weak bands for $Na_V1.7$ and $Na_V1.9$. (B) PCR products were detected for $Na_V1.1$, $Na_V1.6$, $Na_V1.7$, $Na_V1.8$ and $Na_V1.9$ in the rat DRG. (C) PCR products were detected for $Na_V1.1$, $Na_V1.6$ and $Na_V1.7$ in the rat SGN. All tissues were positive for β-actin. (M) Marker lane, 100bp ladder with brightest band representing 500bp. Expected product sizes are given in methods section. PCR was performed either in the presence (+) or absence (-) of reverse transcription.

Rat spiral ganglion: The RT-PCR primers specific for the voltage-gated Na^+ channel α-subunits and β-actin were used to probe the cDNA created from RNA isolated from rat modioli homogenates. Distinct bands at the correct predicted base pair sizes were observed for $Na_V1.1$, $Na_V1.6$ and $Na_V1.7$, as well as the control gene β-actin (Fig. 3.2C). No bands were seen in the lane without reverse transcription, showing that there was no genomic DNA contamination.

Immunocytochemical localization of voltage-gated Na^+ channel alpha subunits in spiral ganglion neurons

$Na_V1.7$: The $Na_V1.7$ antibody strongly labelled the cell bodies of rat SGN using fluorescently tagged secondary antibodies (Figs. 3.3A and B). Labelling was found throughout the cytoplasm of the cell body, with no clear differentiation between membrane and cytoplasmic labelling. Variation was observed in the intensity of labelling, with some neurons strongly labelled and others only faintly labelled (Fig. 3.3B).

When observed through the microscope eyepiece, sections of rat cochlea incubated without the primary antibody the bright green FITC labelling was not observed. Pale yellow puncta were noted throughout the cytoplasm (Fig. 3.3C) that was distinct from the vivid green FITC labelling in the sections incubated with the $Na_V1.7$ antibody. As a monochrome camera was used to capture the microscope images, the distinction between FITC and non-specific fluorescence was lost, and would have been indistinguishable if a standard false-colour look-up table was used.

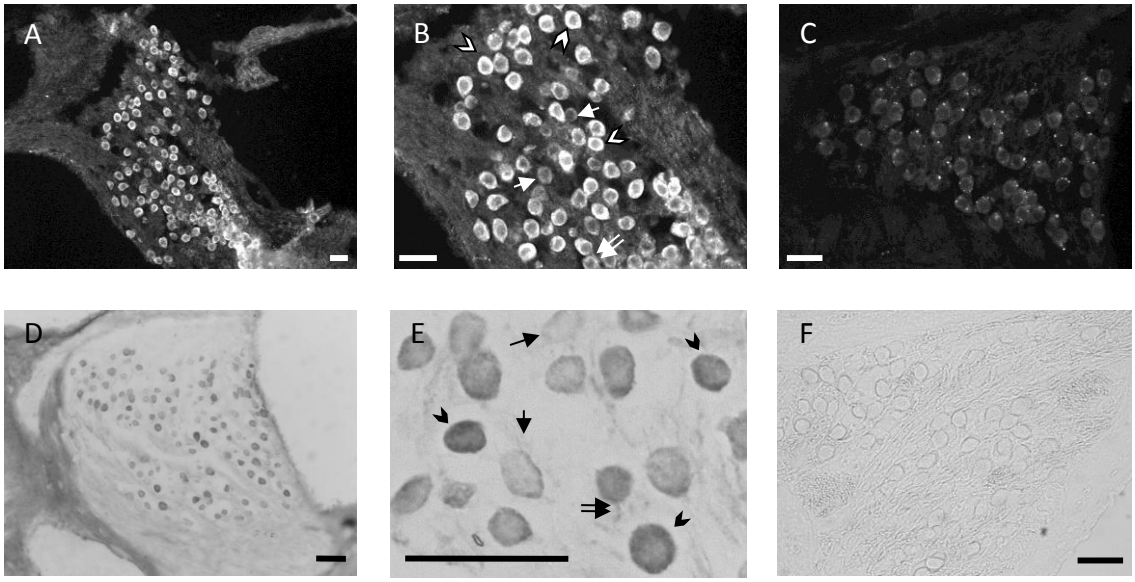

Fig. 3.3. Distribution of $Na_V1.7$ in rat SGN. Micrographs showing $Na_V1.7$ labelling in the rat SGN using fluorescent (A,B) and non-fluorescent (D,E). Both techniques show positive labelling of the neurons although some appear to be less intensely stained (arrow) than others (arrowhead), with staining of the axon observed (double arrows). Labelling of the SGN membrane can be observed in the less intensely labelled neurons (arrows in E). (C) Micrograph showing rat SGN incubated without the primary antibody. (F) Phase contrast micrograph of HRP-DAB labelled SGN incubated without the primary antibody. Scale bars= 30μm for all images.

This punctate labelling was hypothesised to be due to non-specific fluorescence, since similar non-specific labelling has previously been reported when fluorescent methods are used (Samorajski *et al.* 1968, Sans *et al.* 1996). The experiments were repeated using the same $Na_V1.7$ antibody but using a non-fluorescent visualisation method, with streptavidin/horseradish peroxidase (HRP) and DAB to visualise the primary antibody binding. Using this method, the SGN were positively labelled with the dark insoluble reaction product as seen in Figs. 3.3D and E. The positively labelled SGN cell bodies showed variation in staining intensity, similar in appearance to that observed in the fluorescently labelled sections. The less intensely stained neurons showed some evidence of positive staining of their membrane (Fig. 3.3E). Staining of the axon initial segment was also seen (Fig. 3.3E). The sections of rat cochlea incubated without the

primary antibody had no neurons labelled with the reaction product, nor was the punctate labelling observed in the previous controls present when using fluorescently tagged antibodies (Fig. 3.3F). This confirmed that the puncta could be considered as tissue autofluorescence.

$Na_V1.6$: The $Na_V1.6$ antibody strongly labelled the cell bodies of rat SGN (Fig. 3.4A and B). The pattern of distribution was similar to that seen with the $Na_V1.7$ antibody. Labelling was found throughout the cytoplasm of the cell body, with no clear differentiation between membrane and cytoplasmic labelling. There was again considerable variation observed in the intensity of neuronal labelling as seen in Fig. 3.4B. In contrast to the labelling seen with $Na_V1.7$, peripheral and central processes were also strongly labelled for $Na_V1.6$ α-subunits.

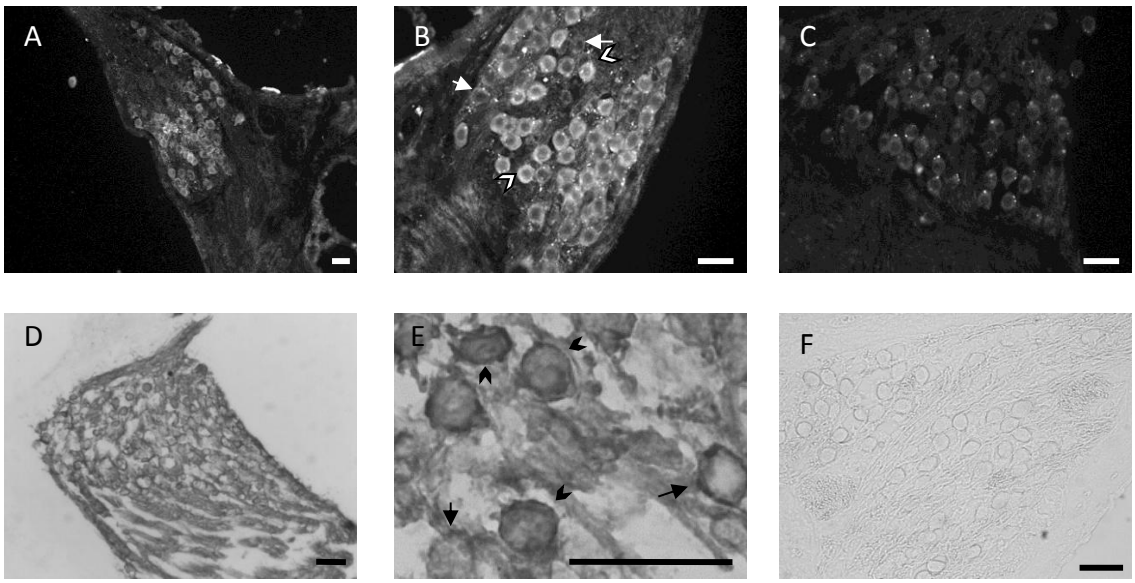

Fig. 3.4. Distribution of $Na_V1.6$ in rat SGN. Micrographs showing $Na_V1.6$ labelling in the rat SGN using fluorescent (A,B) and non-fluorescent (D,E) immunocytochemistry. Both techniques show positive labelling of the neurons although some appear to be less intensely stained (arrow) than others (arrowhead). (C) Micrograph showing rat SGN incubated without the primary antibody. (F) Phase contrast micrograph of HRP-DAB labelled SGN incubated without the primary antibody. Scale bars= 30µm for all images.

As performed previously, the positive FITC labelling was absent in sections of rat cochlea incubated without the primary, although pale yellow puncta were observed throughout the cytoplasm as were also seen for $Na_V1.7$ (Fig. 3.4C). As for $Na_V1.7$, this punctate labelling was demonstrated as non specific autofluorescence by using the HRP/DAB method to non-fluorescently visualise the primary antibody-antigen complex. The SGN were positively stained for $Na_V1.6$ with the insoluble reaction product using this method as seen in Figs. 3.4D and E. Again, positively labelled SGN cell bodies showed variation in staining intensity similar in appearance to that seen with fluorescence imaging. The distinct staining of the neuronal processes was replicated and, in addition, staining of the cell body membranes was observed (Fig. 3.4E). Sections of rat cochlea incubated without the primary antibody did not show neurons labelled with the reaction product nor the punctate labelling observed in the previous fluorescence controls (Fig. 3.4F).

$Na_V1.1$: The $Na_V1.1$ antibody weakly stained the SG neurons and was only detectable using the non-fluorescent HRP/DAB method as seen in Fig. 3.5. Using the fluorescence visualization method, the sections incubated with the $Na_V1.1$ antibody showed non-specific staining (Fig. 3.5A and B), similar to the staining seen in the control without primary antibody (Fig. 3.5C). Weak staining was observed in the SGN cell bodies while darker staining was seen in the neuronal processes, specifically in the central processes (axons), using the non-fluorescence staining method (Fig. 3.5D and E). In the sections of rat cochlea incubated without the primary antibody neurons were not labelled (Fig. 3.5F).

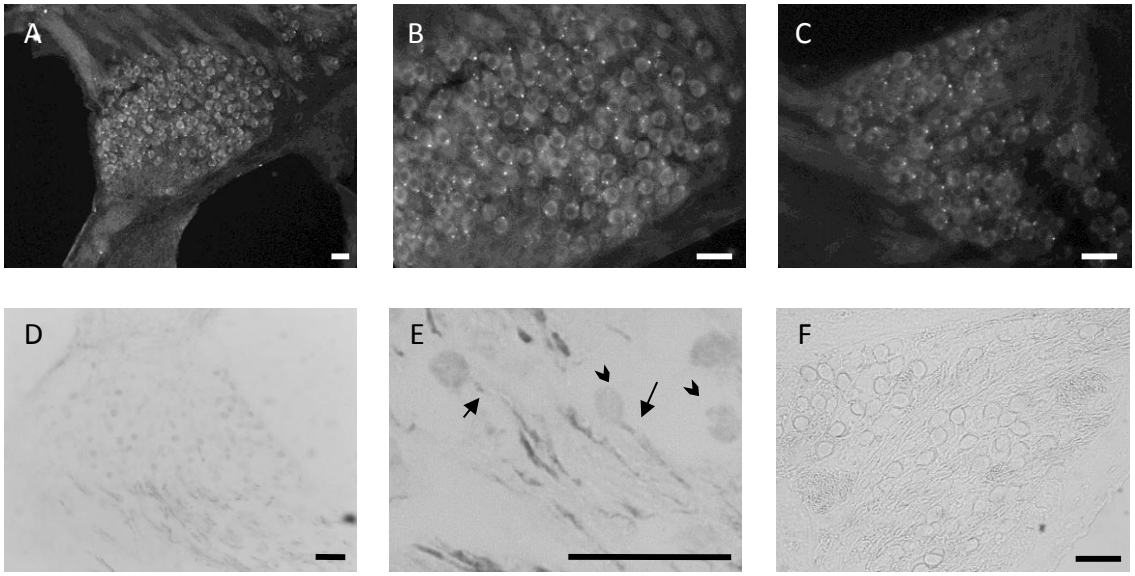

Fig. 3.5. Distribution of $Na_V1.1$ in rat SGN. Micrographs showing $Na_V1.1$ labelling in the rat SGN using fluorescent (A,B) and non-fluorescent (D,E) immunocytochemistry. (A,B) True labelling cannot be identified due to background fluorescence as seen in section with the primary antibody omitted (C). (D, E) Faint labelling of the SGN cell bodies was observed (arrowhead) while the axons were more intensely labelled (arrow) when the non-fluorescence approach was adopted. (F) Phase contrast micrograph showing HRP-DAB labelled SGN incubated without the primary antibody. Scale bars= 30µm for all images.

Other voltage-gated Na^+ channel isoforms: The $Na_V1.2$ antibody did not yield specific staining of the SGN cell bodies or processes (Figs. 3.6A and B), showing similar staining observed in the control without primary antibody (Fig. 3.6C). Staining in cochlear sections incubated with $Na_V1.8$ antibodies showed no specific staining in the SGN cell bodies (Figs. 3.7A and D), which was similar to the staining observed with the sections incubated with $Na_V1.9$ antibodies (Figs. 3.7B and E). Both staining patterns were similar to the staining observed in the control sections incubated without the primary antibodies (Figs. 3.7C and F).

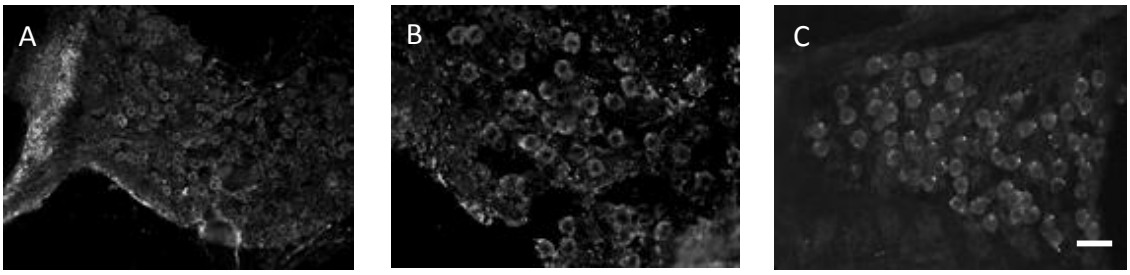

Fig. 3.6. Sections of rat SGN incubated with anti-$Na_V1.2$. Micrographs showing rat SGN (A-B) sections incubated with $Na_V1.2$ antibodies. The sections did not show specific labelling of the neurons, displaying a similar pattern of fluorescence as seen in the control sections taken from the same cochlea (C). Scale bar: A= 60µm B, C= 30µm.

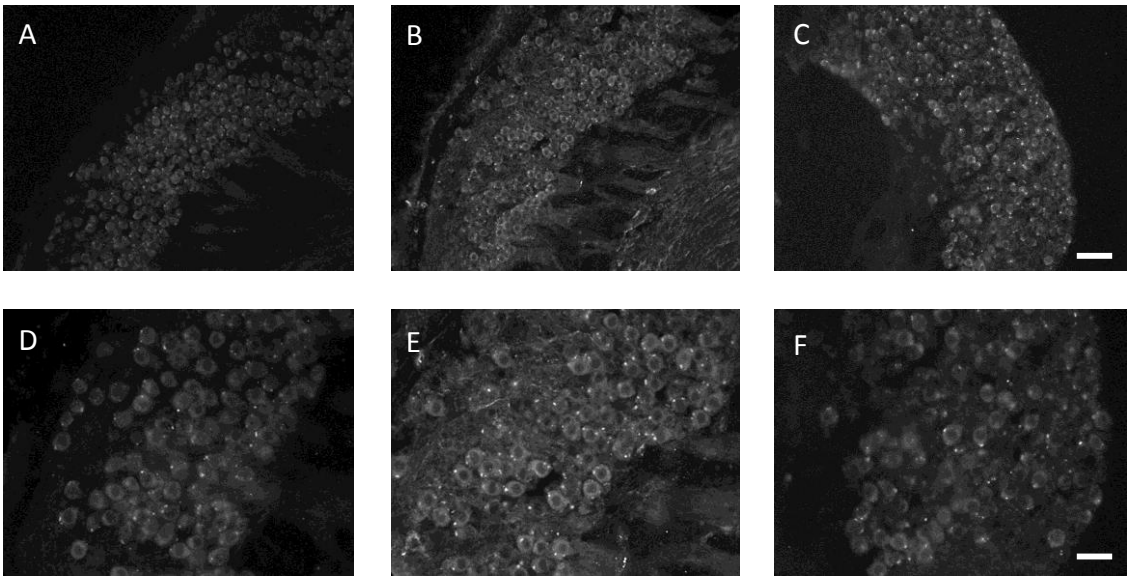

Fig. 3.7. Rat SGN incubated with $Na_V1.8$ and $Na_V1.9$ antibodies. Micrographs showing rat SGN sections incubated with $Na_V1.8$ antibodies (A,D) and $Na_V1.9$ antibodies (B,E). The SGN sections did not show specific labelling of the neurons, displaying a similar pattern of fluorescence as seen in the control sections incubated without the primary antibodies (C and F). Scale bar: A-C= 60µm D-F= 30µm.

Peripherin labelling of spiral ganglion neurons

It has been previously reported that antibodies generated against the intermediate filament protein peripherin, a marker of unmyelinated somatosensory neurons, also preferentially labels Type II SGN in sections of cochlea (Hafidi 1998, Reid *et al.* 2004, Mou *et al.* 1998). A small proportion (33/242 or ≈ 14%) of SGNs was labelled by this

antibody. Most noticeably, all the labelled neurons appeared to be smaller compared to the unlabelled neurons (Fig. 3.8A).

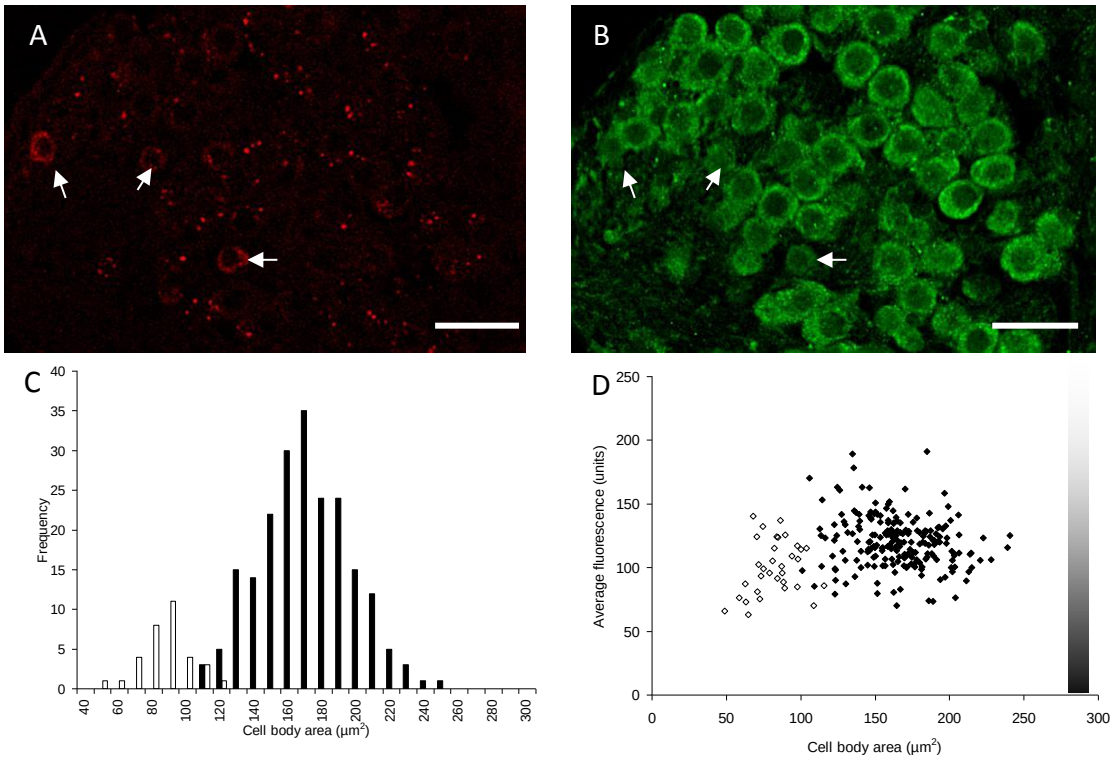

Fig. 3.8. Dual labelling of rat SGN with $Na_V1.7$ and Peripherin. Micrographs showing peripherin (A) and $Na_V1.7$ (B) labelling in the rat SGN. The neurons that are labelled for peripherin appear to have stained weakly for $Na_V1.7$ (arrows point to the position of peripherin positive neurons). Frequency histogram showing the distribution of spiral ganglion cell body areas (C), with a scatter plot of neuronal cell body area versus fluorescent labelling for $Na_V1.7$ (D), showing that the peripherin positive neurons (clear bars/symbols) have smaller cell body area and label less intensely for $Na_V1.7$ than the peripherin negative neurons (filled bars/symbols). Scale bars=30µm. Graduated bar on graphs indicates fluorescence scale (0=black, 255=white).

Peripherin labelling and $Na_V1.7$: The relationship between cell body area and peripherin labelling status was investigated further by dual labelling sections of cochlea with peripherin and $Na_V1.7$ antibodies. This was performed using sections from four cochleae (Fig. 3.8A and B). The frequency histogram of cell body area in Fig. 3.8C shows that distribution in peripherin positive neurons was distinctly separate from that of peripherin negative neurons. The mean difference in peripherin negative

and positive cell body areas was significantly different, 165.3±1.8μm^2 (n=209) and 82.2±2.6μm^2 (n=33) respectively ($p<0.0001$). This represents about a two-fold difference in cell body area.

On visual inspection of the sections it appeared that the peripherin positive neurons were labelled less intensely by the $Na_V1.7$ antibody than the peripherin negative neurons. To investigate the relationship between peripherin and density of $Na_V1.7$ labelling further, the average fluorescence intensity of the neurons labelled with the $Na_V1.7$ antibody was measured in peripherin negative and positive neurons from four cochleae.

The mean $Na_V1.7$ fluorescence was significantly different between the peripherin negative and positive neurons, 120.1±1.4 and 100.2±3.7 respectively ($p<0.01$). This confirmed the impression of differences in staining intensity between the two groups. Combination with the previous data in a scatter plot of cell body area versus average fluorescence in Fig. 3.8D, further illustrates that peripherin negative neurons possess larger cell body areas and label more strongly with $Na_V1.7$ antibody.

Peripherin labelling and $Na_V1.6$: An identical set of dual labelling experiments to those with $Na_V1.7$ were performed, using peripherin and $Na_V1.6$ antibodies with sections from the same rat cochleae that were used previously. Similar initial observations and results with regards to antibody staining, cell body area and fluorescence intensity were made as shown in Fig. 3.9. With the $Na_V1.6$ antibody the difference in distribution and means of cell body area between peripherin negative and positive

neurons was more marked than for $Na_V1.7$. The mean cell body areas were significantly different, with means of 185.7±2.2µm^2 (n=203) and 74.8±3.2µm^2 (n=34) respectively (p <0.001) or about a 2.5 fold difference in cell body area (Fig. 3.9C).

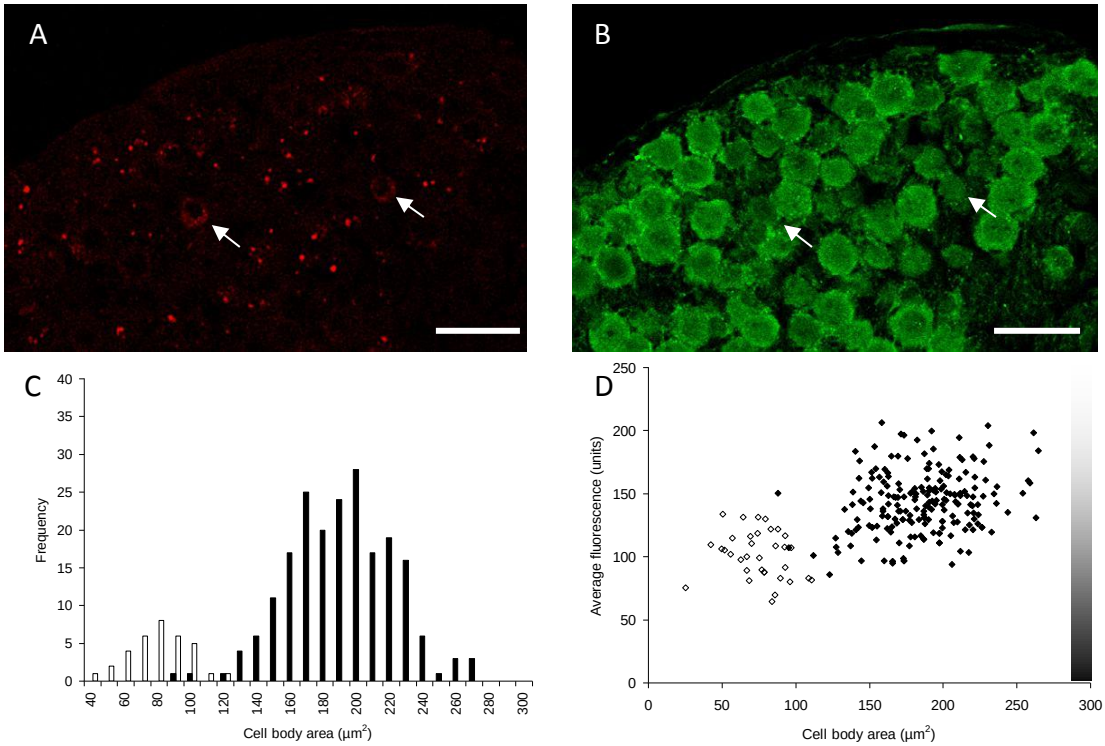

Fig. 3.9. Dual distribution of $Na_V1.6$ and Peripherin in the rat SGN. Micrographs showing peripherin (A) and $Na_V1.6$ (B) labelling in the rat SGN. The neurons that are labelled for peripherin appear to have stained weakly for $Na_V1.6$ (arrows point to the position of peripherin positive neurons). Frequency histograms showing the distribution of spiral ganglion cell body areas (C), with a scatter plot of neuronal cell body area versus fluorescent labelling for $Na_V1.6$ (D), showing that the peripherin positive neurons (clear bars/symbols) have smaller cell body area and label less intensely for $Na_V1.6$ than the peripherin negative neurons (filled bars/symbols). Scale bars=30µm. Graduated bar on graphs indicates fluorescence scale (0=black, 255=white).

On visual inspection, the peripherin positive neurons were again less intensely stained for $Na_V1.6$ than the peripherin negative neurons. Differences in mean $Na_V1.6$ fluorescence between the negative and positive stained peripherin neurons were also significant, 142.6±1.7 (n=203) and 101.6±3.2 (n=34) respectively (p <0.001). Further illustration of the difference between peripherin negative and positive neurons

labelled with the $Na_V1.6$ antibody can be seen in the scatter plot of cell body area versus average fluorescence (Fig. 3.9D).

Comparison of $Na_V1.6$ and $Na_V1.7$ SGN labelling: Direct comparison of $Na_V1.6$ and $Na_V1.7$ fluorescence values was not justified as the relative antibody binding affinities were not known. However, SGN cell body area could be compared directly. The Type I mean areas of 185.7±2.2μm^2 and 165.3±1.8μm^2 for $Na_V1.6$ and $Na_V1.7$ respectively, were highly significantly different at $p < 0.001$. The equivalent difference in Type II cell body areas was 74.8±3.2μm^2 and 82.2±2.6 μm^2 for $Na_V1.6$ and $Na_V1.7$ respectively and this was not significantly different ($p > 0.05$).

Peripherin labelling and $Na_V1.1$: Dual labelling experiments with peripherin and $Na_V1.1$ antibodies could not be performed because of the weak labelling of the SGN cell bodies using $Na_V1.1$ antibodies.

Control experiments into voltage-gated Na^+ channel localisation in tissues from CNS and PNS

Voltage-gated Na^+ channel expression in rat cerebellum: Sections of rat cerebellum were incubated with antibodies against $Na_V1.1$ and $Na_V1.2$ (Fig. 3.10). Positive $Na_V1.1$ staining was observed in the Purkinje cells as well as the granule cell layer (Fig. 3.10A). This staining was absent when the primary antibody was omitted (Fig. 3.10B). Positive staining of the molecular layer was seen in sections incubated with the $Na_V1.2$ antibody (Fig. 3.10C), while no staining was seen in this layer in the absence of the

primary antibody (Fig. 3.10D). Staining was evident in the white matter in both the presence and absence of the primary antibodies.

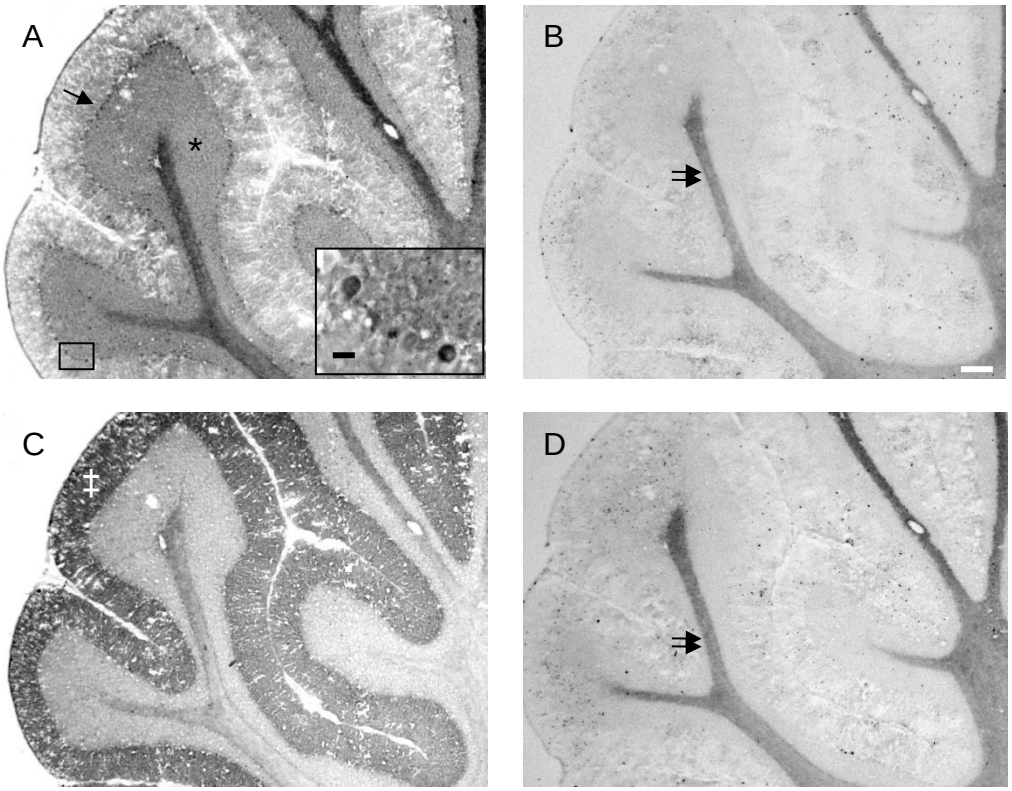

Fig. 3.10. Staining in rat cerebellum for $Na_V1.1$ and $Na_V1.2$. Sections of rat cerebellum incubated in the presence of $Na_V1.1$ antibody (A), $Na_V1.2$ antibody (C) or without primary antibody (B and D). (A) Staining of the Purkinje (arrow) and granule cell layers (*) are observed for $Na_V1.1$, with intense staining seen in the Purkinje cells (inset). (C) Intense staining of the molecular layer (‡) is seen with antibodies against $Na_V1.2$. These staining patterns are not seen in the absence of the primary antibodies (B and D), although staining is seen in the axon trunks (double arrow). Scale bar=200µm, inset 30µm

Voltage-gated Na^+ channel expression in rat DRG: Sections of rat DRG were investigated for expression of $Na_V1.1$, $Na_V1.6$, $Na_V1.7$, $Na_V1.8$ and $Na_V1.9$ (Fig. 3.11). Sections incubated with the antibody against $Na_V1.1$ showed diffuse and faint labelling of the DRG neuron nuclei and cytoplasm (Fig. 3.11A and B). The smaller diameter neurons were intensely stained for $Na_V1.8$, with some faint staining of the medium diameter neurons, and no apparent difference in staining intensity between the

cytoplasm and membrane (Fig. 3.11G and H). In sections incubated with the $Na_V1.9$ antibodies, the smaller and some medium diameter neurons appeared to be stained (Fig. 3.11I and J).

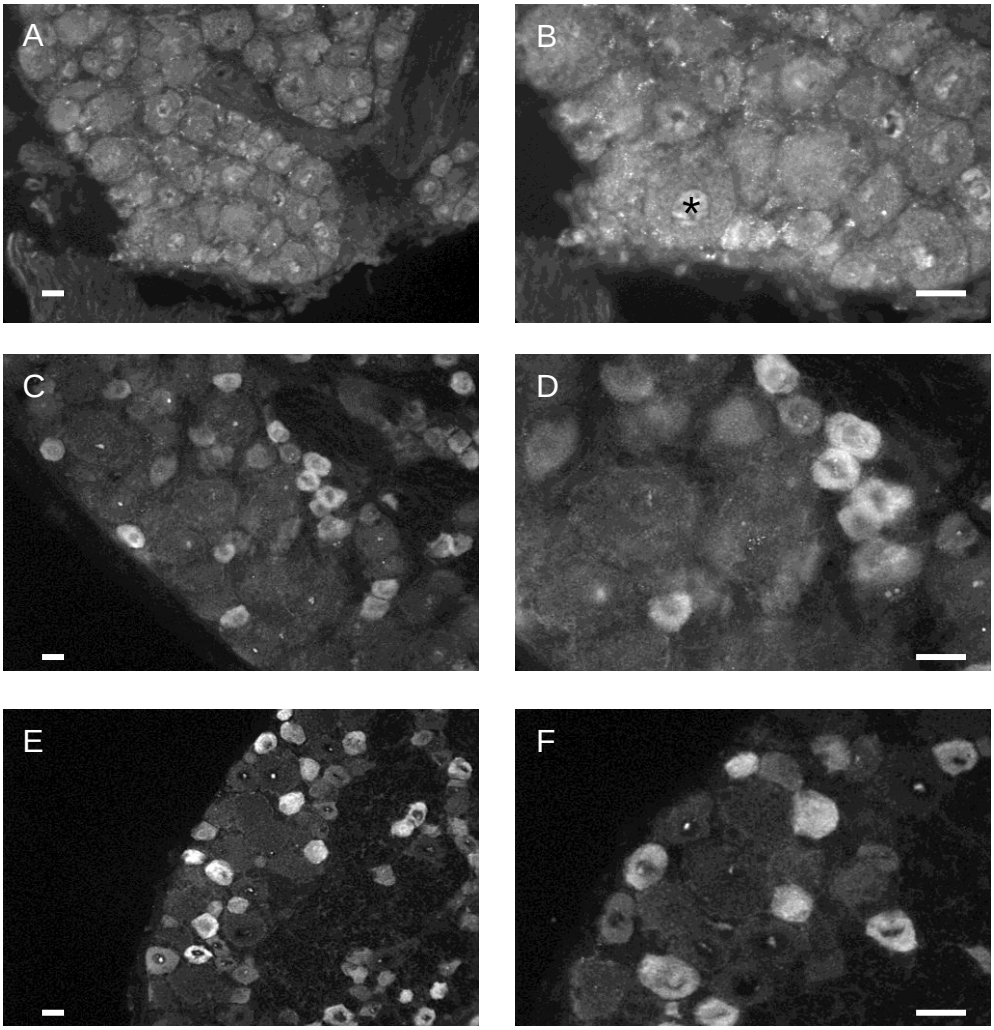

Fig. 3.11. Distribution of voltage-gated Na^+ channels in rat DRG. Micrographs showing rat DRG sections incubated with antibodies against (A,B) $Na_V1.1$, (C,D) $Na_V1.8$ and (E,F) $Na_V1.9$. (A,B) Labelling in the presence of $Na_V1.1$ antibodies is diffuse in the cytoplasm and intense in the nuclei (*). (C,D) The small and medium diameter neurons appear positively stained for $Na_V1.8$, with no clear delineation between the cytoplasm and the membrane. (E,F) Intense labelling with $Na_V1.9$ is restricted to the smaller diameter neurons, with diffuse labeling seen in the medium diameter neurons and no staining seen in the nuclei. Scale bars= 30µm for all images.

Positive staining was seen in the cytoplasm of neurons of all diameters using the antibody against $Na_V1.6$ (Fig. 3.12A and B), with the larger diameter neurons displaying

intense labelling of their membrane compared to the cytoplasm. Intense staining was also seen in all diameter neurons for $Na_V1.7$ (Fig. 3.12C and D). No specific staining was seen in sections incubated without the primary antibodies.

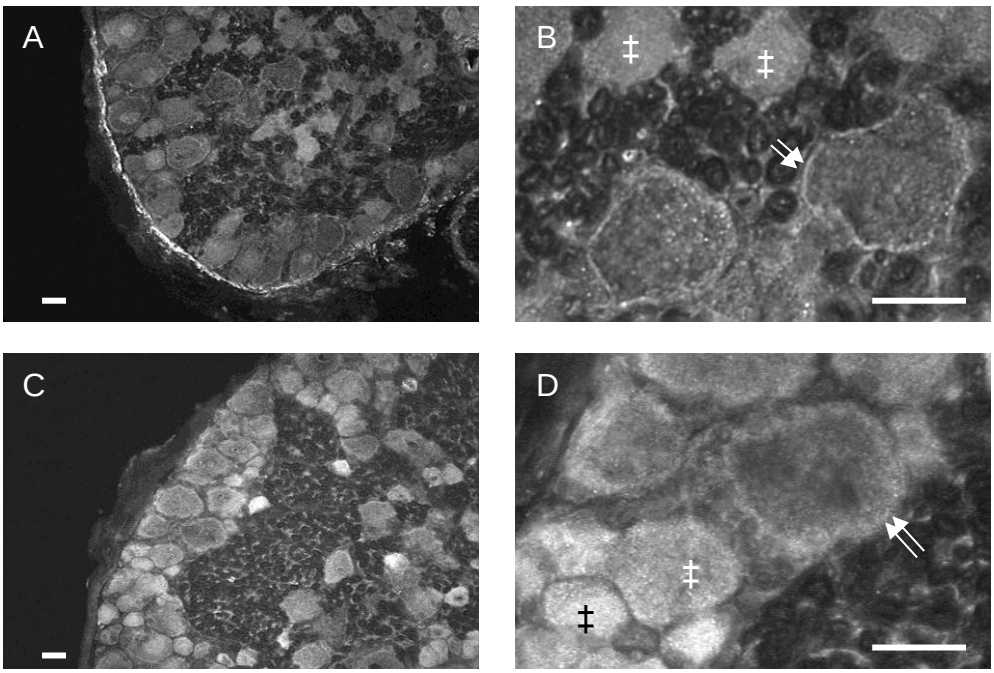

Fig. 3.12. Distribution of $Na_V1.6$ and $Na_V1.7$ in rat DRG. Micrographs showing rat DRG sections incubated with antibodies against (A,B) $Na_V1.6$ and (C,D) $Na_V1.7$. (A,B) Positive staining for $Na_V1.6$ is seen in all diameter neurons, with intense cytoplasmic staining seen in the small diameter neurons (‡) and intense labelling of the membrane in the larger diameter neurons (double arrows). (C,D) Positive staining for $Na_V1.7$ is also seen in all diameter neurons, with intense cytoplasmic staining seen in the small diameter neurons (‡) and intense labelling of the membrane in the larger diameter neurons (double arrows). Scale bars= 30µm for all images.

Discussion

Rat SGN exhibits a unique pattern of voltage-gated Na^+ channel subunit expression

The results presented here provide, for the first time, strong evidence that the α-subunits, $Na_V1.1$, $Na_V1.6$ and $Na_V1.7$, are selectively expressed in adult rat SGNs. These subunits were identified by RT-PCR and immunohistochemistry, which independently verifies the voltage-gated Na^+ channel content in these neurons.

There are a number of unusual features in this pattern of voltage-gated Na^+ channel subunit expression, as they suggest that expression in the SGN does not follow that observed in either the central or peripheral nervous system. Instead, the results presented here show voltage-gated Na^+ channel isoforms normally thought to be selectively expressed in either the peripheral or central nervous system are both expressed in the SGN. The explanation for this may be related to the unique embryological origin of the SGN (Fekete and Wu, 2002). The peripheral and central nervous systems are known to arise from different progenitor cells in the developing embryo. The CNS forms from the dorsal ectoderm through envagination and formation of the neural tube. DRG neurons arise from neural crest cells that migrate laterally to form the peripheral ganglia (Kuan *et al.* 2004, Li *et al.* 2007). In contrast, the SGN develops from a distinct region of neural ectoderm known as the otic placode, which is separate from both the neural tube and neural crest cells (Fekete and Wu 2002, Holley 2005). The results from this study suggest that the otic placode displays an intermediate phenotype with regard to voltage-gated Na^+ channel expression between the CNS and PNS.

$Na_V1.7$ subunit expression: The results presented here show that the $Na_V1.7$ subtype is expressed in the cell bodies and axon initial segments of the rat SGN. In contrast to this rat study, $Na_V1.7$ was not reported to be present in the mouse (Hossain *et al*. 2005). This may reflect a species difference in expression of the $Na_V1.7$ subunit. $Na_V1.7$ is considered to be exclusively expressed by neurons in the PNS, especially in the cell bodies (Sangameswaran *et al.* 1997) and peripheral terminals or growth cones (Toledo-Aral *et al.* 1997) of DRG neurons.

$Na_V1.6$ subunit expression: $Na_V1.6$ labelling was found in the cell body cytoplasm as well as the processes of the rat SGN. The presence of cytoplasmic labelling in the cell body seen here is in agreement with previous reports of $Na_V1.6$ labelling in other sensory ganglia (Krzemien *et al.* 2000, Tzoumaka *et al.* 2000, Black *et al.* 1999). In addition, cytoplasmic labelling has also been reported for potassium channels in the cell bodies of mouse SGN (Adamson *et al.* 2002a) and rat DRG neurons (Rasband *et al.* 2001). This type of labelling is most likely due to the pooling of subunit proteins in the Golgi apparatus, prior to their transport and insertion into the membrane (Krzemien *et al.* 2000). It has been previously reported that the $Na_V1.6$ subtype is expressed in mouse SGN (Hossain *et al.* 2005) with $Na_V1.6$ localised at the initial segment and nodes of Ranvier but not in the cell bodies.

$Na_V1.1$ subunit expression: The preliminary results from this study appear to show that $Na_V1.1$ is expressed in the SGN with strong axonal localisation. Since dual labelling experiments could not be performed using the $Na_V1.1$ antibody, we cannot report if $Na_V1.1$ expression is restricted to the Type I or Type II neurons. $Na_V1.1$ has been

previously been shown to be strongly expressed by neurons in the central nervous system (Whitaker *et al.* 2000, Westenbroek *et al.* 1989, Gordon *et al.* 1987).

Differential expression of $Na_V1.6$ and $Na_V1.7$ in Type I and Type II SGN: The measurement of SGN cell body area along with semi-quantitative fluorescence and non-fluorescence imaging techniques allowed exploration of the evident variation in labelling intensity. This investigation of differential staining intensity was further enhanced by the use of dual labelling with peripherin antibody (Hafidi 1998, Reid *et al.* 2004, Mou *et al.* 1998). The differences in SGN Type I and II cell body area have been reported previously and are confirmed by this study (Berglund and Ryugo 1987).

Whilst reduced fluorescence labelling was apparent in Type II neurons for both $Na_V1.6$ and $Na_V1.7$, the intensity of labelling observed was above background levels, indicating that Type II SGN express these subunits. This would support their possessing some functional capacity. Currently, little electrophysiological evidence exists to identify the specific role of Type II fibres or that they actually exhibit any acoustically driven activity (Robertson *et al.* 1999, Brown 1994), although it has been proposed they may signal static displacement of the basilar membrane (Robertson *et al.* 1999).

The difference in cell area between $Na_V1.6$ and $Na_V1.7$ expressing Type I neurons may be explained in at least two ways. One hypothesis is that the difference may correlate with signalling function as spontaneous activity in mammalian Type I afferents is known to range between 0-120 spikes sec^{-1}, which correlates with axon diameter (Liberman 1982). It would be reasonable to assume that axon diameter also correlates

with cell body area and that the expression of $Na_V1.6$ and $Na_V1.7$ in Type I SGN may then be related to the spontaneous and/or driven activity of Type I fibres. Alternatively, the differences may simply reflect more intense membranous staining by $Na_V1.6$ over $Na_V1.7$. $Na_V1.6$ expression has been previously identified at the nodes of Ranvier of neurons from both the CNS and PNS, suggesting a role for $Na_V1.6$ in action potential initiation and propagation in many neurons (Caldwell *et al.* 2000, Boiko *et al.* 2001). $Na_V1.6$ is also thought to generate a resurgent current, allowing neurons to rapidly generate action potentials, observed in cerebellar Purkinje cells (Raman and Bean 1997, Levin *et al.* 2006) and DRG neurons (Cummins *et al.* 2005), although additional evidence suggests that other voltage-gated Na^+ channel isoforms may contribute to this current (Do and Bean 2004, Kalume *et al.* 2007).

By contrast, $Na_V1.7$, a channel that shows slow inactivation and stays open in response to slow ramp depolarisations (Cummins *et al.* 1998, Herzog *et al.* 2003), may have a role in action potential initiation at the hair cell-afferent fibre synapse. $Na_V1.7$ has been shown to provide a key role in action potential generation in nociceptive fibres. In humans expressing a non-functional $Na_V1.7$ mutant, which confers congenital insensitivity to pain, normal sensation remained in other sensory modalities (Cox *et al.* 2006). This indicates that $Na_V1.7$ is required for action potential initiation in the nociceptive fibres, a role that may be replicated in the SGN. However, Cox *et al*. commented that the subjects who were insensitive to pain had normal hearing, indicating that $Na_V1.7$ may not be essential for the generation of action potentials in the SGN. It could be however that $Na_V1.7$ might be involved in abnormal afferent activity associated with conditions such as tinnitus.

Cellular localisation of voltage-gated Na^+ channel isoforms in SGN: From the immunohistochemistry results, an outline for the cellular localisation of voltage-gated Na^+ channel α-subunits in a typical SGN can be suggested (Fig. 3.13). $Na_V1.7$ staining was observed in the cell body, with no clear delineation between cytoplasm and membrane in the intensely stained neurons whilst membranous labelling was seen in the less intensely stained neurons. Staining was seen along the central processes for $Na_V1.7$ but, in contrast to $Na_V1.1$ staining, it was not seen beyond Rosenthal's canal, indicating that $Na_V1.7$ may be restricted to the axon initial segment. The expression of $Na_V1.7$ in DRG neurons is also seen in the cell body but additionally in the peripheral terminals (Toledo-Aral *et al.* 1997). If this pattern of expression was mirrored in the SGN, this could suggest that $Na_V1.7$ could be localised at the post-synaptic terminal, innervating the hair cells of the organ of Corti. However this theory is speculative, as identifying positive immunostaining from the organ of Corti in frozen cochlea sections is difficult, due to the deformation of the organ of Corti fine morphology during tissue freezing and cryostat sectioning (Fish *et al.* 2001).

$Na_V1.6$ staining was seen along the peripheral and central processes of the SGN as well as the membrane of the cell body. This indicates that $Na_V1.6$ would be expressed along the axon at nodes of Ranvier, generating and conducting action potentials from the axonal hillock and along the processes.

$Na_V1.1$ staining was predominantly seen in the central processes, suggesting that $Na_V1.1$ would be expressed in the axon initial segment and possibly at nodes of

Ranvier along with $Na_V1.6$. This pattern of $Na_V1.1$ expression at nodes of Ranvier and axon initial segments has been identified in mouse spinal cord, along with co-localisation with $Na_V1.6$ in these neurons (Duflocq *et al.* 2008).

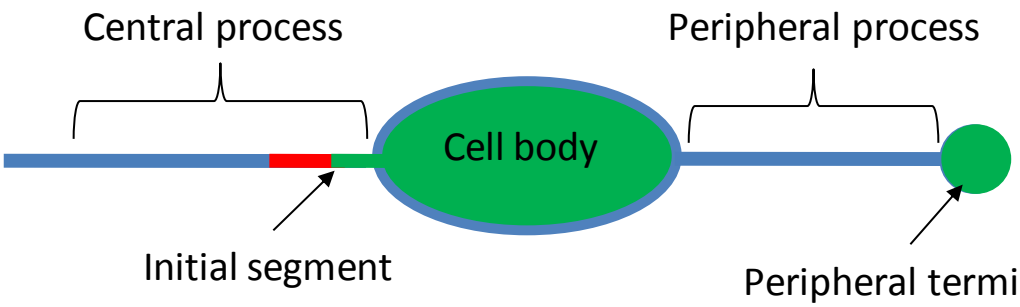

Fig. 3.13. Diagram of voltage-gated Na^+ channel isoform localisation in a typical SGN. Representation of proposed voltage-gated Na^+ channel isoform cellular localisation showing $Na_V1.7$ (green) expressed in the cell body cytoplasm, axon initial segment and peripheral terminal, $Na_V1.6$ (blue) expressed along the peripheral and central processes and the cell body membrane and $Na_V1.1$ (red) expressed at the initial segment of the central process. Diagram is not to scale.

An ideal experiment to test this theory of voltage-gated Na^+ channel distribution would be to dual or triple label SGN sections with antibodies specific to $Na_V1.1$, $Na_V1.6$ and $Na_V1.7$. This cannot be done easily at present as the effective antibodies available were raised in the same host animal.

Variations in staining intensity between SGN: The results presented have shown considerable variation in the staining intensities for both $Na_V1.6$ and $Na_V1.7$ in SGN cell bodies within the same section. Indeed, a similar observation has been noted with regard to the expression of the purinergic receptor, $P2X_2$, in rat SGN (Salih *et al.* 1999). At present it is unclear whether this staining variation results in different functional properties between the individual SGN, as has been shown for K^+ channels (Adamson *et al.* 2002a). However, the differences in staining intensity observed could be due to

transient pooling of the voltage-gated Na^+ channel proteins in the cytoplasm prior to insertion into the membrane.

Expression of other voltage-gated Na^+ channel isoforms in the SGN: The expression of other voltage-gated sodium channel isoforms was also investigated in this study. RT-PCR failed to show the expression of mRNA for $Na_V1.2$, $Na_V1.3$, $Na_V1.8$ and $Na_V1.9$, indicating that these isoforms are not expressed in the rat SGN.

Interestingly, in the mouse study by Hossain *et al*., $Na_V1.2$ expression was observed in the organ of Corti, but only in the efferent innervation to inner and outer hair cells (Hossain *et al.* 2005). The absence of evidence for expression of $Na_V1.8$ and $Na_V1.9$ isoforms in this study is in line with earlier observations that TTX completely abolished inward sodium current in isolated SGN (Santos-Sacchi 1993). $Na_V1.4$ and $Na_V1.5$ expression in the SGN was not studied, as these isoforms are believed to be selectively expressed in skeletal (Trimmer *et al.* 1990) and cardiac (Rogart *et al.* 1989) muscle respectively.

Control results: The extensive analysis and comprehensive documentation of the expression of voltage-gated Na^+ channel subunits in the CNS and PNS neurons provided positive controls for RT-PCR primers used in the current study. CNS neurons have been shown to express $Na_V1.1$, $Na_V1.2$ (Westenbroek *et al.* 1989), $Na_V1.3$ (Beckh *et al.* 1989) and $Na_V1.6$ (Tzoumaka *et al.* 2000), and mRNA isolated from the cerebral cortex was used to test the specificity of the RT-PCR primers designed for these voltage-gated Na^+ channel subunits. $Na_V1.7$ and $Na_V1.9$ were also weakly identified by

the RT-PCR primers. While these proteins have not been identified in the cerebral cortex, the mRNA has been detected in this tissue previously (Dib-Hajj *et al.* 1998, Belcher *et al.* 1995). The mRNA isolated from the DRG was used as a positive control to validate the specificity of the RT-PCR primers designed to detect $Na_V1.7$, $Na_V1.8$ and $Na_V1.9$, as the DRG has been previously reported to express these subunits (Dib-Hajj *et al.* 1998, Dib-Hajj *et al.* 1998, Sangameswaran *et al.* 1997). The RT-PCR primers also identified $Na_V1.1$ mRNA in the DRG tissues. This result has been reported previously (Beckh 1990), but whilst the mRNA for $Na_V1.1$ has been identified in the DRG, the protein has not been detected in the peripheral nervous system (Gordon *et al.* 1987). Both these control tissues presented results that confirmed that the designed primers were specific for their respective voltage-gated Na^+ channel isoforms.

Antibody specificity is essential for the reliable interpretation of immunohistochemical data. Where available, primary antibodies were pre-incubated with their control peptide overnight and reduced the labelling to background levels. Additionally, as with the RT-PCR experiments, tissue taken from the CNS and PNS with known voltage-gated Na^+ channel isoform expression was used as positive controls for the antibodies. Sections of rat cerebellum incubated with the anti-$Na_V1.1$ antibody showed intense staining of the Purkinje and granule cell layers, as has been reported previously (Whitaker *et al.* 2001). In contrast, similar cerebellar sections incubated with antibodies against $Na_V1.2$ showed intense staining of the molecular cell layer, in line with previous reports (Westenbroek *et al.* 1989). Omission of the primary antibodies did not produce specific staining such as that seen in the cell layers of the cerebellum.

The dark staining in the white matter was still seen in the absence of the primary antibodies, indicating that this staining is not specific.

Sections of DRG were also used to validate the antibodies. These sections showed positive staining for $Na_V1.6$ (Tzoumaka *et al.* 2000) and $Na_V1.7$ (Toledo-Aral *et al.* 1997, Sangameswaran *et al.* 1997) in all cell bodies irrespective of diameter. Additionally, positive labelling of the small to medium diameter neurons was observed when the sections were incubated with $Na_V1.8$ and $Na_V1.9$ antibodies, confirming observations from previously published studies (Dib-Hajj *et al.* 1998, Dib-Hajj *et al.* 1998). Some nuclear staining was seen when using the $Na_V1.1$ antibody with the DRG tissue sections, which has been identified previously (Black *et al.* 2004). This indicates that the $Na_V1.1$ protein is not expressed in the cytoplasm of these neurons (Gordon *et al.* 1987), although nuclear staining has been observed for other ion channel proteins (Stonehouse *et al.* 2003). Interestingly, nuclear staining was not seen in SGN incubated with the same $Na_V1.1$ antibodies, suggesting the staining observed in the DRG is either an artefact or is specific.

Sections of rat cochlea incubated without primary antibodies did not display fluorescence specific to the binding of the secondary antibodies to their antigens. However, non-specific cytoplasmic yellow puncta were observed in the SGN cell bodies. These results indicate that in the adult rat SGN there are other sources of endogenous fluorescence, possibly lipofuscin. This has also been reported in other adult neural ganglia, including the retina, vestibular and dorsal root ganglion and cerebellar Purkinje cells (Samorajski *et al.* 1968, Sans *et al.* 1996). Furthermore, the

non-fluorescence DAB/HRP visualisation method validated the original results and demonstrated that these puncta were due to non-specific tissue fluorescence.

Choice of cochlear immunohistochemistry techniques: In this study the cochleae were processed for immunohistochemistry by fixation with 2% PFA, demineralised with 8% EDTA in PBS, infiltrated with 30% sucrose in PBS and Tissue Tek before being oriented and frozen in Tissue Tek over dry ice and hexane. Frozen sections were then cut using a cryostat and melted onto Polysine slides. Due to the osseous nature of the adult rat cochlea, demineralisation was needed to ensure the cochleae were soft enough to section using the cryostat blade while maintaining the morphology of the specimen. While it has been shown that immunohistochemistry can be performed using non-demineralised cochleae (Soliman 1988), the non-specific fluorescence seen from the bone and the possible destruction of morphological integrity indicate that demineralisation is required for good quality cochlear sections.

Cryoprotection and infiltration steps were used in the tissue preparation to fill the canals of the demineralised cochleae, as these precautions have been shown to preserve cochlear morphology during sectioning (Whitlon *et al.* 2006). As mentioned previously, the microarchitecture of the organ of Corti was not readily preserved, probably due to the combination of freezing and mechanical stress during sectioning (Fish *et al.* 2001). While paraffin sectioning would yield superior section morphology (Khan *et al.* 2002), trial experiments with paraffin embedded cochlear sections resulted in overwhelming background fluorescence and reduced DAB staining when using the fluorescence and non-fluorescence imaging techniques, respectively (data

not shown). This indicated that the use of frozen sections was appropriate for the current study as the exposure to heat and organic solvents required for paraffin embedding could influence the antigenicity of the tissue (Whitlon *et al.* 2006).

As the cochleae need to be demineralised prior to sectioning, the tissue was fixed using 2% PFA. Initially the cochleae were fixed for 24 hours to ensure complete fixation of the tissue (Hafidi 1998, Kitahara *et al.* 2005, Jongkamonwiwat *et al.* 2006). However this resulted in high background levels of fluorescence in tissue sections incubated without primary antibodies. The fixation step was reduced to 30 minutes, with the oval and round window membranes carefully punctured and the fixation vial inverted to ensure complete infiltration of the cochlea, with washes in PBS afterwards. This reduced the background fluorescence levels, but non-specific fluorsecence could still be observed. An alternative fixative to PFA could have been used, such as methanol (Soliman 1988), however the non-fluorescence staining technique was developed, as this method gave low levels of background staining in control sections.

Therapeutic applications of characterising voltage-gated Na^+ channel isoforms in the auditory pathway: The characterisation of voltage-gated Na^+ channel isoforms in the periphery of the normal auditory pathway contribute to the development of therapeutics for treating conditions such as tinnitus. The clinical evidence that voltage-gated Na^+ channel blockers may have a role in ameliorating certain types of tinnitus is well documented because lignocaine, a use-dependent sodium channel blocker and local anaesthetic, is the gold standard tinnitolytic agent and is effective in around 50% of patients (Baguley *et al.* 2005). Following ototrauma, it is apparent that marked

plastic changes occur in the auditory pathway some of which have parallels with sensory nerve trauma (Møller 1997, Kaltenbach *et al.* 1998). In models of neuropathic pain this is accompanied by changes in pattern and expression of voltage-gated Na^+ channel subtype in nociceptive nerve fibres and profound changes in neuronal excitability (Novakovic *et al.* 1998, Devor 2006, Cummins and Waxman 1997, Black *et al.* 2004). Several voltage-gated Na^+ channel subtypes including $Na_V1.7$ and $Na_V1.8$ have been implied to regulate spontaneous firing in damaged nociceptive afferents although there is much debate from studies using antisense knock-down methodologies and transgenic animals as to which are the most important (Krafte and Bannon 2008, Momin and Wood 2008).

The use of appropriate models of ototrauma would establish whether similar or other changes in voltage-gated Na^+ channel isoforms may underlie tinnitus. This would provide the basis for optimal matching of tinnitolytic therapeutics to their tinnitogenic target.

In summary, this chapter has shown that the rat SGN express both the mRNA and proteins for three voltage-gated Na^+ channel α-subunits, $Na_V1.1$, $Na_V1.6$ and $Na_V1.7$. $Na_V1.6$ and $Na_V1.7$ were also shown to be expressed in both the Type I and Type II SGN. Furthermore, the subcellular distribution of these α-subunits was characterised, with $Na_V1.1$ expressed predominantly in the central processes, $Na_V1.6$ in the central and peripheral processes as well as the cell bodies, and $Na_V1.7$ expressed in the cell bodies and the proximal regions of the central processes.

The next chapter will discuss the generation of the ototrauma model, using intense sound exposures to generate hearing loss and the use of auditory brainstem responses to measure the degree of hearing threshold changes. This model will then be used to investigate whether the pattern of voltage-gated Na^+ channel expression identified in the normal animals changes following ototrauma.

Chapter 4. ABR measurements and the effect of sound exposure

Introduction

The previous chapter has shown that the rat SGN expresses $Na_V1.7$, $Na_V1.6$ and $Na_V1.1$. As described earlier, somatic nerve damage can lead to altered voltage-gated Na^+ channel expression and redistribution, resulting in hypersensitivity and altered firing patterns of pain fibres.

To investigate whether similar changes in voltage-gated Na^+ channel expression occur following ototrauma in the SGN, a model of moderate ototrauma was devised. This chapter describes the model of hearing loss using a single tone for noise exposure and how the degree of hearing loss was measured using evoked auditory brainstem responses.

What is noise?

The experiments detailed in this chapter use noise exposure to generate deafness in Wistar rats. In general terms, noise is considered to be an unwanted signal or data that perturbs normal perception, be it the hiss from a loud speaker, the 'snow' observed on a detuned television screen or the interference of radio signals.

Acoustic noise exposure: With respect to this investigation the noise used is an acoustic signal. There are two main forms of noise: impulse noise, high intensity but short duration noise generated chiefly from explosions and gunshots; and continuous noise, noise of various frequencies, intensities and durations. In this study continuous noise was used. There are two factors that determine the magnitude of the noise-

induced hearing loss experienced by a subject: intensity or energy and duration. An increase in intensity, measured in dB SPL, will produce hearing loss, with previous studies showing that 85dB SPL will cause hearing loss (Sullivan and Conolly 1988). Additionally the length of the exposure to noise must also be considered. For example two exposures to the same noise source, the first for one hour per day for 10,000 days and the second for 10,000 continuous hours, would subject the cochlea to the same amount of energy but would not necessarily produce the same degree of hearing loss (Rosenblith *et al.* 1954). Indeed it has been shown that exposing guinea pigs to a continuous 4kHz octave band noise delivered at 115dB SPL for 5 hours produced a larger degree of hearing threshold elevation and hair cell loss than the same tones delivered at 125dB SPL but presented in tone bursts (Pourbakht and Yamasoba 2003).

The frequency spectrum of the noise insult is also of consideration. As stated previously, the cochlea is a frequency discriminator, with the basilar membrane resonating at different frequencies along its length. Presenting noise at different frequencies will thus preferentially affect selected regions of the basilar membrane. White noise is noise that has equal energy across all frequencies or a flat spectrum over a defined frequency range, so theoretically all regions of the basilar membrane would be stimulated at the same level. Presenting noise at specific frequencies increases the probability of stimulating a defined region of the basilar membrane, thus damaging hearing at selected frequencies. Many studies have reported using octave band, frequencies across an octave (Ou *et al.* 2000, Hirose *et al.* 2005, König *et al.* 2006), broadband, a large range of frequencies (Kojima *et al.* 2007, Rybalko and Syka 2005, Popelar *et al.* 2008) or narrowband noise, a smaller range of frequencies such as

a single tone (Puel *et al.* 1998, Zhang and Kaltenbach 1998, Finlayson and Kaltenbach 2009). While the overall energy delivered to the cochlea from a high intensity broadband noise may be the same as a high intensity single tone noise stimulus, the increase in frequency bandwidth decreases the intensity of the component frequencies. At the level of the cochlea, the increase in bandwidth will stimulate a larger region of the basilar membrane but, due to the reduced intensity of the component frequencies, the basilar membrane oscillations would not be as large and be expected to result in less physical damage. However, excitotoxic damage would still be evident to due to glutamate release from IHCs across the resonate portions of the basilar membrane.

Noise exposure protocol: In this study, the limitations of the available equipment meant a single tone of 110 dB SPL was used, along with a decision to break the exposure into 2 acute episodes, each lasting 2 hours. It was considered that this exposure would not lead to massive physical damage but would provide moderate hearing loss. There were pragmatic reasons for choosing this exposure regimen, not least on grounds of animal welfare. A single exposure of 4 hours or longer would have been possible but the welfare of the animal would have been compromised by extending the period under which neuroleptanalgesia would have had to be administered. The veterinary staff in the animal facility recommended keeping the period of neuroleptanalgesia to a minimum wherever possible in keeping with primary concern for the welfare of the animal. As a single tone was used, the terms 'noise exposure' and 'sound exposure' are used interchangeably to refer to the current model described below.

Damaging level of noise: As mentioned previously, sound intensity is measured using the decibel scale. This is a logarithmic index that represents a doubling of acoustic intensity (power) for every 3dB SPL increase, a doubling of sound pressure (amplitude) for every 6dB SPL increase and a doubling of the perceived loudness (volume) for every 10dB SPL increase. The relationship between sound pressure, acoustic power and the perception of loudness can be characterised according to Table 4.1. This suggests that constant exposure to noise below 80dB SPL is not considered to generate permanent hearing loss in humans. In man sound intensities appear to show a logarithmic relationship between duration and intensity, such that the more intense the noise, the threshold shifts accumulate more rapidly as the time of the exposure is increased (Miller 1974). For example, noise presented at 120dB SPL for 5 minutes to a typical human subject would generate a dramatic threshold elevation, however to generate a similar threshold shift using 80dB SPL noise would require several hours of continuous exposure (Miller 1974). This relationship informs the basis of international health and safety guidelines for noise exposure limits.

Above about 120 dB SPL the relationship does not hold as sound intensities above this level begin to exceed the gross acoustic capacity of the cochlea. Prolonged duration (i.e. over a few hours) above this level generally leads to loss of physical integrity of cochlear structures (Puel *et al.* 1998, Henderson and Hamernik 1995).

Noise exposure is believed to result in hearing loss in three main ways. First there is the mechanical damage to the cochlea, where noise (in general of above 120dB SPL) is

Sound source examples (with distances)	Sound Pressure Level (dB SPL)	Sound pressure (N m^{-2} or Pa)	Sound intensity (W m^{-2})
Jet engine (50m)	140	200	100
Threshold of pain	130	63.2	10
Threshold of discomfort	120	20	1
Chainsaw (1m)	110	6.3	0.1
Disco loudspeaker (1m)	100	2	0.01
Diesel truck (10m)	90	0.63	0.001
Kerbside of busy road (5m)	80	0.2	0.0001
Vacuum cleaner (1m)	70	0.063	10^{-5}
Conversational speech (1m)	60	0.02	10^{-6}
Average home background	50	6.3x10-2	10^{-7}
Quiet library	40	2x10-3	10^{-8}
Quiet bedroom at night	30	6.3x10-3	10^{-9}
Background in a TV studio	20	2x10-4	10^{-10}
Rustling leaves	10	6.3x10-4	10^{-11}
Threshold of hearing	0	2x10-5	10^{-12}

Table 4.1. The relationship between sound pressure, intensity and SPL, as well as the typical noise sources.

thought to overwhelm the reticular lamina, fusing the stereocilia and damaging the hair cell membranes (Henderson and Hamernik 1995, Spoendlin 1971), resulting in a complete loss of signal transduction.

The second is the metabolic damage of the cochlea, where noise (120dB SPL and below) causes the disruption of the hair cell stereocilia and production of reactive

oxygen species in the hair cells ultimately resulting in cell death. This damage is due to the increased metabolic demands placed upon the cochlear cell types due to the overstimulation by noise, as demonstrated by the increase in deoxyglucose uptake observed in the organ of Corti and cochlear nerve during exposure to white noise (Canlon and Schacht 1983). This metabolic demand increases the oxygen requirement within the cochlea and thus producing a deficit of available oxygen (Spoendlin 1971) and activating apoptotic pathways (Pirvola *et al.* 2000). Indeed treating human patients suffering from noise-induced hearing loss with hyperbaric oxygen therapy, where oxygen is delivered at high pressure to increase oxygen tension in the blood and tissues (Leach *et al.* 1998), has been shown to improve hearing recovery compared to untreated subjects (Ylikoski *et al.* 2008).

The third is the excessive release of glutamate from the stimulated hair cells, resulting in excitotoxicity of the afferent spiral ganglion neuron synapses. The excitotoxic action is generated by the over-activation of the SGN glutamate receptors, which allow the influx of Na^{+} and Ca^{2+}. The excessive influx of these ions results in increased depolarisation of the neuron, increased ATP hydrolysis, activation of Ca^{2+} dependent processes resulting in dendritic swelling and, in extreme cases, neuronal cell death.

The hearing deficit in this study is measured by investigating the threshold of hearing, the lowest intensity of a sound that can be perceived, using the auditory brainstem response (ABR) of the rat. Generally, elevations or shifts in hearing threshold can be classified as a Temporary Threshold Shift (TTS) where the original hearing threshold is restored with recovery, or a Permanent Threshold Shift (PTS) where the original

hearing threshold is not recovered. TTS is thought to be the result of cochlear damage that recovers, such as the repair of the afferent hair cell/spiral ganglion neuron synapse (Puel *et al.* 1998), where as PTS is due to the unrepairable damage or loss of hair cell and/or innervating neurons, which do not regenerate in mammalian cochleae (Holley 2005). Elevated hearing thresholds are not the only descriptor of impaired hearing, as other auditory functions such as localization of sound, perception of loudness and pitch can also be affected, although these functions can not be easily quantified at this time.

Previously published noise-exposure models: The most pertinent studies with which comparisons can be drawn are investigations of noise-induced hearing loss performed by previous students under the supervision of Dr Mulheran using guinea pigs (Etheridge 2002, Fergie 2005). These studies showed that significant, acute elevations in hearing thresholds were evident after 15 minute exposure to modest broadband noise levels (100-110dB SPL) alone or in combination with hypoxia. Additionally, this previous work found that the auditory nerve could be protected from the effect of noise insult by two voltage-gated Na^+ channel blockers, providing a solid platform for the current study.

The published literature surrounding animal models noise induced hearing loss is very disparate with regard to the noise exposure model used. Quite rightly, many previous studies have exposed animals to noise more akin to that experienced in industrial or military environments to investigate the auditory consequences for people working in such conditions, using audible noise, presented at 90-120dB SPL over hours to days

(Sullivan and Conolly 1988, Salvi *et al.* 1979a), or impulse noise, from 150-160dB SPL presented for a few seconds (Hamernik *et al.* 1980, Duan *et al.* 2008), respectively. Previously there has been no investigation of ion channel expression following noise exposure, with the studies focused on creating structural damage to the auditory periphery, significantly elevated CAP or ABR thresholds (Puel *et al.* 1998) and plastic changes that lead to hyperactivity at higher nuclei within the auditory brainstem (Zhang and Kaltenbach 1998, Kaltenbach *et al.* 2004, Bauer *et al.* 2008, Salvi *et al.* 2000). Additionally, to further hinder comparisons, a wide range of animal species have been used to investigate the auditory pathway, from chinchillas and rats to hamsters and cats (Kojima *et al.* 2007, Liberman 1982, Salvi *et al.* 1979a, Heffner and Koay 2005, Kaltenbach *et al.* 2002, Kiang *et al.* 1976, Liberman and Beil 1979).

A fairly systematic study to investigate the effect of white noise exposure on Sprague-Dawley rats showed that hair cell loss and hearing threshold increased when noise intensity was raised from 85dB SPL to 110dB SPL (Sullivan and Conolly 1988). However, it must be noted that this study exposed the rats to noise for 6 hours per day, 5 days per week for 4 weeks in total. Other recent noise induced hearing loss studies using rats (Popelar *et al.* 2008, Chen and Fechter 2003, Perez *et al.* 2004) and mice (Ou *et al.* 2000) have shown similar results to those presented in the current study. It must be noted that all the aforementioned studies use broadband noise, either in the form of white noise or octave band noise, to generate hearing loss, rather than the single tone used here.

Experimental methods

Auditory brainstem response

Experimental set-up: The equipment used to measure the hearing threshold as part of the auditory brainstem response (ABR) is described in Fig. 4.1. This system, designed by Dr Patrick Jones (Applied Technology at GlaxoSmithKline) in collaboration with Dr Mike Mulhearan, generates short, shaped tone pips suitable for eliciting ABRs at frequencies within the documented hearing range of the rat. Specifically, the tone pip test frequencies used in this study were 12kHz, 16kHz, 24kHz and 30kHz.

Three electrodes- the recording, reference and earth electrodes- were inserted subdermally (1) along the mastoid bone below the left ear, (2) between the ears and (3) at the abdomen away from the leg muscles, respectively, in an anaesthetised animal, as described in Chapter 2. These electrodes were connected to an amplifer (Medelec Sapphire 4A, Medelec Ltd, Woking, UK) to amplify the evoked potentials. An Arbitrary Waveform Generator (TGA1230, 30MHz, Thurlby Thandar Instruments Ltd, Huntington, UK) was used to generate cosine enveloped wave forms of the desired frequency (12, 16, 24, 30kHz) with a total length of 5 milliseconds including 1 millisecond rise and fall time.

Tone pips of this duration and shape were used as this configuration has been found to result in optimal stimulation of a discrete, and therefore more easily measured and frequency specific, evoked response in the auditory pathway (Yost 2000). The maximum amplitude of the signal from this generator was 20V peak to peak. The signal from the generator was directed into a sequence of signal attenuators (model

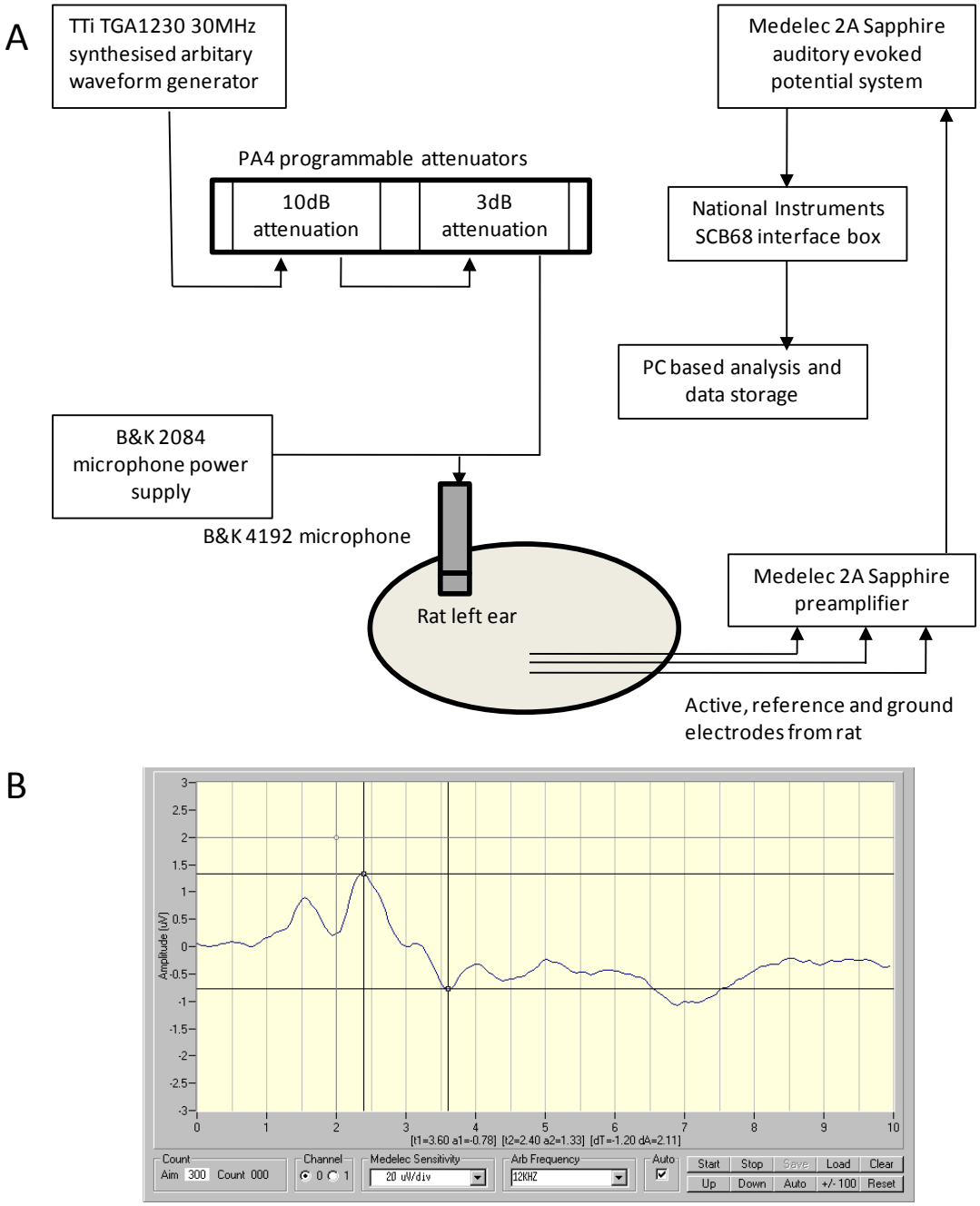

Fig. 4.1. Diagram representing the equipment and experimental set-up for Auditory Brainstem Response recordings. (A) Tone pips of the desired test frequency were generated by the arbitrary waveform generator and delivered to the animal's external auditory meatus via a series of programmable attenuators. Sub-dermal electrodes, placed in the animals scalp, detect the elicited electrical activity which was amplified by the Medelec auditory evoked potential system and recorded by the PC. (B) Example image of the ABR program. The ABR waveform was displayed in the main window with markers t1 and t2 that can be positioned along the waveform to measure the amplitude of the individual waves.

DA-4, Tucker Davis Technologies, Alachua, Florida, USA), which allows incremental attenuation of the maximal output of the signal in user defined intensity steps (measured in dB). One attenuator was set to 10dB steps while the other to 3dB steps. This tone pip signal was then transduced by an ultra high performance reverse driven microphone, used as an acoustic driver (model 4192, Brüel and Kjær Sound and Vibration Measurement A/S, Nærum, Denmark). The driver received a 200V bias current, ensuring the microphone diaphragm was kept in constant electrostatic tension to produce a reliable and flat frequency response (battery operated microphone power supply model 2804 Brüel and Kjær), coupled to the signal line by a 0.01µF capacitor. The driver was positioned approximately 5mm above the entrance to the auditory canal so that the tone pips were delivered directly into the rat's left ear.

The signal generator was electronically controlled by a PC (Kayak XA, Hewlett Packard running Microsoft Windows NT4.0) so that the initiation of the tone pip generation triggered the onset of ABR recording. The signal was repeated and the recording averaged 300 times (count shown in Fig. 4.1B) whilst being continuously displayed by the designed PC software. The ABR recording was pre-amplified (Medelec Sapphire 4A) 10,000 times and filtered between 5Hz-5kHz, and supplied to the PC. The real time recording was digitally sampled using a sampling card (National Instruments Corporation, Austin, Texas, USA) set at 16kHz fitted to a PC. This sampled signal was then averaged with the sensitivity (Volts/division) and time base (ms/division) set by the user. For each recording, the captured data was saved on the PC hard disk for subsequent offline analysis.

Calibration of the reverse driven microphone stimulus: The stimulus used to determine ABR responses was carefully calibrated prior to experimentation as described. As the results presented in the thesis refer to the stimulus level in terms of dB attenuation (dB att), the reader should refer to Table 4.2 for the dB SPL equivalent, where 0dB att is the maximum output delivered at the driver to the rat. As the driver was positioned approximately 5mm above the external auditory canal, the tone pips were not delivered directly to the tympanic membrane, a small degree of output loss can be assumed. Also the degree of destructive and constructive interference due to positional variation and orientation of the pinna could not be directly calculated but would contribute to between animal variability in the ABR (B&K Condenser Microphone Type 4188-4193. Technical Report, Nærum, Denmark).

Frequency (kHz)	Voltage (dB Vrms)	dB SPL
1	-37.2	94
12	-38.3	92.7
16	-38.4	92.6
24	-42.1	88.9
30	-49	82

Table 4.2. Calibration of ABR tone pips. Details of the acoustic driver calibration as described in the methods text. All tones generated from the signal generator except for 1kHz which was generated by the acoustic calibrator.

The driver was coupled via a closed calibration chamber (type 4142, Brüel and Kjær) to a microphone (model 4134, Brüel and Kjær) acting as the reciprocal calibrator. The driver was then continuously driven by at 20 volts peak to peak with the 200V bias voltage provided by the power supply. This power supply also powered the microphone. The output from the microphone was fed into a signal analyser (Hewlett Packard 35665A, Hewlett Packard Ltd, Bracknell, UK), which gave a graphic display of the signal intensity in dB V_{rms}. The driver was calibrated for frequencies between 1 to 30kHz and found to function within the specification provided by the manufacturer. The calibration of the microphone was accomplished by using an acoustical calibrator (model 4231, Brüel and Kjær), generating a 1kHz tone at 94dB SPL.

Data collection and analysis: An example of the ABR data generated is shown in Fig. 4.2. The maximal stimuli, i.e. 0dB att, for each tested frequency are displayed in Table 4.2. The stimulus was attenuated in 10dB steps, from 0dB att to 80dB att, with each step repeated at least twice. The amplitudes and latencies of the individual waveform components were measured using the custom designed software. The ABR data was inserted into Microsoft Excel spreadsheets so an average waveform could be generated for each attenuation step, allowing for the hearing threshold to be established more accurately. The hearing threshold level was established when the P1 component of the ABR waveform could not be detected visually.

ABR waveform components: The rat ABR is composed of four to five waves (labelled P1 to P5, Fig. 4.2) occurring within 6ms of the stimulus onset. The waves are generated by a series of action potentials and post-synaptic potentials produced within the auditory

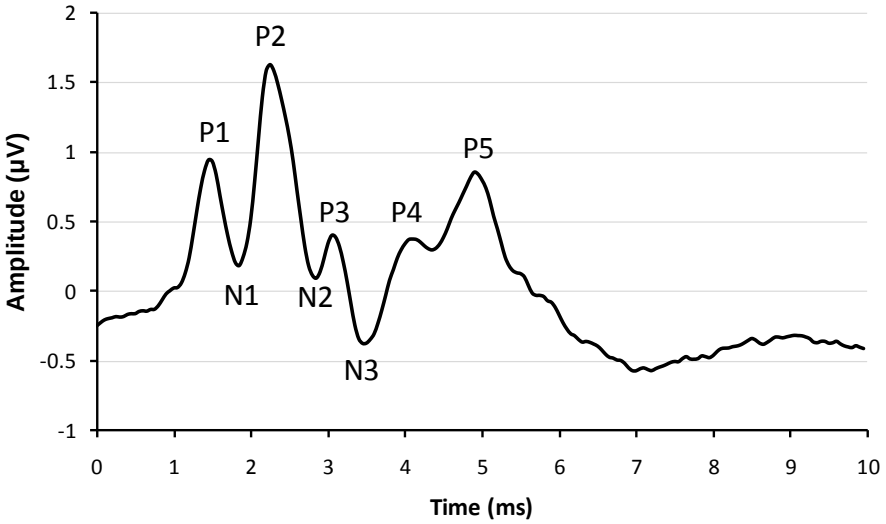

Fig. 4.2. Example ABR waveform. ABR recording elicited from 12kHz tone pip stimulus at 0dB attenuation. The positions of wave components P1 to P5 and N1 to N3 are shown on the trace. The waves are thought to reflect activity from (P1) the cochlear nerve, (P2) the cochlear nucleus, (P3) the superior olivary complex, (P4) the lateral lemniscus, and (P5) the inferior colliculus, medial geniculate body and primary auditory area of the cerebral cortex.

pathway. Many studies have generated evidence to identify the brainstem tracts and nuclei that are responsible for the generation of each wave component (Church and Gritzke 1987, Popelar *et al.* 2008, Starr 1976, Melcher *et al.* 1996, Kaga *et al.* 1997) from the cochlear nerve (P1), the cochlear nucleus (P2), the superior olivary complex (SOC; P3), the lateral lemniscus (P4), and the inferior colliculus (P5), although reports also suggest roles for the medial geniculate body and primary auditory area of the cerebral cortex in generating P5 (Church and Gritzke 1987, Church *et al.* 2007).

Sound exposure

Sound exposure protocol: The sound exposure consisted of a 110dB SPL 14.8 kHz single tone delivered for 2 hours in a soundproof chamber (custom built). The tone was produced by a signal generator (Thurlby Thandar), amplified (custom built amplifier) and delivered to a loud speaker (RS model 250-211, RS components Ltd, Corby, UK)

housed in the lid of the soundproof chamber. 14.8kHz was chosen for a number of reasons: this frequency falls within the most sensitive part of the rat hearing range (Kelly and Masterton 1977); the soundproof chamber provided adequate insulation to prevent the leakage of the tone; using the current loudspeaker arrangement, the 14.8kHz tone was the only frequency that could be presented at 110dB SPL while still being relatively inaudible by experimenters observing the rat in the chamber. It must be noted that even with the attenuation provided by the chamber (approximately 60dB) a 50dB SPL tone at approximately 15kHz would be audible by humans, thus additional hearing protection (ear defenders or ear plugs) was used for animal observation.

The anesthetized animal, under neuroleptanalgesia (see Chapter 2), was placed directly below the loud speaker and was delivered oxygen (500ml flow rate) via a face mask for the duration of the exposure. The rat was under observation at all times and the sound exposure was stopped if the rat displayed any reflex startle response to the sound. Anaesthesia was maintained during the sound exposure to ensure that the animal remained directly under the loudspeaker and to reduce the distress of the animal. The experimental equipment set-up is shown in Fig. 4.3.

Calibration of the sound exposure: The sound exposure equipment was calibrated to ensure that the animal would be subjected to an average of 110dB SPL. The microphone (model 4134, Brüel and Kjær) connected to the signal analyser as used previously, was placed inside the soundproof chamber in several positions, analogous

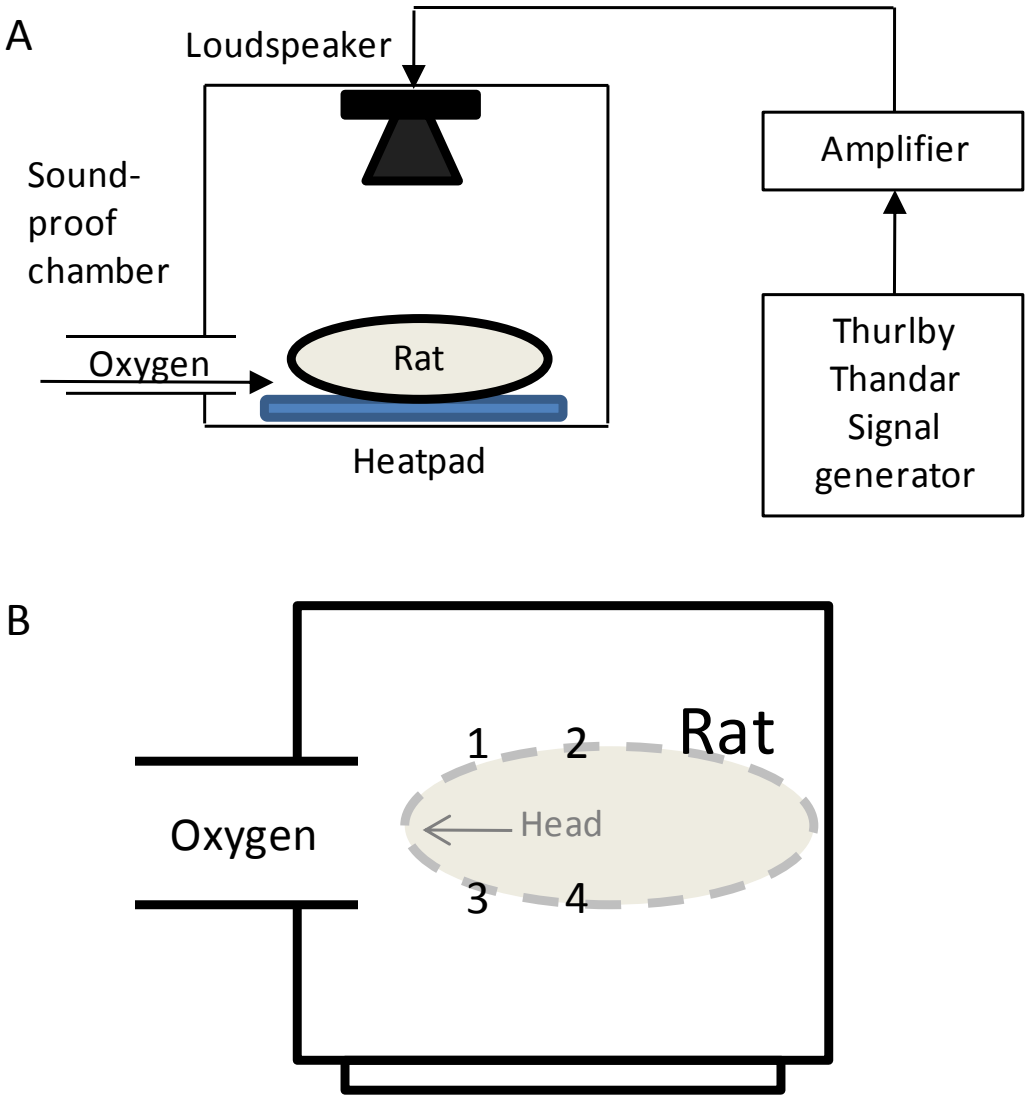

Fig. 4.3. Diagram representing the equipment and experimental set-up for the sound exposure protocol. (A) The rat was placed inside the sound-proof chamber with a loudspeaker housed in the lid. The constant tone was generated by the signal generator, amplified and delivered inside the chamber via the speaker. (B) A top-down view of the sound-proof chamber showing the position of the animal underneath the loudspeaker. The numbers refer to the positions of the microphone used to calibrate the sound to which the animal was exposed.

to where the head of the animal would be when placed in the enclosure. The average sound level in the region of the rat's head was 110dB SPL as shown in Table 4.3.

Position	Voltage (dB Vrms)	dB SPL
1	-17	114
2	-21	110
3	-21	110
4	-24	107
Average	-20.75	110.25

Table 4.3. Calibration of sound exposure chamber. Intensity of 14.8kHz tone generated in the soundproof exposure chamber at positions around the position of the animals head, positions indicated in Fig. 4.3.

Complete ABR and sound exposure regimen: The complete experimental regimen is described in Fig. 4.4. The experimental animals were divided into two groups: sound-exposed animals, which were exposed to the 110dB SPL 14.8kHz tone, and control animals, which were not exposed to sound. On day one, the animals to be exposed were anaesthetised, ABR tested, exposed to the intense sound and allowed to recover. This was repeated on day three. On day nine the animals were anaesthetised and had ABR recordings, were culled and tissues samples were taken. The control animals were treated to the same anaesthesia and ABR regimen but were not exposed to the intense sound.

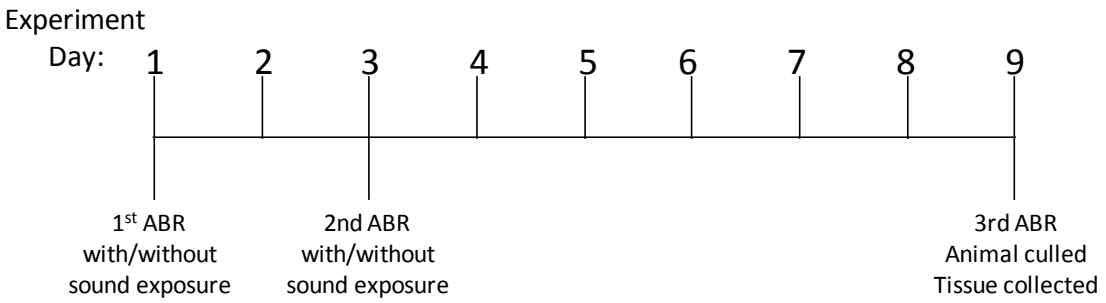

Fig. 4.4. Diagram of the ABR and sound exposure protocol. Representation of the complete ABR and sound exposure protocol. For an animal that is to be exposed to the sound stimulus: day one, the animal has an ABR measurement followed by 2 hours sound exposure; day three, the animal has an ABR measurement followed by 2 hours sound exposure; day nine, the animal has an ABR measurement, is culled at the end of ABR measurements and tissues collected. Control animals are subjected to the same protocol but without the sound exposures.

Data analysis

Statistical analysis was carried out with data entered into a Microsoft Office Excel 2007 spreadsheet. Comparison of ABR thresholds and wave amplitudes from the different data groups was performed using the one-tailed Students t-test. The one-tailed test was used as it was deemed logical that noise exposure would not cause an improvement in hearing function. Specifically the hypothesis was that noise exposure would elevate hearing thresholds. Using the one-tailed test increases the sensitivity in being able to detect a change in the specific direction. Analysis of ABR waveform latency was performed using the two-tailed Students t-test. Results are expressed as means ± SEM and the significance level was set at $p<0.05$ in all experiments.

Results

Unexposed rat ABR measurements

Example control animal hearing thresholds: The ABR waveforms across the tested frequencies from a typical control animal are shown in Fig. 4.5. The hearing threshold for the tested frequencies after the first ABR were (shown here and throughout in dB att, unless stated otherwise) 40dB across all frequencies tested. At the end of the protocol the hearing thresholds after the last ABR were unchanged for 12kHz and 30kHz, although an improvement in hearing threshold of 10dB was seen for 16kHz and 24kHz.

Average hearing threshold results: The average hearing threshold elevations, as well as the average hearing thresholds, from five control animals are presented in Fig. 4.6. There was no detectable increase in hearing threshold in the control, unexposed animals (Fig. 4.6A and B). There was however, a mean decrease (i.e. improvement) in hearing threshold for 16kHz and 24kHz of between 8-10 dB. By using an *a priori* directional one-tailed test these changes were not significant. However empirically, these data suggest modest directional variation in the baseline acoustic threshold at these tested frequencies. This may be attributable to the experimental design, but more importantly it provides clear evidence that the experimental and anaesthetic protocol were not causing a *worsening* of auditory function. The results obtained for ABR amplitude and latency for both P1 and N3 further support this (see below). No significant changes in these were apparent over all stimulus frequencies and intensities used.

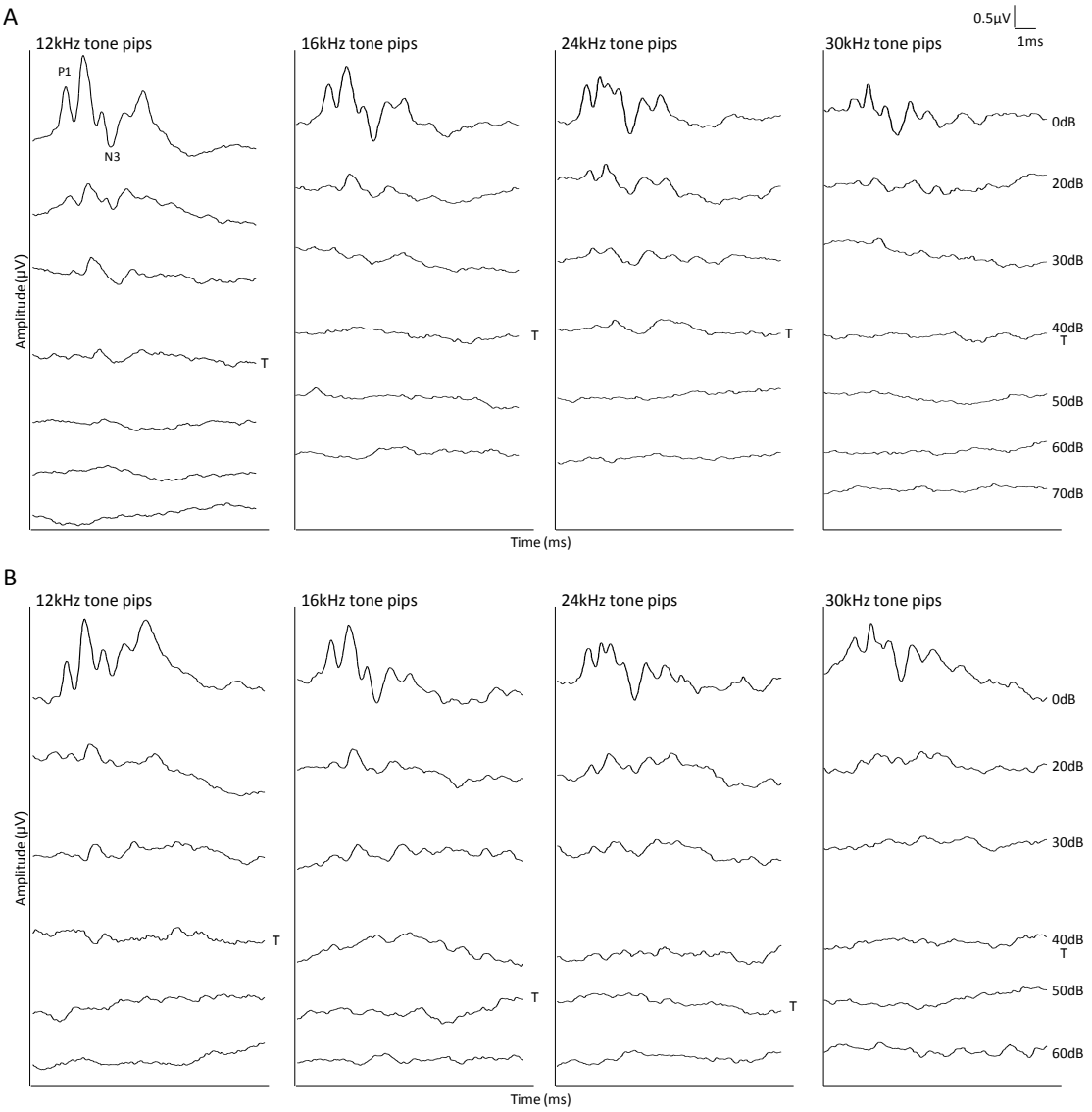

Fig. 4.5. ABR waveforms from an example unexposed animal. ABR waveforms from the first (A) and last (B) ABR from a control animal with each tested frequency and attenuation indicated on the traces. (A) Hearing thresholds for all tested frequencies were 40dB att (threshold indicated by T). (B) Hearing thresholds for 12kHz and 30kHz did not change following the repeated ABR protocols, while the thresholds for 16kHz and 24kHz decreased to 50dB att.

Control animal P1 amplitudes: The P1 amplitudes from the ABR waveforms elicited at 0dB att from the five control animals are shown in Fig. 4.7. The amplitude of P1 in response to the following tone pip frequencies ranged from 0.95±0.063µV to 0.53±0.081µV (Table 4.4). There was no significant difference between P1 amplitudes from the first and last ABR measurements in the control animals ($p>0.05$).

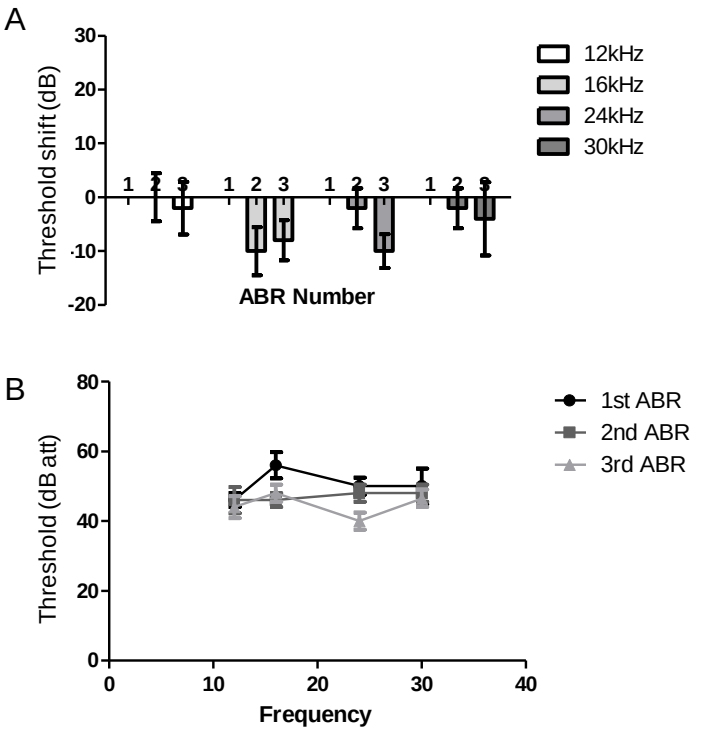

Fig. 4.6. Threshold elevation and hearing thresholds of control animals. Graphs of mean hearing threshold shifts (A) and hearing thresholds (B) of animals unexposed to sound. (A) Hearing thresholds did not increase across the tested frequencies over the repeated ABRs in the unexposed animals. (B) Hearing thresholds did not significantly increase across the tested frequencies over the repeated ABRs in the unexposed animals. Please note that for this and subsequent graphs that ABR number refers to each trial as described in Fig. 4.4.

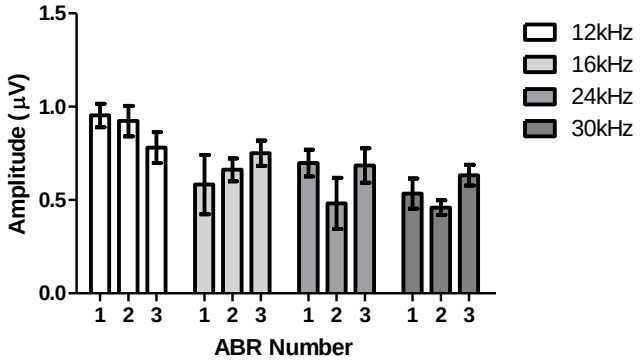

Fig. 4.7. P1 amplitude of control animals. Graphs of mean P1 amplitude of animals unexposed to noise. The P1 amplitude did not significantly change across the tested frequencies over the repeated ABRs in the unexposed animals. ($p>0.05$).

Tone pip frequency (kHz)	P1 amplitude (μV)	
	1st ABR	3rd ABR
12	0.95±0.063	0.78±0.082
16	0.58±0.16	0.75±0.068
24	0.70±0.071	0.69±0.091
30	0.53±0.081	0.63±0.055

Table 4.4. P1 amplitudes from control rats. The amplitude of wave 1 (P1) of the ABR measurements from specific frequency tone pips. No significant difference was detected between the P1 amplitudes from the first and final ABR measurements across all frequencies in the control rats.

The amplitude of P1 with reference to the attenuation of the tone pips at each tested frequency for the unexposed rats is shown in Fig 4.8. As the tone pips were attenuated the amplitude of P1 decreased for all frequencies tested. There appeared to be no alteration in P1 amplitude at the attenuation steps for each ABR for 16kHz and 30kHz upon visual inspection. On visual inspection there appeared to be a decrease in P1 amplitude during the second and third ABRs at 30dB att for the 12kHz and 24kHz tone pips compared to the first ABR measurement, although there was no statistical significant difference in these values ($p>0.05$). The average P1 amplitudes were fitted with a second order polynomial line of best fit, as this fit gave R^2 values (square of the correlation coefficient, with values close to 1 indicating good reliability or fit to the data) typically better than 0.9.. The equations of these fitted lines over the limited stimulus range were of the form:

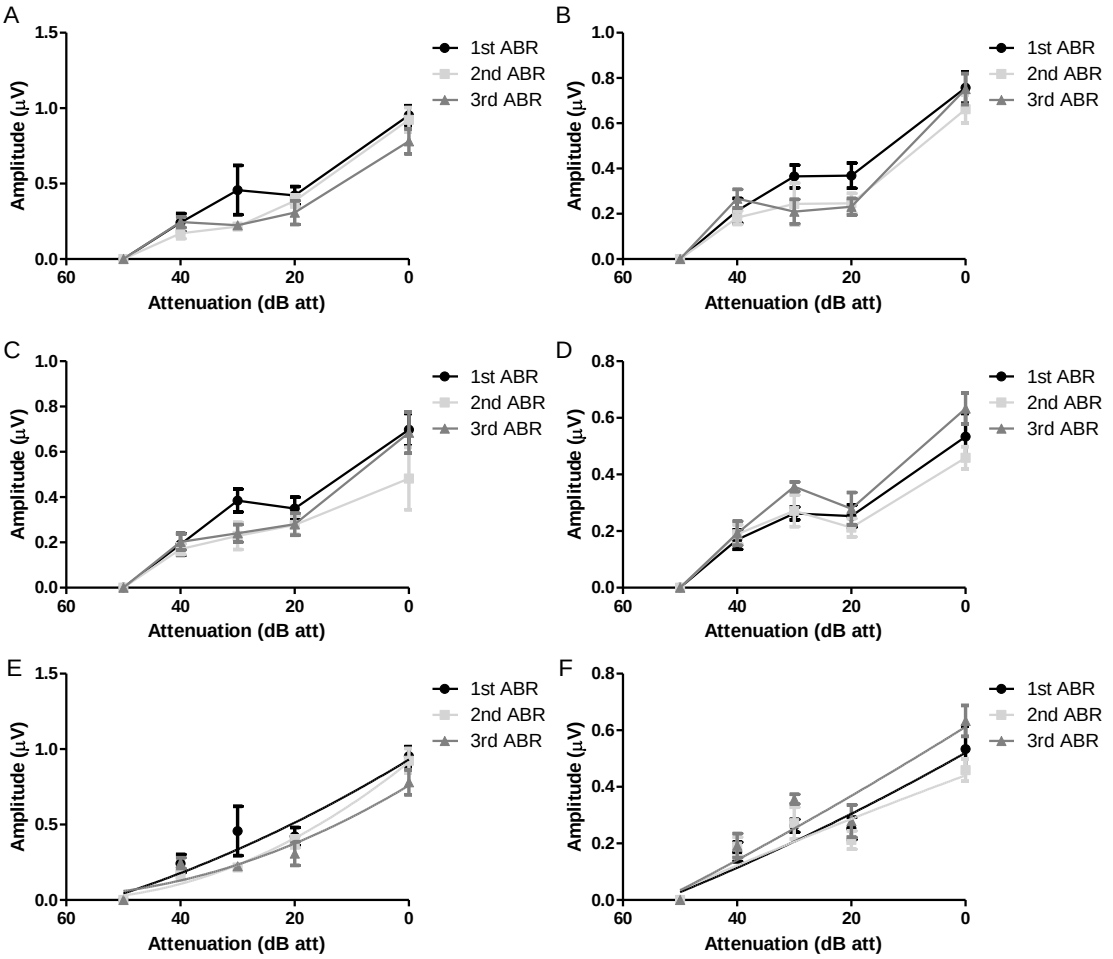

Fig. 4.8. Amplitude of P1 with regard to tone pip attenuation from unexposed rats. The mean amplitude of P1 in response to (A,E) 12kHz, (B) 16kHz, (C) 24kHz and (D,F) 30kHz tone pips for each set of ABR measurements from control rats. For each frequency tested, as the tone pips are attenuated the amplitude of P1 decreases. There was no significant difference between the P1 amplitudes from the ABR measurements at any attenuation in response to the tone pips across all frequencies ($p>0.05$). (E,F) Examples of the data shown in (A) and (D) fitted with a second order polynomial line of best fit. The equations for the lines in (E) and (F) are comparable.

$$y = lx^2 - mx + c$$

This was employed to establish where functional changes may have occurred in the cochlea amplifier. The value of *c* relates to the threshold or sensitivity of the cochlear amplifier, whilst both *l* and *m* relate to the gain function of the cochlear amplifier, By both direct visual and numerical comparison of the forms and their coefficients there was not considered to be any marked difference in these simplified transfer functions

between each ABR measurement across the tested frequencies (Table 4.5). This is taken as support that the sensitivity of the cochlear amplifier, integrity and physiological function of the amplifier remained largely unaffected by the anaesthesia protocol.

Frequency (kHz)	ABR number	Value of		
		I	***m***	***C***
12	1	0.0003	0.031	0.94
	2	0.0002	0.028	0.91
	3	0.0002	0.023	0.76
16	1	0.0002	0.025	0.75
	2	0.0003	0.028	0.66
	3	0.0004	0.032	0.73
24	1	$9x10^{-5}$	0.018	0.69
	2	0.0001	0.016	0.49
	3	0.0003	0.028	0.68
30	1	0.0002	0.020	0.54
	2	0.0002	0.017	0.46
	3	0.0003	0.025	0.63

Table 4.5. Line of best fit equation values for control animal P1 amplitude with attenuation. In this case *I* and *m* refers to the gain and *c* relates to the threshold or sensitivity of the cochlear amplifier.

Control animal P1 latency: Fig. 4.9A shows the average P1 latency at 0dB att from the unexposed rats. The time to the peak of P1 during the first ABR measurements ranged between 1.38±0.042ms and 1.52±0.047ms across the tested frequencies (Table 4.6). There appeared to be some variation in the latency at 24kHz and 30kHz, although statistical significance was not reached when comparing the latency of P1 during the second and final ABR to the data from the first recordings (p>0.05).

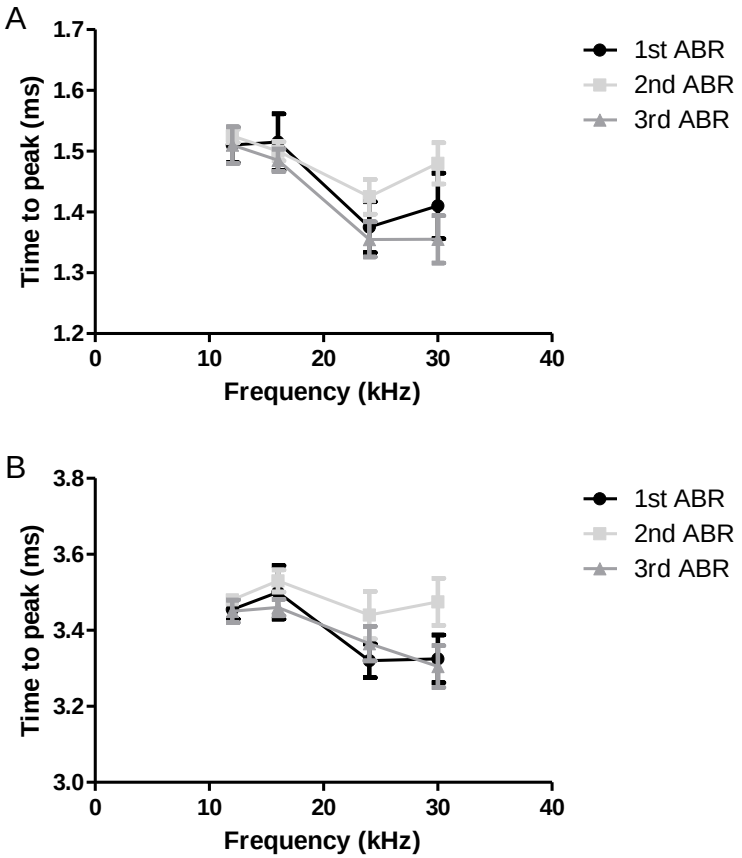

Fig. 4.9. Latency of P1 and N3 from control rats. Graphs showing the time to peak of P1 (A) and N3 (B) from control rats. No significant change in the latency of P1 or N3 was detected in the control animals (p>0.05).

Tone pip frequency (kHz)	P1 time to peak (ms)	
	1st ABR	3rd ABR
12	1.51±0.029	1.51±0.030
16	1.52±0.047	1.49±0.019
24	1.38±0.042	1.36±0.029
30	1.41±0.054	1.36±0.040

Table 4.6. P1 latencies from control rats. The time to the peak of wave 1 (P1) of the ABR measurements from specific frequency tone pips. No significant difference was detected between the P1 latencies from the first and final ABR measurements across all frequencies in the control rats ($p>0.05$).

Fig. 4.10 shows the average P1 latency from the unexposed rats with reference to the attenuation of the tone pip for the tested frequencies. As the tone pips were attenuated the time to the peak of P1 increased across all frequencies tested. Upon visual inspection, there appeared to be no difference in the latency of P1 at each attenuation step between each ABR measurement for each frequency tested, and there was no significant difference between these latencies ($p>0.05$). The mean data for all attenuation steps were fitted with a line of best fit, as for the amplitude data, to give a simplified estimate of temporal processing. The overall form for the control P1 latency was:

$$y = lx^2 + mx + C$$

The equation overall describes the temporal processing related to stimulus intensity in dB attenuation. The term lx^2+mx described the increased latency and therefore travel

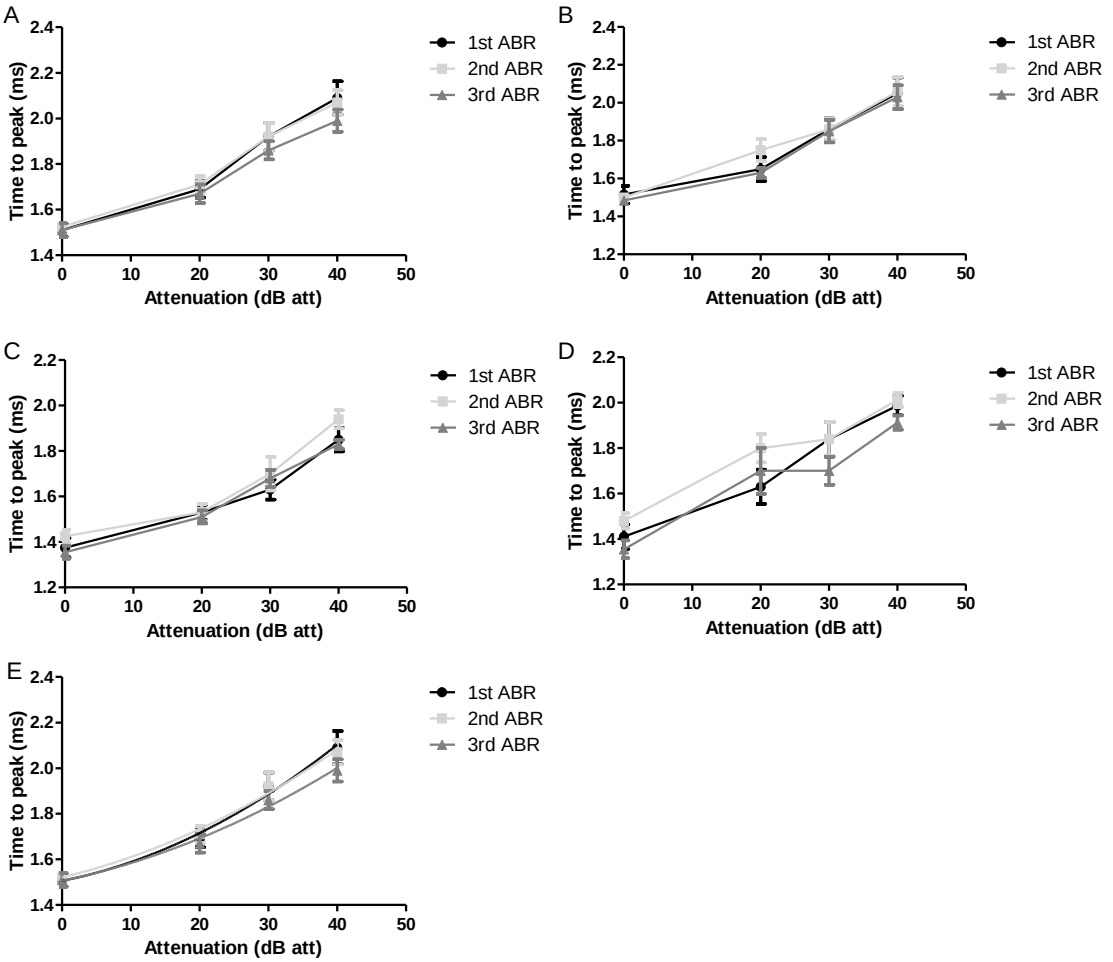

Fig. 4.10. Latency of P1 with regard to tone pip attenuation from unexposed rats. The mean latency of P1 in response to (A,E) 12kHz, (B) 16kHz, (C) 24kHz and (D) 30kHz tone pips for each set of ABR measurements from control rats. For each frequency tested, as the tone pips are attenuated the time to the peak of P1 decreases. There was no significant difference between the P1 latency from the ABR measurements at any attenuation in response to the tone pips across all frequencies ($p>0.05$). (E) Examples of the data shown in (A) and (D) fitted with a second order polynomial line of best fit. The equations for the lines in (E) are comparable.

and processing time of the P1 wave for stimuli below 0dB att (Salvi *et al.* 1979b). The *C* term here is considered to reflect the value or near value of the absolute refractory properties of the ensemble excitable channels in the stimulated neurons of the cochlear nerve (Church *et al.* 2007).

No radical differences in the magnitude of *l*, *m* and *C* were seen in the equations describing latency over the three measurement sessions (Table 4.7). This supports the contention that the anaesthesia or surgical procedure had not affected temporal processing of the cochlea to transduce sound stimuli over the range delivered.

Frequency (kHz)	ABR number	Value of		
		l	***m***	***C***
12	1	$2x10^{-5}$	0.021	1.50
	2	$9x10^{-5}$	0.021	1.52
	3	$7x10^{-5}$	0.019	1.51
16	1	0.0001	0.014	1.51
	2	0.0001	0.022	1.51
	3	$9x10^{-5}$	0.016	1.48
24	1	0.0002	0.010	1.38
	2	0.0004	0.0053	1.43
	3	$1x10^{-5}$	0.016	1.35
30	1	0.0002	0.025	1.41
	2	0.0004	0.027	1.50
	3	0.0003	0.027	1.38

Table 4.7. Line of best fit equation values for control animal P1 latency with attenuation. In this case *l* and *m* are the coefficient of the travel and processing time of the P1 wave and *C* is a relative measure of the absolute refractory period of the cochlear nerve.

Control animal N3 latency: In addition to the time to peak of P1, the time to the prominent negative deflection termed N3 was also measured. The average N3 latencies from the control rats are shown in Fig. 4.9B at 0 dB att. During the first ABR recording the time to the peak of this component ranged from 3.32±0.044ms to 3.50±0.070ms across the tested frequencies (Table 4.8). Although there appeared to be some variation in the latency at 24kHz and 30kHz, statistical significance was not reached when comparing the latency of P1 during the second and final ABR to the data from the first recordings ($p>0.05$).

Tone pip frequency (kHz)	Time to peak (ms)	
	1st ABR	3rd ABR
12	3.46±0.026	3.45±0.030
16	3.50±0.070	3.46±0.022
24	3.32±0.044	3.37±0.045
30	3.33±0.063	3.31±0.055

Table 4.8. N3 latencies from control rats. The time to the peak of wave N3 of the ABR measurements from specific frequency tone pips. No significant difference was detected between the N3 latencies from the first and final ABR measurements across all frequencies in the control rats ($p>0.05$).

Fig. 4.11 shows the average N3 latency from the unexposed rats with reference to the attenuation of the tone pip for the tested frequencies. As the tone pips were attenuated the time to the maximum deflection of N3 increased across all frequencies tested. Upon visual inspection, there appeared to be no differences in the mean latency of N3 at each attenuation step between each ABR measurement for each

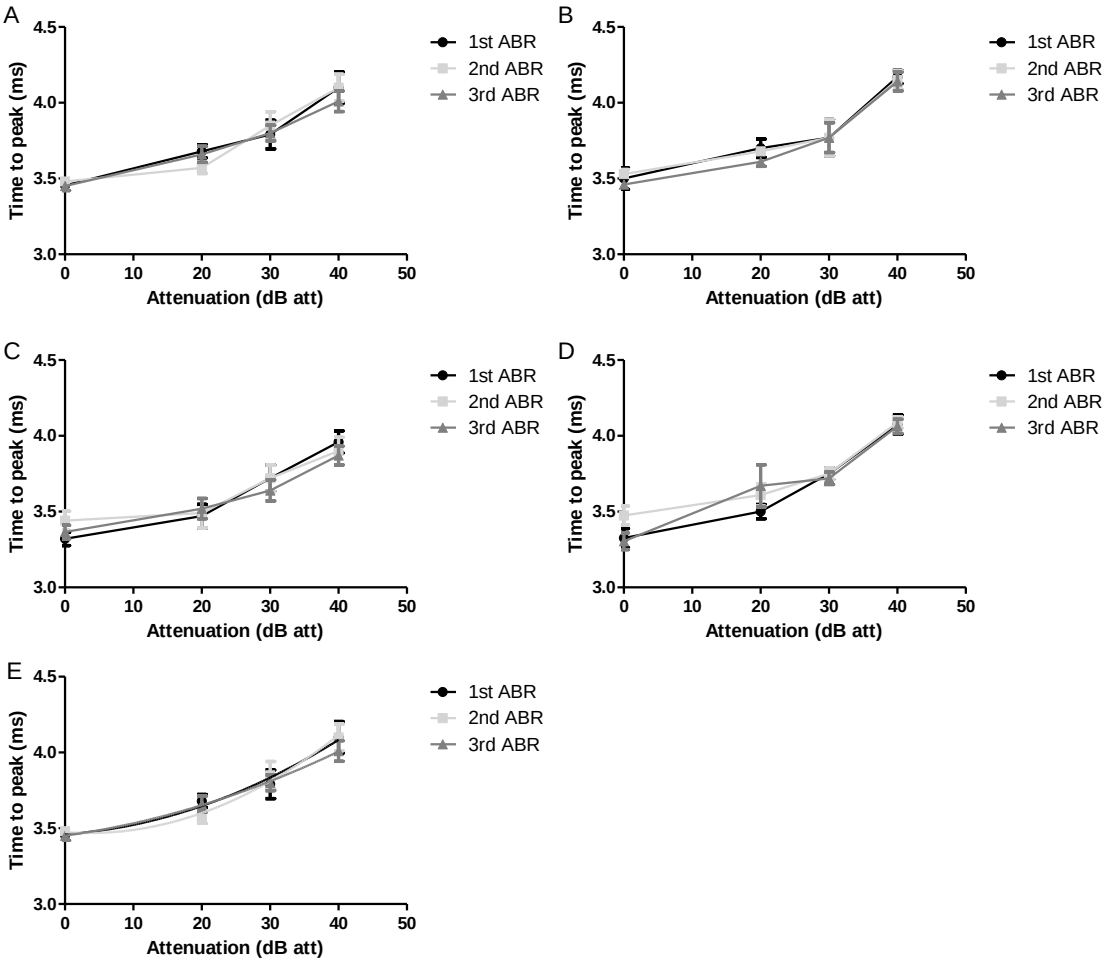

Fig. 4.11. Latency of N3 with regard to tone pip attenuation from unexposed rats. The mean latency of N3 in response to (A,E) 12kHz, (B) 16kHz, (C) 24kHz and (D) 30kHz tone pips for each set of ABR measurements from control rats. For each frequency tested, as the tone pips are attenuated the time to the peak of N3 decreases. There was no significant difference between the N3 latency from the ABR measurements at any attenuation in response to the tone pips across all frequencies ($p>0.05$). (E) Example of the data shown in (A) and fitted with a second order polynomial line of best fit. The equations for the lines in (E) are comparable.

frequency tested, and statistical significance was not reached ($p>0.05$) in all cases. The mean latency data from each ABR was fitted with a line of best fit, as for P1 latency, to provide a simplified transfer function of temporal processing involved from the level of the cochlea through to the SOC (Church *et al*, 2007). Again no differences were seen in the magnitude of the components of these simple fitted equations for each ABR measurement (Table 4.9). This indicates that the temporal processing of the auditory

pathway has not been disrupted by the anaesthesia or experimental protocol in the auditory pathway up to the level of the SOC (Church *et al.* 2007).

Frequency (kHz)	ABR number	Value of		
		l	***m***	***c***
12	1	0.0002	0.014	3.47
	2	0.0004	0.0094	3.47
	3	$2x10^{-17}$	0.018	3.46
16	1	0.0005	0.0058	3.52
	2	0.0006	0.0022	3.55
	3	0.0006	0.0055	3.47
24	1	0.0002	0.015	3.31
	2	0.0003	0.0063	3.43
	3	0.0002	0.011	3.37
30	1	0.0004	0.014	3.33
	2	0.0005	0.0046	3.48
	3	$6x10^{-5}$	0.025	3.34

Table 4.9. Line of best fit equation values for control animal N3 latency with attenuation. In this case *l* and *m* are the coefficient of the travel and processing time of the N3 wave and *C* is a relative measure of the absolute refractory period of the neurons within the auditory brainstem.

Sound-exposed rat ABR measurements

Example sound-exposed animal: The ABR waveforms from a sound-exposed animal are shown in Fig. 4.12. The detected hearing thresholds for this rat after the first ABR were

60dB across all tested frequencies. At the end of the protocol, 6 days after the final sound exposure, the hearing thresholds measured during the final ABR were unchanged for 12kHz and 16kHz. An elevation of 10dB was detected for 24kHz, while an increase of 20dB was noted for 30kHz.

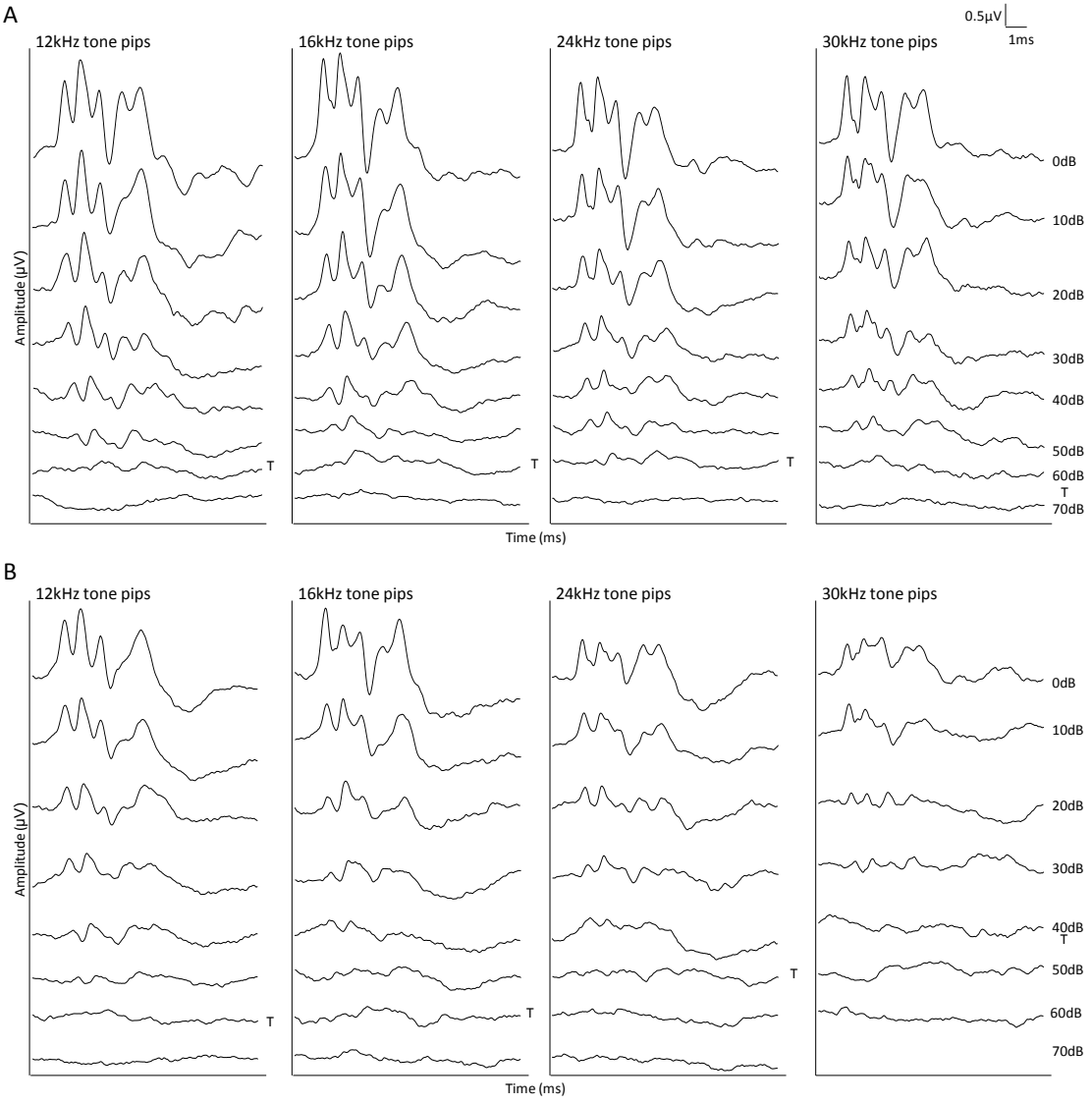

Fig. 4.12. ABR waveforms from an animal exposed to the sound exposure protocol. ABR waveforms from the first (A) and last (B) ABR from a sound-exposed animal with each tested frequency and attenuation indicated on the traces. (A) Hearing thresholds for all tested frequencies were 60dB att (threshold indicated by T). (B) Hearing thresholds for the 12kHz and 16kHz tone pips did not change following the repeated sound exposure and ABR protocol, while the thresholds for 24kHz increased to 50dB att and 30kHz increased to 40dB att. Additionally, a visible decrease in waveform amplitude can be seen following sound exposure for the 24kHz and 30kHz tone pips.

Average sound-exposed hearing thresholds: The average hearing threshold elevations, as well as the average hearing thresholds (in dB att), from eight sound-exposed rats are shown in Fig. 4.13. Following the complete sound exposure protocol, there was no detectable increase in the average hearing threshold at 12kHz. A modestly significant average increase of 6±3dB ($p<0.05$) was seen for the hearing threshold at 16kHz following the complete sound exposure protocol. Significant increases in hearing threshold at 24kHz and 30kHz were observed following the first sound exposure, with an increase in hearing threshold of 10±4dB ($p<0.05$) and 13±3dB ($p<0.005$) respectively. There was further increase in mean ABR threshold following the second sound exposure at 24kHz and 30kHz, of 18±4dB ($p<0.005$) and 24±3dB ($p<0.001$) respectively.

Sound-exposed animal P1 amplitudes: Fig. 4.14 shows the average P1 amplitudes from eight sound-exposed animals in response to tone pips at 0dB att. The P1 amplitudes ranged from 0.93±0.12μV to 0.68±0.13μV (Table 4.10). The P1 amplitudes in response to the 12kHz and 16kHz tone pips were not significantly different following the complete sound exposure protocol ($p>0.05$). However, testing the 24kHz and 30kHz hearing ranges of these animals revealed a significant decrease in P1 amplitude following the final ABR when compared to the first ABR measurements. The average P1 amplitudes generated at both 24kHz and 30kHz decreased by about 35% ($p<0.05$-0.01).

The amplitude of P1 with reference to the attenuation of the tone pips at each tested frequency for the sound-exposed rats was measured and is shown in Fig 4.15. As the

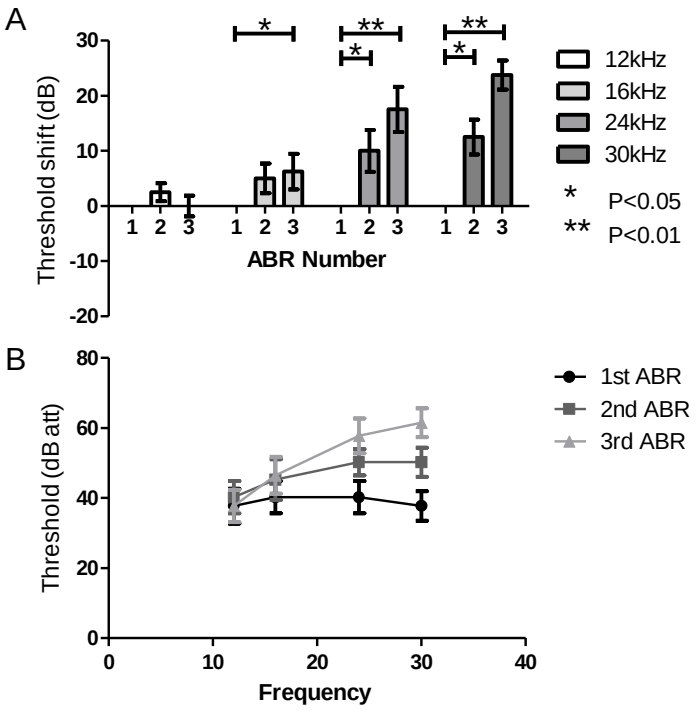

Fig. 4.13. Threshold elevation and hearing thresholds of sound-exposed animals. Graphs of mean hearing threshold shifts (A) and hearing thresholds (B) of animals exposed to sound. (A) Hearing threshold for the 24kHz and 30kHz tone pips significantly increased during the second and third ABRs, following sound exposure. A significant increase in hearing threshold for 16kHz was only detected during the third ABR, after two sound exposures, while the hearing threshold for 12kHz remained unaffected. (D) Hearing threshold for the 24kHz and 30kHz tone pips significantly increased following sound exposure compared to the threshold before sound exposure. A significant increase in hearing threshold for 16kHz was only detected during the third ABR, though the increase was smaller than the elevation seen for 24kHz and 30kHz. The hearing threshold for 12kHz remained unaffected following the complete protocol. Please note that ABR number refers to each trial as described in Fig. 4.4.

tone pips were attenuated the amplitude of P1 decreased for all frequencies tested. On visual inspection there appeared to be no alteration in P1 amplitudes at the attenuation steps for both 12kHz and 16kHz over three ABR measurements. There appeared to be a *decrease* in P1 amplitude during the second and third ABRs at several attenuation steps for the 24kHz and 30kHz tone pips compared to the first ABR measurement, with these decreases reaching significance at $p<0.05$. The average P1

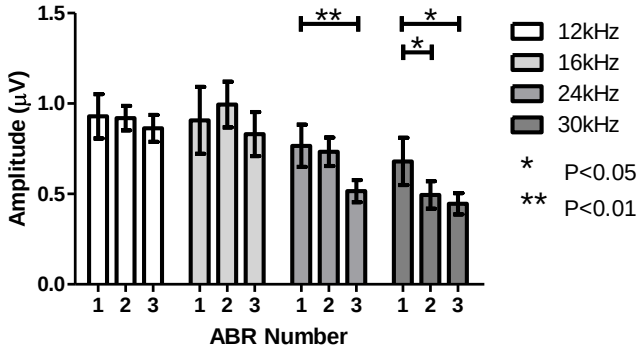

Fig. 4.14. P1 amplitude of sound-exposed animals. Graphs of mean P1 amplitude of animals exposed to noise. P1 amplitude decreased significantly after noise exposure for the 24kHz and 30kHz evoked responses, while the amplitude did not significantly change the lower frequencies tested.

Tone pip frequency (kHz)	P1 amplitude (μV)	
	1st ABR	3rd ABR
12	0.93±0.12	0.86±0.074
16	0.91±0.18	0.83±0.12
24	0.77±0.11	0.52±0.061**
30	0.68±0.13	0.45±0.059*

Table 4.10. P1 amplitudes from noise-exposed rats. The amplitude of wave 1 (P1) of the ABR measurements from specific frequency tone pips. No significant difference was detected between the P1 amplitudes from the first and final ABR measurements at 12kHz and 30kHz ($p>0.05$). A significant decrease in P1 amplitude was detected between the first and final ABR measurement at 24kHz (** $p<0.01$) and 30kHz (* $p<0.05$).

amplitudes forming the simple transfer function were fitted with a second order polynomial line of best fit for each frequency. The equations of these fitted lines over the limited stimulus range were of the form used previously (for P1 amplitude in

control animals). This was employed to establish where functional changes may have occurred in the cochlea amplifier. Again, the value of *c* relates to the threshold or sensitivity of the cochlear amplifier whilst *l* and *m* relates to the gain function of the cochlear amplifier.

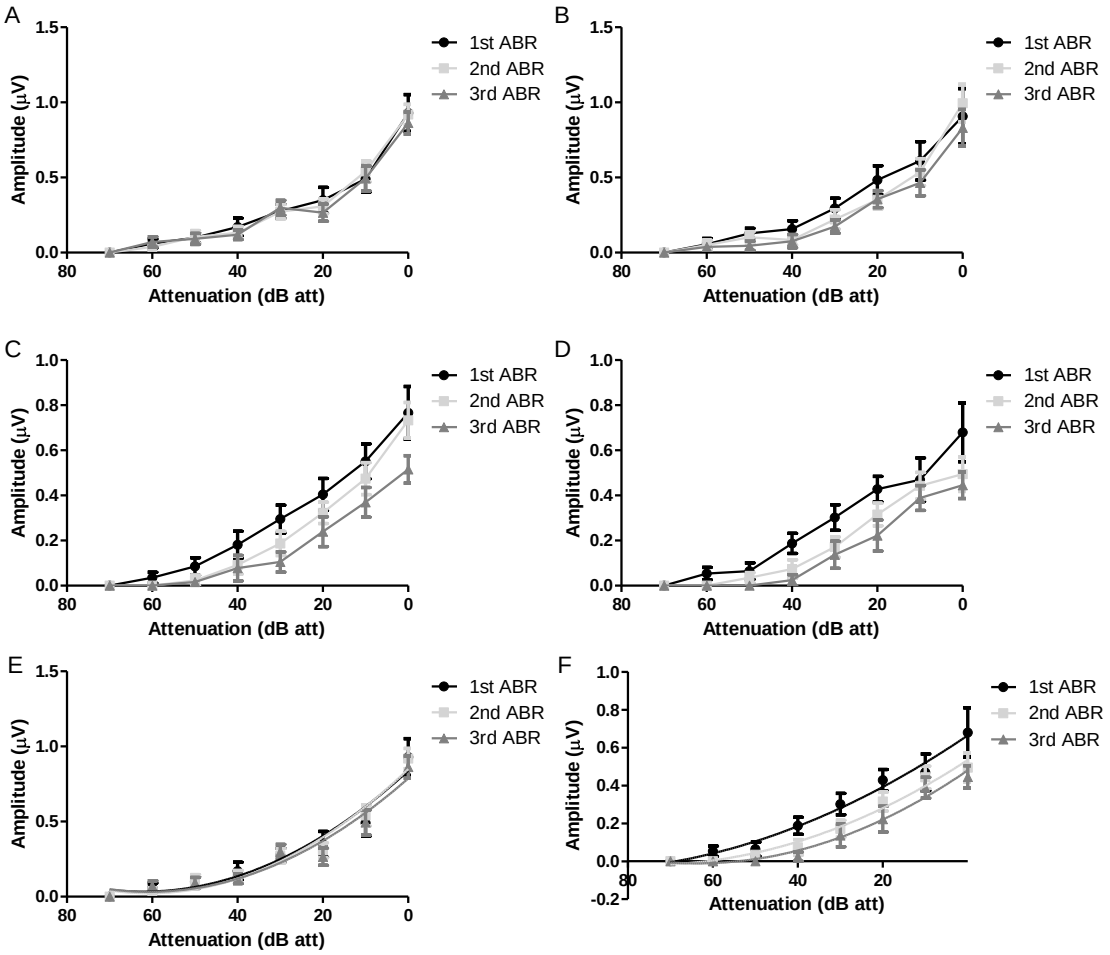

Fig. 4.15. Amplitude of P1 with regard to tone pip attenuation from sound-exposed rats. The mean amplitude of P1 in response to (A,E) 12kHz, (B) 16kHz, (C) 24kHz and (D,F) 30kHz tone pips for each set of ABR measurements. For each frequency tested, as the tone pips are attenuated the amplitude of P1 decreases. There was no significant difference between the P1 amplitudes from the ABR measurements at any attenuation in response to the 12kHz and 16kHz tone pips. However, significant decreases in P1 amplitude in comparison to the 1st ABR were observed during the second and final ABR experiments in response to the 24kHz and 30kHz tone pips ($p<0.05$). (E,F) Examples of the data shown in (A) and (D) fitted with a second order polynomial line of best fit. The equations for the lines in (E) are comparable, while the equations for the lines in (F) only differ with a reduction of the value of *c*.

Frequency (kHz)	ABR number	Value of		
		l	*m*	*c*
12	1	0.0002	0.026	0.84
	2	0.0002	0.027	0.85
	3	0.0002	0.025	0.79
16	1	0.0002	0.025	0.88
	2	0.0003	0.032	0.91
	3	0.0002	0.027	0.78
24	1	0.0001	0.020	0.75
	2	0.002	0.023	0.72
	3	0.0001	0.017	0.52
30	1	$8x10^{-5}$	0.015	0.66
	2	0.0001	0.015	0.54
	3	0.0001	0.015	0.48

Table 4.11. Line of best fit equation values for sound-exposed animal P1 amplitude with attenuation. In this case *l* and *m* refers to the gain and *c* relates to the threshold or sensitivity of the cochlear amplifier.

Visual inspection showed no dramatic changes in the gradients of these fitted lines at all frequencies. There was no difference detected in the equations of the simplified transfer function between each ABR measurement for the 12kHz and 16kHz frequencies (Table 4.11). For 24kHz and 30kHz a decrease in the value of *c* of 0.25 and 0.18, respectively, was returned. This was consistent with the elevations in ABR

threshold. However as can be seen from Fig. 4.15 and Table 4.11, with these simplified transfer functions the general values of *l* and *m* do not appear to change drastically. Interpretation of this analysis is that the sensitivity of the cochlear amplifier was affected but the integrity and physiological function of the amplifier remained largely unaffected by the noise exposure.

Sound-exposed animal P1 latency: Fig. 4.16A shows the average P1 latency from the sound-exposed rats at 0dB att. The time to the peak of P1 during the first ABR measurements ranged between 1.29±0.030ms and 1.48±0.037ms across the tested frequencies (Table 4.12). Following the sound exposure protocol, there was no statistically significant difference in the latency of P1 during the final ABR when compared to the data from the first recordings ($p>0.05$).

Fig. 4.17 shows the average P1 latency from the sound-exposed rats with reference to the attenuation of the tone pip for the tested frequencies. As the tone pips were attenuated the time to the peak of P1 increased across all frequencies tested. Upon visual inspection, there appeared to be no difference in the latency of P1 at each attenuation step between each ABR measurement for each frequency tested, and there was no significant difference between these latencies ($p>0.05$). The data from each ABR was fitted with a second order polynomial line of best fit, of the same form as used previously in the control animals to give a simplified account of temporal processing. No difference was detected in the magnitude of the equation components (Table 4.13), indicating that the ototrauma had not damaged the ability of the cochlea to transduce the sound stimuli.

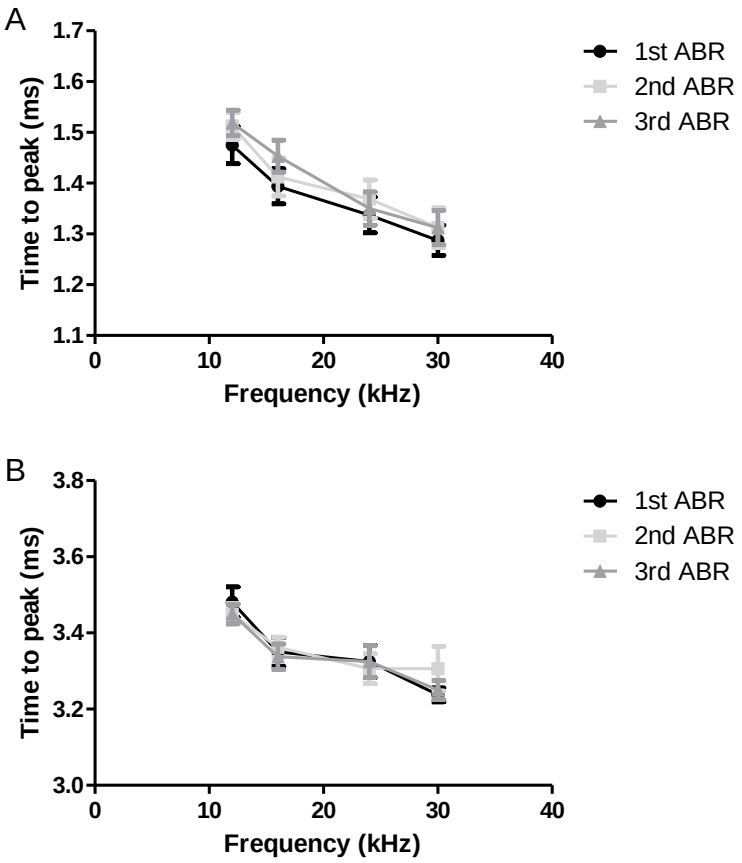

Fig. 4.16. Latency of P1 and N3 from sound-exposed rats. Graphs showing the time to peak of P1 (A) and N3 (B) from sound-exposed rats. No significant change in the latency of P1 or N3 was detected in these animals ($p>0.05$).

Tone pip frequency (kHz)	P1 time to peak (ms)	
	1st ABR	3rd ABR
12	1.48±0.037	1.52±0.025
16	1.40±0.035	1.45±0.031
24	1.34±0.035	1.35±0.033
30	1.29±0.030	1.31±0.034

Table 4.12. P1 latencies from sound-exposed rats. The time to the peak of wave 1 (P1) of the ABR measurements from specific frequency tone pips. No significant difference was detected between the P1 latencies from the first and final ABR measurements across all frequencies in the rats exposed to sound ($p>0.05$).

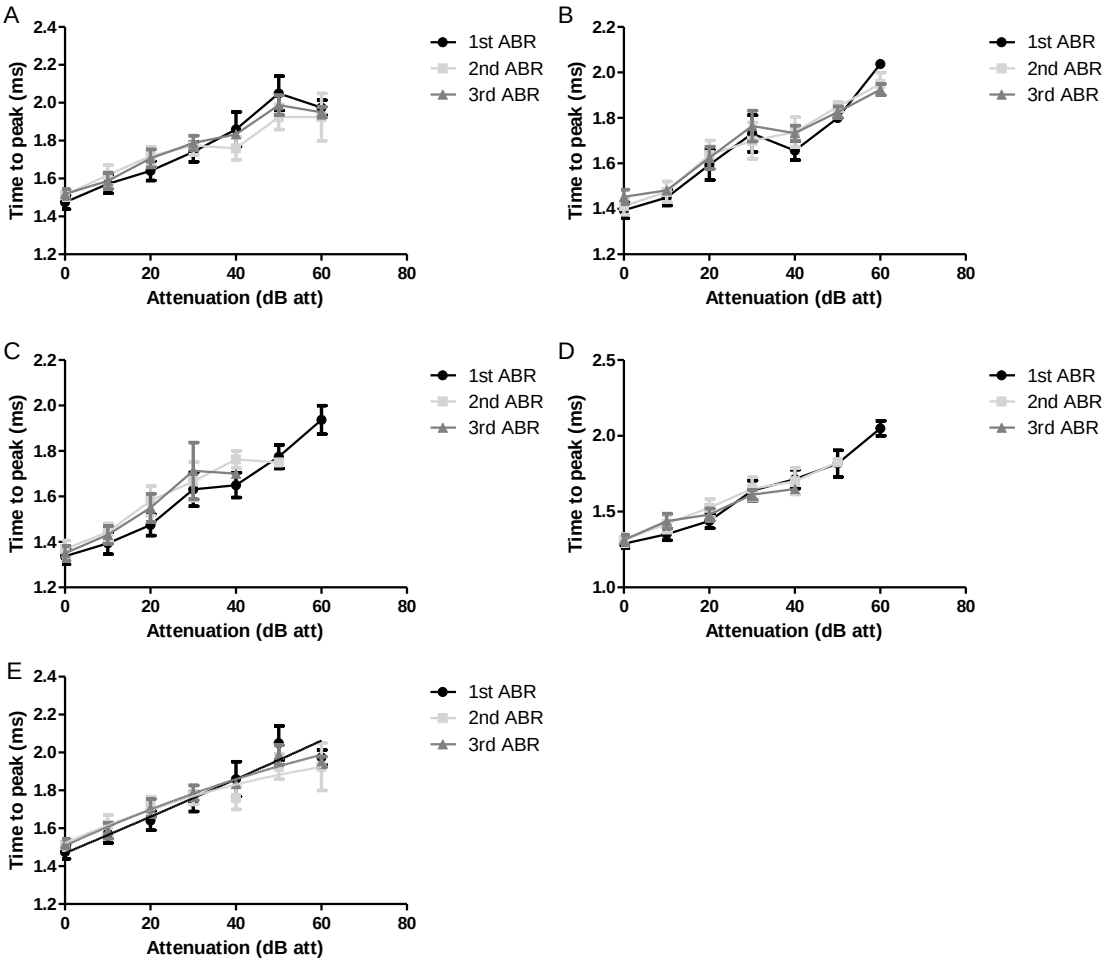

Fig. 4.17. Latency of P1 with regard to tone pip attenuation from sound-exposed rats. The mean latency of P1 in response to (A,E) 12kHz, (B) 16kHz, (C) 24kHz and (D) 30kHz tone pips for each set of ABR measurements from sound-exposed rats. For each frequency tested, as the tone pips are attenuated the time to the peak of P1 decreases. There was no significant difference between the P1 latency from the ABR measurements at any attenuation in response to the tone pips across all frequencies ($p>0.05$). (E) Example of the data shown in (A) fitted with a second order polynomial line of best fit. The equations for the lines in (E) are comparable.

Frequency (kHz)	ABR number	Value of		
		l	*m*	*C*
12	1	$3x10^{-5}$	0.011	1.46
	2	$4x10^{-5}$	0.0092	1.52
	3	$5x10^{-5}$	0.011	1.50
16	1	$6x10^{-5}$	0.0062	1.41
	2	$1x10^{-5}$	0.0096	1.41
	3	$3x10^{-5}$	0.0096	1.44
24	1	$2x10^{-5}$	0.0081	1.33
	2	0.0001	0.014	1.35
	3	0.0001	0.014	1.33
30	1	$3x10^{-5}$	0.0099	1.27
	2	$2x10^{-5}$	0.011	1.31
	3	$6x10^{-5}$	0.011	1.32

Table 4.13. Line of best fit equation values for sound-exposed animal P1 latency with attenuation. In this case *l* and *m* are the coefficient of the travel and processing time of the P1 wave and *C* is a relative measure of the absolute refractory period of the cochlear nerve.

Sound-exposed animal N3 latency: The average N3 latencies from the sound-exposed rats are shown in Fig. 4.16B. The time to the peak of this wave component ranged from 3.41±0.022ms to 3.52±0.016ms during the first ABR measurement (Table 4.14). Following the sound exposure protocol, there was no significant change in the latency

Tone pip frequency (kHz)	Time to peak (ms)	
	1st ABR	3rd ABR
12	3.52±0.016	3.48±0.043
16	3.48±0.034	3.43±0.042
24	3.41±0.022	3.40±0.039
30	3.43±0.027	3.33±0.051

Table 4.14. N3 latencies from sound-exposed rats. The time to the peak of wave N3 of the ABR measurements from specific frequency tone pips. No significant difference was detected between the N3 latencies from the first and final ABR measurements across all frequencies in the rats exposed to sound ($p>0.05$).

of this ABR component when comparing the final ABR measurements to the data from the first recordings ($p>0.05$).

Fig. 4.18 shows the average N3 latency from the sound-exposed rats with reference to the attenuation of the tone pip for the tested frequencies. As the tone pips were attenuated the time to the maximum deflection of N3 increased across all frequencies tested. Upon visual inspection, there appeared to be no difference in the latency of N3 at each attenuation step between each ABR measurement for each frequency tested, and there was no statistical significant difference found between these latencies ($p>0.05$). As before, the data from each ABR was fitted with a line of best fit, with no difference detected in the magnitude of the fitted equation components for each ABR measurement (Table 4.15). This indicates that the temporal processing of the auditory pathway at a level up to the SOC has not been disrupted by the ototrauma protocol.

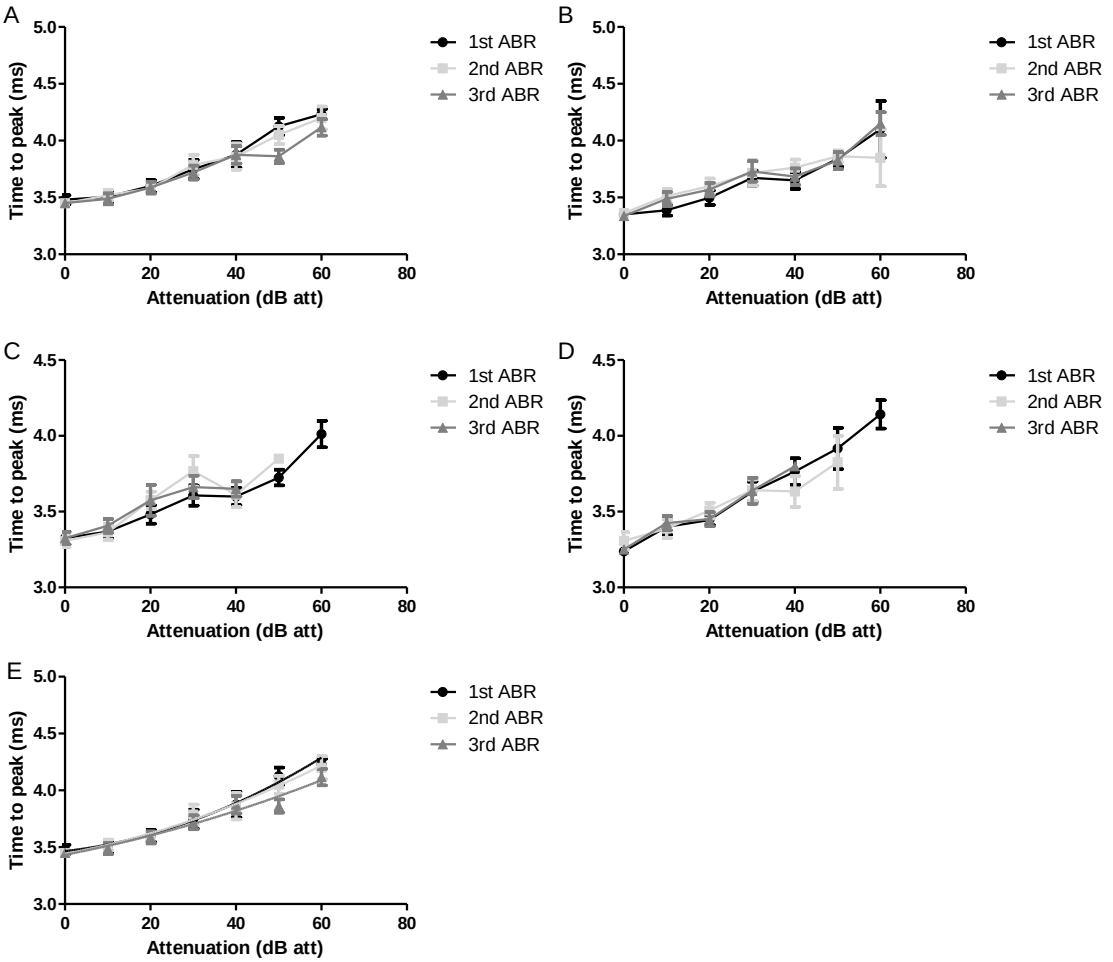

Fig. 4.18. Latency of N3 with regard to tone pip attenuation from sound-exposed rats. The mean latency of N3 in response to (A,E) 12kHz, (B) 16kHz, (C) 24kHz and (D) 30kHz tone pips for each set of ABR measurements from sound-exposed rats. For each frequency tested, as the tone pips are attenuated the time to the peak of N3 decreases. There was no significant difference between the N3 latency from the ABR measurements at any attenuation in response to the tone pips across all frequencies ($p>0.05$). (E) Example of the data shown in (A) and fitted with a second order polynomial line of best fit. The equations for the lines in (E) are comparable.

Frequency (kHz)	ABR number	Value of		
		l	*m*	*C*
12	1	0.0001	0.0052	3.46
	2	$9x10^{-5}$	0.0073	3.44
	3	$7x10^{-5}$	0.0068	3.44
16	1	0.0001	0.0038	3.35
	2	0.0001	0.015	3.36
	3	$9x10^{-5}$	0.006	3.38
24	1	$1x10^{-5}$	0.0087	3.31
	2	0.0001	0.016	3.28
	3	0.0002	0.018	3.30
30	1	$5x10^{-5}$	0.011	3.25
	2	$8x10^{-6}$	0.0095	3.31
	3	0.0001	0.0092	3.27

Table 4.15. Line of best fit equation values for sound-exposed animal N3 latency with attenuation. In this case *l* and *m* are the coefficient of the travel and processing time of the P1 wave and *C* is a relative measure of the absolute refractory period of the auditory brainstem.

Discussion

The primary aim of this study was to develop a robust model of moderate hearing loss in rats. The degree of auditory deficit following exposure was assessed by frequency specific ABR measurements and comparison of hearing threshold as well as ABR waveform amplitude and latency to pre-exposure levels. These could then be further correlated with any changes observed in voltage-gated Na^+ channel expression. The results presented in this chapter have shown that the moderate ototrauma model produces mild but significant hearing threshold elevation, but with no accompanying dramatic changes in the gradient of cochlear gain function or the temporal processing of both the cochlea and the lower half of the auditory brainstem nuclei. This means that any changes seen in voltage-gated Na^+ channel expression were not related to profound loss of cochlear function.

Anaesthesia does not affect ABR measurement

In order to ascertain that the anaesthesia regimen used in this protocol did not adversely modify the ABR results, animals exposed to the same anaesthesia and ABR protocol but which were not exposed to sound were used as the control group. These results show that there was no increase in the hearing threshold and no significant decrease in the P1 amplitude across all tested frequencies for this experimental group.

Additionally, as the frequency of the tone pip stimulus was increased, the time to the peak of the ABR waveforms shortened, due to the higher frequencies activating the hair cells at the more basal regions of the basilar membrane and resulting in a shorter time for the travelling wave to stimulate the appropriate regions of the cochlea

(Church and Kaltenbach 1993). Additionally, as the tone pip stimulus was attenuated the latency of the ABR waveforms increased, which has been reported previously (Salvi *et al.* 1979a, Church and Kaltenbach 1993). While the average P1 and N3 latencies at 0dB att showed some variation across the frequencies tested, there was no significant increase or decrease between the three ABR sessions. The variation observed (Fig. 4.9) is likely due to animal variability and experimental error, exacerbated by the relatively low n number rather than any alteration in auditory processing. Further indication that this variation is not due to altered cochlear function is the low variation seen in the same measurements from the sound-exposed rats (Fig. 4.16).

This shows that the combination of Hypnorm with midazolam was suitable for anesthetizing the rats to generate ABR measurements. This is in contrast to the effects of other anaesthetic agents which have been shown to decrease the amplitude and increase the latency of the ABR waveform components, such as phenobarbital (Shapiro *et al.* 1984), ketamine (Church and Gritzke 1987), and isofluorane (unpublished observations, see Chapter 2).

In human studies using midazolam and fentanyl, there has been no reported effect on evoked ABR waveform amplitudes (Loughnan *et al.* 1987, Hotz *et al.* 2000); however an increase the latency of the mid-latency potentials has been shown in some studies (Morlet *et al.* 1997, Brunner and Vaughan 2000).

Recently there has been a report that the local application of midazolam to the round window can reverse the tinnitogenic effects of salicylate (Panford-Walsh *et al.* 2008). The results presented here from the sound-exposed animals show that hearing thresholds increase following single tone sound exposure with the systemic application of midazolam in addition to Hypnorm. These results indicate that the systemic application of midazolam is insufficient to completely protect the auditory system from damage induced from the sound exposure protocol. Indeed, direct comparison between the current study and the results presented by Panford-Walsh *et al.* is not appropriate due to the completely different route of midazolam administration. Additionally, a previous study investigating the effect of verapamil on quinine induced hearing loss in guinea pigs used the combination of Hypnorm and midazolam anaesthesia to conduct their audiometric recordings (Jager *et al.* 1997). Their results show the guinea pig hearing thresholds were elevated by an average of 16dB following quinine administration (Jager *et al.* 1997). This illustrates that the effects of quinine were not reversed by the use of midazolam. In addition to the results presented in this study, the reversing effect of midazolam on salicylate induced tinnitus may be due to a specific interaction between the two drugs and not a generalized auditory protective action of midazolam. Additional experiments using animals anesthetized with alternative agents, such as ketamine, or awake animals could be performed to determine if a different degree of hearing loss is seen in comparison to the results presented here. However, these experiments could not be performed at present as the Home Office license this study works within does not allow un-anaesthetized animals to be exposed to sound and ketamine anaesthesia was deemed unsuitable for this protocol (see Chapter 2 for details).

While no elevation in hearing thresholds were observed in the animals that were not exposed to sound, a small decrease i.e. *improvement,* in hearing threshold for the 16kHz and 24kHz frequencies during the second and final ABR measurements was seen. As the second and final ABRs are compared to the first ABR measurements, one possible explanation for the improvement in hearing threshold could be that the anaesthesia during the first ABR elevated the hearing threshold of the animal. This explanation seems unlikely as the same anaesthesia regimen did not alter the thresholds for the 12kHz and 30kHz test frequencies or alter the P1 amplitudes in a similar manner. Also, there was no alteration of the ABR waveform component latencies with the repeated sessions of anaesthesia, suggesting that synaptic transmission in the cochlea and auditory brainstem is not hindered by the combination of Hypnorm and midazolam.

The effect of moderate single tone ototrauma on rat ABR

The results presented in this chapter have shown that the sound exposure protocol used generates threshold elevations in the gross ABR at the higher frequencies tested, but without changes in suprathreshold ABR waveform gain or latency P1 amplitude with increased acoustic stimulation. This suggests that the ototrauma used was successful in damaging cochlear sensitivity without disrupting the overall integrity and function of the cochlear amplifier. Additionally, the lack of changes in later ABR waveform latencies beyond the cochlea provides evidence that the gross temporal processing of the auditory brainstem has not been damaged. With reference to human

hearing, the measured deficit of 20dB on average at the higher frequencies tested would be considered a mild loss of hearing sensitivity (Niskar *et al.* 1998).

Possible causes of ABR threshold elevation

The primary ways in which noise can damage the cochlea, physical, metabolic and excitotoxic, could have contributed to the elevated ABR thresholds seen here either alone or in combination. The evidence for each is now considered:

Physical damage: This could have occurred with the present model of ototrauma, with the single tone stimulus used resulting in the hair cell stereocilia becoming damaged and/or losing their precise geometric alignment required for optimal function of the cochlear amplifier (Puel *et al.* 1998, Puel *et al.* 1988). It is however highly unlikely that the reticular lamina and hair cell membranes would become ruptured, as other published noise-exposure studies have shown that these affects are only seen with higher intensity noise insults than used here (Puel *et al.* 1998, Chen *et al.* 1996, Henderson and Hamernik 1995, Spoendlin 1971).

Greater degrees of physical damage than stereocilia disarray and possibly marginal OHC loss would have been expected to result in a steeper gradient of the gain function accompanied by dramatic shifts in suprathreshold latency transfer function as described in other studies (Puel *et al.* 1998, Salvi *et al.* 1979b, Puel *et al.* 1988). This occurs when damage to the cochlear active process occurs and Figs. 4.12-15 clearly show that these were not affected.

Similarly the suprathreshold ABR P1 amplitudes effectively exhibit both the same slope, i.e. *l* and *m,* and form lx^2-*mx*, pre and post noise exposure at all frequencies. This is clear evidence that the cochlea has not sustained gross physical damage (Patuzzi and Robertson 1988). The simple model of threshold elevation due to sub-chronic physical damage proposed in (Hamernik *et al.* 1980) would also account or the magnitude of changes seen here.

Metabolic damage: It is possible that metabolic damage could have contributed to the modest and sustained deficit seen here, although according to Hamernik *et al.* (1980) most metabolic changes will have resolved within the first 24 to 48 hours post insult. However, any acute metabolic changes could contribute to the principle signal triggering more profound changes leading to permanent loss through hair cell apoptosis and necrosis (Hu *et al.* 2000, Hu *et al.* 2002, Hu *et al.* 2009). In this case again the damage sustained in this study suggests that any metabolic changes subsequent to noise exposure did not lead to massive disruption in cochlear physiology.

Excitotoxic damage: Excitotoxic damage, at least acutely, would be expected to result in significantly increased ABR threshold; decreased amplitude and increased ABR latency (Etheridge 2002, Fergie 2005). ABR threshold increases apart, such changes were not apparent in this study. However chronic changes due to excitotoxic damage share a common pathway with metabolic changes as a result of excess ion movement into the neuron (Taylor and Meldrum 1995, Sattler and Tymianski 2000). Therefore it is possible that initial excitotoxic signal could have contributed to some of the

threshold elevation seen here through marginal loss of cochlear hair cells and/or dysfunction of SGN.

Limitations of ABR measurement used in this study

The ABR data provided a simple but very useful gross measure of cochlear and auditory pathway function following the moderate noise insult used in this study. It is however important to discuss the limitations of the techniques used here. The simple quadratic form of the transfer function was based on relatively few dB stimulus intensity data points and was not assumed to be a physiologically precise estimate of the true transfer function, as this estimate also involves the resistance and capacitive components between the auditory pathway and the recording electrodes.

It is also important to acknowledge the possibility that, whilst no gross changes in ABR amplitude and latency were seen, it is possible that changes in both spontaneous and driven temporal discharge patterns at the level of the neuron could have taken place. It is changes in these properties that would provide the actual neurophysiological correlate of processing deficits such as tinnitus (Møller 1997, Eggermont and Roberts 2004).

However the use of this electrophysiological technique has provided a robust estimate of ototraumtic effect that clearly shows no great loss of OHC and IHC function. This is in contrast to many previous studies in which severe noise exposure resulted in profound damage to the auditory periphery often with accompanying plastic changes centrally (Zhang and Kaltenbach 1998, Bauer *et al.* 2008, Kaltenbach *et al.* 1998).

Comparison with previously published studies

As discussed in the introduction of this chapter, the protocols used to investigate noise-induced hearing loss are very disparate, with variations in experimental animal, as well as the intensity, duration and type of noise stimulus used (Kojima *et al.* 2007, Liberman 1982, Sullivan and Conolly 1988, Duan *et al.* 2008, Heffner and Koay 2005, Kaltenbach *et al.* 2002, Salvi *et al.* 1979b). This section of the discussion will compare previously published studies to attempt to uncover a possible cellular correlate for the ABR threshold elevation presented in this chapter.

Hair cell degeneration: Previous studies of noise-induced hearing loss have shown a decrease in the number of hair cells following noise exposure (Ou *et al.* 2000, Sullivan and Conolly 1988, Salvi *et al.* 1979a, Kiang *et al.* 1976, Liberman and Beil 1979, Chen and Fechter 2003), although these studies used noise intensities greater than 110dB SPL. Recent studies have shown the activation of necrosis and apoptosis in small numbers of hair cells following moderate noise exposure (Hu *et al.* 2000, Hu *et al.* 2009). First, 4kHz narrowband noise exposure, delivered to guinea pigs for 4 hours at 110dB SPL, showed swelling of the OHC nuclei at 3 hours as well as 3 and 14 days after noise exposure, indicating OHC necrosis (Hu *et al.* 2000). Exposing chinchillas to the same 4kHz noise for 1 hour induced OHC loss after 30 minutes post-noise via apoptosis and necrosis, with further OHC loss seen over the following two days (Hu *et al.* 2002). While this gives evidence that OHC loss occurs following a moderate, short duration noise exposure, the results are not directly comparable to the current study as rats were not used in these studies. A recent study using Sprague-Dawley rats has revealed

apoptotic IHCs and OHCs following exposure to broadband noise, 1-7kHz delivered at 115dB SPL for 2 hours, at 10 minutes and 4 hours post-exposure (Hu *et al.* 2009). The study reported a decline in apoptotic hair cells at 7 days post-exposure, although this may be due to the removal of the previously dying cells from the organ of Corti. This indicates that 115dB SPL noise is sufficient to induce apoptosis in a select population of hair cells in rat cochleae, although it is difficult to infer if 110dB SPL would yield similar induction of hair cell apoptosis.

As discussed previously, the outer hair cells are thought to be responsible for generating the cochlear amplifier, by altering the cell length to increase or dampen the oscillation of the basilar membrane (Dallos 1992, Davis 1983). It has been shown that the outer hair cells degenerate before the inner hair cells following noise exposure (Sullivan and Conolly 1988). If the outer hair cells were damaged this could result in a decrease in amplification of the basilar membrane vibration at lower stimulus intensities and thus a loss in hearing sensitivity, leading to an increase in hearing threshold. Indeed it has been shown that selective loss of OHC leads to a decrease in hearing sensitivity (Fettiplace and Hackney 2006).

A study investigating noise-induced hearing loss and hair cell loss in Long Evans pigmented rats showed prominent hair cell loss along the basal portion of the basilar membrane in response to octave band noise, delivered above 105dB SPL, with a centre frequency of 13.6kHz (Chen and Fechter 2003). Using the compound action potential (CAP) of the auditory nerve to measure hearing thresholds, no hair cell loss was detected in the basilar membrane regions responsible for the transduction of low

frequencies despite CAP threshold elevation. OHC and IHC loss was seen at higher frequencies, with the more prominent hair cell loss was seen at the 30kHz to 40kHz region, suggesting the OHCs towards the base of the cochlea are more liable to be lost following noise exposure. Additionally, animals that were not exposed to noise also had OHC loss within the 40kHz region of the basilar membrane, indicating a general OHC loss in this cochlear region. While OHC loss was observed towards to the basal region, hearing loss was detected at the lower frequencies tested without hair cell loss at the apical regions. This indicates the hearing loss is due to mechanisms other than the destruction of the hair cells, such as the disruption of the stereocilia.

It must be noted that Chen and Fechter (2003) exposed their animals to sound for 4 hours on average, with some animals kept in hypoxic air during the exposure. As this would result in a greater degree of cochlear damage than evoked in the current study (Etheridge 2002, Chen and Fechter 1999), the results reported by these authors would not be directly comparable to those presented here with regard to any hair cell loss following noise exposure.

Stereocilia disruption: The above study has shown that, although elevations in hearing threshold is associated with hair cell loss, similar threshold elevations can be detected without hair cell loss and, conversely, hair cell loss can occur without threshold elevations (Chen and Fechter 2003). This indicates that more subtle changes may occur to the hair cells following some noise induced hearing loss protocols, such as the disruption of the hair cell stereocilia, rather than complete hair cell loss (Ou *et al.* 2000, Henderson and Hamernik 1995, Liberman and Beil 1979, Clark and Pickles 1996).

This disruption would cause a decrease in sound transduction via loss of hair cell function and thus a decrease in cochlear activity, leading to an increase in hearing threshold, reduction in neurotransmitter release from the basal portion of the hair cells and a decline in SGN depolarisation. Thus the amplitude of P1 would decrease without a decrease in hair cell number.

Glutamate excitotoxicity: The excessive release of glutamate has been shown to cause neuronal degeneration (Lipton and Rosenberg 1994). It has been shown that application of kainic acid, an analogue of glutamate, to chinchilla and guinea pig cochleae can cause the SGN dendrites under the IHCs to swell and degenerate (Pujol *et al.* 1990, Zheng *et al.* 1998). As glutamate has been identified as the neurotransmitter released by the IHCs (Nordang *et al.* 2000, Bobbin 1979), auditory overstimulation would result in an increase in glutamate release and raise the probability of SGN dendrite swelling and deafferentation of the IHCs (Pujol *et al.* 1990, Puel *et al.* 1998). Additionally, the lost of SGN peripheral processes following noise exposure has been documented (Bauer *et al.* 2007). While an increase in hearing thresholds has been reported following the selective loss of SGN following the application of ouabain (Wang *et al.* 2006), it appears that SGN loss following acute sound exposure occurs after the degeneration of the organ of Corti (McFadden *et al.* 2004). This suggests that the hearing threshold elevation observed is unlikely to be due to SGN loss but could be due to degeneration of the synapses between the IHC and the SGN peripheral processes. The recent Kujawa and Liberman paper suggests that dendrite retraction can result in SGN loss after weeks/months following modest

ototrauma (Kujawa and Liberman 2009). This low level loss may be a sub-clinical event that results in an acceleration of age-related hearing loss.

The above studies have shown that there are many possible cellular sites within the cochlea that could result in the hearing loss seen in the sound-exposed rats. As the animals used in this study were not completely deafened, the most likely cellular explanation for the deafness observed would be either disruption/fusion of the hair cell stereocilia or damage to or degeneration of the SGN. Further histology of sound-exposed cochleae would be needed to specifically identify the cellular correlate of deafness from this ototrauma protocol, looking at hair cell number, stereocilia organisation and SGN innervation.

Neuronal consequences following modest ototrauma: While many of the studies cited above have investigated the effect of noise intensities above 110dB SPL on the cochlea, a recent study by Kujawa and Liberman has further highlighted the prominent consequences of more modest ototrauma protocol. In the study (Kujawa and Liberman 2009) mice were exposed to an octave band noise stimulus (8-16kHz) at 100dB SPL for 2 hours, followed by physiological testing of hearing function, using ABR, OAE and CAP measurements, and counting of SGN afferent synapses and cell body numbers. Their results showed a temporary threshold shift with a recovery of hair cell function within 2 weeks. However, there was a decrease in afferent SGN synaptic terminals as well as a decrease in SGN number over time without a decline in hair cell number. This indicates that exposure to modest level of ototrauma can result in accelerated loss of SGN.

The findings presented by Kujawa and Liberman in conjunction with the results presented here add weight to the need for more detailed analysis of the consequences of exposure to modest levels of noise. A more unified, systematic approach is needed to investigate the neuronal consequences of exposure to noise that does not result in catastrophic damage to the cochlea since this better reflects the type of noise exposure and ototrauma experienced by people with early hearing loss.

Other points of interest

While the following points do not directly refer to the analysis of cochlear function following the modest noise exposure protocol, it is felt necessary to discuss them with regard to the wider experimental protocol.

Two sound exposure sessions to produce deafness: The model of noise-induced hearing loss using rats developed in this study exposes the test animal to two sessions of an 110dB SPL 14.8kHz single tone for two hours with 48 hours between the two exposures. The hearing thresholds of the animal were tested before the sound exposure sessions and again six days after the second sound exposure. At the end of the protocol, the higher frequency hearing thresholds were increased by an average of 20dB.

A previously published study rat model of hearing loss, using a single tone sound exposure paradigm very similar to the protocol presented here, has also shown an increase in hearing thresholds of around 20dB six days after a single exposure to

115dB SPL 10kHz single tone (Tan *et al.* 2007). This shows that two exposures to a 14.8kHz tone presented at 110dB SPL can produce a threshold elevation comparable to a single exposure presented at a higher intensity.

Popelar *et al.* showed that one day after a single noise exposure to 118dB SPL white noise for 1 hour the hearing thresholds across all tested frequencies were temporarily shifted, returning to pre-exposure levels when tested 20 days after exposure, suggesting no permanent cochlear damage. Following the second exposure, to 122dB SPL white noise for 1 hour three weeks after the first exposure, there was a larger hearing threshold shift in comparison to the first exposure that did not return to the previous hearing threshold level, indicating that the two exposure protocol produces a permanent hearing threshold shift. Furthermore, a decrease in ABR waveform amplitude was also reported (Popelar *et al.* 2008). This study supports the results presented in this thesis, with a decrease in P1 amplitude following the sound exposure protocol, however it must be noted that Popelar *et al*. used noise exposures at intensities higher than the 110dB SPL tone used in this study and so the conclusions generated may not be directly comparable.

Perez *et al*. used 113dB SPL white noise for 12 hours a day in a two exposure protocol, with six weeks between exposures, across three experimental groups. For the first group the first noise session lasted for 21 days, for group two only 3 days and for group three the rats were not exposed to noise. The second exposure lasted 12 days for all groups. Their results showed that group one had the larger hearing threshold elevation than the other groups after the first noise exposure session. After the second

sound exposure the average hearing threshold for group one had increased but by a smaller degree than the elevations for groups two and three, indicating that the level of threshold elevation diminishes with repeated noise exposures, either by the deafened animals perceiving a lower intensity noise (the intensity of the second exposure reduced by the hearing deficit caused by the first exposure), a reduction in the number of hearing elements that can be damaged by the consequent exposures (such as hair cells or afferent neurons) or the ear becomes conditioned after the first exposure, so that further threshold shifts are resisted by cyto-protective molecules (Perez *et al.* 2004). Again, the results and conclusions generated by Perez *et al*. may not be directly comparable to the results presented in this chapter, due to the length of the noise exposure and the recovery periods being significantly longer than the sound exposure protocol described. The use of extended recovery periods raises the question of whether the auditory deficits presented in the current model recover to normal, pre-exposure levels given time. To investigate this, the rats would have to be allowed to recover following noise-exposure for a period of time longer than the 6 days currently used. While this is possible, the additional recovery time was not practically feasible within the time constraints of this investigation. Additionally, Perez *et al*. reported large variability within the experimental groups, a finding also seen in this thesis, showing that individual animals may be more susceptible to auditory damage.

The above studies show that two noise-exposure sessions result in hearing threshold elevations. However, the above studies further illustrate the disparate nature of noise-exposure models currently used. It must also be noted that this study is not focused on

identifying any differences between hearing loss generated by single or multiple noise exposures. The use of 2 noise exposure sessions was decided upon to safeguard the welfare of the experimental animals, as noise exposure sessions longer than 2 hours would require additional anaesthetic administration. While it would be interesting to investigate whether a single 4 hour noise exposure would generate a similar or distinct pattern of hearing loss, or indeed any consequent changes in voltage-gated Na^+ channel expression, compared to the current protocol, this investigation is beyond the scope of the current study at this time.

Sound exposure affects hearing at higher frequencies: The animals subjected to the 14.8kHz, 110dB SPL sound exposure protocol displayed an increase in hearing thresholds at frequencies above 16kHz. This increase in hearing threshold was also accompanied by a decrease in the P1 wave amplitude at 24kHz and 30kHz, while the P1 amplitude from the lower frequencies remained unchanged. As the P1 wave represents the electrical activity from the cochlea and auditory nerve (Church and Gritzke 1987, Starr 1976), the decrease in amplitude suggests a decrease in evoked cochlear function following sound exposure at these frequencies.

These results indicates that the single tone sound exposure used in this model affects the animals hearing range at frequencies higher than the tone used for the exposure, which has been shown previously (Puel *et al.* 1998, Ou *et al.* 2000, Salvi *et al.* 1979a). This effect is thought to arise from the loss of the active amplification generated in the cochlea by the OHCs (Dallos 1992, Davis 1983). In the normal cochlea, basilar membrane vibrations from low intensity sounds are enhanced by the active motility of

the OHCs, allowing the perception of these sounds. The amplification maximally augments the travelling wave of the basilar membrane at a point a half octave above where the membrane naturally resonates. Thus, this half octave point is more sensitive to damage by frequencies lower than its own point of natural resonance. It is believed that following deafening, the OHCs become damaged at the region of the portion of basilar membrane that responds to frequencies higher than the noise insult (Puel *et al.* 1988) and the amplification is lost, resulting in elevated hearing thresholds (Nouvian *et al.* 2003).

110dB SPL is not extremely traumatic: The sound exposure protocol developed in this study can be considered to be less traumatic when compared to other noise induced hearing loss studies. Indeed the use of noise exposures at higher sound pressure levels, 120-140dB SPL, does result in a greater degree of hearing threshold elevation and deafness than documented here (Spoendlin and Brun 1973, Kojima *et al.* 2007, Heffner and Harrington 2002). In comparison to the noise exposures at such high levels, that would lead to deafness by near complete cochlear destruction, the use of 110dB SPL in the present study would generate a more moderate level of deafness. Additionally, Spoendlin and Brun observed severe damage to the organ of Corti of guinea pigs with noise exposures over 130dB SPL, with reduced hair cell degeneration at exposure intensities below 120dB SPL (Spoendlin and Brun 1973). Interestingly, the noise exposure protocol used by Hu *et al.* 2009, 115dB SPL broadband noise for 2 hours, was used because it induced hearing loss and cell damage but not the immediately destruction of large numbers of hair cells or supporting cells in rat cochleae. Indeed these authors reported a hearing threshold elevation of 24±5.2dB at

7 days post-exposure (Hu *et al.* 2009), which is similar to the hearing threshold elevations reported in this chapter.

Measuring the degree of hearing loss: This study used ABR measurements to determine the hearing threshold of the rats, with the threshold of hearing defined as the point where the ABR waveform components could not be produced reliably (Church *et al*. 2007). The ABR waveform was generated in response to tone pip stimuli that were attenuated in 10dB steps, thus the hearing threshold was defined as the attenuation step that resulted in the loss of the clearly defined ABR waveform. This method would not define the absolute hearing threshold for a given test frequency, as it is conceivable that the absolute hearing threshold would lie somewhere between the attenuation steps.

As this study is interested in measuring any change in hearing threshold following noise exposure, it could be argued that determining the absolute hearing threshold is not essential. This is provided that the ABR results are reproducible, i.e. the ABR waveform declines at the same attenuation step for a rat with undamaged hearing, so that any elevation in hearing threshold is measured relative to the pre-noise exposure value. The ABR results from the control rats show that the hearing threshold does not increase with successive measurements, indicating that comparisons can be made for the noise-exposed rats between the hearing thresholds determined from the first and last ABR. Surprisingly, an improvement in the control animal hearing threshold results was seen for some frequencies following the first ABR. This highlights the need for accurate baseline ABR measurements to ensure that any threshold changes for the

noise-exposed animals are not under estimated. Thus the decision was made to compare hearing thresholds using the 10dB attenuation steps across the test frequencies rather than determining the absolute hearing threshold for each frequency during the complete ABR measurement.

The reason behind measuring only the ABR waveforms in 10dB steps, and not using smaller steps to more accurately define the hearing threshold, is due to methodological restraints. For a precise ABR measurement the rat has to be suitably anaesthetised using neurolepanalgesia. The ABR measurement at each attenuation step takes 30 seconds to complete, with each step repeated at least twice. Each tested frequency consists of between eight and nine attenuation steps (from 0dB to 70dB or 80dB in some cases), with four frequencies tested (12, 16, 24 and 30kHz). Thus the complete ABR protocol takes around 36 minutes to complete. The level of anaesthesia required to suitably measure the ABR provided by Hypnorm and midazolam is between 30 and 40 minutes. Additional top-up injections of anaesthetic could have been given during the ABR protocol to completely define the auditory threshold at each frequency however, to avoid any complications during recovery that could arise from overdosing, top-up injections were kept to a minimum. Hence the set of attenuation steps outlined was used and repeated during each ABR experiment so that the results could be directly compared across the same set of stimuli.

While measuring the hearing thresholds by visual analysis of the ABR waveforms could be considered subjective and possibly inaccurate, additional measures taking into consideration the waveform generated when no tone pips were presented could have

been done. This would have indicated the level of 'noise' generated when the auditory pathway was not directly stimulated and thus could have assisted in determining whether the ABR waveform at a proposed hearing threshold was accurate. However the means to generate such analysis were not available during the investigation. Additional measures were analysed from the ABR recordings to indicate changes in hearing function. As discussed previously, the P1 amplitude, indicating the level of evoked activity from the cochlear nerve, and latency, showing any change in the transfer function from the hair cell activation through to the generation of action potentials by the SGN, were measured.

In summary, this chapter has shown that the newly devised noise exposure protocol produces a mild elevation of hearing thresholds at the higher frequencies tested. While the cellular causes of this increase in hearing threshold have not been directly identified, the results suggest that the integrity of the hair cells and SGN had not been dramatically compromised. Additionally, the control experiments showed that the anaesthesia regimen had not compromised the normal hearing function of the rats.

As shown in this chapter, the model of ototrauma used causes an average increase in hearing threshold of 20dB SPL for the 24kHz and 30kHz tested frequencies. The following chapter will investigate if there is an alteration in the voltage-gated Na^+ channel isoforms expressed in the cochleae from animals exposed to the modest ototrauma protocol.

Chapter 5 Characterization of voltage-gated sodium channel expression of spiral ganglion neurons from sound-exposed animals

Introduction

As shown in the previous chapter, the newly developed sound exposure protocol produces a hearing threshold elevation between 10 and 20dB at the higher frequencies tested. This chapter will investigate if there are any changes in voltage-gated Na^+ channel expression following the sound exposure protocol. The first part will see if there are any changes at the mRNA level, by conducting both RT-PCR and quantitative PCR using sound-exposed modioli.

The second part will look if there any changes in voltage-gated Na^+ channel protein expression and distribution by undertaking immunohistochemistry on sections from sound-exposed rat cochleae. The results will be compared throughout against cochleae extracted from animals that have not been exposed to the sound stimulus but had the same ABR and anaesthesia regimens.

Materials and methods

Sound exposure protocol

Sound exposure method: Animals were divided into two experimental groups. The first group of animals were processed using the sound exposure protocol as described in Chapter 4, referred to as 'sound-exposed animals'. The second group of animals were processed in the same way as the exposed group but were not exposed to the sound stimulus, referred to as 'control animals'. Where possible, one exposed and one control animal were processed in parallel, to ensure that tissue collection and processing for voltage-gated Na^+ channel characterization occurred at the same time.

RT-PCR

RT-PCR method: The RT-PCR experiments were conducted as the method in Chapter 3, using the same primers pairs as detailed in Table 3.1.

Quantitative PCR

In addition to RT-PCR, quantitative (q)PCR was also performed using Taqman fluorogenic probes. The qPCR experiments allow the identification and quantification of the sodium channel mRNA copies present in the rat modioli. This would identify any change in sodium channel mRNA expression in the sound-exposed animals compared against unexposed animals.

Introduction to qPCR: The Taqman method allows the accumulation of PCR products to be measured by an increase in fluorescence intensity using a fluorescent marker during the amplification cycles. As shown in Fig. 5.1, the Taqman probe consists of an

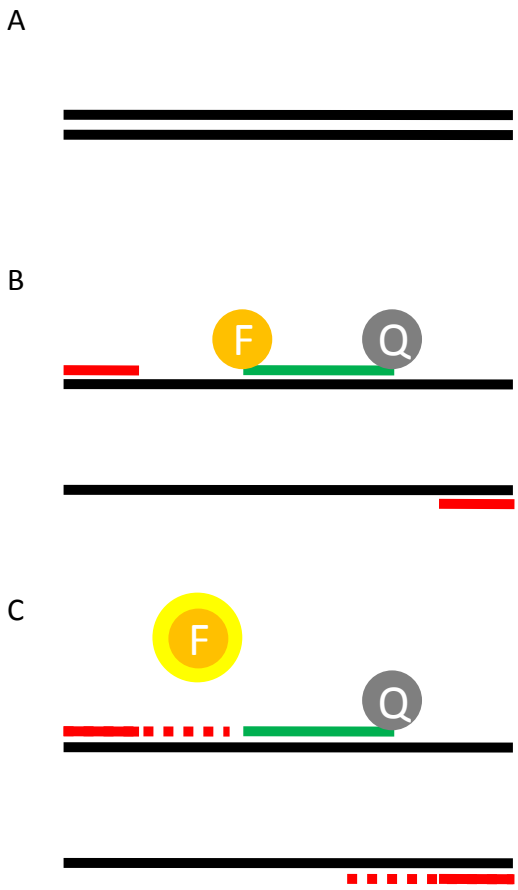

Fig. 5.1. Graphical representation of the Taqman qPCR reaction cycle. (A) The double stranded DNA (black lines) separates to allow the primers (red lines) and Taqman probe (green) to anneal (B). The probe consists of an oligonucleotide sequence with a fluorophore (F) and a fluorescence quencher (Q) attached. (C) The polymerase extends the primers and releases the fluorophore from the Taqman probe, allowing the fluorophore to fluoresce away from the influence of the quencher.

oligonucleotide sequence, designed to be specific for a genomic sequence downstream of a primer, with a fluorophore (6-carboxyfluorescein or 6-FAM) and quencher (tetramethylrhodamine or TAMRA) attached. The fluorophore is prevented from fluorescing due to the proximity of the quencher. During the PCR cycle, when the primer is extended by the Taq polymerase, the fluorophore is released from the probe by the exonuclease activity of the polymerase. As the fluorophore leaves the influence of the quencher, the fluorophore is no longer inhibited and an increase in fluorescence can be detected. The level of fluorescence, detected in the thermal cycler during the

PCR reaction, is directly proportional to the fluorophore release and hence the amount of the DNA template present. At the start of the PCR cycle the number of PCR products will be small and so the level of fluorescence will be indistinguishable from the background fluorescence. The amount of DNA increases with successive PCR cycles and thus the level of fluorescence increases to the point at which the fluorescence can be detected above background levels, known as the threshold cycle (C_T). As the PCR cycles continue the amount of PCR product for each primer pair, and thus fluorescence, will increase exponentially and then reach a plateau, due to a lack of available probes, primers, NTPs or polymerase molecules.

The Applied Biosystems 7500 Fast Real-Time PCR System (Warrington, UK) was used in these experiments, using the Absolute Quantification (AQ) protocol. This protocol determines the absolute quantity of an unknown sample by using a standard curve generated from known copies of genomic standards. AQ is performed using real-time PCR, where the fluorescence data is collected during the PCR process and the reactions are characterised by the point in time during cycling when amplification of a target is first detected, rather than by the amount of target accumulated at the end.

Preparation: The same sterilization and cleaning steps undertaken for RT-PCR, detailed in Chapter 3 were applied for the qPCR experiments.

Tissue extraction: Rat modioli were extracted as described for RT-PCR previously in Chapter 3.

RNA extraction and cDNA synthesis: Two modioli, one from each cochlea of an animal, were pooled for each experiment. mRNA isolation was performed using a QIAGEN RNeasy lipid tissue mini prep kit. For tissue lysis, 1 ml Qiazol reagent was added to the tissues. A clean mixer mill stainless steel ball was added to the tube and the tissues were homogenised in a QIAGEN tissue lyser at 30Hz for 5 minutes. The tissues were left to stand for 5 minutes at room temperature before 200µl chloroform (Sigma) was added to each tube and shaken vigorously for 15 seconds. The tubes were left to stand for 3 minutes at room temperature before being centrifuged at 13,000 rpm for 15 minutes at 4^{o}C to separate phases, with the top aqueous phase containing the genomic material. The aqueous phase was carefully transferred to a fresh 1.5ml eppendorf tube before ethanol (Sigma) was added to the sample to provide appropriate binding conditions before applying the sample to an RNeasy mini spin column, where the total mRNA bound to the column membrane and contaminants were washed away. A DNase solution was added to the column to digest any remaining DNA (Qiagen RNase-free DNase set) before the mRNA was eluted in RNase free water (Applied Biosystems). A NanoDrop ND1000 spectrophotometer (NanoDrop, Wilmingtion, USA) was used to quantify the amount of total mRNA eluted. The total mRNA was transcribed to cDNA using the Applied Biosystems high-capacity cDNA reverse transcription kit using a 96 well plate thermal cycler. The cDNA contained in the well plates were kept at -20^{o}C until use. mRNA from each animal was also processed without reverse transcription to identify any genomic contamination of the samples during the PCR reaction.

PCR reaction: The PCR reaction was performed using the Applied Biosystems 7500 fast thermal cycler AQ protocol. Rat genomic standards with known copy number (Applied Biosystems), no template control (NTC) and 5µl of the sample cDNA with (+) and without (-) reverse transcription were pipetted into the appropriate well of a 96 well plate. The Taqman buffer (Applied Biosystems), 10µM custom designed oligonucleotide primers and Taqman probes (Sigma Genosys) were added to each well, followed by the Taqman master mix (Applied Biosystems). The plates were sealed with an optical adhesive cover, briefly centrifuged and placed in the 7500 fast thermal cycler. The AQ protocol was run and the copy number of the unknown target sequence was calculated by using the standard curve generated from the genomic standards, with the results exported to a Microsoft Excel spreadsheet.

qPCR primers: The details of the primer pairs and Taqman probes specific to the voltage-gated Na^+ channel alpha subunits and the housekeeping genes used for qPCR are detailed in Table 5.1.

Housekeeping gene selection: The housekeeping genes are genes that are constitutively active and maintain the normal functions of the cell. Their expression was used to normalise the voltage-gated Na^+ channel gene expression from each sample, yielding the voltage-gated Na^+ channel gene expression as a percentage of the housekeeping gene. The housekeeping genes selected for this study were β-actin, glyceraldehyde-3-phosphate dehydrogenase (GAPDH) and cyclophilin A (also known as peptidylprolyl isomerase A).

Subunit	Oligonucleotide	Sequence 5'-3'	Subunit	Oligonucleotide	Sequence 5'-3'
$Na_V1.1$ *(Scn1a)*	Forward primer	CTGGCAGAAACCCTAACTATGGT	$Na_V1.7$ *(Scn9a)*	Forward primer	TGACAGCCTGTGAAGGTTGACTC
	Reverse primer	TCAGTCGAAACAGGGACAGAAATG		Reverse primer	GCCATGTGTAAATGCTGCCC
	Taqman probe	CCCAGCTGAAGGTGTC		Taqman probe	AGGCAGCACAGCCATTAGCTCTGATCC
$Na_V1.2$ *(Scn2a)*	Forward primer	GCTCTGCTTTGTGGGAACAG	$Na_V1.8$ *(Scn10a)*	Forward primer	CCTGTCCATTGGGAGTCTGC
	Reverse primer	GCCTTCACACAGATGTATCCTTCT		Reverse primer	GAAGAGGAGGAGGCCGATGT
	Taqman probe	CACTGTCCAGCATCCG		Taqman probe	CTGCTCTTCGCCCTCATGATGTCCCT
$Na_V1.3$ *(Scn3a)*	Forward primer	CCTCTCAGACCTCGCGGACA	$Na_V1.9$ *(Scn11a)*	Forward primer	AAGCCTTTGTGTTCGACCTGG
	Reverse primer	ACGGCAGGTCCATCTGGATT		Reverse primer	ACATCTTTGGGCTGGTCGG
	Taqman probe	CTCCGGCCCTCTTAGAATCCCCAAACC		Taqman probe	TCACAAGCCAGGTCTTTGACGTCATCA
$Na_V1.4$ *(Scn4a)*	Forward primer	AATGCTAGAACTCAGCACACGGG	GAPDH (*Gapdh*)	Forward primer	GAACATCATCCCTGCATCCA
	Reverse primer	CTTGCTTTCAGGCAATGAGAAGAC		Reverse primer	CCAGTGAGCTTCCCGTTCA
	Taqman probe	AAGCCAAGCCTGGTGAGCCTTCTCACT		Taqman probe	CTTGCCCACAGCCTTGGCAGC
$Na_V1.5$ *(Scn5a)*	Forward primer	GGCTGAGGGAAGAGAGGGC	Cyclophilin A (*Ppia*)	Forward primer	TATCTGCACTGCCAAGACTGA
	Reverse primer	GGGAGCCTGGGAAATGGAG		Reverse primer	CCACAATGCTCATGCCTTCTTTCA
	Taqman probe	AGCTGCCCACAGCTGGACACAGTTCAG		Taqman probe	CCAAAGACCACATGCTTGCCATCCA
$Na_V1.6$ *(Scn8a)*	Forward primer	CGTGATGATCCTGACAGTGTTCTG	β-actin (*Actb*)	Forward primer	GAGCTATGAGCTGCCTGAC
	Reverse primer	TGAAGAGCTGCAGGCCAAT		Reverse primer	AGTTTCATGGATGCCACAGGA
	Taqman probe	CAGGGCGAAAACACTC		Taqman probe	CATCACTATCGGCAATGAGCGGTTCC

Table 5.1. Oligonucleotide sequences for the primers and Taqman probes used in the qPCR experiments.

Immunohistochemistry

Immunohistochemistry method: The same immunohistochemistry method and antibodies as detailed in Chapter 3 were used for this study.

Additional precautions: Cochleae from one exposed and one control animal were extracted and processed for immunohistochemistry in parallel. This meant that both sets of cochleae were exposed for the same period of time to each step of the method, from tissue preparation to image capture. This was done to ensure that immunohistochemistry results from an exposed and control animal pair could be compared directly. Also, the gain and exposure of the camera and brightness of the microscope light source settings remained constant for all experiments.

Cell counting: Light micrographs of cochlea sections containing Rosenthal's canal were used to count the number of SGN cell bodies. The images were analyzed using the Cell Counter application in Image J. The area of Rosenthal's canal was also measured to calculate the SGN density.

Results

RT-PCR analysis from sound-exposed and control modioli

ABR thresholds post sound exposure: The average hearing threshold for the 3 sound-exposed animals used for RT-PCR is shown in Fig. 5.2. The hearing thresholds were not elevated for 12kHz or 16kHz at the conclusion of the sound exposure protocol. The average threshold elevation for 12kHz and 16kHz were -3.3±3.3dB SPL and -3.3±8.8dB SPL respectively at the end of the sound exposure regimen. The hearing thresholds for 24kHz and 30kHz were slightly elevated compared to the pre-exposure levels, with mean increases of 3.3±6.7dB SPL and 6.6±6.6dB SPL respectively. However, these threshold elevations did not reach statistical significance ($p>0.05$).

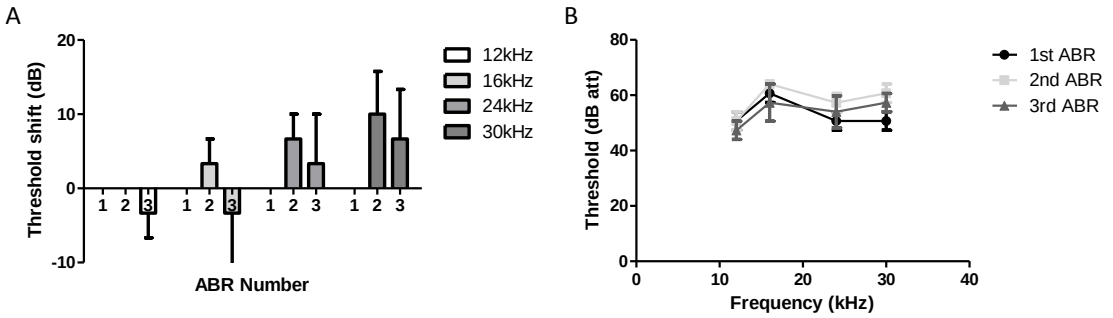

Fig. 5.2. Average hearing thresholds of sound-exposed animals used in RT-PCR experiments. (A) Graph of threshold elevations following sound exposure. No significant increase in hearing thresholds for 12kHz or 16kHz were identified following sound exposure. Slight hearing threshold elevations were identified for 24kHz and 30kHz following sound exposure, although these increases were not statistically significant. (B) Graph showing the average absolute hearing thresholds across the tested frequencies for each ABR (n=3).

Control modioli: The RT-PCR primers specific for the voltage-gated Na^+ channel α-subunits and β-actin were used to probe the cDNA created from mRNA isolated from control modioli homogenates. Bands were detected in the Agarose gel under UV illumination at the correct predicted size for $Na_V1.1$, $Na_V1.6$, $Na_V1.7$ and β–actin (Fig.

5.3A). No bands were seen in the lanes without reverse transcription, indicating no genomic DNA contamination of the samples (n=3).

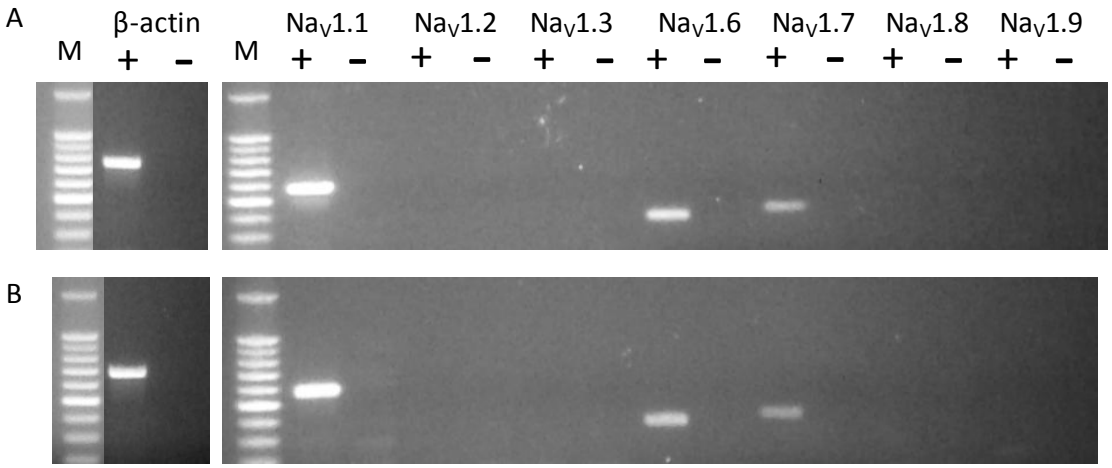

Fig. 5.3. Voltage-gated Na^+ channel mRNA expression in rat SGN following noise exposure. PCR products were separated by electrophoresis on a 1% agarose gel stained with ethidium bromide. (A) PCR products were detected for $Na_V1.1$, 1.6 and 1.7 in the control rat SGN. (B) PCR products were detected for $Na_V1.1$, 1.6 and 1.7 in the rat SGN following sound exposure. All tissues were positive for β-actin. (M) Marker lane, 100bp ladder with brightest band representing 500bp. Expected product sizes are given in methods section of Chapter 3 (Table 3.1). PCR was performed either in the presence (+) or absence (-) of reverse transcription (n=3 for both control and sound-exposed conditions).

Sound-exposed modioli: The same primers were used to probe the cDNA from sound-exposed modioli homogenates. Bands were detected at the correct predicted size for $Na_V1.1$, $Na_V1.6$, $Na_V1.7$ and β-actin (Fig. 5.3B). No bands were identified in the sample lanes prepared without reverse transcription, indicating no contamination from genomic DNA (n=3).

qPCR results from control and sound-exposed modioli

ABR thresholds for sound-exposed animals: The average ABR thresholds for the 7 sound-exposed animals used in these experiments are shown in Fig. 5.4. The average hearing thresholds for 12kHz and 16kHz were slightly elevated following the sound

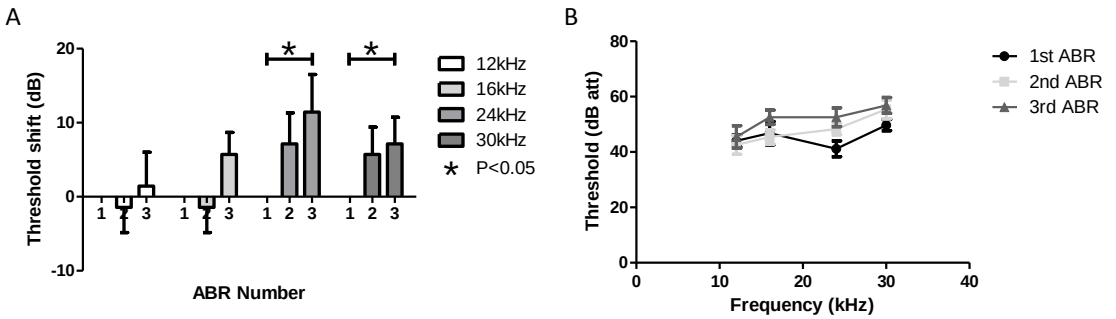

Fig. 5.4. Average hearing thresholds of sound-exposed animals used in qPCR experiments. (A) Graph of threshold elevations following sound exposure. No significant increase in hearing thresholds for 12kHz or 16kHz were identified following sound exposure. Hearing threshold elevations were identified for 24kHz and 30kHz following the conclusion of the sound exposure protocol. These threshold elevations were statistically significant. (B) Graph showing the average absolute hearing thresholds across the tested frequencies for each ABR (n= 7).

exposure protocol. The average hearing threshold elevation for these frequencies was 1.4±4.6dB SPL and 5.7±3.0dB SPL respectively, although these elevations did not reach statistical significance ($p>0.05$). The average hearing thresholds for 24kHz and 30kHz were also elevated compared to the pre-exposure levels. The average threshold for 24kHz had significantly risen by 11.4±5.1dB SPL ($p<0.05$) while the threshold for 30kHz was significantly elevated by 7.1±3.6dB SPL ($p<0.05$).

Housekeeping gene validation: In contrast to RT-PCR, primers and probes for three housekeeping genes were designed and used. Robust signals for β-actin and cyclophilin A were detected from the control modioli cDNA (Fig. 5.5), with average gene copy numbers of $1.36x10^5 \pm 1.13x10^4$ and $4.32x10^4 \pm 3.60x10^3$ respectively. A weaker signal for GAPDH was observed, with an average gene copy number of $1.55x10^3 \pm 1.13x10^2$. Using the cDNA from the exposed modioli, robust signals for β-actin and cyclophilin A were also observed, with average copy numbers of $1.36x10^5 \pm 8.98x10^3$ and $4.83x10^4 \pm 3.55x10^3$ respectively. A weaker signal for GAPDH

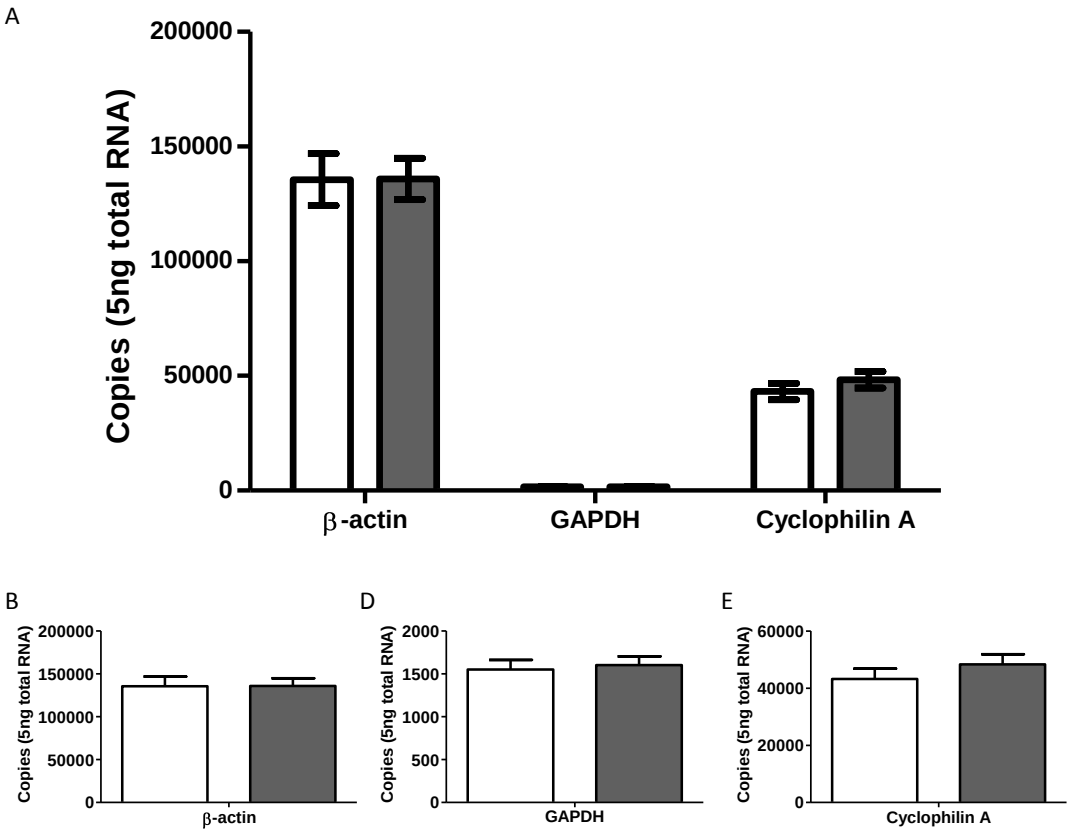

Fig. 5.5. Housekeeping gene mRNA expression. (A) Graph showing expression of all housekeeping genes tested, identifying β-actin, GAPDH and cyclophilin A expressed in both control (clear bars) and sound-exposed (filled bars) animals.(B) Expression of β-actin mRNA remained constant between control and sound-exposed animals. (C) Expression of GAPDH mRNA did not significantly change following sound exposure. (D) Expression of cyclophilin A mRNA slightly but not significantly increased following sound exposure (n= 7 sound-exposed, 6 control).

was also detected, with an average copy number of $1.60x10^3 \pm 1.02x10^2$. From these results, β-actin was used as the reference gene for calculation of the percentage of voltage-gated Na^+ channel mRNA in the tested samples. No significant difference in the housekeeping gene expression between the sound-exposed (n=7) and control modioli (n=6) was detected.

Voltage-gated Na^+ channel mRNA expression from control modioli: Fig. 5.6A shows that qPCR products were detected for $Na_V1.1$, $Na_V1.6$ and $Na_V1.7$ from the control

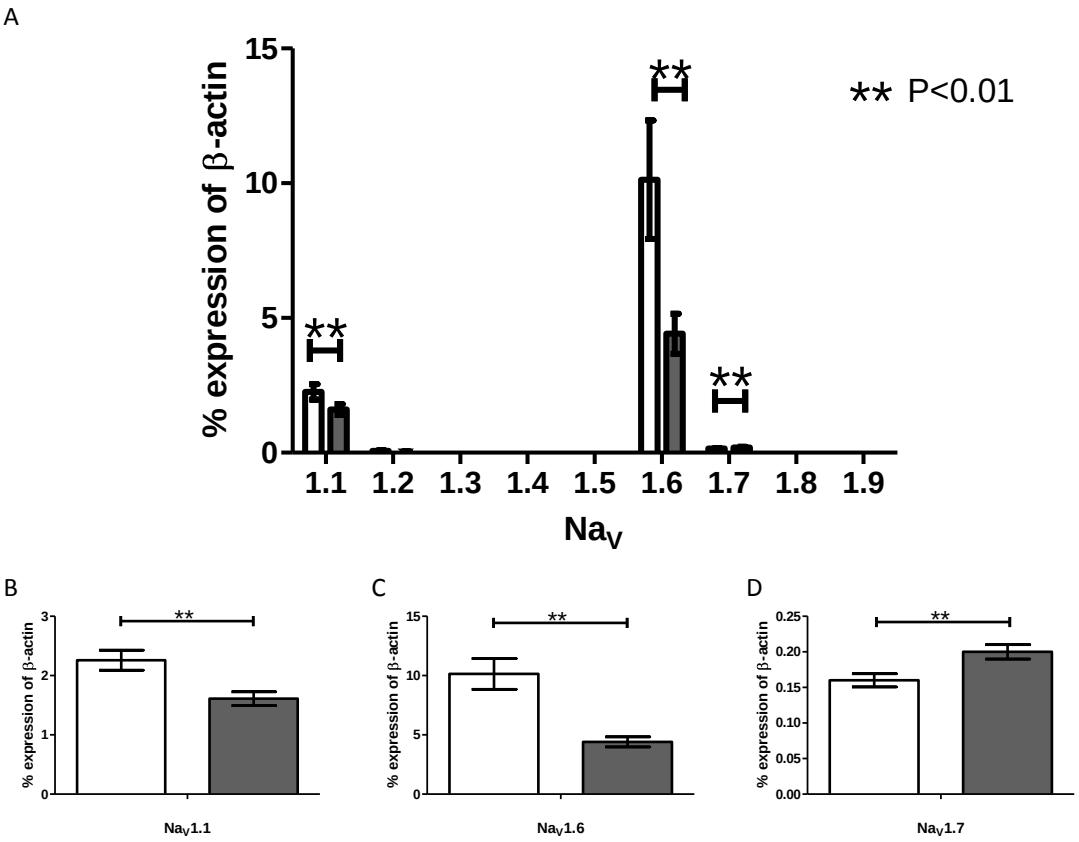

Fig. 5.6. Quantitative PCR results showing voltage-gated Na^+ channel expression as a percentage of the expression of β-actin. Graphs showing voltage-gated Na^+ channel mRNA expression from the modioli of control (clear bars) and sound-exposed (filled bars) animals for (A) all tested voltage-gated Na^+ channels, (B) $Na_V1.1$, (C) $Na_V1.6$ and (D) $Na_V1.7$. (A) High levels of $Na_V1.6$ and $Na_V1.1$ mRNA were detected in the control samples, with $Na_V1.7$ expressed at a lower level and $Na_V1.2$ barely detectable. The expression level of $Na_V1.1$ (B) and $Na_V1.6$ (C) both significantly decreased following sound exposure. (D) The expression of $Na_V1.7$ RNA increased following sound exposure (n= 7 sound-exposed, 6 control).

modioli. The average voltage-gated Na^+ channel expression level, displayed as a percentage of the β-actin expression, for these three isoforms was: $Na_V1.1$, 2.26±0.17%; $Na_V1.6$, 10.1±1.29%; $Na_V1.7$, 0.16±9.22x10^{-3}% ($Na_V1.6$>$Na_V1.1$>$Na_V1.7$).

Voltage-gated Na^+ channel mRNA expression from sound-exposed modioli: Additionally the qPCR results from the sound-exposed modioli are shown in Fig. 5.6B. This shows

that $Na_V1.1$, $Na_V1.6$ and $Na_V1.7$ were also detected from these modioli homogenates. The average expression level for the isoforms was: $Na_V1.1$, 1.61±0.12%; $Na_V1.6$, 4.41±0.42%; $Na_V1.7$, 0.20±0.01%. This shows a statistically significant reduction in gene expression of 29% for $Na_V1.1$ ($p<0.001$) and of 56% for $Na_V1.6$ ($p<0.001$) following the sound exposure protocol compared to the control modioli. Additionally, there was a significant increase in $Na_V1.7$ gene expression following sound exposure of 20% ($p<0.005$), although given the very low copy number in control rats, this was very small compared to the equivalent decrease seen for $Na_V1.6$.

Immunohistochemical localization of voltage-gated Na^+ channel proteins following sound exposure

This section of the immunohistochemistry results will be divided into looking at each voltage-gated Na^+ channel isoform individually. Where appropriate the individual sound-exposed animal will be compared with the control animal processed at the same time.

ABR thresholds for sound-exposed animals: The average ABR thresholds for the 6 sound-exposed animals used for immunohistochemistry are shown in Fig. 5.7. The hearing threshold for 12kHz was not significantly elevated. The hearing threshold for 16kHz was slightly elevated at the conclusion of the sound exposure protocol, by 6.7±3.3dB SPL, although this elevation did not reach statistical significance ($p=0.051$). The hearing thresholds for 24kHz and 30kHz were significantly elevated at the end of the sound exposure protocol. The threshold for 24kHz was elevated by 15.0±5.6dB SPL ($p<0.05$) and the threshold for 30kHz was increased by 23.3±2.1dB SPL ($p<0.0001$).

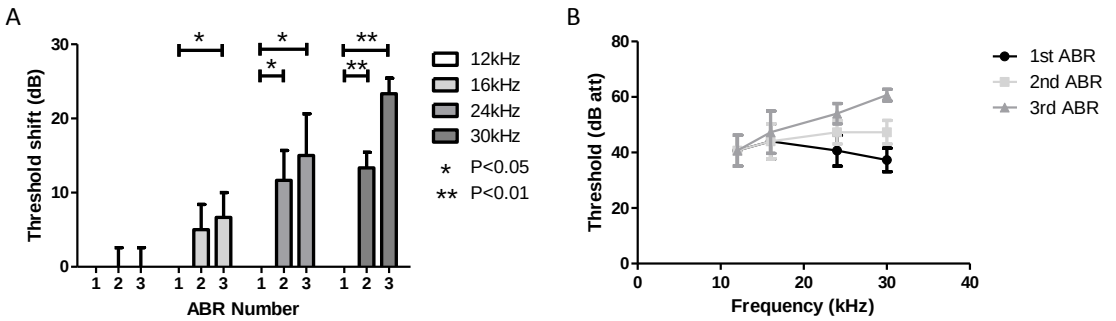

Fig. 5.7. Average hearing thresholds of sound-exposed animals used for immunohistochemistry experiments. (A) Graph of threshold elevations following sound exposure. An increase in hearing threshold for 12kHz was not identified following sound exposure. Significant hearing threshold elevations were identified for 16kHz, 24kHz and 30kHz following the conclusion of the sound exposure protocol. Significant hearing threshold elevations were observed during the second ABR for 16kHz, 24kHz and 30kHz. (B) Graph showing the average absolute hearing thresholds across the tested frequencies for each ABR (n=6).

$Na_V1.7$ in control cochleae: $Na_V1.7$ staining in sections of cochleae from control animals showed a pattern of staining reported previously, with intense $Na_V1.7$ labelling of the SGN cell bodies with variation in staining intensity observed and staining of the axons (Fig. 5.8A and D).

$Na_V1.7$ in sound-exposed cochleae: The staining observed in sections from the six sound-exposed cochleae tested was also seen in the SGN cell bodies, with variation in individual SGN staining intensities seen within the same section. While the distribution of the SGN cell body staining intensity varied within the same section, patterns of staining intensity distribution emerged, with some sections appearing to have a greater proportion of darker stained neurons than the sections from control cochlea. Conversely, some sections from sound-exposed cochleae appeared to display a large proportion of SGN that were less intensely stained compared to their control cochleae counterparts. From the six animals investigated, four groupings of $Na_V1.7$ staining

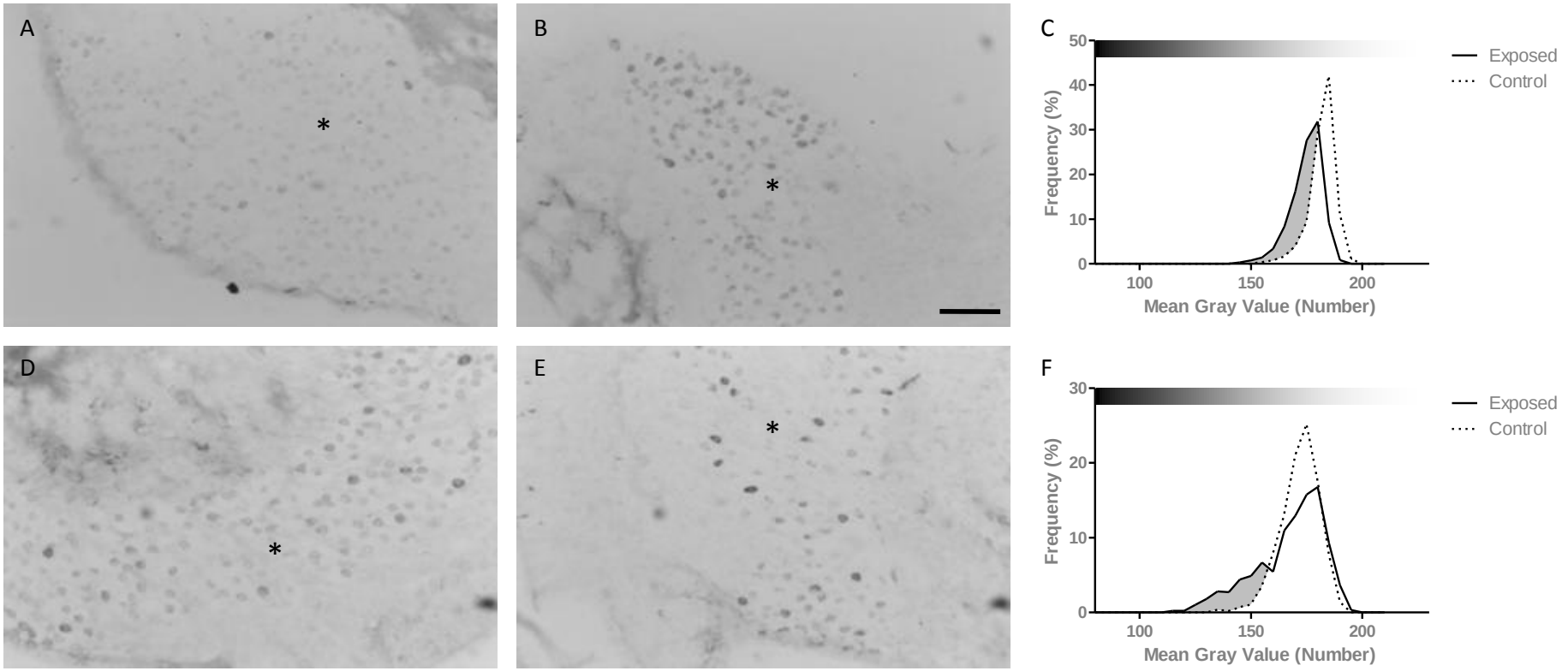

Fig. 5.8. $Na_V1.7$ staining in sound-exposed cochlear SGN. Micrographs of cochlea sections stained for $Na_V1.7$ from control (A,D) and sound-exposed (B,E) animals. Robust staining can be seen in the SGN cell bodies (*) from the control animals (A,D). Frequency pictographs of the SGN cell body mean gray value (C,F) show an increase in frequency of the darker stained neurons (shaded region) following sound exposure (solid line) compared to the control SGN (dotted line). Data for graph C taken from the cochlea of the animals represented by A and B while the data for graph F was generated from the cochlea of the animals represented by D and E. Scale bar= 50µm in all micrographs. Gray Values, 0= black, 255= white, indicated by bar above pictographs.

intensity could be identified. These observations were (with the number of animals in each group): 1) cochleae that showed an increase in frequency of darker stained SGN compared to their control cochleae (3 rats); 2) cochleae that showed an increased frequency of less intensely stained SGN (1 rat); 3) cochleae that showed an increase in frequency of both darker and lighter stained SGN (1 rat); 4) cochleae that showed no change in SGN staining intensity distribution (1 rat). The specific details of each case will be described in the following text and figures, with the respective ABR measurements for each group also reported for overall consideration.

Group 1) Increase in frequency of darker stained SGN: The majority of the sound-exposed cochleae were found to have SGN with qualitatively more intensely stained neurons for $Na_V1.7$ (Fig. 5.8B and E) compared to their respective control animal counterparts (Fig. 5.8A and D), with three out of six animals displaying this pattern. The minimum and maximum mean gray values for the neurons from the sound-exposed and unexposed animals are provided in Table 5.2. These values show that the mean gray value ranges for SGN from sound-exposed and control cochleae are very similar, with an average increase in darkest staining of 11 units. While there appears to be no difference in the mean gray value ranges, further analysis revealed an increase in the frequency of the darker stained neurons in the sound-exposed cochleae compared to their control counterparts (Fig. 5.8C and F).

		Mean gray values from			
		Unexposed rats		Sound-exposed rats	
Group	Animal	Minimum	Minimum	Maximum	Maximum
1	A	140	141	192	189
	B	132	107	187	187
	C	126	117	184	185
2	D	108	101	165	178
3	E	92	77	182	187
4	F	131	129	189	189

Table 5.2. Mean gray value ranges for SGN labelled for $Na_V1.7$. Table displaying the minimum and maximum mean gray values from SGN labelled with the $Na_V1.7$ antibody from unexposed and sound-exposed animals (where 0=black and 255=white). The case number refers to the pattern of $Na_V1.7$ labelling seen in the sound-exposed animals where: group 1, an increase in the frequency of darker stained neurons; group 2, an increase in frequency of lighter stained neurons; group 3, an increase in frequency of both darker and lighter stained neurons; group 4, no change seen.

The hearing threshold data for these three animals in group 1 is shown in Fig. 5.9. An increase in threshold elevation in response to the 12kHz tone pips was not detected in all three animals following sound exposure. An increase of the threshold for the 16kHz

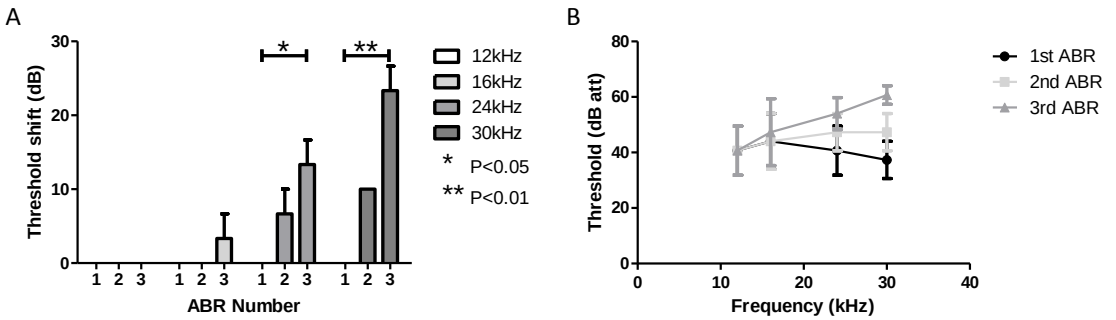

Fig. 5.9. Hearing thresholds of sound-exposed animals shown in Fig. 5.8. (A) Graph of the average threshold elevations following sound exposure. No increase in hearing threshold for 12kHz was identified following sound exposure. Hearing threshold elevations were identified for 16kHz following the conclusion of the sound exposure protocol although this elevation did not reach statistical significance. Significant hearing threshold increases were observed for 24kHz and 30kHz during the final ABR ($P<0.05$ and 0.01 respectively). (B) Graph showing the average hearing thresholds for each animal across the tested frequencies from each ABR recording (n=3).

tone of 3.3±3.3dB following the complete sound exposure protocol. An average increase in the hearing threshold of 6.7±3.3dB for the 24kHz tone was detected during the second ABR recording, while an average increase of 13.3±3.3dB was measured after the complete sound exposure protocol. The hearing threshold for 24kHz was increased by 6.7±3.3dB during the second ABR recording and 13.3±3.3dB after the third ABR recording. An average elevation of the hearing threshold in response to the 30kHz tone pips was detected during the second (10±0dB) and final (23.3±3.3dB) ABR recordings were detected in these rats.

Group 2) Increase in frequency of lighter stained SGN: One sound-exposed animal displayed an apparent increase in the number of less intensely stained SGN cell bodies (Fig. 5.10B) compared to the appropriate control animal SGN (Fig. 5.10A). The minimum and maximum mean gray values for the sound-exposed and control neurons are also presented in Table 5.2. While the mean gray value range appears similar

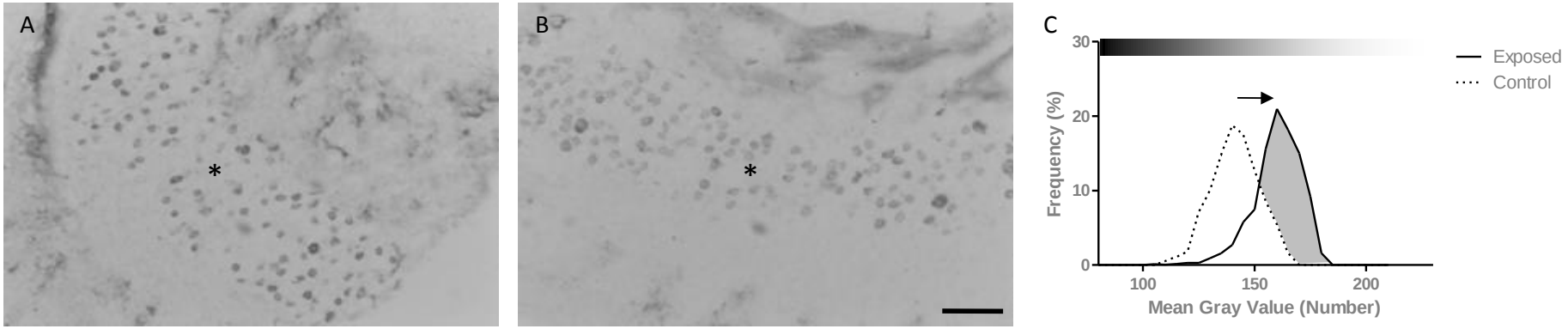

Fig. 5.10. $Na_V1.7$ staining in sound-exposed cochlear SGN. Micrographs of cochlea sections stained for $Na_V1.7$ from control (A) and sound-exposed (B) animals. Robust staining can be seen in the SGN cell bodies (*) from the control animals (A). Following sound exposure there was a decrease in SGN cell body staining intensity (B) compared to the control cochlea section (A). This is shown in the frequency pictograph for the animals represented in A and B (C). This frequency pictograph shows an increase in the frequency of the less intensely stained SGN cell bodies (shaded region) following sound exposure (solid line) compared to the control animal (dotted line). Scale bar= 50µm in all micrographs. Gray Values, 0= black, 255= white, indicated by bar above pictographs.

between these cochleae, further analysis showed an increase in the frequency of the less intensely stained neurons from the sound-exposed cochlea when compared to the control cochlea (Fig. 5.10C).

The ABR measurements for this subject (Fig. 5.11) revealed threshold elevations at all frequencies tested. The hearing threshold for the 12kHz tone pips had increased by 10dB during the second and final ABR recording, while the threshold elevation seen for the 16kHz frequency was 20dB during these measurements. The 24kHz tone pips uncovered an increase in hearing threshold of 30dB during the second ABR measurement and 40dB during the final ABR measurement. The threshold to illicit a response from the 30kHz tones had increased by 20dB, as measured during the second ABR recording, and 30dB SPL during the final ABR measurement.

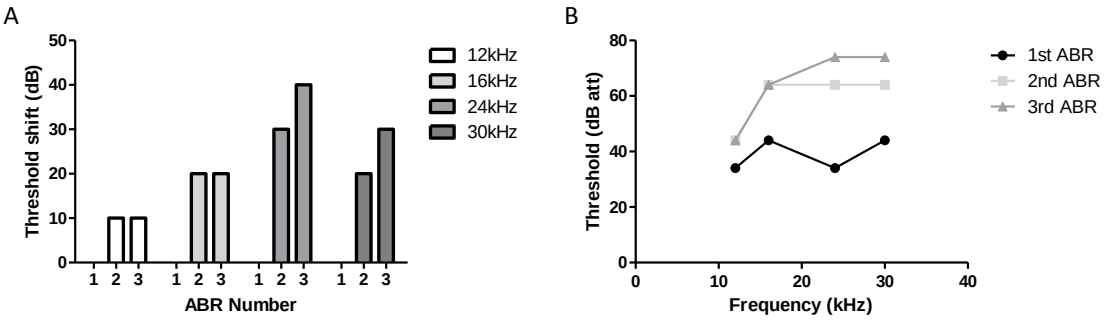

Fig. 5.11. Hearing thresholds of sound-exposed animal shown in Fig. 5.10. (A) Graph of threshold elevations following sound exposure. Hearing threshold elevations were identified for 12kHz, 16kHz, 24kHz and 30kHz following the conclusion of the sound exposure protocol. (B) Graph showing the hearing thresholds across the tested frequencies for each ABR.

Group 3) Increase in frequency of darker and lighter stained SGN: The third group showed one sound-exposed animal with an increase in both the lighter and darker labelled SGN cell bodies for $Na_V1.7$ (Fig. 5.12B) compared to the sections from the

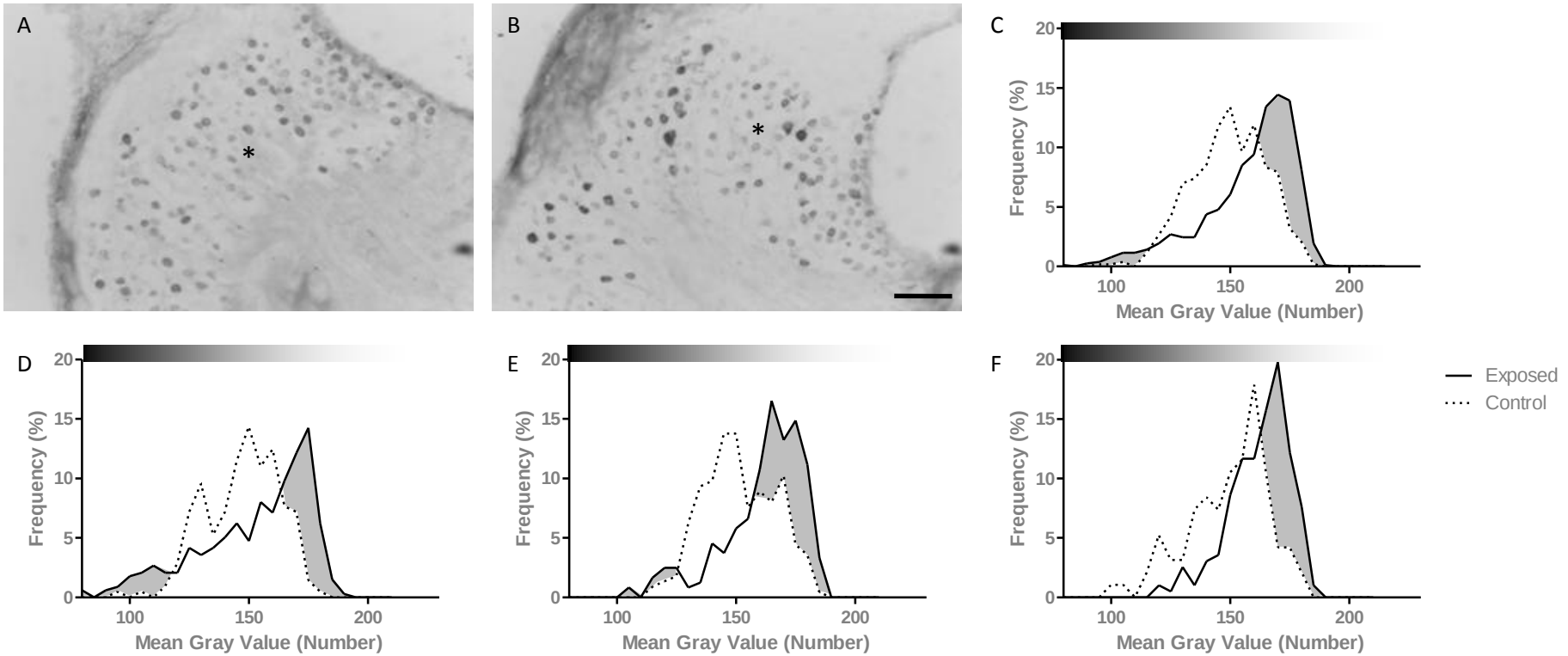

Fig. 5.12. $Na_V1.7$ staining in sound-exposed cochlear SGN. Micrographs of cochlea sections stained for $Na_V1.7$ from control (A) and sound-exposed (B) animals. Robust staining can be seen in the SGN cell bodies (*) from the control animals (A). Frequency pictograph of the SGN cell body mean gray value (C) show a decrease in $Na_V1.7$ staining intensity following sound exposure (solid line), with a small increase in frequency of the more intensely stained cell bodies, compared to the control cochlea (dotted line). (D) The SGN staining from the apical region of the sound-exposed cochlea show an increase in the frequency of the darker and lighter stained neurons compared to the control cochlea (shaded regions). The SGN from the middle (E) and basal (F) portions of the sound-exposed cochlea show an increase in the frequency of the lighter stained neurons compared to the control cochlea. Data for graphs C-F taken from the cochlea of the animals represented in A and B. Scale bar= 50µm in all micrographs. Gray Values, 0= black, 255= white, indicated by bar above pictograph

control animal processed at the same time (Fig. 5.12A). The minimum and maximum mean gray values for the sound-exposed neurons was 77 and 187 respectively, while the minimum and maximum mean gray values of the SGN from the control animal were 92 and 182 respectively (Table 5.2). Further analysis revealed an increase in frequency of both the darker and lighter stained SGN from the sound-exposed cochlea when compared to the control cochlea (Fig. 5.12C).

Additionally, an increase in the frequency of the darker and lighter stained SGN in the apical region of the sound-exposed cochlea compared to the similar region from the control cochlea was observed in this group (Fig. 5.12D). The SGN from the middle showed a small increase in the frequency of darker stained neurons with a larger increase in the frequency of the less intensely stained neurons (Fig. 5.12E). The SGN from the basilar regions of the sound-exposed cochlea only showed an increase in the frequency of the lighter stained neurons compared to the similar regions in the control cochlea (Fig. 5.12F).

The ABR measurements for this subject are shown in Fig. 5.13. There was no threshold elevation in response to the 12kHz tone pips following sound exposure. A threshold elevation of 10dB was seen for 16kHz and 24kHz during the second ABR measurement, but the threshold elevation was absent at these frequencies during the final ABR recording. Testing using the 30kHz tone pips revealed a hearing threshold elevation of 10dB during the second ABR, increasing to 20dB during the final ABR measurements.

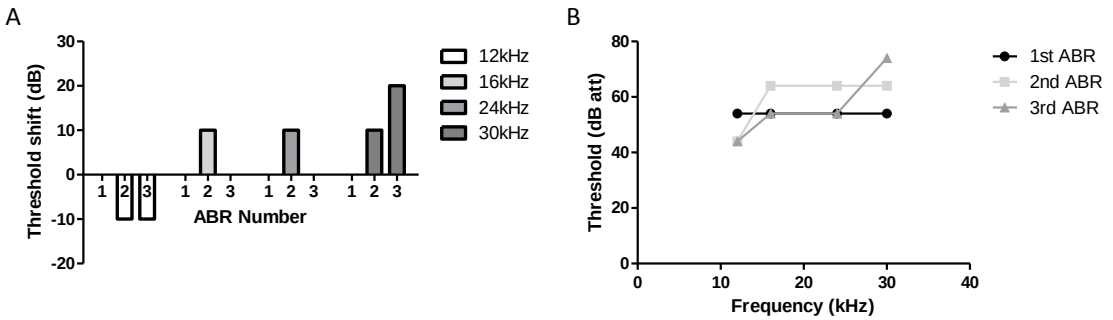

Fig. 5.13. Hearing thresholds of sound-exposed animal shown in Fig. 5.12. (A) Graph of threshold elevations following sound exposure. No increase in hearing threshold for 12kHz was identified following sound exposure. Hearing threshold elevations were identified for 30kHz following the conclusion of the sound exposure protocol. Hearing threshold elevations seen for 16kHz and 24kHz during the second ABR were not observed during the final ABR, indicating a temporary threshold shift at these frequencies. (B) Graph showing the hearing thresholds across the tested frequencies for each ABR.

Group 4) No change in SGN staining intensity: In the fourth group one sound-exposed animal showed no detectable difference in the SGN staining intensity distribution for $Na_V1.7$ (Fig. 5.14B) when compared to the appropriate control cochleae (Fig. 5.14A). The minimum and maximum mean gray values for the sound-exposed neurons was 131 and 189 respectively, while the minimum and maximum mean gray values of the SGN from the control animal were 129 and 189 respectively (Table 5.2). Further analysis showed no difference in the distribution of SGN staining intensities between the sound-exposed and control cochleae (Fig. 5.14C)

The ABR measurements for this animal (Fig. 5.15) showed no threshold elevation for the 12kHz test frequency following sound exposure. An elevation of 10dB was seen for 16kHz following the conclusion of the sound exposure protocol. Hearing threshold elevations were observed for both 24kHz and 30kHz during the second and last ABR. The threshold increase seen for 24kHz was 10dB for the second and final ABR while

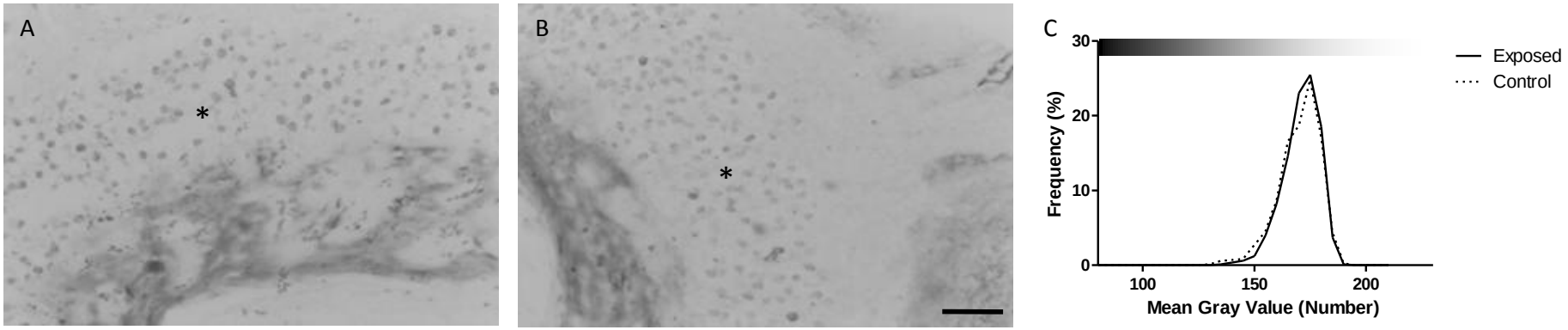

Fig. 5.14. $Na_V1.7$ staining in sound-exposed cochlear SGN. Micrographs of cochlea sections stained for $Na_V1.7$ from control (A) and sound-exposed (B) animals. Robust staining can be seen in the SGN cell bodies (*) from the control animal (A). Frequency pictograph of the SGN cell body mean gray value (C) from the cochleae represented in A and B show no difference in the staining intensity distribution for $Na_V1.7$ between the control (dotted line) and sound-exposed (solid line) animals. Scale bar= 50µm in all micrographs. Gray Values, 0= black, 255= white, indicated by bar above pictographs.

the threshold for hearing the 30kHz tones was raised by 20dB during the same recordings.

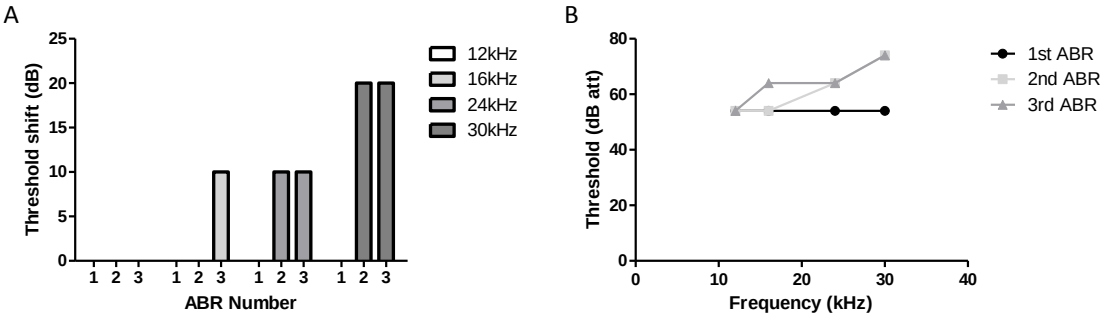

Fig. 5.15. Hearing thresholds of sound-exposed animal shown in Fig. 5.14. (A) Graph of threshold elevations following sound exposure. No increase in hearing threshold for 12kHz was identified following sound exposure. Hearing threshold elevations were identified for 16kHz, 24kHz and 30kHz following the conclusion of the sound exposure protocol. (B) Graph showing the absolute hearing thresholds across the tested frequencies for each ABR.

$Na_V1.6$: The staining seen with the $Na_V1.6$ antibody in sections of control cochleae was similar to that reported in the previous chapter. There was intense labelling of both the SGN central and peripheral processes as well as the cell bodies (Fig. 5.16A and D). Using sections of cochleae from sound-exposed animals, the pattern of SGN staining was identical to that seen from the unexposed control animals. On visual inspection, there appeared to be no difference in the intensity of the $Na_V1.6$ staining in SGN processes and cell bodies (Fig. 5.16B and E). The analysis of cell body staining intensity showed that there was no difference in the $Na_V1.6$ staining intensity distribution between the control and sound-exposed SGN (Fig. 5.16C and F).

$Na_V1.1$: Using the $Na_V1.1$ antibody with sections of control cochleae showed a similar pattern of staining observed previously. With this antibody, there was very faint

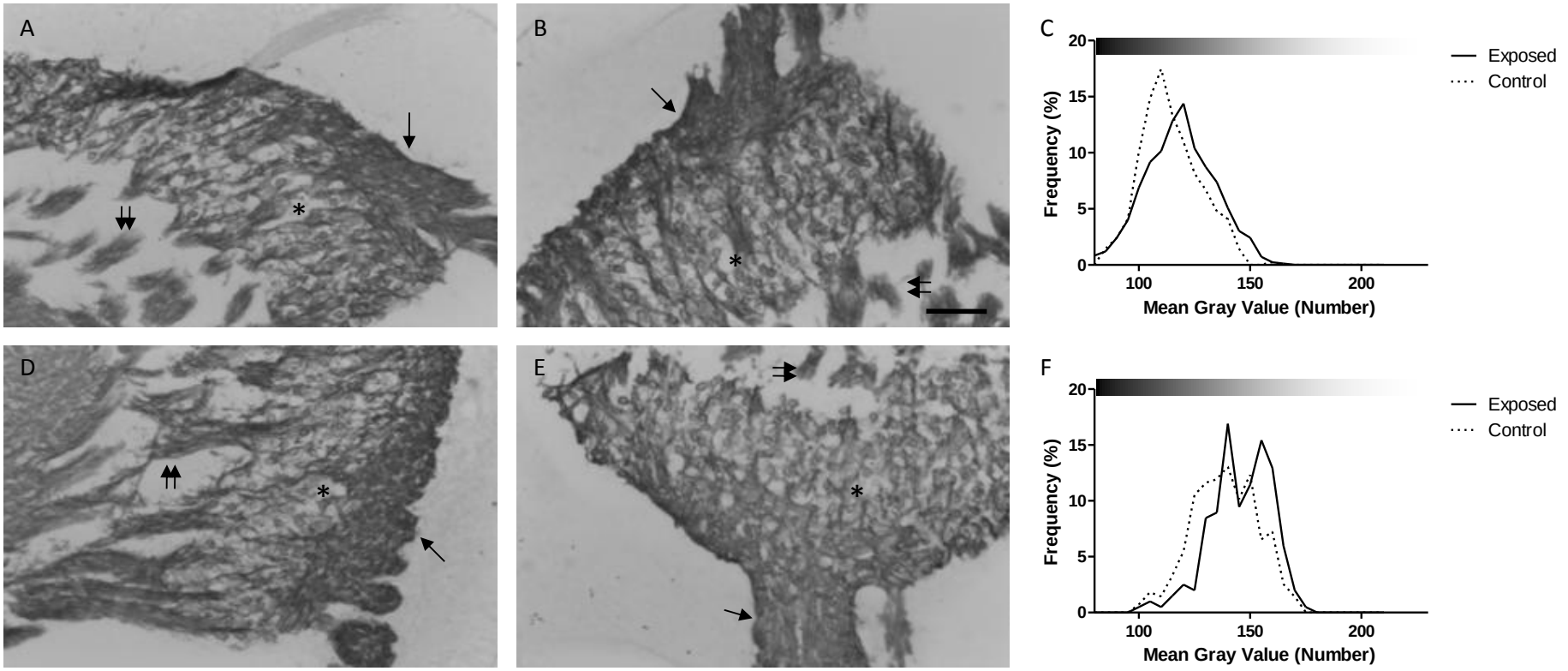

Fig. 5.16. $Na_V1.6$ staining in sound-exposed cochlear SGN. Micrographs of cochlea sections stained for $Na_V1.6$ from control (A,D) and sound-exposed (B,E) animals. Robust staining can be seen in the SGN cell bodies (*), peripheral processes (single arrow) and central processes (double arrow) from the control animals (A,D). Following sound exposure, cell body, peripheral process and central process staining appears similar to the control animals (B,E). Frequency pictographs of the SGN cell body mean gray value (C,F) show no difference in the staining intensity distribution for $Na_V1.6$ between the control (dotted line) and sound-exposed (solid line) animals. Data for graph C taken from the cochlea of the animals represented by A and B while the data for graph F was generated from the cochlea of the animals represented by D and E. Scale bar= 50µm in all micrographs. Gray Values, 0= black, 255= white, indicated by bar above pictographs.

staining of the SGN cell bodies with more intense labelling of the central processes (Fig. 5.17A and D).

The sections of cochleae from sound-exposed animals showed a different pattern of $Na_V1.1$ expression. Staining was still observed in the central processes but intense staining was also observed in the peripheral processes from the exposed cochleae (Fig. 5.17B and E). On visual inspection this peripheral process staining appeared to be more intense in the exposed cochleae than the control cochleae. There was no detectable change in $Na_V1.1$ SGN cell body staining intensity between the exposed and control cochleae (Fig. 5.17C and F).

Further analysis showed that the peripheral processes from the exposed cochleae were significantly more intensely labelled for $Na_V1.1$ than the peripheral processes from the control cochleae (Fig. 5.18). The average mean gray value for the peripheral processes from the sound-exposed animals were 145.1±3.63 while the value from the control animals were 158.7±4.28 ($p<0.05$).

Is there evidence for SGN cell loss following noise exposure? The number of SGN cell bodies was counted in sections of cochleae from three sound-exposed and three control animals. Additionally the area of Rosenthal's canal, in which the SGNs reside, was also measured so that the density of the SGN could be calculated. The analysis showed that on average there were 32.3±2.2 SGN per 10,000μm^2 in the sections taken from control cochleae. From the sections taken from sound-exposed cochleae the mean density of SGN was 33.6±0.9 cell bodies per 10,000μm^2 (Fig. 5.19A). There was

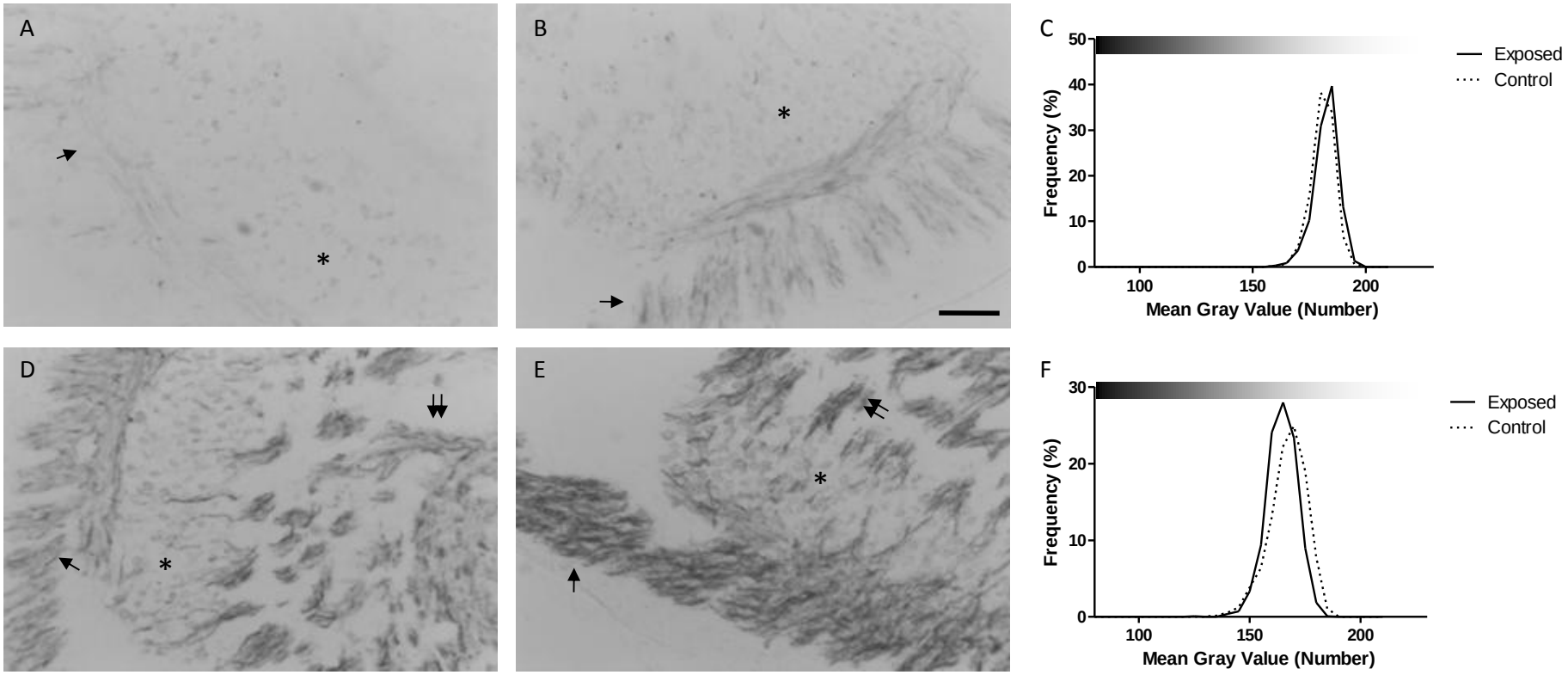

Fig. 5.17. $Na_V1.1$ staining in sound-exposed cochlear SGN. Micrographs of cochlea sections stained for $Na_V1.1$ from control (A,D) and sound-exposed (B,E) animals. Faint staining can be seen in the SGN cell bodies (*) and peripheral processes (single arrow) with more intense labelling observed in the central processes (double arrow) from the control animals (A,D). Following sound exposure, cell body and central process staining appear similar to the control animals, while an increased staining can be observed in the peripheral processes (B,E). Frequency pictographs of the SGN cell body mean gray value (C,F) show no difference in the staining intensity distribution for $Na_V1.1$ between the control (dotted line) and sound-exposed (solid line) animals. Data for graph C taken from the cochlea of the animals represented by A and B while the data for graph F was generated from the cochlea of the animals represented by D and E. Gray Values, 0= black, 255= white, indicated by bar above pictographs.

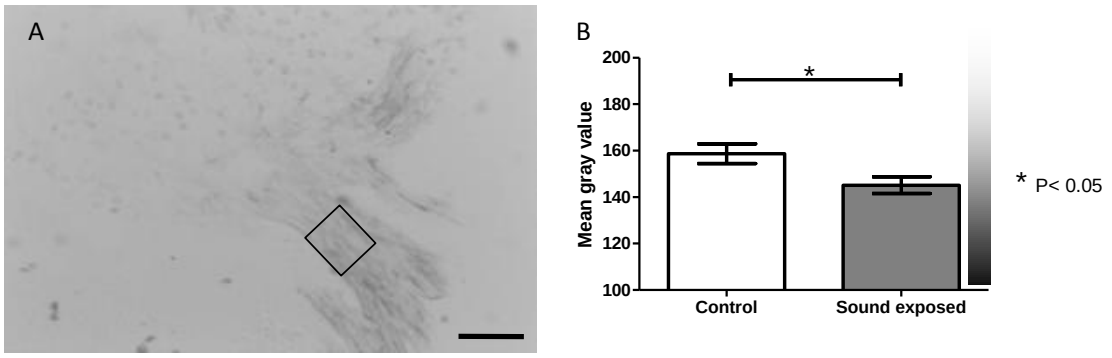

Fig. 5.18. Staining intensity of peripheral processes labelled with $Na_V1.1$. (A) Micrograph of a cochlea section labelled with $Na_V1.1$ showing the area of the peripheral processes that was measured (square). (B) Graph showing the mean gray values of the peripheral processes from control and sound-exposed animals. Scale bar= 50µm. Gray value scale, 255= white, 0= black as indicated by graduated bar (n=3 for both conditions).

no significant difference in the mean density of SGN between the control and sound-exposed groups ($p>0.05$). Additionally, there was no significance in the SGN density in sections taken from the apex, middle and base of cochleae from sound-exposed and control animals (Fig. 5.19B).

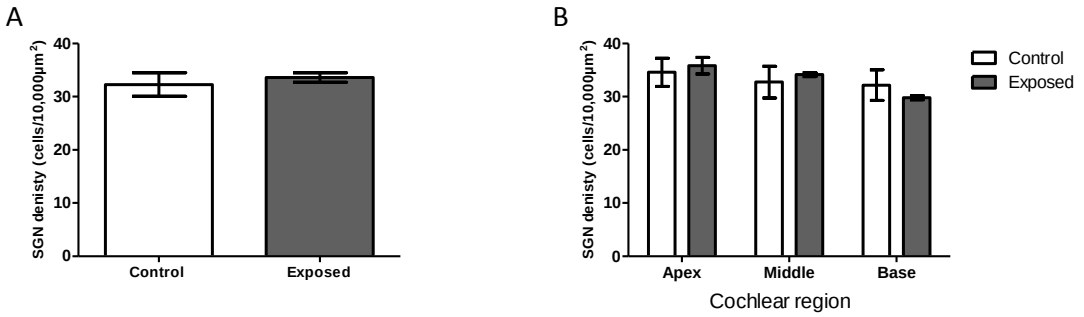

Fig. 5.19. SGN cell body density. Graphs showing the mean SGN cell body density from control (clear bars) and sound-exposed (filled bars) animals. (A) The average SGN cell body density from all cochlear sections shows no significant difference in the number of SGN following the sound exposure protocol. (B) The average SGN cell body density from cochlear sections representing the apex, middle and base show no significant difference between the control and sound-exposed animals (n=3 for each condition).

Discussion

Does sound exposure affect SGN voltage-gated Na^+ channel composition?

RNA expression following sound exposure: The RT-PCR results showed that only the mRNA for $Na_V1.1$, $Na_V1.6$ and $Na_V1.7$ were detected following the sound exposure protocol. This indicates that the mRNA for other voltage-gated Na^+ channel isoforms are either not expressed in the SGN following sound exposure or are expressed at such a low level that they are undetectable using the RT-PCR technique. This result is in contrast to studies demonstrating that $Na_V1.3$, an isoform predominantly expressed during embryonic development (Waxman *et al.* 1994), is expressed following damage to the adult somatic sensory neurons, seen for example in DRG (Black *et al.* 1999, Dib-Hajj *et al.* 1996, Dib-Hajj *et al.* 1999) and the dorsal horn of the spinal cord (Hains *et al.* 2003). This re-expression of $Na_V1.3$ is believed to cause these sensory neurons to become hyperexcitable, as $Na_V1.3$ rapidly recovers from inactivation and thus allows faster action potential generation (Cummins and Waxman 1997, Cummins *et al.* 2001), and contributes to the sensation of neuropathic pain.

While no additional voltage-gated Na^+ channel isoform mRNA was detected, there was a difference in the quantity of the mRNA for the established voltage-gated Na^+ channel isoforms following sound exposure. A significant decrease in $Na_V1.6$ mRNA expression was observed following sound exposure. Also there was a small yet significant decrease in the expression of $Na_V1.1$ and a significant increase in $Na_V1.7$ expression. As the cell counting experiments showed no difference in the total number of SGN cell bodies between the sound-exposed and control modioli, this suggests that the drop in $Na_V1.6$ mRNA expression is the result of a cellular response to the sound exposure as

opposed to a decrease in SGN number, caused by cell death by necrosis or apoptosis. These results demonstrate, for the first time, that sound exposure can induce changes in the level of ion channel expression in the peripheral auditory system, an observation that may have a bearing on the regulation of neuronal excitability at this site.

Immunohistochemistry as a measure of protein expression: In this study we sought to establish whether antibody labelling changed in parallel to gene expression and mRNA levels. To this end, the intensity of staining observed in the SGN cell bodies was measured and contrasted between sound-exposed and control rats.

The measurement of fluorescent or non-fluorescent immunohistochemical staining intensity is, at best, a semi-quantitative measure of protein expression. Immunohistochemistry, much like RT-PCR, gives an indication of whether the protein of interest is expressed by a tissue or cell and also the location of the protein in the section. The staining intensity gives an indication of the relative levels of protein expression in each cell, with strongly stained cells believed to have high levels of protein compared to weakly stained cells. However, measuring intensity of staining does not yield an absolute measure of protein expression. This is because the relationship between protein expression and measured intensity may not be linear; for instance do cells that are twice as dark as others contain twice as much protein? Added to this is the saturation of the staining; the point where the intensity of the staining does not increase despite the presence of the antigen. As demonstrated in Fig. 5.20, the linear increase in protein concentration may not be fully represented by

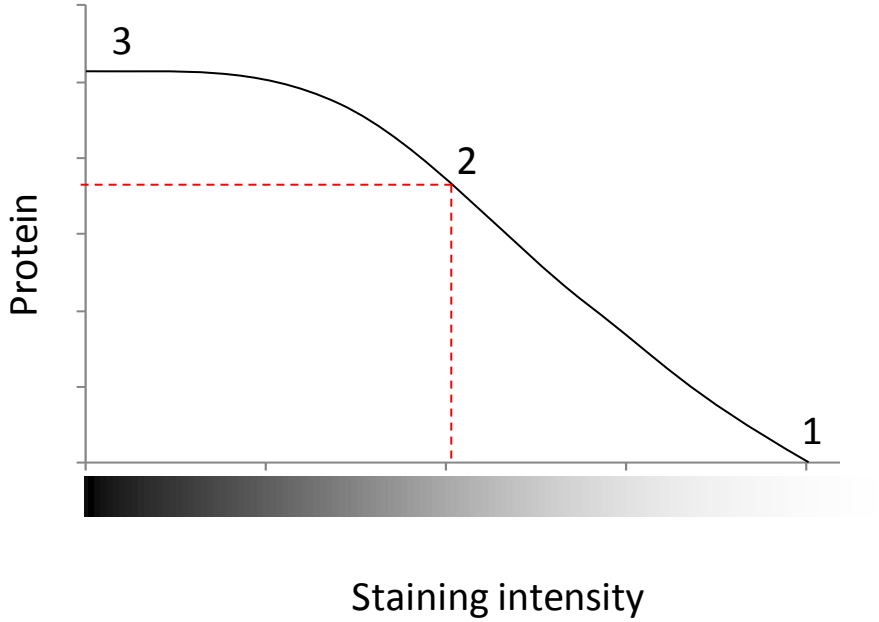

Fig. 5.20. Measuring staining intensity as an indication of protein content. Diagram representing the possible relationship between the measurement of non-flouresent immunohistochemical staining intensity and protein expression level. 1) No staining (white) indicates a lack of antibody binding and thus no expression of the protein of interest. 2) Increase in staining intensity indicates an increase in protein content but as the staining saturates (3) the resolution is lost and a two-fold increase in staining intensity does not indicate the same level of protein content.

the increase in staining intensity. A further consideration in this instance is the use of the horseradish peroxidase detection, as the development of the stain is dependent on the activity of the enzyme, alterations in environmental temperature between experiments could have profound effects on staining intensity and time to develop staining. Thus using the intensity of staining is best suited for identifying profound changes in comparative protein expression, where staining alters from very light to very dark, as opposed to subtler changes. For more quantitative description of protein expression other methods, such as Western blotting, could be used, although even this method fails to provide a precise measure of absolute protein levels.

As stated above, the staining intensity of the SGN cell bodies was measured. These measurements were taken as the cell bodies appeared to be robustly labelled for the voltage-gated Na^+ channel isoforms of interest (as shown in Chapter 3). However, identifying any changes in antibody labelling at regions of the SGN responsible for action potential generation and propagation, such as the nodes of Ranvier or along the post-synaptic membrane innervating the hair cells, would be more beneficial in indicating a functional role of any changes in voltage-gated Na^+ channel expression. As discussed in Chapter 3, the microarchitecture of the organ of Corti is not well preserved using the cochlear sectioning methods, precluding the analysis of the post-synaptic region of the SGN. Additionally, the immunohistochemistry labelling failed to clearly identify clustering of voltage-gated Na^+ channels along the neuronal processes that would indicate nodes of Ranvier. Electron microscopy and immunogold labelling would provide better identification of nodes of Ranvier (Rieger *et al.* 1986, Steffensen *et al.* 1997), although these were not preformed due to the time constraints of the project. Thus measuring the SGN cell bodies was primarily performed to indicate protein expression.

$Na_V1.7$ protein expression: The pattern of $Na_V1.7$ labelling seen in the SGN from sound-exposed animals showed a large degree of variation between the experimental subjects. In comparison with control animals processed for immunohistochemistry simultaneously, three animals showed an increase in the frequency of the darker stained neurons; one animal showed an increase in the frequency of lightly stained neurons; one animal showed an increase in the frequency of both the lightly and darker stained neurons; and one animal showed no change in SGN staining intensity

distribution. This shows there is a degree of variability in the results gathered between animals that have been exposed to the same sound exposure protocol. Other studies have shown variability in the cellular responses following noise induced hearing loss experiments, especially when investigating hair cell loss (Ou *et al.* 2000, Perez *et al.* 2004, Bauer *et al.* 2007). This demonstrates that the cellular response to sound exposure is not uniform even in animals from the same strain. It must also be noted that the changes in staining intensity seen were not dramatic. In many cases the SGN staining intensities between the sound-exposed and control cochleae were within the same mean gray value range. This suggests subtle changes in cell body $Na_V1.7$ staining intensity distribution, with subpopulations of the SGN showing altered $Na_V1.7$ expression following sound exposure rather than changes to the whole SGN population.

Half of the sound-exposed rats showed an increase in the frequency of the darker stained SGN cell bodies compared to the appropriate control cochleae (group 1, 3 out of 6 rats analysed). This indicates an increase in $Na_V1.7$ protein expression in these neurons following sound exposure. This is complemented by the qPCR results which showed an increase in $Na_V1.7$ mRNA in the sound-exposed modioli. These results are similar to those reported for $Na_V1.9$ expression in models of inflammatory pain. An increase in $Na_V1.9$ mRNA (Tate *et al.* 1998) and protein (Amaya *et al.* 2006) have been reported in DRG cell bodies seven days after the injection of Freund's complete adjuvant. While these increases have been seen in the DRG cell bodies, no increase in $Na_V1.9$ has been identified in the processes following inflammation (Coggeshall *et al.* 2004). However, $Na_V1.9$ knock-out mice have shown a reduction in inflammatory pain

behaviour (Amaya *et al.* 2006) indicating $Na_V1.9$ is important in the generation of inflammatory pain. This suggests that the increase in $Na_V1.7$ staining following noise exposure could contribute to an increase neuronal excitability, in a similar fashion to the up-regulation of $Na_V1.9$ associated with inflammatory pain, without the observed neuronal translocation observed with $Na_V1.8$ in neuropathic pain studies (Novakovic *et al.* 1998, Thakor *et al.* 2009).

One sound-exposed animal showed an increase in the frequency of lighter stained SGN cell bodies compared to the appropriate control animal (group 2). This suggests a decrease in $Na_V1.7$ protein expression in the SGN cell bodies following sound exposure, comparative to changes in the pattern of $Na_V1.8$ staining seen in DRG neurons following axotomy (Novakovic *et al.* 1998). The decrease in $Na_V1.8$ staining observed in the DRG cell bodies was attributed to the translocation of the protein from the cell body to the site of injury, suggesting that the $Na_V1.7$ protein could be transported from the SGN cell body to the synapse innervating the organ of Corti. One sound-exposed animal showed an increase in the frequency of the darker and lighter stained SGN cell bodies, compared to the appropriate control cochlea (group 3). This suggests a combination of both an up-regulation of $Na_V1.7$ expression restricted to the apical and middle regions and a down-regulation of $Na_V1.7$ throughout all regions of the cochlea in this subject. The remaining sound-exposed animal showed no change in SGN $Na_V1.7$ staining intensity when compared to the control animal (group 4), despite the animal presenting elevated hearing thresholds, 10dB at 24kHz and 20dB at 30kHz, prior to dissection and increased $Na_V1.1$ staining along the SGN peripheral processes. It must be noted that for groups 2 through 4, only one animal was identified in each

pattern of $Na_V1.7$ expression. Further cochleae would have to be investigated to ensure if the expression patterns classified here are repeatable.

One interpretation of the different $Na_V1.7$ expression patterns observed following sound exposure would be that the different groups represent different stages in a response to the sound exposure protocol and deafness. The response starts with an increase in $Na_V1.7$ expression (case 1) followed by a gradual down-regulation starting at the basal SGN and spreading apically (case 3) until $Na_V1.7$ expression in the cell bodies has decreased to the level seen in case 2. The three animals that showed an increase in darker stained neurons would represent the starting point after sound exposure, where there is an increase in $Na_V1.7$ expression. The cochlea that showed the increase in both darker and lighter stained neurons would represent the midpoint, where $Na_V1.7$ expression is reduced predominantly at the basal SGN. The cochlea that showed the increase in the lighter stained neurons would represent the endpoint, where $Na_V1.7$ expression is down-regulated at all levels of the cochlea.

The reason why the animals show different $Na_V1.7$ staining patterns following the same sound exposure could be related to their individual susceptibility to sound-induced hearing loss. The group 1 animals could represent the majority of the animals that are normally sensitive, while group 2 could be more vulnerable to sound exposure as the animal showed the greatest threshold elevations across all tested frequencies. The animal in group 4 could be tolerant to the effects of the sound exposure protocol, although the ABR threshold elevations were similar to the animals in group 1. This proposed difference in susceptibility could mean that the cochleae are responding at

different rates according to vulnerability, representing different points along the hypothesised $Na_V1.7$ expression response. To test whether the $Na_V1.7$ expression changes over time following sound exposure, further cochleae would be investigated for $Na_V1.7$ expression at different times after the last sound exposure, such as before and after the six days currently used. Additional sound exposures could also be performed to investigate whether the degree of $Na_V1.7$ expression change in the SGN is related to the extent of the animals hearing loss.

The cellular cues for these changes in $Na_V1.7$ expression are difficult to identify at this time. The increase in $Na_V1.7$ expression could be in response to the degeneration of the SGN peripheral processes following glutamate excitotoxicity, as production of the protein could be increased as the neuron re-innervates the hair cell. The down-regulation of $Na_V1.7$ could be due to changes of the neurotrophic support from the hair cells, due to hair cell damage, the initiation of apoptosis/necrosis or gene expression following sound exposure. It has been shown that the hair cells produce neurotrophins that support the SGN, particularly neurotrophin 3 (NT-3) produced by IHC to support Type I SGN (Ylikoski *et al.* 1993, Ernfors *et al.* 1995). Noise induced hearing loss has also been shown to induce the transcription of immediate early response genes that encode for neurotrophins and transcription factors (Tan *et al.* 2007, Cho *et al.* 2004). As the hair cells in the basal portion of the cochlea have been shown to be more prone to damage than their apical counterparts (Chen and Fechter 2003) it would be reasonable to think that any change in hair cell function or neurotrophin production would be observed in the basal hair cells first. Hence, the

basal SGN would respond to the altered hair cell function before the apical SGN, and a decrease in $Na_V1.7$ expression could be seen beginning with the basal SGN.

In vitro studies have shown the expression of voltage-gated K^+ channels can be altered by incubating SGN explants in media containing different concentrations of neurotrophins, particularly NT-3 and brain derived neurotrophic factor (BDNF) (Adamson *et al.* 2002b). Furthermore, it has been recently shown in rat DRG that NT-3 can reduce voltage-gated Na^+ channel expression following sciatic nerve constriction injury (Wilson-Gerwing *et al.* 2008) and BDNF can increase neuronal excitability *in vitro* (Zhang *et al.* 2008). Thus, the decrease in $Na_V1.7$ expression seen in the SGN could be due to an increase in NT-3 expression. Additionally, BDNF expression in the cochlea has been shown to increase following noise exposure (Tan *et al.* 2007), which could result in increased SGN excitability. In summary, if neurotrophin levels were altered in the cochlea by noise exposure then changes in ion channel expression and SGN excitability could ensue. Further experiments, such as those performed in Tan *et al*. (2007), could be performed to investigate the level of neurotrophin expression in the SGN before and following the sound exposure protocol devised in this study.

Another potential explanation for the variation in $Na_V1.7$ staining would be to consider the prevalence of tinnitus generation in animal models following noise exposure. As tinnitus is a perceptual condition, evaluating whether an animal experiences tinnitus following exposure to an intense sound or noise must be done using behavioural experiments. Many of the published studies investigating tinnitus state that the animals “may” or “usually” develop tinnitus following sound exposure, indicating

overlap in the behaviours performed by the sound-exposed and control animal groups (Kaltenbach *et al.* 2004, Heffner and Harrington 2002). This demonstrates that only a proportion of the animals exposed to sound generate tinnitus like behaviour. One of the findings of the current study that echoes the published incidence of tinnitus behaviour is that changes in $Na_V1.7$ expression following sound exposure is not consistent across the investigated animals. While the majority of the cochleae investigated show an increase in $Na_V1.7$ expression in the SGN, cochleae from other individuals do not. While the prevalence of tinnitus behaviour and the increased expression of $Na_V1.7$ may be coincidental, further experiments would have to be performed to determine if there is any correlation between the incidence of tinnitus behaviour and increased expression of $Na_V1.7$ in sound-exposed animals. These would require determining if the rats experience tinnitus, through conditioned behavioural responses or gap detection methods as described in Chapter 6, and subsequently analysing their cochleae for $Na_V1.7$ immunoreactivity.

The variation in $Na_V1.7$ staining intensity could also be due to limitations of the non-fluorescence staining technique. As this technique depends on the enzymatic breakdown of DAB, any variations in ambient temperature or exposure time could result in darker or lighter staining. Precautions were taken to reduce this variability, with the slides from control and exposed cochleae processed in parallel under a fume hood.

Additionally, the variations in $Na_V1.7$ staining seen could be due to biological variability between the rats tested. Further cochleae from sound-exposed rats would have to be

investigated to determine if $Na_V1.7$ expression falls into one of the 4 groups put forward in this chapter. The qPCR experiments have shown that the expression of mRNA for $Na_V1.7$ is at a much lower level than $Na_V1.1$ or $Na_V1.6$. This suggests that $Na_V1.7$ is not the predominant isoform expressed in the SGN and that the variations in staining reported here may not lead to changes in SGN function. However, mRNA level does not necessarily correlate with protein expression level, especially as the immunohistochemistry results showed very strong $Na_V1.7$ staining despite the low mRNA level, and additional experiments would need to be performed to investigate whether altered $Na_V1.7$ expression results in altered SGN function. At present, little is known about how quickly or slowly voltage-gated Na^+ channels are replaced in the neuronal membrane, or how quickly changes in mRNA expression result in altered protein expression. While details have emerged about how voltage-gated Na^+ channels are inserted and removed from the membrane (Ekberg and Adams 2006), it is currently unknown how these processes are altered following neuronal damage. Further experiments investigating any change in the expression and function of ankyrin, annexin II and contactin to insert the voltage-gated Na^+ channels into the SGN membrane (Chahine *et al.* 2005), or ubiquitin ligases of the Nedd4 family promoting Na^+ channel degradation (Fotia *et al.* 2004), could be performed to investigate whether the alterations in immunohistochemistry staining observed following noise exposure are a result of increased Na^+ channel insertion or removal.

The functional significance of any alteration in $Na_V1.7$ expression must be considered, as $Na_V1.7$ has been shown to remain open in response to slow ramp depolarisations (Cummins *et al.* 1998, Herzog *et al.* 2003). It is currently unclear how the functional

properties of the SGN would be affected by an alteration in $Na_V1.7$ expression. In a recent human study, mutations that result in a non-functional $Na_V1.7$ protein have been shown to confer insensitivity to painful stimuli while retaining all other sensory modalities, including hearing (Cox *et al.* 2006). While this suggests that $Na_V1.7$ is not essential for normal hearing in humans, no implication is made as to the contribution of the protein following noise induced hearing loss or induction of tinnitus. Also, there are gain of function mutations of $Na_V1.7$ that cause pain, such as paroxysmal extreme pain disorder (PEPD), previously known as familial rectal pain (Fertleman *et al.* 2006), and primary erythromelalgia (Yang *et al.* 2004, Dib-Hajj *et al.* 2005). These mutations are believed to reduce the threshold of activation of action potentials and generating the sensation of pain (Dib-Hajj *et al.* 2007). It appears that these mutations do not generate hearing disorders or tinnitus, at least these symptoms are not reported, but no implication is made as to how the increase in neuronal activity would affect the auditory pathway following noise-induced hearing loss.

$Na_V1.6$ protein expression: As shown previously, a dramatic decrease in $Na_V1.6$ mRNA was identified following sound exposure, indicating that sound exposure can induce changes in $Na_V1.6$ mRNA expression in the cochlea. Following this, the immunohistochemistry experiments showed no difference detected in the $Na_V1.6$ labelling at the cell bodies of sound-exposed and control SGN. This does not definitively mean that there is no change in protein expression between the sound-exposed and control SGN. If there was a change in $Na_V1.6$ expression at the afferent dendrite synapse, between the SGN and the hair cell, then this could not be detected due to the poor preservation of the morphology of the organ of Corti. Additionally, any

subtle changes in protein expression at nodes of Ranvier would also be undetected at this point. A decrease in $Na_V1.6$ mRNA could lead to a decrease of $Na_V1.6$ channels at nodes, resulting in decreased Na^+ current at these regions and the possible failure to propagate action potentials. This could lead to a decrease in axonal firing frequency, a result seen with the decrease in P1 amplitude following sound exposure (Chapter 4).

As the immunohistochemistry technique used here is semi-quantitative, subtle changes in protein expression would not necessarily be detected. A more suitable quantitative method would be needed to ascertain if $Na_V1.6$ protein levels change following sound exposure, such as Western blotting or mass spectrometry. However certain technical limitations prevent this from being performed at this time, particularly the small size of the cochlea and the tiny amount of detectable protein that can be extracted from the SGN. It must also be considered that a change in mRNA does not necessarily indicate a change in protein expression (Anderson and Seilhamer 1997).

$Na_V1.1$ protein expression: There was an increase in the staining for $Na_V1.1$ seen in the peripheral process of the SGN following sound exposure, while the staining in the cell bodies and central processes remained similar to sections from unexposed control animals. This indicates an increase in protein expression along the SGN dendrites that innervate the hair cells.

This change in staining pattern is similar to that observed for $Na_V1.8$ in somatosensory nerves following sciatic nerve injury. Using sciatic nerve lesions in rat models of

neuropathic pain, an increase in $Na_V1.8$ staining was seen in the injured nerve while no change was observed in the contralateral nerve (Novakovic *et al.* 1998, Thakor *et al.* 2009). The increase in labelling was also accompanied by an increase in neuronal excitability and TTX resistant current. In addition, a decrease in $Na_V1.8$ staining in the DRG cell bodies ipsilateral to the sciatic nerve injury was observed, thought to be due to translocation of the protein from the cell body to the site of injury (Novakovic *et al.* 1998). The increase in $Na_V1.1$ staining in the peripheral processes of the SGN parallels the expression of $Na_V1.8$ in damaged sciatic nerve, indicating that the increase in $Na_V1.1$ staining might be due to peripheral translocation of the $Na_V1.1$ protein. It must be noted that a decrease in $Na_V1.1$ staining in the SGN cell bodies following sound exposure was not seen. As the staining for $Na_V1.1$ in the SGN cell bodies from control cochleae was very faint, a decrease in staining intensity might not be detectable using the current methodology.

In addition, Thakor *et al*. reported an increase in $Na_V1.8$ mRNA in the injured sciatic nerve, believed to be transported from the neuronal cell body to the site of injury for local translation (Thakor *et al.* 2009), despite the general view that proteins are created and transported from the cell body. This chapter has reported that that an overall decrease in $Na_V1.1$ mRNA was detected in the sound-exposed animals, using mRNA isolated from the whole SGN. If the mRNA was isolated from just the SGN peripheral processes there may be evidence of localised elevated mRNA levels due to transportation from the cell bodies, mirroring the results reported in the sciatic nerve injury model. Further experiments, such as *in situ* hybridization (Hiel *et al.* 1996, Ruan *et al.* 2008, Taranda *et al.* 2009) or careful dissection of the SGN peripheral processes

(Whitlon *et al.* 2006), would be required to investigate first whether there is transportation of the mRNA for $Na_V1.1$ from the cell bodies along the peripheral processes and if there are any changes following sound exposure.

Other human pain states have provided a link between an increase in voltage-gated Na^+ channel expression in nerve fibres and the sensation of pain. Samples taken from patients suffering from pulpitis (tooth pain) have shown an increase in $Na_V1.7$ (Luo *et al.* 2008) while sufferers of rhinitis showed increase in $Na_V1.7$, $Na_V1.8$ and $Na_V1.9$ (Keh *et al.* 2008) labelling in the respective nerve fibres. In addition, it has been shown that injection of substances that can generate inflammatory pain, such as FCA and carrageenan, can up-regulate voltage-gated Na^+ channel expression in rat DRG (Strickland *et al.* 2008, Black *et al.* 2004, Tate *et al.* 1998, Amaya *et al.* 2006, Coggeshall *et al.* 2004). If neuronal damage following sound exposure resulted in an inflammatory response from the cochlea, then a redistribution of voltage-gated Na^+ channel might occur, such as the observed expression of $Na_V1.1$ along the SGN peripheral processes following sound exposure, and this could influence nerve excitability. It has been shown experimentally that the cochlea can generate an immune response to injected immunogenic molecules (Ma *et al.* 2000). It has also been shown that the cochlea can produce inflammation following exposure to damaging levels of noise (Fujioka *et al.* 2006), with the infiltration of the cochlea by macrophages believed to remove the cellular debris of damaged hair cells and to preserve the integrity of the basilar membrane partition (Hirose *et al.* 2005, Tornabene *et al.* 2006, Miyao *et al.* 2008). How this inflammatory response affects the SGN is unknown, although histological analysis of Rosenthal's canal for any interaction

between SGN and inflammatory cells could be performed (Hirose *et al.* 2005, Tornabene *et al.* 2006, Miyao *et al.* 2008).

ABR threshold elevation variations between sound-exposed animals: The ABR results presented here reveal a degree of variability in the threshold elevations generated by exposing animals from the same strain to the same sound exposure protocol. The three animals used for RT-PCR analysis did not show statistically significant average hearing threshold elevations at 24kHz and 30kHz, in contrast to the animals used for qPCR and immunohistochemistry. While the threshold elevations were not statistically significant in these three rats, hearing threshold elevations were evident, indicating a variable degree of hearing loss in these animals that may not have reached statistical significance due to a very small sample size. This observation is similar to the variability seen in other noise induced hearing loss studies (Ou *et al.* 2000, Perez *et al.* 2004). Interestingly, the animals used for the qPCR experiments had significantly elevated hearing thresholds and produced results similar to those seen from the RT-PCR gels, further illustrating that the model of ototrauma does not result in additional voltage-gated Na^+ channel mRNA expression. Whether an even greater degree of hearing loss, caused from additional sound exposures or similar, would cause other voltage-gated Na^+ channel genes to be transcribed would have to be investigated further.

Voltage-gated Na^+ channel expression changes following nerve damage: This discussion has drawn many parallels between the redistribution of voltage-gated Na^+ channel isoforms in neuropathic and inflammatory pain states with the voltage-gated

Na^+ channel expression observed in the SGN following sound exposure. One of the recurring characteristics of voltage-gated Na^+ channel expression in models of neuropathic pain is the redistribution of voltage-gated Na^+ channel isoforms at the site of nerve damage, particularly where the nerve has been lesioned (Novakovic *et al.* 1998, Thakor *et al.* 2009). It has been reported that noise exposure, shown to generate tinnitus behaviour using a conditioned response suppression method, can result in a decrease in density of processes within the OSL (Kujawa and Liberman 2009, Bauer *et al.* 2007). This decrease in processes could be due to deafferentation of the hair cells and be considered as a lesion of the SGN peripheral processes, similar to the axotomy of the sciatic nerve. Similar rigorous histology to that performed by Bauer *et al*. would be required however to determine if analogous peripheral fibre loss occurred in the present study of sound exposure (Bauer *et al.* 2007).

The decrease in neuronal processes following noise exposure could be due to glutamate neurotoxicity. Local application of glutamate to the cochlea has been shown to disrupt the afferent synapse between the hair cell and SGN (Pujol *et al.* 1990). Similar dendritic disruption was also seen following noise exposure, and prevented with the application of the broad glutamate receptor antagonist kynurenate (Puel *et al.* 1998). This shows that noise exposure can separate the SGN from their target hair cells in a manner that can be considered comparable to the lesion of the sciatic nerve seen in pain models. It has been shown that voltage-gated Na^+ channel channels can accumulate in sectioned nerves in human painful neuromas, and that this accumulation generates the hypersensitivity associated with the neuroma (England *et al.* 1996, Kretschmer *et al.* 2002). If a similar pattern of voltage-gated Na^+ channel

accumulation occurred in the SGN, such as the staining seen for $Na_V1.1$ following sound exposure, this could confer altered sensitivity to the afferent synapse as it re-establishes the connection to the hair cell. This could potentially contribute to the generation of tinnitus or hyperacusis, as the SGN would require a smaller stimulus following noise exposure to generate action potentials. Hence, action potentials could be generated in periods of silence or sounds below the threshold of hearing, potentially generating the sensation of tinnitus or altered susceptibility to sound.

It is of interest to note that sound exposure experiments by Puel *et al*. used a 6kHz single tone presented for 15 minutes to guinea pigs at either 100/110dB or 120/130dB. The 100/110dB presentation showed no disruption of the dendrites while the 120/130dB tone showed a large degree of dendritic damage. While this suggests that the 110dB 14.8kHz tone used in this study may not cause the dendritic swelling documented in guinea pigs, the rats were exposed to the tone for a total of 4 hours (two sessions, two hours per session). This increase in duration may well cause dendritic swelling, although probably to a smaller degree than observed for the 130dB tone presentation. Further investigation would determine if the sound exposure protocol results in the disruption of the SGN dendrites, such as evaluation using electron microscopy (Pujol *et al.* 1990, Puel *et al.* 1998).

Noise exposure has also been shown to generate a general inflammatory response in the cochlea (Hirose *et al.* 2005, Tornabene *et al.* 2006, Miyao *et al.* 2008). This response is thought to be due to hair cell loss, with the cochlear macrophages removing the cellular debris and repairing the reticular lamina. This inflammatory

response can arise from complete hair cell loss, although partial hair cell loss has been shown to generate the same inflammatory reaction (Hirose *et al.* 2005). However, how the SGN are affected in this inflammatory process is currently unknown.

While the results presented here show an increase in $Na_V1.1$ staining in the peripheral processes following sound exposure, changes in $Na_V1.7$ and $Na_V1.6$ were not apparent in the processes innervating the organ of Corti. If there was increased voltage-gated Na^+ channel accumulation at the synapse between the hair cell and SGN then this would be undetected using the current methodology, as the morphology of the organ of Corti is not preserved. Changing the frozen sectioning for paraffin or plastic embedding and sectioning would increase the preservation of the organ of Corti (Maison *et al.* 2007), although it has been the laboratory's experience that the antigenicity of the sections is reduced when using paraffin embedded sections. An alternative to sectioning would be to extract the organ of Corti using a surface preparation (Ruan *et al.* 2008, Kohonen and Tarkkanen 1966, Axelsson *et al.* 1975, Shibata *et al.* 2007). This technique would also allow the counting of the hair cells following sound exposure experiments as well as investigating the condition of the hair cell stereocilia and membranes.

One drawback from the experimental approach adopted is that the PCR and immunohistochemistry experiments are performed using cochleae from different individual animals. As the ABR and $Na_V1.7$ immunohistochemistry results from this study have shown, there can be a degree of variability in the results gathered between animals that have been exposed to the same sound exposure protocol. Additionally,

other studies have shown that variability is inherent in experiments investigating noise induced hearing loss (Ou *et al.* 2000, Perez *et al.* 2004). The ideal solution would be to process the cochleae from a single animal for both PCR and immunohistochemistry. While this cannot be conducted at present, recent publications using laser microdissection have shown that it is possible to collect SGN from cochlea sections for PCR analysis that have been previously used for immunohistochemistry (Pagedar *et al.* 2006, Torkos *et al.* 2008). This method would allow a direct comparison of mRNA and protein expression, as well as threshold elevation following sound exposure, from a single cochlea. Furthermore, this technique would allow the collection of samples containing only SGN cell bodies, peripheral processes or central processes. Characterisation of voltage-gated Na^+ channel protein and any mRNA differences between these neuronal regions could then be conducted.

Moderate sound exposure does not alter SGN density: Severe noise damage, above 120dB SPL, has been shown to result in the loss of SGNs (Spoendlin 1971, Spoendlin 1975, Fredelius *et al.* 1988) following hair cell loss (Spoendlin and Brun 1973, McFadden *et al.* 2004, Spoendlin 1971). As stated above, the cell counting experiments showed that there was no difference in the SGN density in the cochleae from sound-exposed and control animals over the time period of the experiment. This indicates that the moderate sound exposure protocol used here does not acutely decrease the number of SGN. It also suggests that the elevation of hearing thresholds and decrease in P1 amplitudes seen after sound exposure is not due to a dramatic loss of the SGNs. The hearing loss seen in the sound-exposed animals could be due to damage to the organ of Corti and/or the afferent synapses between the hair cells and

the SGNs. As stated previously, a decrease in afferent processes has been identified following noise exposure with no correlation between hair cell loss and threshold elevations (Bauer *et al.* 2007). These authors did not however investigate any correlation between SGN density and threshold elevation following noise exposure, so it is unknown whether the fibre reduction is due to SGN loss or degeneration of the peripheral processes.

Additionally, a recent study presenting 100dB SPL octave band (8-16kHz) noise to mice for 2 hours showed a temporary hearing threshold elevation at tested frequencies greater than the noise exposure and reduction of afferent fibres without any decrease in IHC numbers at the corresponding regions of the cochlea (Kujawa and Liberman 2009). However, during the following months of recovery, these authors found a decrease in the SGN population of 40-60% and a decrease in the number of IHC ribbon synapses without a decrease in IHC number at the high frequency regions of the cochlea. This indicates that even a modest ototrauma insult that does not cause the degeneration of IHCs can result in the loss of SGN over time. Further experiments using prolonged recovery periods, similar to those by Kujawa and Liberman (2009), would have to be performed to investigate whether the moderate sound exposure protocol used in this study would ultimately result in a delayed degeneration of the SGN.

While there was no identified reduction in SGN density following sound exposure, further investigation could be performed to assess the SGN health post sound exposure. Studies investigating SGN apoptosis following the application of ototoxic

drugs, such as cisplatin (Alam *et al.* 2000, Lee *et al.* 2003) and ouabain (Lang *et al.* 2005), have identified several immunohistochemical markers that may prove useful in discovering the start of an apoptotic cascade following sound exposure. These include cytochrome C labelling in the cytoplasm, indicating apoptosis via mitochondria disruption, and increase in caspase 3 staining.

Additionally, the terminal deoxynucleotidyl transferase (TdT)-mediated dUTP-biotin nick end labelling (TUNEL) assay has been shown to be useful in identifying apoptosis in cochlear sections (Lee *et al.* 2003, Martinez-Monedero *et al.* 2006). The TUNEL assay allows the identification of fragmented DNA, as occurs in apoptosis. This is done by visualising the DNA/TdT complex by biotinylated dUTP and avidin-peroxidase (Gavrieli *et al.* 1992), either fluorescently (Lee *et al.* 2003) or non-fluorescently (Steinbach and Lutz 2007). It must be noted that the TUNEL assay could also reveal necrotic cell death as opposed to apoptosis (Charriaut-Marlangue and Ben-Ari 1995). Either the immunohistochemical markers or TUNEL assay could be used on cochlear sections to identify apoptotic or necrotic SGN following sound exposure.

Does sound exposure alter SGN function? While the results presented here show alterations in voltage-gated Na^+ channel α-subunit expression in the SGN following sound exposure, the issue of whether these changes result in altered neuronal function is currently unaddressed. Many of the above cited pain models link the altered voltage-gated Na^+ channel expression with an increase in neuronal excitability. The hypothesis that the changes in voltage-gated Na^+ channel expression changes in

the SGN following sound exposure reported here results in an increase in SGN excitability would have to be investigated.

Many studies have been performed to investigate the membrane properties of SGN using the whole cell patch clamp technique. However this requires access to the SGN membrane, no mean feat considering the architecture of the cochlea.

Dissecting and dissociating the neurons from the modiolus, generating free SGN adhering to a cover slip or similar, has proved to be a popular method. This involves the mechanical isolation of the neurons from the modiolus through careful trituration using pipettes (Adamson *et al.* 2002a, Santos-Sacchi 1993). Additional enzymatic digestion steps have also been documented to release the neurons from the modiolus, using enzymes such as thermolysin (Ripoll and Rebillard 1997), trypsin (Moore *et al.* 1996), collagenase and pronase (Szabo *et al.* 2002, Szabo *et al.* 2003). Although an enzyme inhibition step would be required to halt the complete digestion of the neurons. Once adhered to the cover slip, the neurons can be used for electrophysiology directly or stored in cell culture. While cell culture with media containing neurotrophins (Whitlon *et al.* 2006) has been shown to promote neuronal survival (Mou *et al.* 1998), prolonged exposure would likely be disadvantageous as neurotrophin application has been shown to alter ion channel expression in these neurons (Adamson *et al.* 2002b). An alternative method would be to generate a cochlear slice preparation. This has been shown to produce access to SGN for electrophysiology (Jagger *et al.* 2000, Jagger and Housley 2003) as well as calcium imaging (Lin *et al.* 2003).

Many the studies cited above have used cochleae from early postnatal animals, ranging from P0 to P14. This is because the cochlea has not fully ossified at this stage of development, so removing the otic capsule and modiolar bone is relatively easy. The animals used in this study were adult Wistar rats, ensuring the cochleae investigated were fully developed. While cell culture methods may be best suited for developing neurons, the dissociation and electrophysiological study of SGN from adult guinea pigs (250-300g) has been documented (Szabo *et al.* 2002, Szabo *et al.* 2003). Also, while cochlear slice preparations may favour the juvenile cochleae, hemicochlear sections may be more suitable for accessing adult SGN (Teudt and Richter 2007).

The contributions of the different voltage-gated Na^+ channel isoforms to the whole cell Na^+ current could be separated by pharmacological means. While the application of TTX would identify TTX resistant currents, and TTX sensitive currents by subtraction (Catterall 2000), other toxins can be used to identify the components of the TTX-S current. The $Na_V1.6$ current could be blocked by the application of a TTX metabolite 4,9-anhydro-TTX (Rosker *et al.* 2007). Additionally, a tarantula venom peptide ProTx-II has been shown to selectively block $Na_V1.7$ currents (Schmalhofer *et al.* 2008). While a $Na_V1.1$ specific blocker is not currently available, the combination of ProTx-II and 4,9-anhydro-TTX could be used and the remaining current would be due to $Na_V1.1$ activity in the SGN. These tools would identify any change in the voltage-gated Na^+ channel current contribution from the voltage-gated Na^+ channel isoforms identified following sound exposure. Alternatively, transgenic mice with the voltage-gated Na^+ channel isoforms knocked out could be used (Do and Bean 2004).

Anaesthesia does not alter voltage-gated Na^+ channel subunit expression

Voltage-gated Na^+ channel expression from control animals: The RT-PCR results from the modioli of control animals showed distinct bands for $Na_V1.1$, $Na_V1.6$ and $Na_V1.7$ only. This result was identical to the RT-PCR results presented in Chapter 3, which indicates that the anaesthesia protocol does not alter the voltage-gated Na^+ channel subunit mRNA expression. The qPCR experiments also showed that the mRNA for these voltage-gated Na^+ channel subunits was robustly identified in the control animals. However, as the qPCR experiments were not performed on mRNA isolated from animals that had not been anaesthetised previously, no conclusion can be drawn whether the anaesthesia has any effect on the level of voltage-gated Na^+ channel mRNA expression in the cochlea. The immunohistochemistry experiments showed positive staining for $Na_V1.1$, $Na_V1.6$ and $Na_V1.7$ in the SGN from unexposed animals, with labelling identical to that seen in the SGN previously. This indicates that the anaesthetics do not alter the pattern of protein expression in these neurons.

The local application of midazolam to the cochlea has been shown to reverse the increase of BDNF mRNA and Arg3.1 protein expression in rat SGN caused by salicylate (Panford-Walsh *et al.* 2008). These increases have been shown to coincide with tinnitus behaviour generation in a model of noise exposure (Tan *et al.* 2007). Additionally, tinnitus behaviour in the salicylate treated animals was also reduced with the local application of midazolam (Panford-Walsh *et al.* 2008), although these experiments were not repeated with animals experiencing tinnitus following noise exposure.

This does not necessarily mean that the use of midazolam in the current study will affect the voltage-gated Na^+ channel mRNA and protein expression following sound exposure. The application of midazolam was systemic in the current investigation while midazolam was delivered locally to the round window of the cochlea in the aforementioned study. Changes in voltage-gated Na^+ channel mRNA and protein expression were detected between the sound-exposed and control animals that were anaesthetised, while no changes were observed between the control animals and animals that were not anaesthetised before sacrifice. Whether the magnitude of the mRNA and protein expression changes were reduced by the use of midazolam could be addressed by the use of an anaesthetic regimen that does not use midazolam. However, as described in Chapter 2, the administration of midazolam with Hypnorm was found to give the best balance between depth of anaesthesia (neuroleptanalgesia), generating stable and repeatable ABR measurements and recovery of the animal at the conclusion of the experiment. Also, the qPCR results for the housekeeping genes showed no significant difference in mRNA levels between the sound-exposed and unexposed control animals, indicating that the anaesthesia does not universally affect the mRNA levels of the neurons.

Housekeeping gene validation: The housekeeping genes are used as internal standards against which the qPCR results are normalised. The proteins these genes encode for are required for the maintenance of the cell and the mRNA is believed to be transcribed at a constant level. While mRNA for β-actin (Choi *et al.* 1991), GAPDH (Tang *et al.* 1996) and cyclophilin A (Bjarnason *et al.* 1998) has been widely scrutinized

in many tissues, certain issues over gene expression consistency have arisen. Differences in gene expression of these housekeepers between male and female rats (Verma and Shapiro 2006), after food deprivation (Yamada *et al.* 1997) and essential amino acid withdrawal (Marten *et al.* 1994) have highlighted that the expression of these constituently active genes is not constant in certain conditions.

The three aforementioned housekeeping genes were analysed in the qPCR experiments, in case the sound exposure protocol altered the expression of these genes. As shown in Fig. 5.6, there was no difference in the average copy numbers for β-actin, GAPDH or cyclophilin A between the control and sound-exposed animals. This shows that the expression of the housekeeping genes is not altered by this sound exposure protocol. While GAPDH has been used previously as the reference gene in studies using cochlear tissue (Torkos *et al.* 2008), β-actin was used to normalise the voltage-gated Na^+ channel gene expression data in this study. This was due to the low copy number of GAPDH, which has been reported in smaller tissues (Barber *et al.* 2005).

In review, this chapter has shown the cohort of voltage-gated Na^+ channel α-subunits expressed in the rat SGN is dramatically altered following the noise exposure protocol. While the RT-PCR results showed no additional voltage-gated Na^+ channel isoforms were detected following noise exposure, the qPCR clearly showed that the levels of mRNA expression of $Na_V1.1$ and $Na_V1.6$ were significantly reduced and $Na_V1.7$ was significantly increased following noise exposure. Additionally, the immunohistochemistry experiments revealed an increase in $Na_V1.1$ labelling in the

SGN peripheral processes and marked changes in $Na_V1.7$ labelling in the SGN cell bodies. This provides evidence, for the first time, that noise exposure, that generates mild hearing loss, can produce altered voltage-gated Na^+ channel expression in the rat SGN.

Chapter 6. Final conclusions and future work.

This thesis has clearly demonstrated, for the first time, that rat SGNs express the mRNA and proteins for three α-subunits of the voltage-gated Na^+ channel family, $Na_V1.1$, $Na_V1.6$ and $Na_V1.7$. It has also been shown that, following exposure to a modest ototrauma model that produces elevated hearing threshold levels without catastrophic reduction of cochlear function, the mRNA levels of these channels, particularly for $Na_V1.6$, alters significantly when investigated 6 days after the noise insult. There is also evidence for altered voltage-gated Na^+ channel protein expression in these neurons, particularly with regard to $Na_V1.1$ and $Na_V1.7$. This suggests that voltage-gated Na^+ channel expression in the SGN can be altered by noise exposure, and expression of these channels may alter following what would be considered as normal variations in the sound intensity of the external acoustic environment. The results also show that reorganisation of the voltage-gated Na^+ channels is not a unique feature of somatosensory neurons.

What has not been addressed is whether the changes in sodium channel expression result in altered SGN activity. To answer this query, electrophysiological recordings of SGN from noise-exposed cochleae would have to be undertaken, particularly looking at action potential generation and ionic conductances, and compared to SGN from unexposed animals. As discussed in Chapter 5, many functional studies of SGN have been published and thus there are a large number of methods that could be used or adapted for the electrophysiological recording of adult rat SGN.

The current investigation has also provided a good foundation for future investigation of voltage-gated Na^+ channels in rat SGN following noise exposure. While the results presented here did not show a decrease in SGN number at 6 days following noise exposure, a recent study has shown that a modest noise insult can generate SGN loss during an extended period of recovery (Kujawa and Liberman 2009). Thus it would be prudent to investigate SGN number and voltage-gated Na^+ channel expression following the current noise exposure protocol at time points beyond the current 6 day recovery period, from between 2 and 50 weeks, to see whether SGN number declines following noise exposure and whether voltage-gated Na^+ channel expression is altered at these points.

What is potassium channel expression in rat SGN and are there any changes following noise exposure? While this thesis has concentrated specifically on voltage-gated Na^+ channels, investigating the expression of other ion channels that contribute to neuronal excitability would be of interest following noise exposure, particularly potassium channels. As mentioned in Chapter 1, the expression of voltage-gated and calcium-activated potassium channels has been characterised in mouse SGN. First, it would be logical to determine if rat SGN express the same compliment of potassium channels as their mouse counterparts and if any tonotopic gradients are replicated, using PCR and immunohistochemistry methods detailed in this thesis. Following this characterisation, potassium channel expression would be investigated following the sound exposure protocol used previously, with sound-exposed and control SGN compared and contrasted. Additionally, potassium channel expression could also be

identified at additional time points during the recovery from sound exposure, as outlined previously for voltage-gated sodium channel expression.

Are ion channel expression changes related to the magnitude of the noise exposure protocol? This thesis has shown that a relatively modest sound exposure protocol can result in profound changes in voltage-gated Na^+ channel expression. An interesting progression of this work would be to investigate whether voltage-gated Na^+ channel expression is related to the magnitude of the sound exposure protocol. The current protocol uses two sound exposure sessions, with each session lasting two hours. It would be possible to expose the rats to addition sessions or to increase the length of each session to increase the sound insult to the animal. The hearing function of the rats would be tested, to detect whether increasing the sound exposure results in further hearing threshold elevations, followed by the expression of voltage-gated Na^+ channels and K^+ channels using PCR and immunohistochemistry techniques.

Additionally, as the results presented have shown that voltage-gated Na^+ channel expression in the SGN can be altered following a modest noise insult, the question of whether ion channel expression could be altered by even less intense sound exposures arises. Experiments to investigate this would require exposing rats to noise intensities of between 100dB SPL and 80dB SPL and below, then detecting voltage-gated Na^+ channel, as well as other ion channel, expression using PCR and immunohistochemistry. These experiments would broaden our understanding of SGN response noise exposure that generates sub-clinical hearing threshold elevation and

perhaps highlight ion channel changes that could be responsible for hearing disorders, such as tinnitus, presbycusis and hyperacusis.

Are ion channel expression changes a consequence of glutamate excitotoxicity? The model of ototrauma used in this thesis was devised to reduce any physical and metabolic damage sustained by the cochlea. Indeed, the ABR results from Chapter 4 demonstrate that there was no change in the temporal processing or amplification function of the cochleae from sound-exposed rats, indicating post-synaptic changes consequent of excitotoxic damage. Experiments acutely perfusing glutamate receptor agonists, akin to those performed in Montpellier (Puel *et al.* 1998, Puel *et al.* 1997, d'Aldin *et al.* 1997), into the cochlea could be performed to investigate the previous excitotoxicity postulations. In addition, the previous PCR and immunohistochemistry experiments could then be performed on the glutamate receptor agonist perfused cochleae to investigate any alterations in ion channel expression following exogenously induced excitotoxicity.

Does sound exposure generate tinnitus? While it has been shown previously that exposure to noise can generate the sensation of tinnitus in humans (Henry *et al.* 2005) and animal models, it is currently unknown if the rats used in this study experience tinnitus following the sound exposure protocol. As tinnitus is a subjective condition, behavioural models have been used to identify the generation of tinnitus in animals in response to tinnitogenic agents such as salicylate (Jastreboff and Brennan 1994, Rüttiger *et al.* 2003) and noise exposure (Tan *et al.* 2007, Heffner and Harrington 2002). These models involved conditioning the test animal to perform or cease a

particular behaviour, such as pressing a lever, in the absence of a background sound. The theory being that if the animal experiences tinnitus, following noise exposure or application of the tinnitogenic drug, the animal will behave normally in the periods of silence, as the perceived tinnitus sound will fill the silent periods. Heffner and Harrington (2002) identified tinnitus behaviour in hamsters exposed to a 10kHz tone above 120dB for two to four hours, with an average hearing threshold increase of 40dB. This shows that exposure to a single tone for 2 to 4 hours can generate tinnitus behaviour. However the generation of tinnitus by the model of hearing loss presented in this study cannot be directly inferred. This is because of the same species of animal was not used and the hearing threshold elevation seen in this study is smaller than the results published by Heffner and Harrington (2002).

An alternative to conditioned behavioural testing has been identified, using the gap detection deficit method to indicate tinnitus generation in animals exposed to noise (Turner *et al.* 2006). This method measures the magnitude of the startle response elicited by a loud sound stimulus in the presence of a constant background sound. Turner *et al*. have shown that the startle response in normal hearing animals is smaller when a short period of silence (or gap) in the background sound is presented before the sound stimulus. However, no difference in the startle response is seen using animals exposed to noise, suggesting that the noise-exposed animals do not detect the gap because the silence is filled with the perception of tinnitus. While this method has no behavioural training and thus does not rely on a conditioned response, it is limited by the background sound generation, either generated single tones or broadband noise. The gap detection deficit method presumes that the background sound is

similar to the perception of tinnitus experienced by the sufferer but if the tinnitus perception changed frequency, or consisted of many different frequencies, then this would not be represented by the constant background sound.

Either similar behavioural or gap detection studies would have to be performed to establish whether the Wistar rats in this study do experience tinnitus following the sound exposure protocol. While the link between threshold elevation and tinnitus has been shown (Tan *et al.* 2007, Heffner and Koay 2005, Heffner and Harrington 2002), it has also been reported that tinnitus behaviour can be detected in animals that do not have hearing loss (Heffner and Koay 2005). In humans tinnitus can be generated by exposure to acoustic trauma (Mrena *et al.* 2004) yet the sensation of tinnitus can persist when hearing thresholds have recovered (Nottet *et al.* 2006). This indicates that there is a link between hearing loss and the generation of tinnitus but the two conditions can occur independently of each other. It would also be interesting to compare voltage-gated Na^+ channel expression in sound-exposed and control cochleae with the detection of tinnitus behaviour for any correlation.

Appendix- Manuscript of published work

The following manuscript was submitted for publication in the journal of Molecular and Cellular Neuroscience. The reference for the publication is:

Fryatt AG, Vial C, Mulheran M, Gunthorpe MJ, Grubb BD (2009) Voltage-gated sodium channel expression in rat spiral ganglion neurons. Mol Cell Neurosci 42:399-407.

Voltage-Gated Sodium Channel Expression in Rat Spiral Ganglion Neurons

Fryatt A.G[1], Vial C[1], Mulheran M[1], Gunthorpe M.J.[2], Grubb B.D[1]

[1]Department of Cell Physiology and Pharmacology, University of Leicester, University Road, Leicester, United Kingdom LE1 9HN

[2]Neurosciences Centre of Excellence for Drug Discovery, GlaxoSmithKline Research & Development, New Frontiers Science Park, Harlow, Essex, United Kingdom. CM19 5AW

Correspondence: AG Fryatt,

Email: agf4@le.ac.uk

Telephone: 0044 116 252 3087

Fax: 0044 116 252 5045

Abstract

The spiral ganglion neurons (SGN) provide the afferent innervation of the hair cells in the organ of Corti and relay auditory information from the inner ear to the brain. Voltage-gated sodium channels (Na_V) initiate and propagate action potentials that encode this sensory information but little is known regarding the subtypes expressed in these cells. We have used RT-PCR and immunohistochemistry to study the compliment and anatomical distribution of Na_V channels in rodent SGN. $Na_V1.1$, $Na_V1.6$ and $Na_V1.7$ were all detected at the mRNA level. Fluorescence or streptavidin-horseradish peroxidase immunohistochemistry extended these findings, demonstrating predominant localisation of $Na_V1.6$ and $Na_V1.7$ on SGN cell bodies and $Na_V1.1$ on axonal processes. Dual labelling with peripherin demonstrated higher $Na_V1.6$ and $Na_V1.7$ expression on Type I, rather than Type II neurons. These results provide evidence for selective expression and variations in the distribution of VGSC in the rodent SGN, which may guide further studies into afferent function in the auditory pathway and therapeutic approaches for diseases such as hearing loss and tinnitus.

Keywords: Cochlea; immunohistochemistry; peripherin; RT-PCR; spiral ganglion neurons; voltage-gated sodium channels

Introduction

There are nine recognised members of the voltage-gated sodium channel family (VGSC; $Na_V1.1$-1.9). Of these $Na_V1.1$, 1.2, 1.3, and 1.6 are highly (but not exclusively) expressed in the central nervous system (Westenbroek, Merrick and Catterall, 1989, Beckh et al., 1989, Whitaker et al., 2000, Whitaker et al., 2001, Tzoumaka et al., 2000)

whereas $Na_V1.7$, 1.8 and 1.9 demonstrate a more restricted expression pattern, in autonomic and sensory neurons in the peripheral nervous system (Sangameswaran et al., 1997, Toledo-Aral et al., 1997, Sangameswaran et al., 1996, Dib-Hajj et al., 1998a), and $Na_V1.4$ and $Na_V1.5$ represent the predominant skeletal muscle and cardiac sodium channels, respectively (Trimmer et al., 1990, Rogart et al., 1989). The $Na_V1.6$ sub-type is also highly expressed in the peripheral nervous system where it is enriched at the nodes of Ranvier of myelinated axons and contributes to saltatory conduction (Caldwell et al., 2000, Krzemien et al., 2000).

The spontaneously active spiral ganglion neurons (SGN) form the afferent conduction pathway in the auditory periphery. There are two types of SGN, Type I neurons that innervate the inner hair cells and Type II neurons that innervate the outer hair cells (Dallos, 1992). The conduction of nerve impulses along these afferents is controlled by a number of ion channels including the voltage-gated sodium channels. Clearly, establishing the expression and distribution of the sodium channels expressed in the auditory periphery could impact our understanding of action potential dynamics and coding of auditory stimuli as well as normal and abnormal phenotypes (Patuzzi et al., 2004, Hossain et al., 2005). This knowledge would also contribute to the development of putative therapeutics for disorders such as tinnitus, enabling more precise targeting of channels involved in tinnitogenesis and, potentially provide opportunities for the rational development of sub-type selective ligands to address this area of unmet need (Vio and Holme, 2005). To date, only one study has been reported that has examined VGSC expression and distribution in SGN (Hossain *et al*., 2005) but this was limited to $Na_V1.2$, and $Na_V1.6$. The aim of this study, therefore, was to fully characterise the

expression and distribution pattern of relevant VGSCs using RT-PCR and Na_V subtype selective antibodies in rat SGN.

Results

Na_V alpha subunit expression using RT-PCR

Validation of primer specificity in Rat cerebral cortex and DRG: To confirm the specificity of the primers used, tissue with previously documented Na_V α subunit expression were utilised. Distinct bands at the correct predicted sizes were observed for $Na_V1.1$, $Na_V1.2$, $Na_V1.3$ and $Na_V1.6$ in the cerebral cortex, with weak bands present for $Na_V1.7$ and $Na_V1.9$ (Fig. 1A). With the mRNA isolated from the rat DRG, distinct bands were seen for $Na_V1.1$, $Na_V1.7$, $Na_V1.8$ and $Na_V1.9$ while a weak band was observed for $Na_V1.6$ (Fig. 1B).

Rat spiral ganglion: The RT-PCR primers specific for the Na_V α subunits and β-actin were used to probe the cDNA created from mRNA isolated from rat modioli homogenates. Distinct bands at the correct predicted molecular weight were observed for $Na_V1.7$, $Na_V1.6$ and $Na_V1.1$, as well as the control gene β-actin (Fig. 1C). No bands were seen in the lane without reverse transcription, showing that there was no genomic DNA contamination.

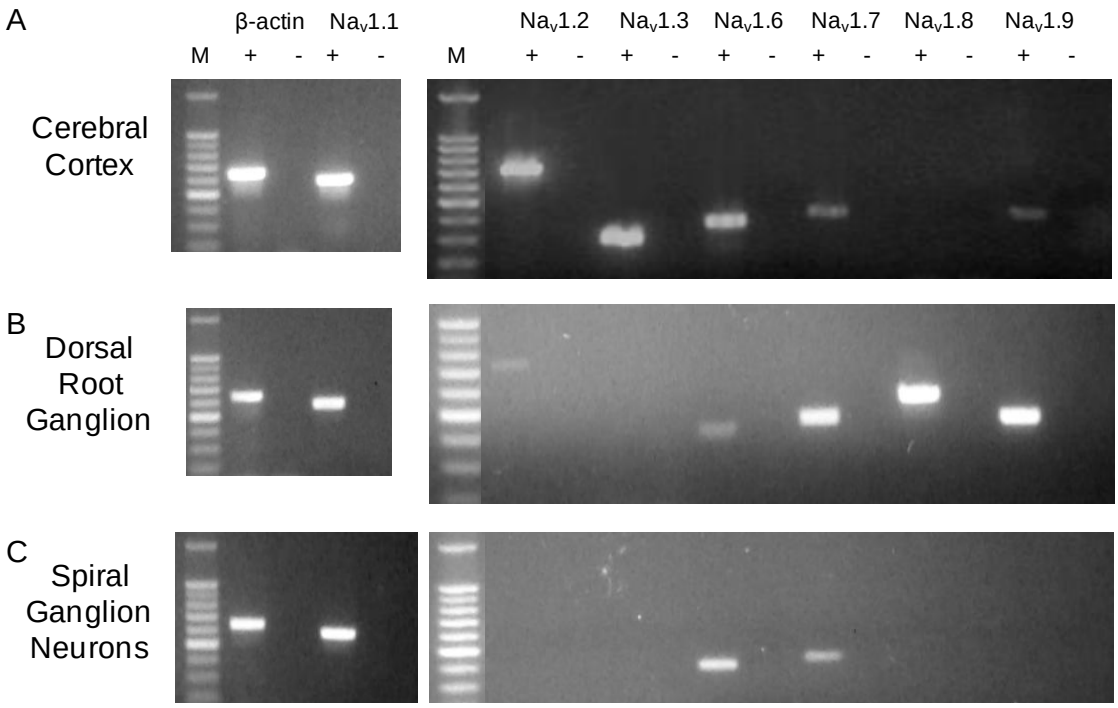

Fig. 1. Na_V mRNA channel expression in adult rat nervous tissues. PCR products were separated by electrophoresis on a 1% agarose gel stained with ethidium bromide. (A) PCR products were detected for $Na_V1.1$, 1.2, 1.3 and 1.6 in the rat cerebral cortex, with weak bands for $Na_V1.7$ and $Na_V1.9$. (B) PCR products were detected for $Na_V1.1$, 1.6, 1.7, 1.8 and 1.9 in the rat DRG. (C) PCR products were detected for Na_V 1.1, 1.6 and 1.7 in the rat SGN. All tissues were positive for β-actin. M lane, 100bp ladder with brightest band representing 500bp. Expected product sizes are given in methods section. PCR was performed either in the presence (+) or absence (-) of reverse transcription.

Immunocytochemical localization of Na_V alpha subunits in spiral ganglion neurons

$Na_V1.7$: The $Na_V1.7$ antibody strongly labelled the cell bodies of rat SGN using fluorescently tagged secondary antibodies (Fig. 2A and B). Labelling was found throughout the cytoplasm of the cell body, with no clear differentiation between membrane and cytoplasmic labelling. Variation was observed in the intensity of labelling, with some neurons strongly labelled and others only faintly labelled (Fig. 2B).

In sections of rat cochlea incubated without the primary antibody, the labelling was reduced to background levels although pale yellow puncta were noted throughout the cytoplasm (Fig. 2C).

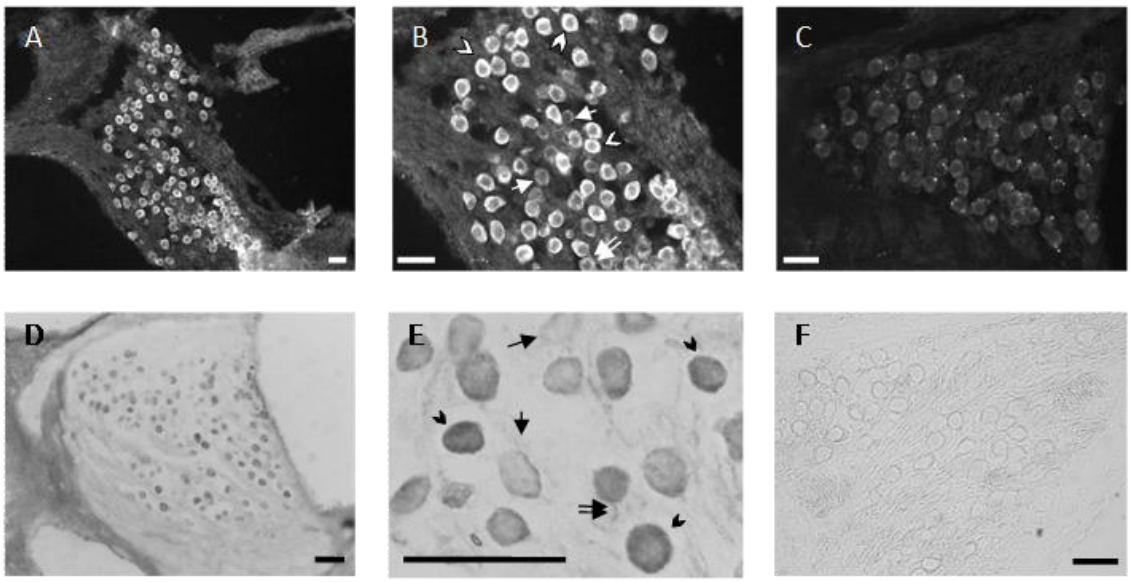

Fig. 2. Distribution of $Na_V1.7$ in rat SGN. Micrographs showing $Na_V1.7$ labelling in the rat SGN using fluorescent (A,B) and non-fluorescent (D,E) immunohistochemistry. Both techniques show positive labelling of the neurons although some appear to be less intensely stained (arrow) than others (arrowhead). (C) Micrograph showing rat SGN incubated without the primary antibody. (F) Phase contrast micrograph of HRP-DAB labelled SGN incubated without the primary antibody. Scale bars= 30µm for all images.

To demonstrate that this punctate labelling was due to non-specific fluorescence, experiments were repeated using the same $Na_V1.7$ antibody but with streptavidin/horseradish peroxidase (HRP) and DAB to non-fluorescently visualise the primary antibody binding. Using this method, the SGN were positively labelled with brown reaction product as seen in Figs. 2D and E. The positively labelled SGN cell bodies showed variation in staining intensity, similar in appearance to that observed in the fluorescence imaging technique. Additionally, the sections of rat cochlea incubated without the primary antibody did not show neurons labelled with the brown reaction product, nor the punctate labelling observed in the previous controls using

fluorescently tagged antibodies (Fig. 2F). This confirmed that the puncta could be considered as tissue autofluorescence.

$Na_V1.6$: The $Na_V1.6$ antibody strongly labelled the cell bodies of rat SGN (Fig. 3A and B). The pattern of distribution was similar to that seen with the $Na_V1.7$ antibody. Labelling was found throughout the cytoplasm of the cell body, with no clear differentiation between membrane and cytoplasmic labelling. Additionally, there was again considerable variation observed in the intensity of neuronal labelling as seen in Fig. 3B. In contrast to the labelling seen with $Na_V1.7$, peripheral and central processes were also strongly labelled for $Na_V1.6$ α-subunits.

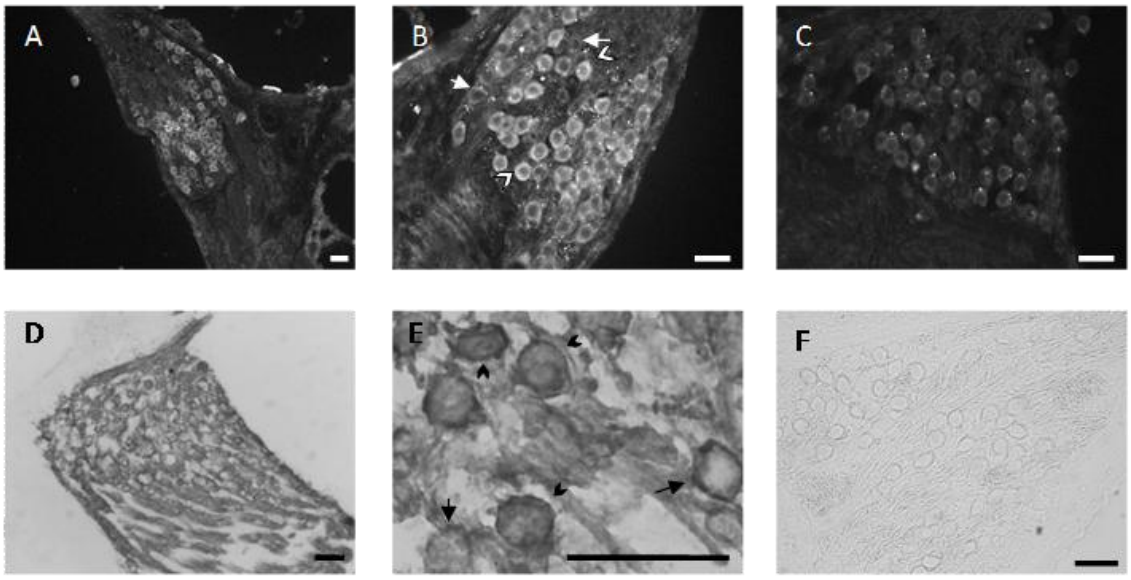

Fig. 3. Distribution of $Na_V1.6$ in rat SGN. Micrographs showing $Na_V1.6$ labelling in the rat SGN using fluorescent (A,B) and non-fluorescent (D,E) immunohistochemistry. Both techniques show positive labelling of the neurons although some appear to be less intensely stained (arrow) than others (arrowhead). (C) Micrograph showing rat SGN incubated without the primary antibody. (F) Phase contrast micrograph of HRP-DAB labelled SGN incubated without the primary antibody. Scale bars= 30μm for all images.

As performed previously, sections of rat cochlea incubated without the primary antibody the labelling was reduced to background levels, although pale yellow

autofluorescent puncta were observed throughout the cytoplasm as were also seen for $Na_V1.7$ (Fig. 3C). As for $Na_V1.7$, this punctate labelling was demonstrated as non specific by using the HRP/DAB method to visualise non-fluorescently primary antibody binding. The SGN were positively stained for $Na_V1.6$ with the brown reaction product using this method as seen in Figs. 3D and E. Again, positively labelled SGN cell bodies showed variation in staining intensity similar in appearance to that seen with fluorescence imaging. The distinct staining of the neuronal processes was replicated and, in addition, staining of the cell body membranes was observed (Fig. 3E). Sections of rat cochlea incubated without the primary antibody did not show neurons labelled with the brown reaction product nor the punctate labelling observed in the previous fluorescence controls (Fig. 3F).

$Na_V1.1$: The $Na_V1.1$ antibody weakly stained the SG neurons and was only detectable using the non-fluorescent HRP/DAB method as seen in Fig. 4. Weak staining was observed in the SGN cell bodies while darker staining was seen in the neuronal processes, specifically in the axons (Fig. 4A and B). The sections of rat cochlea incubated without the primary antibody did not show labelled neurons (Fig. 4C).

Peripherin labelling of spiral ganglion neurons

It has been previously reported that antibodies generated against the intermediate filament protein, peripherin, preferentially label Type II SGN in sections of cochlea (Hafidi, 1998, Mou, Adamson and Davis, 1998, Reid, Flores-Otero and Davis, 2004). A small proportion (33/242 or $\approx$ 14%) of SGN were labelled by this antibody. Most

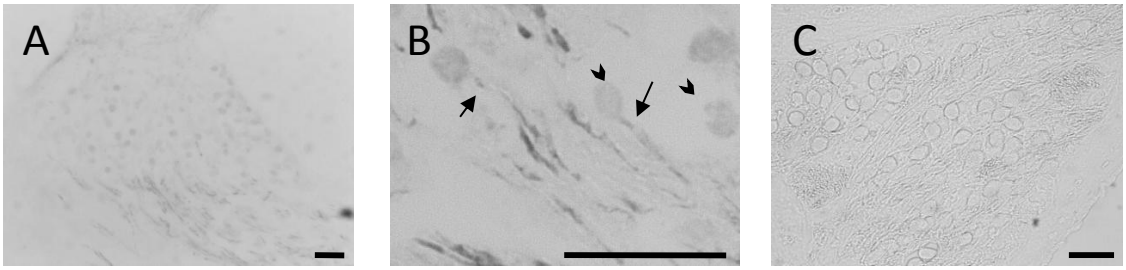

Fig. 4. Distribution of $Na_V1.1$ in rat SGN. Micrographs showing $Na_V1.1$ labelling in the rat SGN using non-fluorescent immunohistochemistry. (A,B) Faint labelling of the SGN cell bodies was observed (arrowhead) while the axons were more intensely labelled (arrow). (C) Phase contrast micrograph showing rat SGN incubated without the primary antibody. Scale bars= 30µm for all images.

noticeably, all the labelled neurons appeared to be smaller compared to the unlabelled neurons (Fig. 5A).

Peripherin labelling status and $Na_V1.7$: The relationship between cell body area and peripherin labelling status was investigated further by dual labelling sections of cochlea with peripherin and $Na_V1.7$ antibodies. This was performed using sections from four cochleae (Fig. 5A and B). The frequency histogram of cell body area in Fig. 5C shows that distribution in peripherin positive neurons was distinctly separate from that of peripherin negative neurons. The mean difference in peripherin negative and positive cell body areas was significantly different, from 165.3 μm^2 ±1.8 (n=209) vs 82.2 μm^2 ±2.6 (n=33) respectively, $p< 0.0001$. This represents about a two-fold difference in cell body area.

On visual inspection of the sections it appeared that the peripherin positive neurons were labelled less intensely by the $Na_V1.7$ antibody than the peripherin negative neurons. To investigate the relationship between peripherin and density of $Na_V1.7$ labelling further, the average fluorescence intensity of the neurons labelled with the

$Na_V1.7$ antibody was measured in peripherin negative and positive neurons from four cochleae.

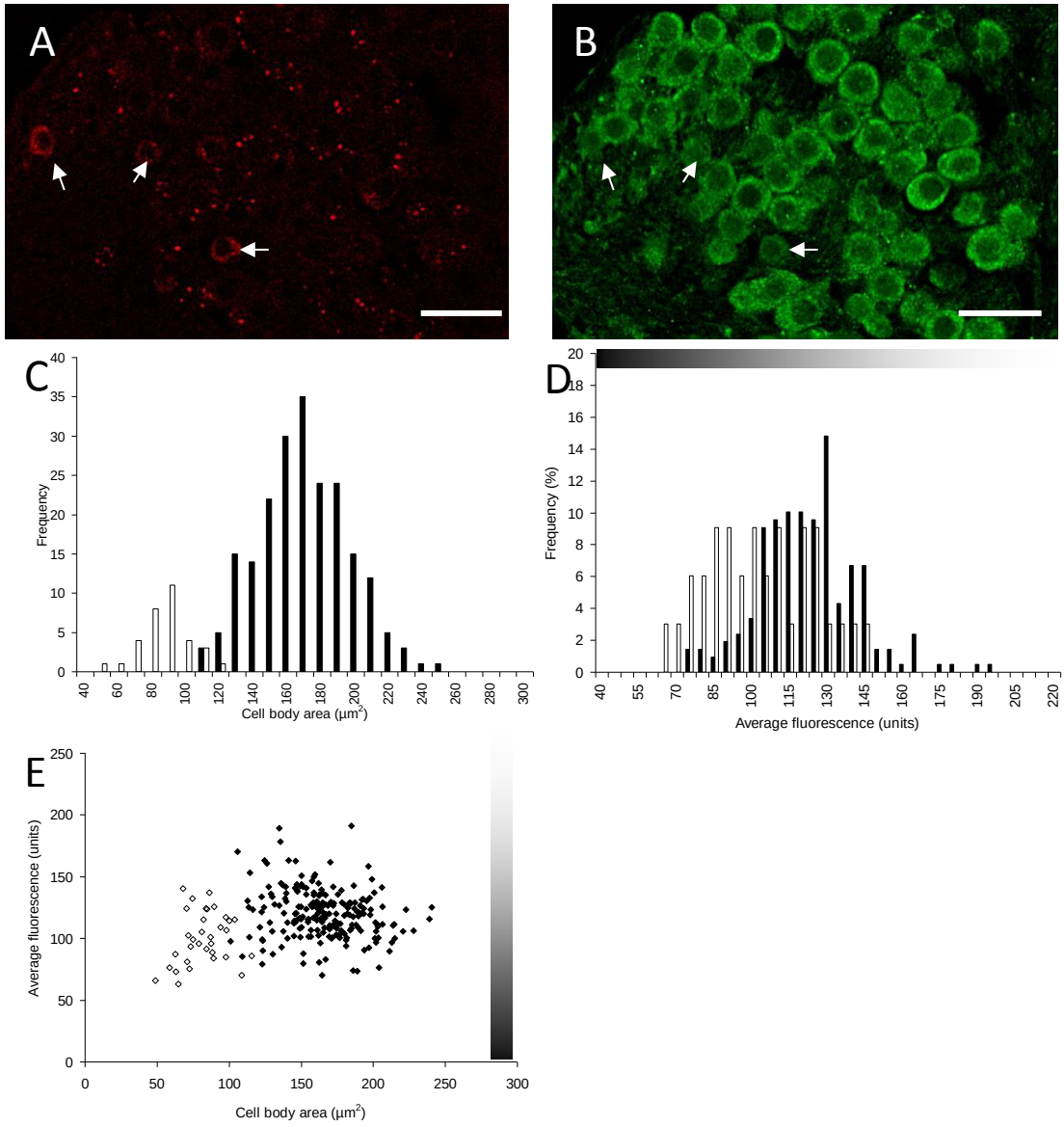

Fig. 5. Dual labelling of rat SGN with $Na_V1.7$ and Peripherin. Micrographs showing peripherin (A) and $Na_V1.7$ (B) labelling in the rat SGN. The neurons that are labelled for peripherin appear to have stained weakly for $Na_V1.7$ (arrows point to the position of peripherin positive neurons). Frequency histograms showing the distribution of spiral ganglion cell body areas (C) and normalised average fluorescent labelling for $Na_V1.7$ (D), with a scatter plot of neuronal cell body area versus fluorescent labelling for $Na_V1.7$ (E), showing that the peripherin positive neurons (clear bars/symbols) have smaller cell body area and label less intensely for $Na_V1.7$ than the peripherin negative neurons (filled bars/symbols). Scale bars=30µm. Graduated bar on graphs indicates fluorescence scale (0=black, 255=white).

The mean $Na_V1.7$ fluorescence was significantly different between the peripherin negative and positive neurons, from 120.1±1.4 vs 100.2±3.7 respectively at $p<0.01$. This confirmed the impression of differences in staining intensity between the two groups. Combination with the previous data in a scatter plot of cell body area versus average fluorescence in Fig. 5E, further illustrates that peripherin negative neurons possess larger cell body areas and label more strongly with $Na_V1.7$ antibody.

Peripherin labelling status and $Na_V1.6$: An identical set of dual labelling experiments to those with $Na_V1.7$ were performed, using peripherin and $Na_V1.6$ antibodies and sections from the same rat cochleae that were used previously. Similar initial observations and results with regards to antibody staining, cell body area and fluorescence intensity were obtained as shown in Figs. 6 A-E. With $Na_V1.6$ the difference in distribution and means of cell body area between peripherin negative and positive neurons was more marked than for $Na_V1.7$. The differences in mean cell body area were significantly different with means of 185.7±2.2μm^2 (n=203) vs 74.8±3.2μm^2 (n=34) respectively, $p<0.001$, or about a 2.5 fold difference in cell body area.

Differences in mean $Na_V1.6$ fluorescence between the negative and positive stained peripherin neurons were also significantly different, with mean difference of about 40 units; 142.6±1.7 (n=203) vs 101.6±3.2 (n=34) respectively, $p<0.001$.

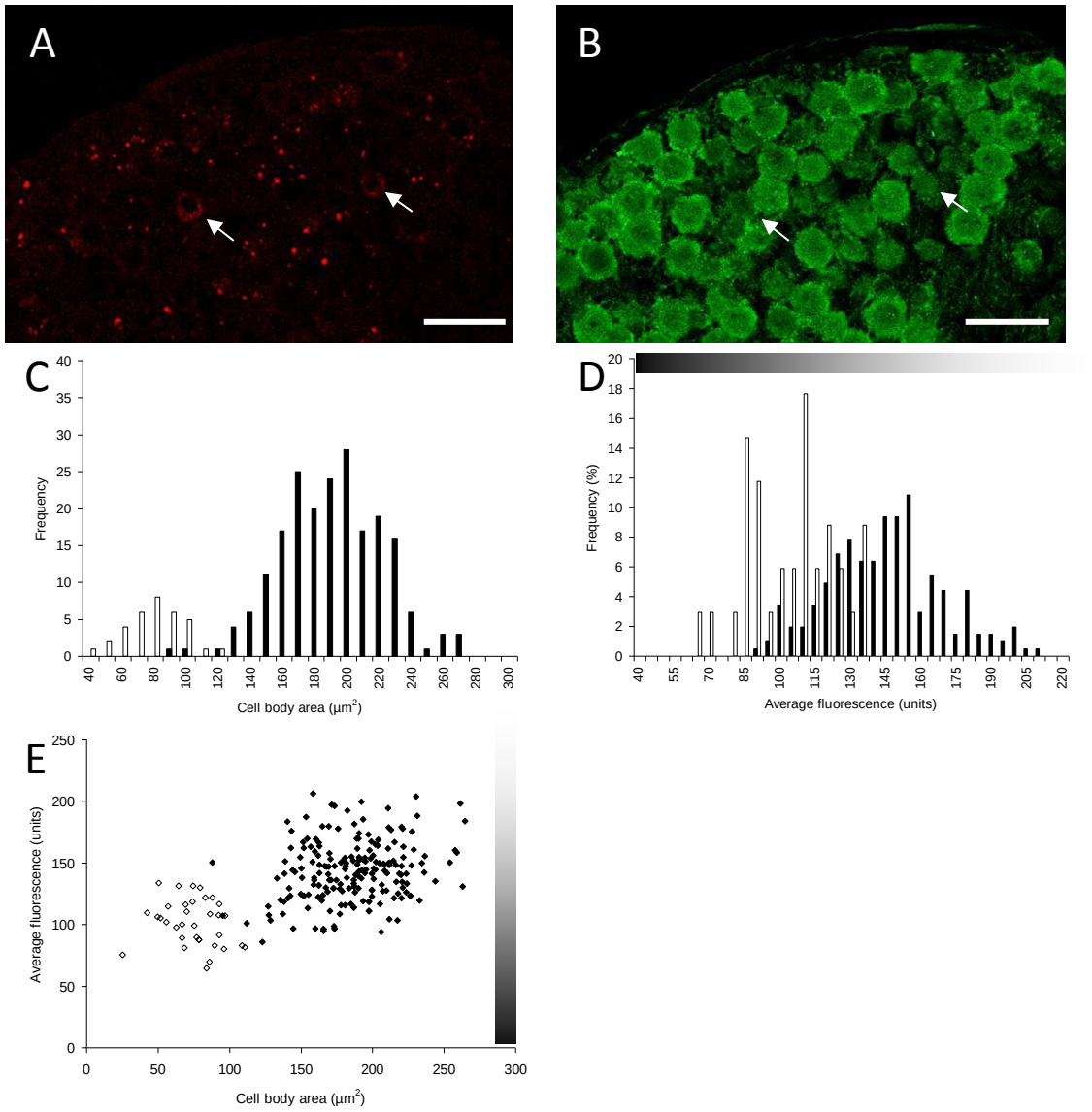

Fig. 6. Dual distribution of $Na_V1.6$ and Peripherin in the rat SGN. Micrographs showing peripherin (A) and $Na_V1.6$ (B) labelling in the rat SGN. The neurons that are labelled for peripherin appear to have stained weakly for $Na_V1.6$ (arrows point to the position of peripherin positive neurons). Frequency histograms showing the distribution of spiral ganglion cell body areas (C) and normalised average fluorescent labelling for $Na_V1.6$ (D), with a scatter plot of neuronal cell body area versus fluorescent labelling for $Na_V1.6$ (E), showing that the peripherin positive neurons (clear bars/symbols) have smaller cell body area and label less intensely for $Na_V1.6$ than the peripherin negative neurons (filled bars/symbols). Scale bars=30µm. Graduated bar on graphs indicates fluorescence scale (0=black, 255=white).

Combination of the two parameters in a scatter plot of cell body area versus average fluorescence in Fig 5E, further illustrates that peripherin negative neurons label more intensely than with $Na_V1.6$ antibody.

Comparison of $Na_V1.6$ and $Na_V1.7$ SGN labelling: Direct comparison of $Na_V1.6$ and $Na_V1.7$ immunofluorescence values was not justified as the relative antibody binding affinities were not known. However, SGN cell body area could be compared directly. The Type I means of 185.7±2.2µm^2 vs 165.3 µm^2 ±1.8µm^2 for $Na_V1.6$ and $Na_V1.7$ respectively, were highly significantly different at $p < 0.001$. The respective difference in Type II means, 74.8±3.2µm^2 vs 82.2 µm^2 ±2.6, for $Na_V1.6$ and $Na_V1.7$ was not significant at $p > 0.05$.

Peripherin labelling status and $Na_V1.1$: Dual labelling experiments with peripherin and $Na_V1.1$ antibodies could not be performed because of the weak labelling of the SGN cell bodies using $Na_V1.1$ antibodies.

Discussion

Rat SGN exhibits a unique pattern of Na_V subunit expression: The results presented here provide for the first time strong evidence that the α-subunits, $Na_V1.7$, $Na_V1.6$ and $Na_V1.1$, are selectively expressed in adult rat SGNs. There are a number of unusual features in this pattern of Na_V subunit expression, as they suggest that expression in the SGN does not follow that observed in either the central or peripheral nervous system. Instead, the results presented here show Na_V isoforms normally considered to be specific to the peripheral and central nervous system are both expressed in the

SGN. The explanation for this may be related to the independent embryological origins of the SGN (Fekete and Wu, 2002). The peripheral and central nervous systems are known to arise from different progenitor cells in the developing embryo. The CNS forms from the dorsal ectoderm through envagination and formation of the neural tube. DRG neurons arise from neural crest cells that migrate laterally to form the peripheral ganglia (Kuan et al., 2004, Li, Say and Zhou, 2007). In contrast, the SGN develops from a distinct region of neural ectoderm known as the otic placode, which is separate from both the neural tube and neural crest cells (Holley, 2005, Fekete and Wu, 2002). The results from this study suggest that the otic placode displays an intermediate phenotype with regard to Na_V channel expression between the CNS and PNS.

Na_V1.1 subunit expression: Na_V1.1 has been previously been shown to be strongly expressed by neurons in the central nervous system (Westenbroek, Merrick and Catterall, 1989). The preliminary results from this study appear to show that Na_V1.1 is weakly expressed in the SGN with strong axonal localisation. As dual labelling experiments could not be performed using the Na_V1.1 antibody, we cannot report if Na_V1.1 expression is restricted to the Type I or Type II neurons.

Na_V1.7 subunit expression: Na_V1.7 is considered to be exclusively expressed by neurons in the PNS, especially in the cell bodies (Sangameswaran et al., 1997) and peripheral terminals or growth cones (Toledo-Aral et al., 1997) of DRG neurons. The results presented here also show that the Na_V1.7 subtype is expressed in the cell bodies of the rat SGN. In contrast to this rodent model, Na_V1.7 was not reported to be

present in the murine model of Hossain *et al*., (2005). This may reflect a species difference in expression of the $Na_V1.7$ subunit.

$Na_V1.6$ subunit expression: It has been previously reported that the $Na_V1.6$ subtype is expressed in murine SGN (Hossain et al., 2005) with $Na_V1.6$ localised at the initial segment and nodes of Ranvier and not in the cell bodies. The results here in the rat SGN are also partly in line with this earlier study. $Na_V1.6$ labelling was found in the cell body cytoplasm as well as the processes of the rat SGN. The presence of cytoplasmic labelling in the cell body seen here is in agreement with previous reports of $Na_V1.6$ labelling in other sensory ganglia (Tzoumaka et al., 2000, Krzemien et al., 2000, Black et al., 1999). In addition, cytoplasmic labelling has also been reported for potassium channels in the cell bodies of murine SGN (Adamson et al., 2002) and rat DRG neurons (Rasband et al., 2001). This type of labelling is most likely due to the pooling of subunit proteins in the Golgi apparatus, prior to their transport and insertion into the membrane.

Differential expression of $Na_V1.6$ and $Na_V1.7$ in SGN Type 1 and Type II: The measurement of SGN cell body area along with semi-quantitative fluorescence and non-fluorescence imaging techniques enabled the evident variation in labelling intensity to be explored in more detail. Resolution of differential expression was further enhanced by the use of dual labelling with peripherin antibody (Hafidi, 1998, Mou, Adamson and Davis, 1998, Reid, Flores-Otero and Davis, 2004). The differences in SGN Type 1 and II cell body area have been reported previously and are confirmed by this study (Berglund and Ryugo, 1987).

Whilst reduced fluorescence for both $Na_V1.6$ and 1.7 was apparent in Type II neurons, the intensity of labelling observed was above background levels, indicating that Type II SGN express these subunits. This would support their possessing some functional capacity. Currently, little electrophysiological evidence exists to identify the specific role of Type II fibres or that they actually exhibit any acoustically driven activity (Brown, 1994, Robertson, Sellick and Patuzzi, 1999), although it has been proposed they may signal static displacement of the basilar membrane (Robertson, Sellick and Patuzzi, 1999).

The difference in cell area between $Na_V1.6$ and 1.7 expressing Type I neurons may be explained in at least two ways. One hypothesis is that the difference may correlate with signalling function as spontaneous activity in mammalian Type I afferents is known to range between 0-120 spikes sec^{-1}, which correlates with axon diameter (Liberman, 1982). It would be reasonable to assume that axon diameter also correlates with cell body area and that the expression of $Na_V1.6$ and 1.7 in Type I SGN may then be related to the spontaneous and/or driven activity of Type I fibres. Alternatively, the differences may simply reflect more intense membranous staining by $Na_V1.6$ over 1.7. $Na_V1.6$ has a role in action potential initiation and propagation in many neurons due to its localisation at the axon hillock and nodes of Ranvier, respectively. By contrast $Na_V1.7$, a channel that shows slow inactivation and stays open in response to slow ramp depolarisations, may have a role in initiating action potential initiation at the hair cell-afferent fibre synapse.

Expression of other Na_V isoforms in the SGN: The expression of other voltage-gated sodium channel isoforms was also investigated in this study. RT-PCR failed to show the expression of mRNA for $Na_V1.2$, $Na_V1.3$, $Na_V1.8$ and $Na_V1.9$, indicating that these isoforms are not expressed in the rat SGN.

Interestingly, in the murine study by Hossain *et al*., (2005), $Na_V1.2$ expression in the in the organ of Corti was observed, but only in the efferent innervation to inner and outer hair cells (Hossain et al., 2005). The absence of evidence for expression of $Na_V1.8$ and $Na_V1.9$ isoforms in this study is in line with earlier observations that TTX completely abolished inward sodium current in isolated SGN (Santos-Sacchi, 1993). $Na_V1.4$ and $Na_V1.5$ expression in the SGN was not studied, as these isoforms are believed to be selectively expressed in skeletal and cardiac muscle respectively (Trimmer et al., 1990, Rogart et al., 1989, Catterall, Goldin and Waxman, 2005).

Control results: The extensive analysis and comprehensive documentation of the expression of Na_V subunits in the CNS and PNS neurons provided positive controls for RT-PCR primers used in the current study. CNS neurons have been shown to express $Na_V1.1$, $Na_V1.2$ (Westenbroek, Merrick and Catterall, 1989), $Na_V1.3$ (Beckh et al., 1989) and $Na_V1.6$ (Tzoumaka et al., 2000), and mRNA isolated from the cerebral cortex was used to test the specificity of the RT-PCR primers designed for these Na_V subunits. $Na_V1.7$ and $Na_V1.9$ were also weakly identified by the RT-PCR primers. While these proteins have not been identified in the cerebral cortex, the mRNA has been detected in this tissue previously (Dib-Hajj et al., 1998a, Belcher et al., 1995). The mRNA isolated from the DRG was used as a positive control to validate the specificity of the RT-PCR

primers designed to detect $Na_V1.7$, $Na_V1.8$ and $Na_V1.9$, as the DRG has been previously reported to express these subunits (Sangameswaran et al., 1997, Dib-Hajj et al., 1998a, Dib-Hajj et al., 1998b). The RT-PCR primers also identified $Na_V1.1$ mRNA in the DRG tissues. This result has been reported previously (Beckh, 1990), but whilst the mRNA for $Na_V1.1$ has been identified in the DRG, the protein has not been detected in the peripheral nervous system (Gordon et al., 1987). Both these control tissues yielded results that confirmed that the designed primers were specific for their respective Na_V isoforms.

Antibody specificity is necessary for the reliable interpretation of immunohistochemical data. Sections of rat cochlea without primary antibodies did not display fluorescence specific to the binding of the secondary antibodies to their antigens. However, non-specific cytoplasmic yellow puncta were observed in the SG cell bodies. These results indicate that in the adult rat SGN there are other sources of endogenous fluorescence, possibly lipofuscin. This has also been reported in other adult neural ganglia, including the retina, vestibular and dorsal root ganglion and cerebellar Purkinje cells (Sans, Bartolami and Fraysse, 1996, Samorajski, Ordy and Rady-Reimer, 1968). Furthermore, we are confident that these puncta were due to non-specific fluorescence, since we used non-fluorescence DAB/HRP visualisation methods to validate the original results.

Characterising Na_V Isoforms in the Auditory pathway- Therapeutic Applications: The characterisation of Na_V isoforms in the periphery of the normal auditory pathway contribute to the development of therapeutics for treating conditions such as tinnitus.

The clinical evidence that voltage-gated sodium blockers may have a role in ameliorating certain types of tinnitus is well documented because lignocaine, a use-dependent sodium channel blocker and local anaesthetic, is the gold standard tinnitolytic agent and is effective in around 50% of patients (Baguley et al., 2005). Following ototrauma, it is apparent that marked plastic changes occur in the auditory pathway some of which have parallels with sensory nerve trauma (Moller, 1997, Kaltenbach et al., 1998). In models of neuropathic pain this is accompanied by changes in pattern and expression of Na_V subtype and profound changes in neuronal excitability (Devor, 2006, Novakovic et al., 1998, Black et al., 2004, Cummins and Waxman, 1997). Several Na_V channel subtypes including $Na_V1.7$ and $Na_V1.8$ have been implied to regulate spontaneous firing in damaged nociceptive afferents although there is much debate from studies using antisense knock-down methodologies and transgenic animals as to which are the most important (for reviews see Krafte and Bannon, 2008, Momin and Wood, 2008).

The use of appropriate models of ototrauma would establish whether similar or other changes in Na_V isoforms may underlie tinnitus. This would provide the basis for optimal matching of tinnitolytic therapeutics to their tinnitogenic target.

Experimental Methods

RT-PCR

Tissue extraction: Male Wistar rats (250-400g) were sacrificed using Euthanal® (IP) in accordance with UK Home Office Animals Act 1986 (schedule 1). The dorsal root ganglia (DRG) and cerebral cortex were rapidly excised and frozen over dry ice in a

sterile RNase/DNase free tube. The temporal bones were removed and excess bone was removed to leave the bony inner ear segment that contained the cochlea. The otic capsule of the cochlea was removed to reveal the modiolus, which was then carefully removed from the remaining bone and frozen over dry ice as above.

mRNA isolation and cDNA synthesis: Two modioli- from the left and right ear of one animal- six DRGs and 35 mg of cerebral cortex were used per analysis. The tissues were homogenised separately in lysis buffer, by pestle and mortar, and centrifuged in a QIAshredder (QIAGEN, Crawley, UK). The total RNA was isolated from the homogenates using the RNeasy mini kit (QIAGEN). The RNA was eluted in RNase free water and the remaining DNA was removed by using DNase I (Invitrogen, Paisley, UK). The total RNA was reverse transcribed to complementary (c)DNA using SuperScript^{TM} III Reverse Transcriptase (Invitrogen) The cDNA was stored at -80^{o}C until use.

PCR reaction: The PCR reaction was performed using BIOTAQ DNA polymerase (Bioline, London, UK), custom designed sense and antisense primers at 0.5µM final concentration (Sigma Genosys, Cambridge, UK) and 1µl of cDNA using a T-Gradient Biometra thermocycler (Biotron, Göttingen, Germany). Thirty-five PCR cycles were performed using annealing temperatures between 54 and 59^{o}C. The PCR products were separated by electrophoresis on a 1% agarose gel with ethidium bromide and a 100 base pair DNA ladder (Promega, Southampton, UK) at 110V. The gel was photographed under ultraviolet illumination using a digital camera and Kodak digital science 1D software (Kodak). The mRNA isolation, cDNA synthesis and PCR reaction was repeated four times, using modioli from a fresh rat each time.

Primer design: Primer pairs specific to the Na_V alpha subunits and β-actin used are summarised in table 1. The primer pairs were designed to cross intron-exon boundaries as determined from the rat sequences. This would show any genomic DNA contamination of the PCR products as a higher base pair size band than the calculated band. The identity of PCR products was confirmed by sequencing.

Tissue preparation for immunohistochemistry

Cochlea extraction: Male Wistar rats (250-300g) were sacrificed using Euthanal® (IP) in accordance with UK Home Office Animals Act 1986 (schedule 1). The circulatory system of the animal was flushed transcardially with warm PBS supplemented with heparin. For fixation the animal was perfused transcardially with warm 2%

Subunit	Forward primer 5'-3'	Reverse primer 5'-3'	Predicted band size (bp)	Annealing temperature (^{o}C)
$Na_V1.1$	GCGTGCTGCCGGGAAAACATAC	ACGTCCTTCGCTCGCCCTCTGA	576	59
$Na_V1.2$	CGTCCGCAGAATCCAGAGA	CTTGAAGGGTCTTCCAACAAGTC	705	58
$Na_V1.3$	AGGGAAGGATTGACTTGCC	TGGACCTCTCCTTAGAGTCCA	295	58
$Na_V1.6$	AAGTGGACAGCCTACGGC	TTGTTGACAATATCGATTTCGAACCG	364	58
$Na_V1.7$	GACGACAGCGGCACGACTAAT	AGCTGCGAAGATCCCTGTAAAGA	402	54
$Na_V1.8$	GATCCGTGGAACTGGCTGGA	GAGGAATGCCCACGCAAAGGAATC	482	58
$Na_V1.9$	CCCTGCTGCGCTCGGTGAAGAA	GACAAAGTAGATCCCAGAGG	395	58
B-actin	TACAACCTCCTTGCAGCTCC	GGATCTTCATGAGGTAGTCTGTC	630	59

Table 1. PCR Primers. Primers were either designed or modified from others previously published. $Na_V1.2$, $Na_V1.3$, $Na_V1.6$ (Wooltorton *et al.*, 2007); $Na_V1.8$ (Dib-Hajj *et al.*, 1998a); $Na_V1.9$ (Dib-Hajj *et al.*, 1998b); β- actin (Raff *et al.*, 1997).

paraformaldehyde solution. The temporal bones were dissected and excess bone was removed to leave the bony inner ear segment that contained the cochlea. The cochleae were placed in 2% paraformaldehyde solution for 30 minutes and demineralised in 8% EDTA until soft (4 to 10 days at 4^{o}C). They were then placed in PBS with 30% sucrose overnight at 4^{o}C and then were infiltrated with Tissue Tek OCT overnight at 4^{o}C (Cho et al., 2004). The fixed cochleae were quickly frozen in Tissue Tek over dry ice/hexane and stored at -20^{o}C. Frozen 10μm sections were cut from tissue blocks, mounted on Polysine^{TM} slides and air dried. Tissue sections were washed (1x15 mins) in PBS.

Immunohistochemistry on frozen sections

Antibody information: Information about the primary and secondary antibodies used in this study is presented in table 2.

Fluorescent probe staining: For detection of sodium channel subtypes, the slides were incubated in the following: (1) Blocking solution of PBS containing 10% goat serum, supplemented with 0.5% Triton X-100 for 30 min at room temperature; (2) Sodium channel subtype specific primary polyclonal antibodies raised in rabbit (see table 2 for details) diluted in blocking solution and incubated overnight at 4^{o}C; (3) Goat anti-rabbit IgG conjugated with fluorescein isothiocyanate (FITC) for 2 hours at room temperature. Between each incubation step, the sections were thoroughly washed with PBS. Sections were mounted with Citifluor AF1 mountant (UKC Chem. Lab, Kent, UK).

Antibody	Host	Dilution	Supplier	Product code
Anti-$Na_V1.1$	Rabbit	1:200	Alomone labs	ASC-001
Anti-$Na_V1.6$	Rabbit	1:200	Alomone labs	ASC-009
Anti-$Na_V1.7$	Rabbit	1:200	Alomone labs	ASC-008
Anti-Peripherin	Mouse	1:100	Millipore	MAB1527
Anti-rabbit/FITC	Goat	1:400	Jackson ImmunoResearch	111-095-144
Anti-mouse/Texas red	Goat	1:400	Jackson ImmunoResearch	115-075-146
Anti-rabbit/Biotin	Swine	1:350	DAKO	E0353

Table 2. Immunohistochemistry antibodies. Details of the antibodies used in the study. Entries with / indicates a conjugation, i.e. anti-rabbit/biotin means anti-rabbit conjugated with biotin. Antibodies diluted in either 10% goat serum PBS for fluorescence immunohistochemistry or 10% swine serum PBS for non-fluorescence immunohistochemistry.

Control experiments were carried out to determine the amount of non-specific binding by omitting the primary antiserum from the incubation media. Pre-incubation of primary antibody with the blocking peptide overnight reduced the labelling to background levels.

For identification of Type II SG neurons, experiments were carried out using an anti-peripherin monoclonal antibody MAB 1527 raised in mouse (Millipore, Watford, UK) as this protein is known to be selectively expressed in Type II SG neurons (Hafidi, 1998, Mou, Adamson and Davis, 1998, Reid, Flores-Otero and Davis, 2004). Immunostaining was visualised with goat anti-mouse secondary antibodies conjugated with Texas Red (Jackson ImmunoResearch).

The sections were viewed using a Nikon Labophot 2A microscope equipped for epifluorescense imaging and photography, with a monochromatic CCD camera, frame grabber card and software (Scion Image^{TM}). Photography of tissue sections was carried out with the appropriate filters for FITC or Texas Red.

Scion Image^{TM} (Scion Corporation, Frederick, Maryland USA) was used to measure the cell body area and average fluorescence of the neurons from the epifluorescent images. Only neurons that showed an unlabelled nucleus and an intact cell body were measured. The fluorescence scale ranged from: 0= black; 255= white. Unless otherwise stated, this scale is used throughout the results and discussion sections.

Non-fluorescence DAB/HRP staining: For non-fluorescence detection of sodium channel subtypes, the tissue sections were incubated sequentially in the following solutions: (1) 0.2% Hydrogen peroxide in methanol for 15 minutes; (2) 10% swine serum and 0.5% Triton X-100 in PBS for 30 minutes at room temperature; (3) Anti-rabbit polyclonal antibodies as described above, overnight at 4^{o}C; (5) Swine anti-rabbit biotin conjugated IgG, diluted with 10% swine serum in PBS for 35 minutes at room temperature (DAKO, Ely, UK); (6) Streptavidin-Horseradish peroxidase (HRP) conjugate prediluted for 30 minutes at room temperature (DAKO); (7) 3, 3'-diaminobenzidine solution (DAB substrate kit, DAKO) for 4 minutes at room temperature; (8) 70% IMS for 5 minutes followed by 100% IMS for 5 minutes and 100% xylene twice for 5 minutes. Between steps 1 and 8 the tissue sections were thoroughly washed with PBS. Sections were mounted using DPX (RA Lamb, Eastbourne, UK).

The slides were examined using a light microscope equipped with a digital camera (Moticam 2300, GT Vision, Haverhill, Suffolk, UK) and images were captured using Motic Images Plus 2.0

Statistical Analysis

Statistical analysis was carried out with data entered into a Microsoft Office Excel 2007 spreadsheet. Comparison of different data groups was performed using the two-tailed Students t-test. Results are expressed as means ± se and a p=0.05 significance level was adopted throughout.

Acknowledgements

AF was in receipt of BBSRC CASE studentship in association with GlaxoSmithKline and a grant from the Ménière's Society. The authors would like to thank Mrs Susan Giblett for providing valuable help in the HRP/DAB staining and Dr Amit Prasai for conducting the preliminary experiments in this study.

References

Adamson CL, Reid MA, Mo Z, Bowne-English J, Davis RL (2002) Firing features and potassium channel content of murine spiral ganglion neurons vary with cochlear location. The Journal of Comparative Neurology 447:331-350.

Baguley DM, Jones S, Wilkins I, Axon PR, Moffat DA (2005) The inhibitory effect of intravenous lidocaine infusion on tinnitus after translabyrinthine removal of vestibular schwannoma: A double-blind, placebo-controlled, crossover study. Otology & Neurotology 26:169-176.

Beckh S, Noda M, Lubbert H, Numa S (1989) Differential regulation of three sodium channel messenger RNAs in the rat central nervous system during development. EMBO J 8:3611-3616.

Beckh S (1990) Differential expression of sodium channel mRNAs in rat peripheral nervous system and innervated tissues. FEBS Lett 262:317-322.

Belcher SM, Zerillo CA, Levenson R, Ritchie JM, Howe JR (1995) Cloning of a sodium channel alpha subunit from rabbit schwann cells. Proc Natl Acad Sci U S A 92:11034-11038.

Berglund AM, Ryugo DK (1987) Hair cell innervation by spiral ganglion neurons in the mouse. J Comp Neurol 255:560-570.

Black JA, Cummins TR, Plumpton C, Chen YH, Hormuzdiar W, Clare JJ, Waxman SG (1999) Upregulation of a silent sodium channel after peripheral, but not central, nerve injury in DRG neurons. J Neurophysiol 82:2776-2785.

Black JA, Liu S, Tanaka M, Cummins TR, Waxman SG (2004) Changes in the expression of tetrodotoxin-sensitive sodium channels within dorsal root ganglia neurons in inflammatory pain. Pain 108:237-247.

Brown MC (1994) Antidromic responses of single units from the spiral ganglion. J Neurophysiol 71:1835-1847.

Caldwell JH, Schaller KL, Lasher RS, Peles E, Levinson SR (2000) Sodium channel $Na_V1.6$ is localized at nodes of ranvier, dendrites, and synapses. PNAS 97:5616-5620.

Catterall WA, Goldin AL, Waxman SG (2005) International union of pharmacology. XLVII. nomenclature and structure-function relationships of voltage-gated sodium channels. Pharmacol Rev 57:397-409.

Cho Y, Gong TL, Kanicki A, Altschuler RA, Lomax MI (2004) Noise overstimulation induces immediate early genes in the rat cochlea. Molecular Brain Research 130:134-148.

Cummins TR, Waxman SG (1997) Downregulation of tetrodotoxin-resistant sodium currents and upregulation of a rapidly repriming tetrodotoxin-sensitive sodium current in small spinal sensory neurons after nerve injury. Journal of Neuroscience 17:3503-3514.

Dallos P (1992) The active cochlea. The Journal of Neuroscience 12:4575-4585.

Devor M (2006) Sodium channels and mechanisms of neuropathic pain. Journal of Pain 7:S3-S12.

Dib-Hajj SD, Tyrrell L, Black JA, Waxman SG (1998a) NaN, a novel voltage-gated na channel, is expressed preferentially in peripheral sensory neurons and down-regulated after axotomy. Proc Natl Acad Sci U S A 95:8963-8968.

Dib-Hajj SD, Black JA, Cummins TR, Kenney AM, Kocsis JD, Waxman SG (1998b) Rescue of alpha-SNS sodium channel expression in small dorsal root ganglion neurons after axotomy by nerve growth factor in vivo. J Neurophysiol 79:2668-2676.

Fekete DM, Wu DK (2002) Revisiting cell fate specification in the inner ear. Curr Opin Neurobiol 12:35-42.

Gordon D, Merrick D, Auld V, Dunn R, Goldin AL, Davidson N, Catterall WA (1987) Tissue-specific expression of the RI and RII sodium channel subtypes. Proc Natl Acad Sci U S A 84:8682-8686.

Hafidi A (1998) Peripherin-like immunoreactivity in type II spiral ganglion cell body and projections. Brain Res 805:181-190.

Holley MC (2005) Keynote review: The auditory system, hearing loss and potential targets for drug development. Drug Discov Today 10:1269-1282.

Hossain WA, Antic SD, Yang Y, Rasband MN, Morest DK (2005) Where is the spike generator of the cochlear nerve? voltage-gated sodium channels in the mouse cochlea. Journal of Neuroscience 25:6857-6868.

Kaltenbach JA, Godfrey DA, Neumann JB, McCaslin DL, Afman CE, Zhang J (1998) Changes in spontaneous neural activity in the dorsal cochlear nucleus following exposure to intense sound: Relation to threshold shift. Hear Res 124:78-84.

Krafte DS, Bannon AW (2008) Sodium channels and nociception: Recent concepts and therapeutic opportunities. Current Opinion in Pharmacology 8:50-56.

Krzemien DM, Schaller KL, Levinson SR, Caldwell JH (2000) Immunolocalization of sodium channel isoform NaCh6 in the nervous system. J Comp Neurol 420:70-83.

Kuan CY, Tannahill D, Cook GM, Keynes RJ (2004) Somite polarity and segmental patterning of the peripheral nervous system. Mech Dev 121:1055-1068.

Li HY, Say EH, Zhou XF (2007) Isolation and characterization of neural crest progenitors from adult dorsal root ganglia. Stem Cells 25:2053-2065.

Liberman MC (1982) Single-neuron labeling in the cat auditory nerve. Science 216:1239-1241.

Moller AR (1997) Similarities between chronic pain and tinnitus. The American Journal of Otology 18:577-585.

Momin A, Wood JN (2008) Sensory neuron voltage-gated sodium channels as analgesic drug targets. Curr Opin Neurobiol 18:383-388.

Mou K, Adamson CL, Davis RL (1998) Time-dependence and cell-type specificity of synergistic neurotrophin actions on spiral ganglion neurons. J Comp Neurol 402:129-139.

Novakovic SD, Tzoumaka E, McGivern JG, Haraguchi M, Sangameswaran L, Gogas KR, Eglen RM, Hunter JC (1998) Distribution of the tetrodotoxin-resistant sodium channel PN3 in rat sensory neurons in normal and neuropathic conditions. Journal of Neuroscience 18:2174-2187.

Patuzzi RB, Brown DJ, McMahon CM, Halliday AF (2004) Determinants of the spectrum of the neural electrical activity at the round window: Transmitter release and neural depolarisation. Hear Res 190:87-108.

Raff T, van der Giet M, Endemann D, Wiederholt T, Paul M (1997) Design and testing of beta-actin primers for RT-PCR that do not co-amplify processed pseudogenes. Biotechniques 23:456-460.

Rasband MN, Park EW, Vanderah TW, Lai J, Porreca F, Trimmer JS (2001) Distinct potassium channels on pain-sensing neurons. Proc Natl Acad Sci U S A 98:13373-13378.

Reid MA, Flores-Otero J, Davis RL (2004) Firing patterns of type II spiral ganglion neurons in vitro. Journal of Neuroscience 24:733-742.

Robertson D, Sellick PM, Patuzzi R (1999) The continuing search for outer hair cell afferents in the guinea pig spiral ganglion. Hear Res 136:151-158.

Rogart RB, Cribbs LL, Muglia LK, Kephart DD, Kaiser MW (1989) Molecular cloning of a putative tetrodotoxin-resistant rat heart na+ channel isoform. Proc Natl Acad Sci U S A ; Proceedings of the National Academy of Sciences of the United States of America 86:8170-8174.

Samorajski T, Ordy JM, Rady-Reimer P (1968) Lipofuscin pigment accumulation in the nervous system of aging mice. Anat Rec 160:555-573.

Sangameswaran L, Delgado SG, Fish LM, Koch BD, Jakeman LB, Stewart GR, Sze P, Hunter JC, Eglen RM, Herman RC (1996) Structure and function of a novel voltage-gated, tetrodotoxin-resistant sodium channel specific to sensory neurons. J Biol Chem 271:5953-5956.

Sangameswaran L, Fish LM, Koch BD, Rabert DK, Delgado SG, Ilnicka M, Jakeman LB, Novakovic S, Wong K, Sze P, Tzoumaka E, Stewart GR, Herman RC, Chan H, Eglen RM, Hunter JC (1997) A novel tetrodotoxin-sensitive, voltage-gated sodium channel expressed in rat and human dorsal root ganglia. J Biol Chem 272:14805-14809.

Sans A, Bartolami S, Fraysse B (1996) Histopathology of the peripheral vestibular system in small vestibular schwannomas. Am J Otol 17:326-324.

Santos-Sacchi J (1993) Voltage-dependent ionic conductances of type I spiral ganglion cells from the guinea pig inner ear. Journal of Neuroscience 13:3599-3611.

Toledo-Aral JJ, Moss BL, He ZJ, Koszowski AG, Whisenand T, Levinson SR, Wolf JJ, Silos-Santiago I, Halegoua S, Mandel G (1997) Identification of PN1, a predominant voltage-dependent sodium channel expressed principally in peripheral neurons. Proc Natl Acad Sci U S A 94:1527-1532.

Trimmer JS, Cooperman SS, Agnew WS, Mandel G (1990) Regulation of muscle sodium channel transcripts during development and in response to denervation. Dev Biol 142:360-367.

Tzoumaka E, Tischler AC, Sangameswaran L, Eglen RM, Hunter JC, Novakovic SD (2000) Differential distribution of the tetrodotoxin-sensitive rPN4/NaCh6/Scn8a sodium channel in the nervous system. J Neurosci Res 60:37-44.

Vio MM, Holme RH (2005) Hearing loss and tinnitus: 250 million people and a US$10 billion potential market. Drug Discov Today 10:1263-1265.

Westenbroek RE, Merrick DK, Catterall WA (1989) Differential subcellular localization of the RI and RII na+ channel subtypes in central neurons. Neuron 3:695-704.

Whitaker WR, Clare JJ, Powell AJ, Chen YH, Faull RL, Emson PC (2000) Distribution of voltage-gated sodium channel alpha-subunit and beta-subunit mRNAs in human hippocampal formation, cortex, and cerebellum. J Comp Neurol 422:123-139.

Whitaker WRJ, Faull RLM, Waldvogel HJ, Plumpton CJ, Emson PC, Clare JJ (2001) Comparative distribution of voltage-gated sodium channel proteins in human brain. Mol Brain Res 88:37-53.

Wooltorton JR, Gaboyard S, Hurley KM, Price SD, Garcia JL, Zhong M, Lysakowski A, Eatock RA (2007) Developmental changes in two voltage-dependent sodium currents in utricular hair cells. J Neurophysiol 97:1684-1704.

Bibliography

Abrashkin, K.A., Izumikawa, M., Miyazawa, T., Wang, C., Crumling, M.A., Swiderski, D.L., Beyer, L.A., Gong, T.L. and Raphael, Y., 2006. The fate of outer hair cells after acoustic or ototoxic insults. *Hear.Res.,* **218,** 20-29.

Adamson, C.L., Reid, M.A., Mo, Z., Bowne-English, J. and Davis, R.L., 2002a. Firing features and Potassium channel content of murine spiral ganglion neurons vary with cochlear location. *J.Comp.Neurol.,* **447,** 331-350.

Adamson, C.L., Reid, M.A. and Davis, R.L., 2002b. Opposite Actions of Brain-Derived Neurotrophic Factor and Neurotrophin-3 on Firing Features and Ion Channel Composition of Murine Spiral Ganglion Neurons. *J.Neurosci.,* **22,** 1385-1396.

Akopian, A.N., Souslova, V., England, S., Okuse, K., Ogata, N., Ure, J., Smith, A., Kerr, B.J., McMahon, S.B., Boyce, S., Hill, R., Stanfa, L.C., Dickenson, A.H. and Wood, J.N., 1999. The tetrodotoxin-resistant sodium channel SNS has a specialized function in pain pathways. *Nat.Neurosci.,* **2,** 541-548.

Alam, S.A., Ikeda, K., Oshima, T., Suzuki, M., Kawase, T., Kikuchi, T. and Takasaka, T., 2000. Cisplatin-induced apoptotic cell death in Mongolian gerbil cochlea. *Hear.Res.,* **141,** 28-38.

Amaya, F., Decosterd, I., Samad, T.A., Plumpton, C., Tate, S., Mannion, R.J., Costigan, M. and Woolf, C.J., 2000. Diversity of Expression of the Sensory Neuron-Specific TTX-Resistant Voltage-Gated Sodium Ion Channels SNS and SNS2. *Mol.Cell.Neurosci.,* **15,** 331-342.

Amaya, F., Wang, H., Costigan, M., Allchorne, A.J., Hatcher, J.P., Egerton, J., Stean, T., Morisset, V., Grose, D., Gunthorpe, M.J., Chessell, I.P., Tate, S., Green, P.J. and Woolf, C.J., 2006. The Voltage-Gated Sodium Channel Nav1.9 Is an Effector of Peripheral Inflammatory Pain Hypersensitivity. *J.Neurosci.,* **26,** 12852-12860.

Amir, R., Michaelis, M. and Devor, M., 1999. Membrane Potential Oscillations in Dorsal Root Ganglion Neurons: Role in Normal Electrogenesis and Neuropathic Pain. *J.Neurosci.,* **19,** 8589-8596.

Anderson, L. and Seilhamer, J., 1997. A comparison of selected mRNA and protein abundances in human liver. *Electrophoresis,* **18,** 533-537.

Aubry, U., Carignan, G., Charette, D., Keeri-Szanto, M. and Lavallee, J.P., 1966. Neuroleptanalgesia with fentanyl-droperidol: an appreciation based on more than 1000 anaesthetics for major surgery. *Can.Anaesth.Soc.J.,* **13,** 263-271.

Axelsson, A., Miller, J. and Larsson, B., 1975. A Modified "Soft Surface Specimen Technique" For Examination Of The Inner Ear. *Acta Otolaryngol.,* **80,** 362.

Baguley, D.M., Jones, S., Wilkins, I., Axon, P.R. and Moffat, D.A., 2005. The inhibitory effect of intravenous lidocaine infusion on tinnitus after translabyrinthine removal of vestibular schwannoma: a double-blind, placebo-controlled, crossover study. *Otol.Neurotol.,* **26,** 169-176.

Baguley, D.M., 2002. Mechanisms of tinnitus. *Br.Med.Bull.,* **63,** 195-212.

Baker, M.D. and Bostock, H., 1997. Low-Threshold, Persistent Sodium Current in Rat Large Dorsal Root Ganglion Neurons in Culture. *J.Neurophysiol.,* **77,** 1503-1513.

Balaban, C.D., Zhou, J. and Li, H., 2003. Type 1 vanilloid receptor expression by mammalian inner ear ganglion cells. *Hear.Res.,* **175,** 165-170.

Barber, R.D., Harmer, D.W., Coleman, R.A. and Clark, B.J., 2005. GAPDH as a housekeeping gene: analysis of GAPDH mRNA expression in a panel of 72 human tissues. *Physiol.Genomics,* **21,** 389-395.

Bauer, C.A., Turner, J.G., Caspary, D.M., Myers, K.S. and Brozoski, T.J., 2008. Tinnitus and inferior colliculus activity in chinchillas related to three distinct patterns of cochlear trauma. *J.Neurosci.Res.,* **86,** 2564-2578.

Bauer, C.A., Brozoski, T.J. and Myers, K., 2007. Primary afferent dendrite degeneration as a cause of tinnitus. *J.Neurosci.Res.,* **85,** 1489-1498.

Beckh, S., 1990. Differential expression of sodium channel mRNAs in rat peripheral nervous system and innervated tissues. *FEBS Lett.,* **262,** 317-322.

Beckh, S., Noda, M., Lubbert, H. and Numa, S., 1989. Differential regulation of three sodium channel messenger RNAs in the rat central nervous system during development. *EMBO J.,* **8,** 3611-3616.

Belcher, S.M., Zerillo, C.A., Levenson, R., Ritchie, J.M. and Howe, J.R., 1995. Cloning of a sodium channel alpha subunit from rabbit Schwann cells. *Proc.Natl.Acad.Sci.U.S.A.,* **92,** 11034-11038.

Berglund, A.M. and Ryugo, D.K., 1991. Neurofilament Antibodies and Spiral Ganglion Neurons of the Mammalian Cochlea. *J.Comp.Neurol.,* **306,** 393-408.

Berglund, A.M. and Ryugo, D.K., 1987. Hair cell innervation by spiral ganglion neurons in the mouse. *J.Comp.Neurol.,* **255,** 560-570.

Birks, J. and Grimley Evans, J., 2009. Ginkgo biloba for cognitive impairment and dementia.[update of Cochrane Database Syst Rev. 2007;(2):CD003120; PMID: 17443523]. *Cochrane Database of Systematic Reviews,* 003120.

Bjarnason, R., Wickelgren, R., Hermansson, M., Hammarqvist, F., Carlsson, B. and Carlsson, L.M.S., 1998. Growth Hormone Treatment Prevents the Decrease in Insulin-

Like Growth Factor I Gene Expression in Patients Undergoing Abdominal Surgery. *J.Clin.Endocrinol.Metab.,* **83,** 1566-1572.

Black, J.A., Cummins, T.R., Plumpton, C., Chen, Y.H., Hormuzdiar, W., Clare, J.J. and Waxman, S.G., 1999. Upregulation of a silent sodium channel after peripheral, but not central, nerve injury in DRG neurons. *J.Neurophysiol.,* **82,** 2776-2785.

Black, J.A., Dib-Hajj, S., McNabola, K., Jeste, S., Rizzo, M.A., Kocsis, J.D. and Waxman, S.G., 1996. Spinal sensory neurons express multiple sodium channel α-subunit mRNAs. *Mol.Brain Res.,* **43,** 117-131.

Black, J.A., Liu, S., Tanaka, M., Cummins, T.R. and Waxman, S.G., 2004. Changes in the expression of tetrodotoxin-sensitive sodium channels within dorsal root ganglia neurons in inflammatory pain. *Pain,* **108,** 237-247.

Bobbin, R.P., 1979. Glutamate and aspartate mimic the afferent transmitter in the cochlea. *Exp.Brain Res.,* **34,** 389-393.

Boiko, T., Rasband, M.N., Levinson, S.R., Caldwell, J.H., Mandel, G., Trimmer, J.S. and Matthews, G., 2001. Compact Myelin Dictates the Differential Targeting of Two Sodium Channel Isoforms in the Same Axon. *Neuron,* **30,** 91-104.

Bonner, T.I., Buckley, N.J., Young, A.C. and Brann, M.R., 1987. Identification of a family of muscarinic acetycholine receptor genes. *Science,* **237,** p527(6).

Brandt, A., Striessnig, J. and Moser, T., 2003. CaV1.3 Channels Are Essential for Development and Presynaptic Activity of Cochlear Inner Hair Cells. *J.Neurosci.,* **23,** 10832-10840.

Brown, M.C., 1994. Antidromic responses of single units from the spiral ganglion. *J.Neurophysiol.,* **71,** 1835-1847.

Brownell, W.E., Bader, C.R., Bertrand, D. and De Ribaupierre, Y., 1985. Evoked mechanical responses of isolated cochlear outer hair cells. *Science,* **227,** 194-196.

Brunner, M. and Vaughan, D., 2000. Evoked potential monitoring in anaesthesia and analgesia. *Anaesthesia,* **55,** 823-825.

Butt, A.M. and Kalsi, A., 2006. Inwardly rectifying potassium channels (Kir) in central nervous system glia: a special role for Kir4.1 in glial functions. *J.Cell.Mol.Med.,* **10,** 33-44.

Caldwell, J.H., Schaller, K.L., Lasher, R.S., Peles, E. and Levinson, S.R., 2000. Sodium channel $Na_V1.6$ is localized at nodes of Ranvier, dendrites, and synapses. *Proc.Natl.Acad.Sci.U.S.A.,* **97,** 5616-5620.

Canlon, B. and Schacht, J., 1983. Acoustic stimulation alters deoxyglucose uptake in the mouse cochlea and inferior colliculus. *Hear.Res.,* **10,** 217-226.

Catterall, W.A., 2000. From ionic currents to molecular mechanisms: The structure and function of Voltage-Gated Sodium Channels. *Neuron,* **26,** 13-25.

Catterall, W.A., Goldin, A.L. and Waxman, S.G., 2005a. International Union of Pharmacology. XLVII. Nomenclature and structure-function relationships of voltage-gated sodium channels. *Pharmacol.Rev.,* **57,** 397-409.

Catterall, W.A., Perez-Reyes, E., Snutch, T.P. and Striessnig, J., 2005b. International Union of Pharmacology. XLVIII. Nomenclature and structure-function relationships of voltage-gated calcium channels. *Pharmacol.Rev.,* **57,** 411-425.

Chahine, M., Ziane, R., Vijayaragavan, K. and Okamura, Y., 2005. Regulation of Nav channels in sensory neurons. *Trends Pharmacol.Sci.,* **26,** 496-502.

Charriaut-Marlangue, C.C.A. and Ben-Ari, Y., 1995. A cautionary note on the use of the TUNEL stain to determine apoptosis. *Neuroreport,* **7,** 61-64.

Chen, G.D. and Fechter, L.D., 2003. The relationship between noise-induced hearing loss and hair cell loss in rats. *Hear.Res.,* **177,** 81-90.

Chen, G. and Fechter, L.D., 1999. Potentiation of octave-band noise induced auditory impairment by carbon monoxide. *Hear.Res.,* **132,** 149-159.

Chen, G. and Jastreboff, P.J., 1995. Salicylate-induced abnormal activity in the inferior colliculus of rats. *Hear.Res.,* **82,** 158-178.

Chen, L., Trautwein, P.G., Shero, M. and Salvi, R.J., 1996. Tuning, spontaneous activity and tonotopic map in chicken cochlear ganglion neurons following sound-induced hair cell loss and regeneration. *Hear.Res.,* **98,** 152-164.

Chen, Y.H., Dale, T.J., Romanos, M.A., Whitaker, W.R.J., Xie, X.M. and Clare, J.J., 2000. Cloning, distribution and functional analysis of the type III sodium channel from human brain. *Eur.J.Neurosci.,* **12,** 4281-4289.

Cho, Y., Gong, T.L., Kanicki, A., Altschuler, R.A. and Lomax, M.I., 2004. Noise overstimulation induces immediate early genes in the rat cochlea. *Mol.Brain Res.,* **130,** 134-148.

Choi, D.W. and Rothman, S.M., 1990. The Role of Glutamate Neurotoxicity in Hypoxic-Ischemic Neuronal Death. *Annu.Rev.Neurosci.,* **13,** 171-182.

Choi, J.K., Holtzer, S., Chacko, S.A., Lin, Z.X., Hoffman, R.K. and Holtzer, H., 1991. Phorbol esters selectively and reversibly inhibit a subset of myofibrillar genes responsible for the ongoing differentiation program of chick skeletal myotubes. *Mol.Cell.Biol.,* **11,** 4473-4482.

Church, M.W. and Gritzke, R., 1987. Effects of ketamine anesthesia on the rat brain-stem auditory evoked potential as a function of dose and stimulus intensity. *Electroencephalogr.Clin.Neurophysiol.,* **67,** 570-583.

Church, M.W., Jen, K.L., Stafferton, T., Hotra, J.W. and Adams, B.R., 2007. Reduced auditory acuity in rat pups from excess and deficient omega-3 fatty acid consumption by the mother. *Neurotox.Teratol.,* **29,** 203-210.

Church, M.W. and Kaltenbach, J.A., 1993. The hamster's auditory brain stem response as a function of stimulus intensity, tone burst frequency, and hearing loss. *Ear Hear.,* **14,** 249-257.

Clapham, D.E., 2003. TRP channels as cellular sensors. *Nature,* **426,** 517-524.

Clapham, D.E., Julius, D., Montell, C. and Schultz, G., 2005. International Union of Pharmacology. XLIX. Nomenclature and Structure-Function Relationships of Transient Receptor Potential Channels. *Pharmacol.Rev.,* **57,** 427-450.

Clark, J.A. and Pickles, J.O., 1996. The effects of moderate and low levels of acoustic overstimulation on stereocilia and their tip links in the guinea pig. *Hear.Res.,* **99,** 119-128.

Coggeshall, R.E., Tate, S. and Carlton, S.M., 2004. Differential expression of tetrodotoxin-resistant sodium channels Nav1.8 and Nav1.9 in normal and inflamed rats. *Neurosci.Lett.,* **355,** 45-48.

Corey, D.P., 2006. What is the hair cell transduction channel? *The Journal of Physiology,* **576,** 23-28.

Coward, K., Plumpton, C., Facer, P., Birch, R., Carlstedt, T., Tate, S., Bountra, C. and Anand, P., 2000. Immunolocalization of SNS/PN3 and NaN/SNS2 sodium channels in human pain states. *Pain,* **85,** 41-50.

Cox, J.J., Reimann, F., Nicholas, A.K., Thornton, G., Roberts, E., Springell, K., Karbani, G., Jafri, H., Mannan, J., Raashid, Y., Al-Gazali, L., Hamamy, H., Valente, E.M., Gorman, S., Williams, R., McHale, D.P., Wood, J.N., Gribble, F.M. and Woods, C.G., 2006. An SCN9A channelopathy causes congenital inability to experience pain. *Nature,* **444,** 894-898.

Cummins, T.R. and Waxman, S.G., 1997. Downregulation of tetrodotoxin-resistant sodium currents and upregulation of a rapidly repriming tetrodotoxin-sensitive sodium current in small spinal sensory neurons after nerve injury. *J.Neurosci.,* **17,** 3503-3514.

Cummins, T.R., Aglieco, F., Renganathan, M., Herzog, R.I., Dib-Hajj, S.D. and Waxman, S.G., 2001. Nav1.3 Sodium Channels: Rapid Repriming and Slow Closed-State Inactivation Display Quantitative Differences after Expression in a Mammalian Cell Line and in Spinal Sensory Neurons. *J.Neurosci.,* **21,** 5952-5961.

Cummins, T.R., Dib-Hajj, S.D., Black, J.A., Akopian, A.N., Wood, J.N. and Waxman, S.G., 1999. A Novel Persistent Tetrodotoxin-Resistant Sodium Current In SNS-Null And Wild-Type Small Primary Sensory Neurons. *J.Neurosci.,* **19,** 43RC.

Cummins, T.R., Dib-Hajj, S.D., Herzog, R.I. and Waxman, S.G., 2005. Nav1.6 channels generate resurgent sodium currents in spinal sensory neurons. *FEBS Lett.,* **579,** 2166-2170.

Cummins, T.R., Howe, J.R. and Waxman, S.G., 1998. Slow Closed-State Inactivation: A Novel Mechanism Underlying Ramp Currents in Cells Expressing the hNE/PN1 Sodium Channel. *J.Neurosci.,* **18,** 9607-9619.

d'Aldin, C.G., Ruel, J., Assie, R., Pujol, R. and Puel, J.L., 1997. Implication of NMDA type glutamate receptors in neural regeneration and neoformation of synapses after excitotoxic injury in the guinea pig cochlea. *Int.J.Dev.Neurosci.,* **15,** 619-629.

Dallos, P., 1992. The active cochlea. *J.Neurosci.,* **12,** 4575-4585.

Dallos, P. and Fakler, B., 2002. Prestin, a new type of motor protein. *Nat.Rev.Mol.Cell.Biol,* **3,** 104-111.

Dallos, P. and Harris, D., 1978. Properties of auditory nerve responses in absence of outer hair cells. *J.Neurophysiol.,* **41,** 365-383.

Dart, C., Leyland, M.L., Barrett-Jolley, R., Shelton, P.A., Spencer, P.J., Conley, E.C., Sutcliffe, M.J. and Stanfield, P.R., 1998. The dependence of Ag+ block of a potassium channel, murine kir2.1, on a cysteine residue in the selectivity filter. *J.Physiol.(Lond.),* **511,** 15-24.

Daudet, N., Vago, P., Ripoll, C., Humbert, G., Pujol, R. and Lenoir, M., 1998. Characterization of atypical cells in the juvenile rat organ of corti after aminoglycoside ototoxicity. *J.Comp.Neurol.,* **401,** 145-162.

Davies, E., 2004. The Pharmacological Management of Tinnitus. *Audiol.Med.,* **2,** 26-28.

Davis, H., 1983. An active process in cochlear mechanics. *Hear.Res.,* **9,** 79-90.

Davis, R.L., 2003. Gradients of neurotrophins, ion channels, and tuning in the cochlea. *The Neuroscientist,* **9,** 311-316.

Devor, M., 2006. Sodium channels and mechanisms of neuropathic pain. *J.Pain,* **7,** S3-S12.

Dhaka, A., Viswanath, V. and Patapoutian, A., 2006. TRP ion channels and temperature sensation. *Annu.Rev.Neurosci.,* **29,** 135-161.

Dib-Hajj, S., Black, J. ., Felts, P. and Waxman, S. ., 1996. Down-regulation of transcripts for Na channel α-SNS in spinal sensory neurons following axotomy. *Proc.Natl.Acad.Sci.U.S.A.,* **93,** 14950-14954.

Dib-Hajj, S.D., Black, J.A., Cummins, T.R., Kenney, A.M., Kocsis, J.D. and Waxman, S.G., 1998. Rescue of alpha-SNS sodium channel expression in small dorsal root ganglion neurons after axotomy by nerve growth factor in vivo. *J.Neurophysiol.,* **79,** 2668-2676.

Dib-Hajj, S.D., Fjell, J., Cummins, T.R., Zheng, Z., Fried, K., LaMotte, R., Black, J.A. and Waxman, S.G., 1999. Plasticity of sodium channel expression in DRG neurons in the chronic constriction injury model of neuropathic pain. *Pain,* **83,** 591-600.

Dib-Hajj, S.D., Rush, A.M., Cummins, T.R., Hisama, F.M., Novella, S., Tyrrell, L., Marshall, L. and Waxman, S.G., 2005. Gain-of-function mutation in Nav1.7 in familial erythromelalgia induces bursting of sensory neurons. *Brain,* **128,** 1847-1854.

Dib-Hajj, S.D., Tyrrell, L., Black, J.A. and Waxman, S.G., 1998. NaN, a novel voltage-gated Na channel, is expressed preferentially in peripheral sensory neurons and down-regulated after axotomy. *Proc.Natl.Acad.Sci.U.S.A.,* **95,** 8963-8968.

Dib-Hajj, S.D., Cummins, T.R., Black, J.A. and Waxman, S.G., 2007. From genes to pain: Nav1.7 and human pain disorders. *Trends Neurosci.,* **30,** 555-563.

Dietrich, P.S., McGivern, J.G., Delgado, S.G., Koch, B.D., Eglen, R.M., Hunter, J.C. and Sangameswaran, L., 1998. Functional analysis of a voltage-gated sodium channel and its splice variant from rat dorsal root ganglia. *J.Neurochem.,* **70,** 2262-2272.

Djouhri, L., Fang, X., Okuse, K., Wood, J.N., Berry, C.M. and Lawson, S.N., 2003. The TTX-Resistant Sodium Channel Nav1.8 (SNS/PN3): Expression and Correlation with Membrane Properties in Rat Nociceptive Primary Afferent Neurons. *J.Physiol.,* **550,** 739-752.

Do, M.T.H. and Bean, B.P., 2004. Sodium Currents in Subthalamic Nucleus Neurons From Nav1.6-Null Mice. *J.Neurophysiol.,* **92,** 726-733.

Dobie, R.A., 1999. A review of randomized clinical trials in tinnitus. *Laryngoscope,* **109,** 1202-1211.

Dodson, P.D., Barker, M.C. and Forsythe, I.D., 2002. Two Heteromeric Kv1 Potassium Channels Differentially Regulate Action Potential Firing. *J.Neurosci.,* **22,** 6953-6961.

Drew, S. and Davies, E., 2001. Effectiveness of Ginkgo biloba in treating tinnitus: double blind, placebo controlled trial. *BMJ,* **322,** 73.

Duan, M., Laurell, G., Qiu, J. and Borg, E., 2008. Susceptibility to impulse noise trauma in different species: guinea pig, rat and mouse. *Acta Otolaryngol.,* **128,** 277.

Duflocq, A., Le Bras, B., Bullier, E., Couraud, F. and Davenne, M., 2008. Nav1.1 is predominantly expressed in nodes of Ranvier and axon initial segments. *Mol.Cell.Neurosci.,* **39,** 180-192.

Dulon, D., Luo, L., Zhang, C. and Ryan, A.F., 1998. Expression of small-conductance calcium-activated potassium channels (SK) in outer hair cells of the rat cochlea. *Eur.J.Neurosci.,* **10,** 907-915.

Eggermont, J.J. and Roberts, L.E., 2004. The neuroscience of tinnitus. *Trends Neurosci.,* **27,** 676-682.

Ekberg, J. and Adams, D.J., 2006. Neuronal voltage-gated sodium channel subtypes: Key roles in inflammatory and neuropathic pain. *Int.J.Biochem.Cell Biol.,* **38,** 2005-2010.

Elgoyhen, A.B., Vetter, D.E., Katz, E., Rothlin, C.V., Heinemann, S.F. and Boulter, J., 2001. α10: A determinant of nicotinic cholinergic receptor function in mammalian vestibular and cochlear mechanosensory hair cells. *Proc.Natl.Acad.Sci.U.S.A.,* **98,** 3501-3506.

Elgoyhen, A.B., Johnson, D.S., Boulter, J., Vetter, D.E. and Heinemann, S., 1994. α9: An acetylcholine receptor with novel pharmacological properties expressed in rat cochlear hair cells. *Cell,* **79,** 705-715.

England, J.D., Happel, L.T., Kline, D.G., Gamboni, F., Thouron, C.L., Liu, Z.P. and Levinson, S.R., 1996. Sodium channel accumulation in humans with painful neuromas. *Neurology,* **47,** 272-276.

Ernfors, P., Van De Water, T., Loring, J. and Jaenisch, R., 1995. Complementary roles of BDNF and NT-3 in vestibular and auditory development. *Neuron,* **14,** 1153-1164.

Ertel, E.A., Campbell, K.P., Harpold, M.M., Hofmann, F., Mori, Y., Perez-Reyes, E., Schwartz, A., Snutch, T.P., Tanabe, T., Birnbaumer, L., Tsien, R.W. and Catterall, W.A., 2000. Nomenclature of Voltage-Gated Calcium Channels. *Neuron,* **25,** 533-535.

Etheridge, S., 2002. An acute experimental model of hearing loss using noise in combination with hypoxia and its use in the investigation of a putative cochleoprotectant. PhD. University of Leicester.

Eybalin, M., 1993. Neurotransmitters and neuromodulators of the mammalian cochlea. *Physiol.Rev.,* **73,** 309-373.

Fang, X., Djouhri, L., Black, J.A., Dib-Hajj, S.D., Waxman, S.G. and Lawson, S.N., 2002. The Presence and Role of the Tetrodotoxin-Resistant Sodium Channel Nav1.9 (NaN) in Nociceptive Primary Afferent Neurons. *J.Neurosci.,* **22,** 7425-7433.

Fekete, D.M. and Wu, D.K., 2002. Revisiting cell fate specification in the inner ear. *Curr.Opin.Neurobiol.,* **12,** 35-42.

Fekete, D.M., 1996. Cell fate specification in the inner ear. *Curr.Opin.Neurobiol.,* **6,** 533-541.

Felix, D. and Ehrenberger, K., 1992. The efferent modulation of mammalian inner hair cell afferents. *Hear.Res.,* **64,** 1-5.

Felts, P.A., Yokoyama, S., Dib-Hajj, S., Black, J.A. and Waxman, S.G., 1997. Sodium channel alpha-subunit mRNAs I, II, III, NaG, Na6 and hNE (PN1): different expression patterns in developing rat nervous system. *Brain Res.Mol.Brain Res.,* **45,** 71-82.

Fergie, N., 2005. Investigation of voltage-dependent sodium channel modulators as cochleoprotectants. MD. University of Leicester.

Fertleman, C.R., Baker, M.D., Parker, K.A., Moffatt, S., Elmslie, F.V., Abrahamsen, B., Ostman, J., Klugbauer, N., Wood, J.N., Gardiner, R.M. and Rees, M., 2006. SCN9A mutations in paroxysmal extreme pain disorder: allelic variants underlie distinct channel defects and phenotypes. *Neuron,* **52,** 767-774.

Fettiplace, R. and Hackney, C.M., 2006. The sensory and motor roles of the auditory hair cells. *Nat.Rev.Neurosci.,* **7,** 19-29.

Filipo, R., Barbara, M., Cordier, A., Mafera, B., Romeo, R., Attanasio, G., Mancini, P. and Marzetti, A., 1997. Osmotic Drugs in the Treatment of Cochlear Disorders: A Clinical and Experimental Study. *Acta Otolaryngol.,* **117,** 229.

Finlayson, P.G. and Kaltenbach, J.A., 2009. Alterations in the spontaneous discharge patterns of single units in the dorsal cochlear nucleus following intense sound exposure. *Hear.Res.,* **256,** 104-117.

Fish, J.H.,3rd, Scholtz, A.W., Hussl, B., Kammen-Jolly, K., Ichiki, H., Kreczy, A. and Schrott-Fischer, A., 2001. Immunohistochemical and morphological studies on the human fetal cochlea: a comparative view on methods. *Tissue Cell,* **33,** 189-199.

Flecknell, P.A. and Mitchell, M., 1984. Midazolam and fentanyl-fluanisone: assessment of anaesthetic effects in laboratory rodents and rabbits. *Lab.Anim.,* **18,** 143-146.

Forsythe, I.D., 2002. Auditory processing. *Encyclopaedia of Life Sciences.* Chichester, UK: John Wiley & Sons, Ltd. www.els.net.

Fotia, A.B., Ekberg, J., Adams, D.J., Cook, D.I., Poronnik, P. and Kumar, S., 2004. Regulation of Neuronal Voltage-gated Sodium Channels by the Ubiquitin-Protein Ligases Nedd4 and Nedd4-2. *J.Biol.Chem.,* **279,** 28930-28935.

Fredelius, L., Rask-Andersen, H., Johansson, B., Urquiza, R., Bagger-Sjoback, D. and Wersall, J., 1988. Time sequence of degeneration pattern of the organ of Corti after acoustic overstimulation. A light microscopical and electrophysiological investigation in the guinea pig. *Acta Otolaryngol.,* **106,** 81-93.

Fregni, F., Marcondes, R., Boggio, P.S., Marcolin, M.A., Rigonatti, S.P., Sanchez, T.G., Nitsche, M.A. and Pascual-Leone, A., 2006. Transient tinnitus suppression induced by repetitive transcranial magnetic stimulation and transcranial direct current stimulation. *Eur.J.Neurol.,* **13,** 996-1001.

Fuchs, P.A., Glowatzki, E. and Moser, T., 2003. The afferent synapse of cochlear hair cells. *Curr.Opin.Neurobiol.,* **13,** 452-458.

Fujioka, M., Kanzaki, S., Okano, H.J., Masuda, M., Ogawa, K. and Okano, H., 2006. Proinflammatory cytokines expression in noise-induced damaged cochlea. *J.Neurosci.Res.,* **83,** 575-583.

Furness, D.N., Hulme, J.A., Lawton, D.M. and Hackney, C.M., 2002. Distribution of the glutamate/aspartate transporter GLAST in relation to the afferent synapses of outer hair cells in the guinea pig cochlea. *JARO,* **3,** 234-247.

Gavrieli, Y., Sherman, Y. and Ben-Sasson, S., 1992. Identification of programmed cell death in situ via specific labeling of nuclear DNA fragmentation. *J.Cell Biol.,* **119,** 493-501.

Geisler, C.D., 1998. *From sound to synapse: physiology of the mammalian ear.* New York; Oxford: Oxford University Press.

Gelfand, S.A., 2001. Anatomy and physiology of the auditory system. *Essentials of audiology.* 2nd ed. New York: Thieme. 37-89.

Glowatzki, E. and Fuchs, P.A., 2002. Transmitter release at the hair cell ribbon synapse. *Nat.Neurosci.,* **5,** 147-154.

Goldin, A.L., 2001. Resurgence of sodium channel research. *Ann.Rev.Physiol.,* **63,** 871-894.

Goldstein, M.E., House, S.B. and Gainer, H., 1991. NF-L and peripherin immunoreactivities define distinct classes of rat sensory ganglion cells. *J.Neurosci.Res.,* **30,** 92-104.

Goldstein, S.A., Bayliss, D.A., Kim, D., Lesage, F., Plant, L.D. and Rajan, S., 2005. International Union of Pharmacology. LV. Nomenclature and molecular relationships of two-P potassium channels. *Pharmacol.Rev.,* **57,** 527-540.

Gordon, D., Merrick, D., Auld, V., Dunn, R., Goldin, A.L., Davidson, N. and Catterall, W.A., 1987. Tissue-specific expression of the RI and RII sodium channel subtypes. *Proc.Natl.Acad.Sci.U.S.A.,* **84,** 8682-8686.

Green, C.J., 1975. Neuroleptanalgesic drug combinations in the anaesthetic management of small laboratory animals. *Lab.Anim.,* **9,** 161-178.

Green, G.E., Khan, K.M., Beisel, K.W., Drescher, M.J. and Hatfield, J.S., 1996. Calcium Channel Subunits in the Mouse Cochlea. *J.Neurochem.,* **67,** 37-45.

Hafidi, A., 1998. Peripherin-like immunoreactivity in type II spiral ganglion cell body and projections. *Brain Res.,* **805,** 181-190.

Hafidi, A., Beurg, M. and Dulon, D., 2005. Localization and developmental expression of BK channels in mammalian cochlear hair cells. *Neurosci.,* **130,** 475-484.

Hains, B.C., Klein, J.P., Saab, C.Y., Craner, M.J., Black, J.A. and Waxman, S.G., 2003. Upregulation of sodium channel Nav1.3 and functional involvement in neuronal hyperexcitability associated with central neuropathic pain after spinal cord injury. *J.Neurosci.,* **23,** 8881-8892.

Hains, B.C., Saab, C.Y., Klein, J.P., Craner, M.J. and Waxman, S.G., 2004. Altered sodium channel expression in second-order spinal sensory neurons contributes to pain after peripheral nerve injury. *J.Neurosci.,* **24,** 4832-4839.

Hamernik, R.P., Henderson, D. and Salvi, R.J., 1980. Contribution of animal studies to our understanding of impulse noise induced hearing loss. *Scand.Audiol.,* **Supplementum,** 128-146.

Hamid, M.A., 2009. Meniere's disease. *Pract.Neurol.,* **9,** 157-162.

Heffner, H.E. and Harrington, I.A., 2002. Tinnitus in hamsters following exposure to intense sound. *Hear.Res.,* **170,** 83-95.

Heffner, H.E. and Koay, G., 2005. Tinnitus and hearing loss in hamsters (Mesocricetus auratus) exposed to loud sound. *Behav.Neurosci.,* **119,** 734-742.

Henderson, D. and Hamernik, R.P., 1995. Biologic bases of noise-induced hearing loss. *Occup.Med.,* **10,** 513-534.

Henry, J.A., Loovis, C., Montero, M., Kaelin, C., Anselmi, K.A., Coombs, R., Hensley, J. and James, K.E., 2007. Randomized clinical trial: group counseling based on tinnitus retraining therapy. *J.Rehabil.Res.Devel.,* **44,** 21-32.

Henry, J.A., Dennis, K.C. and Schechter, M.A., 2005. General Review of Tinnitus: Prevalence, Mechanisms, Effects, and Management. *J.Speech Lang.Hear.Res.,* **48,** 1204-1235.

Herzog, R.I., Cummins, T.R., Ghassemi, F., Dib-Hajj, S.D. and Waxman, S.G., 2003. Distinct repriming and closed-state inactivation kinetics of Nav1.6 and Nav1.7 sodium channels in mouse spinal sensory neurons. *J.Physiol.,* **551,** 741-750.

Hiel, H., Elgoyhen, A.B., Drescher, D.G. and Morley, B.J., 1996. Expression of nicotinic acetylcholine receptor mRNA in the adult rat peripheral vestibular system. *Brain Res.,* **738,** 347-352.

Hirose, K., Discolo, C.M., Keasler, J.R. and Ransohoff, R., 2005. Mononuclear phagocytes migrate into the murine cochlea after acoustic trauma. *J.Comp.Neurol.,* **489,** 180-194.

Hodgkin, A.L. and Huxley, A.F., 1952. A quantitative description of membrane current and its application to conduction and excitation in nerve. *J.Physiol,* **117,** 500-544.

Holley, M.C., 2005. Keynote review: The auditory system, hearing loss and potential targets for drug development. *Drug Discov.Today,* **10,** 1269-1282.

Hong, S., Morrow, T.J., Paulson, P.E., Isom, L.L. and Wiley, J.W., 2004. Early Painful Diabetic Neuropathy Is Associated with Differential Changes in Tetrodotoxin-sensitive and -resistant Sodium Channels in Dorsal Root Ganglion Neurons in the Rat. *J.Biol.Chem.,* **279,** 29341-29350.

Hossain, W.A., Antic, S.D., Yang, Y., Rasband, M.N. and Morest, D.K., 2005. Where is the spike generator of the cochlear nerve? Voltage-gated sodium channels in the mouse cochlea. *J.Neurosci.,* **25,** 6857-6868.

Hotz, M.A., Ritz, R., Linder, L., Scollo-Lavizzari, G. and Haefeli, W.E., 2000. Auditory and electroencephalographic effects of midazolam and alpha-hydroxy-midazolam in healthy subjects. *Br.J.Clin.Pharmacol.,* **49,** 72-79.

House, J.W. and Brackmann, D.E., 1981. Tinnitus: surgical treatment. *Ciba Found.Symp.,* **85,** 204-216.

Hsu, W., 1981. Xylazine-induced depression and its antagonism by alpha adrenergic blocking agents. *J.Pharmacol.Exp.Ther.,* **218,** 188-192.

Hu, B.H., Cai, Q., Manohar, S., Jiang, H., Ding, D., Coling, D.E., Zheng, G. and Salvi, R., 2009. Differential expression of apoptosis-related genes in the cochlea of noise-exposed rats. *Neuroscience,* **161,** 915-925.

Hu, B.H., Guo, W., Wang, P.Y., Henderson, D. and Jiang, S.C., 2000. Intense noise-induced apoptosis in hair cells of guinea pig cochleae. *Acta Otolaryngol.,* **120,** 19-24.

Hu, B.H., Henderson, D. and Nicotera, T.M., 2002. Involvement of apoptosis in progression of cochlear lesion following exposure to intense noise. *Hear.Res.,* **166,** 62-71.

Huang, C.L., 2004. The transient receptor potential superfamily of ion channels. *J.Am.Soc.Nephrol.,* **15,** 1690-1699.

Inagaki, A., Ugawa, S., Yamamura, H., Murakami, S. and Shimada, S., 2008. The CaV3.1 T-type Ca2+channel contributes to voltage-dependent calcium currents in rat outer hair cells. *Brain Res.,* **1201,** 68-77.

Inoue, M., Ates, N., Vossen, J.M.H. and Coenen, A.M.L., 1994. Effects of the neuroleptanalgesic fentanyl-fluanisone (Hypnorm) on spike-wave discharges in epileptic rats. *Pharmacol.Biochem.Behav.,* **48,** 547-551.

Ishibashi, T., Takumida, M., Akagi, N., Hirakawa, K. and Anniko, M., 2009. Changes in transient receptor potential vanilloid (TRPV) 1, 2, 3 and 4 expression in mouse inner ear following gentamicin challenge. *Acta Otolaryngol.,* **129,** 116-126.

Jager, W., Idrizbegovic, E., Karlsson, K.K. and Alvan, G., 1997. Quinine-induced hearing loss in the guinea pig is not affected by the Ca2+ channel antagonist verapamil. *Acta Otolaryngol.,* **117,** 46-48.

Jagger, D.J. and Housley, G.D., 2003. Membrane properties of type II spiral ganglion neurones identified in a neonatal rat cochlear slice. *J.Physiol.(Lond.),* **552,** 525-533.

Jagger, D.J., Robertson, D. and Housley, G.D., 2000. A technique for slicing the rat cochlea around the onset of hearing. *J.Neurosci.Methods,* **104,** 77-86.

Jastreboff, P.J. and Brennan, J.F., 1994. Evaluating the Loudness of Phantom Auditory Perception (Tinnitus) in Rats. *Int.J.Audiol.,* **33,** 202.

Jenkinson, D.H., 2006. Potassium channels--multiplicity and challenges. *Br.J.Pharmacol.,* **147,** S63-71.

Jessell, T.M. and Sanes, J.R., 2000. The induction and patterning of the nervous system. In Kandel, E. R., Schwartz, J. H. and Jessell, T. M., eds, *Principles of neural science.* Fourth edition ed. USA: McGraw-Hill. 1019.

Jongkamonwiwat, N., Phansuwan-Pujito, P., Casalotti, S.O., Forge, A., Dodson, H. and Govitrapong, P., 2006. The existence of opioid receptors in the cochlea of guinea pigs. *Eur.J.Neurosci.,* **23,** 2701-2711.

Jordt, S.E., Bautista, D.M., Chuang, H.H., McKemy, D.D., Zygmunt, P.M., Hogestatt, E.D., Meng, I.D. and Julius, D., 2004. Mustard oils and cannabinoids excite sensory nerve fibres through the TRP channel ANKTM1. *Nature,* **427,** 260-265.

Jordt, S., McKemy, D.D. and Julius, D., 2003. Lessons from peppers and peppermint: the molecular logic of thermosensation. *Curr.Opin.Neurobiol.,* **13,** 487-492.

Kaga, K., Shinoda, Y. and Suzuki, J.-., 1997. Origin of Auditory Brainstem Responses in Cats: Whole Brainstem Mapping, and a Lesion and HRP Study of the Inferior Colliculus. *Acta Otolaryngol.,* **117,** 197.

Kaltenbach, J.A., Godfrey, D.A., Neumann, J.B., McCaslin, D.L., Afman, C.E. and Zhang, J., 1998. Changes in spontaneous neural activity in the dorsal cochlear nucleus following exposure to intense sound: relation to threshold shift. *Hear.Res.,* **124,** 78-84.

Kaltenbach, J.A., Rachel, J.D., Mathog, T.A., Zhang, J., Falzarano, P.R. and Lewandowski, M., 2002. Cisplatin-Induced Hyperactivity in the Dorsal Cochlear Nucleus and Its Relation to Outer Hair Cell Loss: Relevance to Tinnitus. *J.Neurophysiol.,* **88,** 699-714.

Kaltenbach, J.A., Zacharek, M.A., Zhang, J. and Frederick, S., 2004. Activity in the dorsal cochlear nucleus of hamsters previously tested for tinnitus following intense tone exposure. *Neurosci.Lett.,* **355,** 121-125.

Kalume, F., Yu, F.H., Westenbroek, R.E., Scheuer, T. and Catterall, W.A., 2007. Reduced Sodium Current in Purkinje Neurons from NaV1.1 Mutant Mice: Implications for Ataxia in Severe Myoclonic Epilepsy in Infancy. *J.Neurosci.,* **27,** 11065-11074.

Kedei, N., Szabo, T., Lile, J.D., Treanor, J.J., Olah, Z., Iadarola, M.J. and Blumberg, P.M., 2001. Analysis of the Native Quaternary Structure of Vanilloid Receptor 1. *J.Biol.Chem.,* **276,** 28613-28619.

Keh, S.M.M.R.C.S., Facer, P.M.P., Simpson, K.D., Sandhu, G.F.R.C.S., Saleh, H.A.F.R.C.S. and Anand, P.F.R.C.P., 2008. Increased Nerve Fiber Expression of Sensory Sodium Channels Nav1.7, Nav1.8, and Nav1.9 in Rhinitis. *Laryngoscope,* **118,** 573-579.

Kelly, J.B. and Masterton, B., 1977. Auditory sensitivity of the albino rat. *J.Comp.Physiol.Psychol.,* **91,** 930-936.

Kemp, D.T., 2002. Otoacoustic emissions, their origin in cochlear function, and use. *Br.Med.Bull.,* **63,** 223-241.

Kennedy, H.J., Crawford, A.C. and Fettiplace, R., 2005. Force generation by mammalian hair bundles supports a role in cochlear amplification. *Nature,* **433,** 880-883.

Khan, K.M., Drescher, M.J., Hatfield, J.S., Khan, A.-. and Drescher, D.G., 2002. Muscarinic receptor subtypes are differentially distributed in the rat cochlea. *Neuroscience,* **111,** 291-302.

Kiang, N.Y., Liberman, M.C. and Levine, R.A., 1976. Auditory-nerve activity in cats exposed to ototoxic drugs and high-intensity sounds. *Ann.Otol.Rhinol.Laryngol.,* **85,** 752-768.

Kitahara, T., Li, H.S. and Balaban, C.D., 2005. Changes in transient receptor potential cation channel superfamily V (TRPV) mRNA expression in the mouse inner ear ganglia after kanamycin challenge. *Hear.Res.,* **201,** 132-144.

Knipper, M., Zimmermann, U., Köpschall, I., Rohbock, K., Jüngling, S. and Zenner, H.P., 1995. Immunological identification of candidate proteins involved in regulating active shape changes of outer hair cells. *Hear.Res.,* **86,** 100-110.

Koester, J. and Siegelbaum, S.A., 2000a. Local signaling: Passive electrical properties of the neuron. In Kandel, E. R., Schwartz, J. H. and Jessell, T. M., eds, *Principles of neural science.* Fourth edition ed. USA: McGraw-Hill. 140.

Koester, J. and Siegelbaum, S.A., 2000b. Membrane potential. In Kandel, E. R., Schwartz, J. H. and Jessell, T. M., eds, *Principles of neural science.* Fourth edition ed. USA: McGraw-Hill. 125.

Koester, J. and Siegelbaum, S.A., 2000c. Propagated signaling: The action potential. In Kandel, E. R., Schwartz, J. H. and Jessell, T. M., eds, *Principles of neural science.* Fourth edition ed. USA: McGraw-Hill. 150.

Kohonen, A. and Tarkkanen, J.V., 1966. Dihydrostreptomycin and kanamycin ototoxicity. An experimental study by surface preparation technique. *Laryngoscope,* **76,** 1671-1680.

Kohrs, R. and Durieux, M., 1998. Ketamine: teaching an old drug new tricks. *Anesth.Analg.,* **87,** 1186-1193.

Kojima, K., Matsumoto, M. and Ito, J., 2007. Severe acoustic trauma in adult rats induced by short duration high intensity sound. *Acta Otolaryngol.Supp.,* 26-29.

König, O., Schaette, R., Kempter, R. and Gross, M., 2006. Course of hearing loss and occurrence of tinnitus. *Hear.Res.,* **221,** 59-64.

Kössl, M., Richardson, G.P. and Russell, I.J., 1990. Stereocilia bundle stiffness: Effects of neomycin sulphate, A23187 and Concanavalin A. *Hear.Res.,* **44,** 217-229.

Krafte, D.S. and Bannon, A.W., 2008. Sodium channels and nociception: recent concepts and therapeutic opportunities. *Curr.Opin.Neurobiol.,* **8,** 50-56.

Kretschmer, T., Happel, L.T., England, J.D., Nguyen, D.H., Tiel, R.L., Beuerman, R.W. and Kline, D.G., 2002. Accumulation of PN1 and PN3 sodium channels in painful human neuroma-evidence from immunocytochemistry. *Acta Neurochir.,* **144,** 803-810.

Krzemien, D.M., Schaller, K.L., Levinson, S.R. and Caldwell, J.H., 2000. Immunolocalization of sodium channel isoform NaCh6 in the nervous system. *J.Comp.Neurol.,* **420,** 70-83.

Kuan, C.Y., Tannahill, D., Cook, G.M. and Keynes, R.J., 2004. Somite polarity and segmental patterning of the peripheral nervous system. *Mech.Dev.,* **121,** 1055-1068.

Kubista, M., Andrade, J.M., Bengtsson, M., Forootan, A., Jonak, J., Lind, K., Sindelka, R., Sjoback, R., Sjogreen, B., Strombom, L., Stahlberg, A. and Zoric, N., 2006. The real-time polymerase chain reaction. *Mol.Aspects Med.,* **27,** 95-125.

Kujawa, S.G., Glattke, T.J., Fallon, M. and Bobbin, R.P., 1992. Intracochlear application of acetylcholine alters sound-induced mechanical events within the cochlear partition. *Hear.Res.,* **61,** 106-116.

Kujawa, S.G. and Liberman, M.C., 2009. Adding Insult to Injury: Cochlear Nerve Degeneration after "Temporary" Noise-Induced Hearing Loss. *J.Neurosci.,* **29,** 14077-14085.

Kwan, K.Y., Allchorne, A.J., Vollrath, M.A., Christensen, A.P., Zhang, D.S., Woolf, C.J. and Corey, D.P., 2006. TRPA1 contributes to cold, mechanical, and chemical nociception but is not essential for hair-cell transduction. *Neuron,* **50,** 277-289.

Lang, H., Schulte, B.A. and Schmiedt, R.A., 2005. Ouabain induces apoptotic cell death in type I spiral ganglion neurons, but not type II neurons. *JARO,* **6,** 63-74.

Larsen, M. and Langmoen, I.A., 1998. The effect of volatile anaesthetics on synaptic release and uptake of glutamate. *Toxicol.Lett.,* **100-101,** 59-64.

Larsen, M., Grøndahl, T.Ø., Haugstad, T.S. and Langmoen, I.A., 1994. The effect of the volatile anesthetic isoflurane on Ca2+-dependent glutamate release from rat cerebral cortex. *Brain Res.,* **663,** 335-337.

Leach, R.M., Rees, P.J. and Wilmshurst, P., 1998. Hyperbaric oxygen therapy. *BMJ,* **317,** 1140-1143.

Lee, J.E., Nakagawa, T., Kim, T.S., Iguchi, F., Endo, T., Dong, Y., Yuki, K., Naito, Y., Lee, S.H. and Ito, J., 2003. A novel model for rapid induction of apoptosis in spiral ganglions of mice. *Laryngoscope,* **113,** 994-999.

Lee, J.H. and Marcus, D.C., 2003. Endolymphatic sodium homeostasis by Reissner's membrane. *Neuroscience,* **119,** 3-8.

Legan, P.K., Lukashkina, V.A., Goodyear, R.J., Lukashkin, A.N., Verhoeven, K., Van Camp, G., Russell, I.J. and Richardson, G.P., 2005. A deafness mutation isolates a second role for the tectorial membrane in hearing. *Nat.Neurosci.,* **8,** 1035-1042.

Leonova, E.V. and Raphael, Y., 1997. Organization of cell junctions and cytoskeleton in the reticular lamina in normal and ototoxically damaged organ of Corti. *Hear.Res.,* **113,** 14-28.

Levin, S.I., Khaliq, Z.M., Aman, T.K., Grieco, T.M., Kearney, J.A., Raman, I.M. and Meisler, M.H., 2006. Impaired Motor Function in Mice With Cell-Specific Knockout of Sodium Channel Scn8a (NaV1.6) in Cerebellar Purkinje Neurons and Granule Cells. *J.Neurophysiol.,* **96,** 785-793.

Levine, R.A., 1999. Somatic (Craniocervical) Tinnitus and the Dorsal Cochlear Nucleus Hypothesis. *Am.J.Otolaryngol.,* **20,** 351-362.

Li, H.Y., Say, E.H. and Zhou, X.F., 2007. Isolation and characterization of neural crest progenitors from adult dorsal root ganglia. *Stem Cells,* **25,** 2053-2065.

Liberman, M.C., 1982. Single-neuron labeling in the cat auditory nerve. *Science,* **216,** 1239-1241.

Liberman, M.C. and Beil, D.G., 1979. Hair cell condition and auditory nerve response in normal and noise-damaged cochleas. *Acta Otolaryngol.,* **88,** 161-176.

Liberman, M.C. and Dodds, L.W., 1984. Single-neuron labeling and chronic cochlear pathology. II. Stereocilia damage and alterations of spontaneous discharge rates. *Hear.Res.,* **16,** 43-53.

Liberman, M.C., Gao, J., He, D.Z., Wu, X., Jia, S. and Zuo, J., 2002. Prestin is required for electromotility of the outer hair cell and for the cochlear amplifier. *Nature,* **419,** 300-304.

Liberman, M.C., Dodds, L.W. and Pierce, S., 1990. Afferent and efferent innervation of the cat cochlea: Quantitative analysis with light and electron microscopy. *J.Comp.Neurol.,* **301,** 443-460.

Lin, X., Webster, P., Li, Q., Chen, S. and Ouyang, Y., 2003. Optical recordings of Ca2+ signaling activities from identified inner ear cells in cochlear slices and hemicochleae. *Brain Res.Brain Res.Protocol.,* **11,** 92-100.

Lipton, S.A. and Rosenberg, P.A., 1994. Excitatory amino acids as a final common pathway for neurologic disorders.[see comment]. *N.Engl.J.Med.,* **330,** 613-622.

Loughnan, B.L., Sebel, P.S., Thomas, D., Rutherfoord, C.F. and Rogers, H., 1987. Evoked potentials following diazepam or fentanyl. *Anaesthesia,* **42,** 195-198.

Lumpkin, E.A., Marquis, R.E. and Hudspeth, A.J., 1997. The selectivity of the hair cell's mechanoelectrical-transduction channel promotes Ca2+ flux at low Ca2+ concentrations. *Proc.Natl.Acad.Sci.U.S.A.,* **94,** 10997-11002.

Luo, S., Perry, G.M., Levinson, S.R. and Henry, M.A., 2008. Nav1.7 expression is increased in painful human dental pulp. *Mol.Pain,* **4,** 16.

Ma, C., Billings, P., Harris, J.P. and Keithley, E.M., 2000. Characterization of an experimentally induced inner ear immune response. *Laryngoscope,* **110,** 451-456.

Maison, S.F., Parker, L.L., Young, L., Adelman, J.P., Zuo, J. and Liberman, M.C., 2007. Overexpression of SK2 channels enhances efferent suppression of cochlear responses without enhancing noise resistance. *J.Neurophysiol.,* **97,** 2930-2936.

Marcus, N.J., 2005. Pain in cancer patients unrelated to the cancer or treatment. *Cancer Invest.,* **23,** 84-93.

Marten, N., Burke, E., Hayden, J. and Straus, D., 1994. Effect of amino acid limitation on the expression of 19 genes in rat hepatoma cells. *FASEB J.,* **8,** 538-544.

Martinez-Monedero, R., Corrales, C.E., Cuajungco, M.P., Heller, S. and Edge, A.S., 2006. Reinnervation of hair cells by auditory neurons after selective removal of spiral ganglion neurons. *J.Neurobiol.,* **66,** 319-331.

McFadden, S.L., Ding, D., Jiang, H. and Salvi, R.J., 2004. Time course of efferent fiber and spiral ganglion cell degeneration following complete hair cell loss in the chinchilla. *Brain Res.,* **997,** 40-51.

Melcher, J.R., Guinan Jr., J.J., Knudson, I.M. and Kiang, N.Y.S., 1996. Generators of the brainstem auditory evoked potential in cat. II. Correlating lesion sites with waveform changes. *Hear.Res.,* **93,** 28-51.

Millan, M.J., 1999. The induction of pain: an integrative review. *Prog.Neurobiol.,* **57,** 1-164.

Miller, J.D., 1974. Effects of noise on people. *J.Acoust.Soc.Am.,* **56,** 729-764.

Mintz, I.M., Venema, V.J., Swiderek, K.M., Lee, T.D., Bean, B.P. and Adams, M.E., 1992. P-type calcium channels blocked by the spider toxin omega-Aga-IVA. *Nature,* **355,** 827-829.

Miyao, M., Firestein, G.S. and Keithley, E.M., 2008. Acoustic trauma augments the cochlear immune response to antigen. *Laryngoscope,* **118,** 1801-1808.

Mo, Z.L. and Davis, R.L., 1997. Endogenous firing patterns of murine spiral ganglion neurons. *J.Neurophysiol.,* **77,** 1294-1305.

Møller, A.R., 1997. Similarities between Chronic Pain and Tinnitus. *Am.J.Otol.,* **18,** 577-585.

Momin, A. and Wood, J.N., 2008. Sensory neuron voltage-gated sodium channels as analgesic drug targets. *Curr.Opin.Neurobiol.,* **18,** 383-388.

Moore, E.J., Hall, D.B. and Narahashi, T., 1996. Sodium and Potassium Currents of Type I Spiral Ganglion Cells from Rat. *Acta Otolaryngol.,* **116,** 552.

Morlet, D., Bertrand, O., Salord, F., Boulieu, R., Pernier, J. and Fischer, C., 1997. Dynamics of MLAEP changes in midazolam-induced sedation. *Electroencephalogr.Clin.Neurophysiol.,* **104,** 437-446.

Mou, K., Adamson, C.L. and Davis, R.L., 1998. Time-dependence and cell-type specificity of synergistic neurotrophin actions on spiral ganglion neurons. *J.Comp.Neurol.,* **402,** 129-139.

Mrena, R., Savolainen, S., Pirvola, U. and Ylikoski, J., 2004. Characteristics of acute acoustical trauma in the Finnish Defence Forces -- Las características del trauma acústico agudo en las Fuerzas de Defensa de Finlandia. *Int.J.Audiol.,* **43,** 177.

Newcomb, R., Szoke, B., Palma, A., Wang, G., Chen, X., Hopkins, W., Cong, R., Miller, J., Urge, L., Tarczy-Hornoch, K., Loo, J.A., Dooley, D.J., Nadasdi, L., Tsien, R.W., Lemos, J. and Miljanich, G., 1998. Selective peptide antagonist of the class E calcium channel from the venom of the tarantula Hysterocrates gigas. *Biochemistry (N.Y.),* **37,** 15353-15362.

Niedzielski, A. and Wenthold, R., 1995. Expression of AMPA, kainate, and NMDA receptor subunits in cochlear and vestibular ganglia. *J.Neurosci.,* **15,** 2338-2353.

Niskar, A.S., Kieszak, S.M., Holmes, A., Esteban, E., Rubin, C. and Brody, D.J., 1998. Prevalence of Hearing Loss Among Children 6 to 19 Years of Age: The Third National Health and Nutrition Examination Survey. *JAMA,* **279,** 1071-1075.

Nordang, L., Cestreicher, E., Arnold, W. and Anniko, M., 2000. Glutamate is the afferent neurotransmitter in the human cochlea. *Acta Otolaryngol.,* **120,** 359-362.

Nottet, J.B., Moulin, A., Brossard, N., Suc, B. and Job, A., 2006. Otoacoustic emissions and persistent tinnitus after acute acoustic trauma. *Laryngoscope,* **116,** 970-975.

Nouvian, R., Ruel, J., Wang, J., Guitton, M.J., Pujol, R. and Puel, J., 2003. Degeneration of sensory outer hair cells following pharmacological blockade of cochlear KCNQ channels in the adult guinea pig. *Eur.J.Neurosci.,* **17,** 2553-2562.

Novakovic, S.D., Tzoumaka, E., McGivern, J.G., Haraguchi, M., Sangameswaran, L., Gogas, K.R., Eglen, R.M. and Hunter, J.C., 1998. Distribution of the tetrodotoxin-resistant sodium channel PN3 in rat sensory neurons in normal and neuropathic conditions. *J.Neurosci.,* **18,** 2174-2187.

Ohlemiller, K.K. and Gagnon, P.M., 2004. Apical-to-basal gradients in age-related cochlear degeneration and their relationship to "primary" loss of cochlear neurons. *J.Comp.Neurol.,* **479,** 103-116.

Ohmori, H., 1985. Mechano-electrical transduction currents in isolated vestibular hair cells of the chick. *J.Physiol.,* **359,** 189-217.

Olivera, B.M., Rivier, J., Scott, J.K., Hillyard, D.R. and Cruz, L.J., 1991. Conotoxins. *J.Biol.Chem.,* **266,** 22067-22070.

Ou, H.C., Bohne, B.A. and Harding, G.W., 2000. Noise damage in the C57BL/CBA mouse cochlea. *Hear.Res.,* **145,** 111-122.

Ozawa, S., Kamiya, H. and Tsuzuki, K., 1998. Glutamate receptors in the mammalian central nervous system. *Prog.Neurobiol.,* **54,** 581-618.

Pagedar, N.A., Wang, W., Chen, D.H.-., Davis, R.R., Lopez, I., Wright, C.G. and Alagramam, K.N., 2006. Gene expression analysis of distinct populations of cells isolated from mouse and human inner ear FFPE tissue using laser capture microdissection – a Technical report based on preliminary findings. *Brain Res.,* **1091,** 289-299.

Palmer, A.M. and Carter, N., 2002. The role of sodium channels in disease. *The newsletter for the society for medicines research,* **8,** 1-14.

Panford-Walsh, R., Singer, W., Ruttiger, L., Hadjab, S., Tan, J., Geisler, H.S., Zimmermann, U., Kopschall, I., Rohbock, K., Vieljans, A., Oestreicher, E. and Knipper, M., 2008. Midazolam reverses salicylate-induced changes in brain-derived neurotrophic factor and arg3.1 expression: implications for tinnitus perception and auditory plasticity. *Mol.Pharmacol.,* **74,** 595-604.

Panici, P.B., Greggi, S., Scambia, G., Baiocchi, G., Lomonaco, M., Conti, G. and Mancuso, S., 1993. Efficacy and toxicity of very high-dose cisplatin in advanced ovarian carcinoma: 4-year survival analysis and neurological follow-up. *Int.J.Gynecol.Cancer,* **3,** 44-53.

Patuzzi, R. and Robertson, D., 1988. Tuning in the mammalian cochlea. *Physiol.Rev.,* **68,** 1009-1082.

Perez, R., Freeman, S. and Sohmer, H., 2004. Effect of an initial noise induced hearing loss on subsequent noise induced hearing loss. *Hear.Res.,* **192,** 101-106.

Pieri, L., Schaffner, R., Scherschlicht, R., Polc, P., Sepinwall, J., Davidson, A., Mohler, H., Cumin, R., Da Prada, M., Burkard, W.P., Keller, H.H., Muller, R.K., Gerold, M., Pieri, M., Cook, L. and Haefely, W., 1981. Pharmacology of midazolam. *Arzneimittelforschung,* **31,** 2180-2201.

Pirvola, U., Xing-Qun, L., Virkkala, J., Saarma, M., Murakata, C., Camoratto, A.M., Walton, K.M. and Ylikoski, J., 2000. Rescue of Hearing, Auditory Hair Cells, and Neurons by CEP-1347/KT7515, an Inhibitor of c-Jun N-Terminal Kinase Activation. *J.Neurosci.,* **20,** 43-50.

Platzer, J., Engel, J., Schrott-Fischer, A., Stephan, K., Bova, S., Chen, H., Zheng, H. and Striessnig, J., 2000. Congenital deafness and sinoatrial node dysfunction in mice lacking class D L-type Ca2+ channels. *Cell,* **102,** 89-97.

Popelar, J., Grecova, J., Rybalko, N. and Syka, J., 2008. Comparison of noise-induced changes of auditory brainstem and middle latency response amplitudes in rats. *Hear.Res.,* **245,** 82-91.

Pourbakht, A. and Yamasoba, T., 2003. Cochlear damage caused by continuous and intermittent noise exposure. *Hear.Res.,* **178,** 70-78.

Pridmore, S., Kleinjung, T., Langguth, B. and Eichhammer, P., 2006. Transcranial magnetic stimulation: potential treatment for tinnitus? *Psych.Clin.Neurosci.,* **60,** 133-138.

Puel, J.L., 1995. Chemical synaptic transmission in the cochlea. *Prog.Neurobiol.,* **47,** 449-476.

Puel, J.L., Bobbin, R.P. and Fallon, M., 1988. The active process is affected first by intense sound exposure. *Hear.Res.,* **37,** 53-63.

Puel, J.L., d'Aldin, C., Ruel, J., Ladrech, S. and Pujol, R., 1997. Synaptic repair mechanisms responsible for functional recovery in various cochlear pathologies. *Acta Otolaryngol.,* **117,** 214-218.

Puel, J.L., Ruel, J., d'Aldin, C.G. and Pujol, R., 1998. Excitotoxicity and repair of cochlear synapses after noise-trauma induced hearing loss. *Neuroreport,* **9,** 2109-2114.

Pujol, R., Rebillard, G., Puel, J.L., Lenoir, M., Eybalin, M. and Recasens, M., 1990. Glutamate neurotoxicity in the cochlea: a possible consequence of ischaemic or anoxic conditions occurring in ageing. *Acta Otolaryngol.Supp.,* **476,** 32-36.

Pulec, J.L., 1995. Cochlear nerve section for intractable tinnitus. *Ear Nose Throat J.,* **74,** 468.

Raff, T., van der Giet, M., Endemann, D., Wiederholt, T. and Paul, M., 1997. Design and testing of beta-actin primers for RT-PCR that do not co-amplify processed pseudogenes. *Biotechniques,* **23,** 456-460.

Raman, I.M. and Bean, B.P., 1997. Resurgent Sodium Current and Action Potential Formation in Dissociated Cerebellar Purkinje Neurons. *J.Neurosci.,* **17,** 4517-4526.

Rasband, M.N., Park, E.W., Vanderah, T.W., Lai, J., Porreca, F. and Trimmer, J.S., 2001. Distinct potassium channels on pain-sensing neurons. *Proc.Natl.Acad.Sci.U.S.A.,* **98,** 13373-13378.

Rask-Andersen, H., Friberg, U., Johansson, M. and Stjernschantz, J., 2005. Effects of intratympanic injection of latanoprost in Meniere's disease: a randomized, placebo-controlled, double-blind, pilot study. *Otolaryngol.Head Neck Surg.,* **133,** 441-443.

Reed, W.D., Hopkins, B.E., Joske, R.A. and Laurence, B.H., 1971. A comparative study of conventional premedication (pethidine, promethazine, and atropine) and neuroleptanalgesia (droperidol and phenoperidine) for peroral endoscopy. *Gut,* **12,** 736-738.

Reid, M.A., Flores-Otero, J. and Davis, R.L., 2004. Firing patterns of type II spiral ganglion neurons in vitro. *J.Neurosci.,* **24,** 733-742.

Richter, G.T., Mennemeier, M., Bartel, T., Chelette, K.C., Kimbrell, T., Triggs, W. and Dornhoffer, J.L., 2006. Repetitive transcranial magnetic stimulation for tinnitus: a case study. *Laryngoscope,* **116,** 1867-1872.

Rieger, F., Daniloff, J., Pincon-Raymond, M., Crossin, K., Grumet, M. and Edelman, G., 1986. Neuronal cell adhesion molecules and cytotactin are colocalized at the node of Ranvier. *J.Cell Biol.,* **103,** 379-391.

Ripoll, C. and Rebillard, G., 1997. A simple technique to efficiently dissociate primary auditory neurons from 5 day-old rat cochleas. *J.Neurosci.Methods,* **73,** 123-128.

Robertson, D., Sellick, P.M. and Patuzzi, R., 1999. The continuing search for outer hair cell afferents in the guinea pig spiral ganglion. *Hear.Res.,* **136,** 151-158.

Robertson, D., 1984. Horseradish peroxidase injection of physiologically characterized afferent and efferent neurones in the guinea pig spiral ganglion. *Hear.Res.,* **15,** 113-121.

Rogart, R.B., Cribbs, L.L., Muglia, L.K., Kephart, D.D. and Kaiser, M.W., 1989. Molecular cloning of a putative tetrodotoxin-resistant rat heart Na+ channel isoform. *Proc.Natl.Acad.Sci.U.S.A.,* **86,** 8170-8174.

Rogers, M., Tang, L., Madge, D.J. and Stevens, E.B., 2006. The role of sodium channels in neuropathic pain. *Semin.Cell Dev.Biol.,* **17,** 571-581.

Rosenblith, W.A., Rudmose, W., Davis, H., Glorig, A., Hardy, H.C., Hoople, G.D., House, H., Parrack, H.O., Schowalter, E.J. and Walmer, C.R., 1954. The Relations of Hearing Loss to Noise Exposure. *AMA Arch.Otolaryngol.,* **60,** 261-a-262.

Rosker, C., Lohberger, B., Hofer, D., Steinecker, B., Quasthoff, S. and Schreibmayer, W., 2007. The TTX metabolite 4,9-anhydro-TTX is a highly specific blocker of the Nav1.6 voltage-dependent sodium channel. *Am J Physiol Cell Physiol,* **293,** C783-789.

Rothman, S.M. and Olney, J.W., 1986. Glutamate and the pathophysiology of hypoxic-ischemic brain damage. *Ann.Neurol.,* **19,** 105-111.

Ruan, Q., Chen, D., Wang, Z., Chi, F., Yin, S. and Wang, J., 2008. Topological and developmental expression gradients of Kir2.1, an inward rectifier K+ channel, in spiral ganglion and cochlear hair cells of mouse inner ear. *Dev.Neurosci.,* **30,** 374-388.

Ruel, J., Chabbert, C., Nouvian, R., Bendris, R., Eybalin, M., Leger, C.L., Bourien, J., Mersel, M. and Puel, J., 2008. Salicylate Enables Cochlear Arachidonic-Acid-Sensitive NMDA Receptor Responses. *J.Neurosci.,* **28,** 7313-7323.

Ruel, J., Nouvian, R., d'Aldin, C.G., Pujol, R., Eybalin, M. and Puel, J., 2001. Dopamine inhibition of auditory nerve activity in the adult mammalian cochlea. *Eur.J.Neurosci.,* **14,** 977-986.

Rush, A.M., Bräu, M.E., Elliott, A.A. and Elliott, J.R., 1998. Electrophysiological properties of sodium current subtypes in small cells from adult rat dorsal root ganglia. *J.Physiol.,* **511,** 771-789.

Rush, A.M., Dib-Hajj, S.D., Liu, S., Cummins, T.R., Black, J.A. and Waxman, S.G., 2006. A single sodium channel mutation produces hyper- or hypoexcitability in different types of neurons. *Proc.Natl.Acad.Sci.U.S.A.,* **103,** 8245-8250.

Rush, A.M., Dib-Hajj, S.D. and Waxman, S.G., 2005. Electrophysiological properties of two axonal sodium channels, Nav1.2 and Nav1.6, expressed in mouse spinal sensory neurones. *J.Physiol.,* **564,** 803-815.

Rüttiger, L., Ciuffani, J., Zenner, H. and Knipper, M., 2003. A behavioral paradigm to judge acute sodium salicylate-induced sound experience in rats: a new approach for an animal model on tinnitus. *Hear.Res.,* **180,** 39-50.

Rybak, L.P. and Whitworth, C.A., 2005. Ototoxicity: therapeutic opportunities. *Drug Discov.Today,* **10,** 1313-1321.

Rybalko, N. and Syka, J., 2005. Effect of noise exposure on gap detection in rats. *Hear.Res.,* **200,** 63-72.

Sala, T., 1997. Transtympanic gentamicin in the treatment of Meniere's disease. *Auris Nasus Larynx,* **24,** 239-246.

Salih, S.G., Housley, G.D., Raybould, N.P. and Thorne, P.R., 1999. ATP-gated ion channel expression in primary auditory neurones. *Neuroreport,* **10,** 2579-2586.

Salvi, R.J., Hamernik, R.P. and Henderson, D., 1979a. Auditory nerve activity and cochlear morphology after noise exposure. *Arch.Otorhinolaryngol.,* **224,** 111-116.

Salvi, R.J., Henderson, D. and Hamernik, R.P., 1979b. Single auditory nerve fiber and action potential latencies in normal and noise-treated chinchillas. *Hear.Res.,* **1,** 237-251.

Salvi, R.J., Wang, J. and Ding, D., 2000. Auditory plasticity and hyperactivity following cochlear damage. *Hear.Res.,* **147,** 261-274.

Samorajski, T., Ordy, J.M. and Rady-Reimer, P., 1968. Lipofuscin pigment accumulation in the nervous system of aging mice. *Anat.Rec.,* **160,** 555-573.

Sangameswaran, L., Fish, L.M., Koch, B.D., Rabert, D.K., Delgado, S.G., Ilnicka, M., Jakeman, L.B., Novakovic, S., Wong, K., Sze, P., Tzoumaka, E., Stewart, G.R., Herman, R.C., Chan, H., Eglen, R.M. and Hunter, J.C., 1997. A novel tetrodotoxin-sensitive, voltage-gated sodium channel expressed in rat and human dorsal root ganglia. *J.Biol.Chem.,* **272,** 14805-14809.

Sans, A., Bartolami, S. and Fraysse, B., 1996. Histopathology of the peripheral vestibular system in small vestibular schwannomas. *Am.J.Otol.,* **17,** 326-324.

Santarelli, R., Arslan, E., Carraro, L., Conti, G., Capello, M. and Plourde, G., 2003. Effects of Isoflurane on the Auditory Brainstem Responses and Middle Latency Responses of Rats. *Acta Otolaryngol.,* **123,** 176.

Santos-Sacchi, J., 1993. Voltage-dependent ionic conductances of type I spiral ganglion cells from the guinea pig inner ear. *J.Neurosci.,* **13,** 3599-3611.

Sargent, P.B., 1993. The Diversity of Neuronal Nicotinic Acetylcholine Receptors. *Annu.Rev.Neurosci.,* **16,** 403-443.

Sattler, R. and Tymianski, M., 2000. Molecular mechanisms of calcium-dependent excitotoxicity. *J.Mol.Med.,* **78,** 3-13.

Schmalhofer, W.A., Calhoun, J., Burrows, R., Bailey, T., Kohler, M.G., Weinglass, A.B., Kaczorowski, G.J., Garcia, M.L., Koltzenburg, M. and Priest, B.T., 2008. ProTx-II, a Selective Inhibitor of NaV1.7 Sodium Channels, Blocks Action Potential Propagation in Nociceptors. *Mol.Pharmacol.,* **74,** 1476-1484.

Schmuziger, N., Patscheke, J. and Probst, R., 2006. Hearing in nonprofessional pop/rock musicians. *Ear Hear.,* **27,** 321-330.

Shapiro, S.M., Møller, A.R. and Shiu, G.K., 1984. Brain-stem auditory evoked potentials in rats with high-dose pentobarbital. *Electroencephalogr.Clin.Neurophysiol.,* **58,** 266-276.

Shibata, S.B., Osumi, Y., Yagi, M., Kanda, S., Kawamoto, K., Kuriyama, H., Nishiyama, T. and Yamashita, T., 2007. Administration of amitriptyline attenuates noise-induced hearing loss via glial cell line-derived neurotrophic factor (GDNF) induction. *Brain Res.,* **1144,** 74-81.

Siegel, J.H. and Kim, D.O., 1982. Efferent neural control of cochlear mechanics? Olivocochlear bundle stimulation affects cochlear biomechanical nonlinearity. *Hear.Res.,* **6,** 171-182.

Simpson, J.J. and Davies, W.E., 1999. Recent advances in the pharmacological treatment of tinnitus. *Trends Pharmacol.Sci.,* **20,** 12-18.

Skinner, L.J., Enee, V., Beurg, M., Jung, H.H., Ryan, A.F., Hafidi, A., Aran, J. and Dulon, D., 2003. Contribution of BK Ca2+-activated K+ channels to auditory neurotransmission in the guinea pig cochlea. *J.Neurophysiol.,* **90,** 320-332.

Soliman, A.M., 1988. A comparative immunofluorescent study of fixed decalcified tissue and frozen non-decalcified tissue from the guinea pig cochlea. *Arch.Otorhinolaryngol.,* **244,** 337-341.

Spoendlin, H., 1975. Retrograde degeneration of the cochlear nerve. *Acta Otolaryngol.,* **79,** 266-275.

Spoendlin, H., 1971. Primary Structural Changes in the Organ of Corti After Acoustic Overstimulation. *Acta Otolaryngol.,* **71,** 166.

Spoendlin, H. and Brun, J.P., 1973. Relation of structural damage to exposure time and intensity in acoustic trauma. *Acta Otolaryngol.,* **75,** 220-226.

Starr, A., 1976. Correlation between confirmed sites of neurological lesions and abnormalities of far-field auditory brainstem responses. *Electroencephalogr.Clin.Neurophysiol.,* **41,** 595-608.

Starr, A., Sininger, Y., Nguyen, T., Michalewski, H.J., Oba, S. and Abdala, C., 2001. Cochlear Receptor (Microphonic and Summating Potentials, Otoacoustic Emissions) and Auditory Pathway (Auditory Brain Stem Potentials) Activity in Auditory Neuropathy. *Ear Hear.,* **22,** 91-99.

Steffensen, I., Waxman, S.G., Mills, L. and Stys, P.K., 1997. Immunolocalization of the Na+–Ca2+ exchanger in mammalian myelinated axons. *Brain Res.,* **776,** 1-9.

Steinbach, S. and Lutz, J., 2007. Glutamate induces apoptosis in cultured spiral ganglion explants. *Biochem.Biophys.Res.Commun.,* **357,** 14-19.

Stonehouse, A.H., Grubb, B.D., Pringle, J.H., Norman, R.I., Stanfield, P.R. and Brammar, W.J., 2003. Nuclear immunostaining in rat neuronal cells using two anti-Kir2.2 ion channel polyclonal antibodies. *J.Mol.Neurosci.,* **20,** 189-194.

Strickland, I.T., Martindale, J.C., Woodhams, P.L., Reeve, A.J., Chessell, I.P. and McQueen, D.S., 2008. Changes in the expression of NaV1.7, NaV1.8 and NaV1.9 in a distinct population of dorsal root ganglia innervating the rat knee joint in a model of chronic inflammatory joint pain. *Eur.J.Pain,* **12,** 564-572.

Sullivan, M.J. and Conolly, R.B., 1988. Dose-response hearing loss for white noise in the Sprague-Dawley rat. *Fundam.Appl.Toxicol.,* **10,** 109-113.

Szabo, Z., Harasztosi, C., Szucs, G., Sziklai, I. and Rusznak, Z., 2003. A detailed procedure and dissection guide for the isolation of spiral ganglion cells of the guinea pig for electrophysiological experiments. *Brain Res.Brain Res.Protocol.,* **10,** 139-147.

Szabo, Z.S., Harasztosi, C.S., Sziklai, I., Szucs, G. and Rusznak, Z., 2002. Ionic currents determining the membrane characteristics of type I spiral ganglion neurons of the guinea pig. *Eur.J.Neurosci.,* **16,** 1887-1895.

Tabuchi, K., Suzuki, M., Mizuno, A. and Hara, A., 2005. Hearing impairment in TRPV4 knockout mice. *Neurosci.Lett.,* **382,** 304-308.

Takumida, M., Kubo, N., Ohtani, M., Suzuka, Y. and Anniko, M., 2005. Transient receptor potential channels in the inner ear: presence of transient receptor potential channel subfamily 1 and 4 in the guinea pig inner ear. *Acta Otolaryngol.,* **125,** 929.

Tan, J., Ruttiger, L., Panford-Walsh, R., Singer, W., Schulze, H., Kilian, S.B., Hadjab, S., Zimmermann, U., Kopschall, I., Rohbock, K. and Knipper, M., 2007. Tinnitus behavior and hearing function correlate with the reciprocal expression patterns of BDNF and Arg3.1/arc in auditory neurons following acoustic trauma. *Neuroscience,* **145,** 715-726.

Tang, W.W., Qi, M., Van, G.Y., Wariner, G.P. and Samal, B., 1996. Leukemia inhibitory factor ameliorates experimental anti-GBM Ab glomerulonephritis. *Kidney Int.,* **50,** 1922-1927.

Taranda, J., Ballestero, J.A., Hiel, H., de Souza, F.S., Wedemeyer, C., Gomez-Casati, M.E., Lipovsek, M., Vetter, D.E., Fuchs, P.A., Katz, E. and Elgoyhen, A.B., 2009. Constitutive expression of the alpha10 nicotinic acetylcholine receptor subunit fails to maintain cholinergic responses in inner hair cells after the onset of hearing. *JARO,* **10,** 397-406.

Tate, S., Benn, S., Hick, C., Trezise, D., John, V., Mannion, R.J., Costigan, M., Plumpton, C., Grose, D., Gladwell, Z., Kendall, G., Dale, K., Bountra, C. and Woolf, C.J., 1998. Two sodium channels contribute to the TTX-R sodium current in primary sensory neurons. *Nat.Neurosci.,* **1,** 653-655.

Taylor, C.P. and Meldrum, B.S., 1995. Na+ channels as targets for neuroprotective drugs. *Trends Pharmacol.Sci.,* **16,** 309-316.

Teudt, I.U. and Richter, C.P., 2007. The hemicochlea preparation of the guinea pig and other mammalian cochleae. *J.Neurosci.Methods,* **162,** 187-197.

Thakor, D.K., Lin, A., Matsuka, Y., Meyer, E.M., Ruangsri, S., Nishimura, I. and Spigelman, I., 2009. Increased peripheral nerve excitability and local NaV1.8 mRNA up-regulation in painful neuropathy. *Mol.Pain,* **5,** 14.

Thalmann, R., Marcus, D.C. and Thalmann, I., 1981. Physiological chemistry of cochlear duct. *Acta Otolaryngol.,* **91,** 535-540.

Toledo-Aral, J.J., Moss, B.L., He, Z.J., Koszowski, A.G., Whisenand, T., Levinson, S.R., Wolf, J.J., Silos-Santiago, I., Halegoua, S. and Mandel, G., 1997. Identification of PN1, a predominant voltage-dependent sodium channel expressed principally in peripheral neurons. *Proc.Natl.Acad.Sci.U.S.A.,* **94,** 1527-1532.

Tombola, F., Pathak, M.M. and Isacoff, E.Y., 2006. How does voltage open an ion channel? *Ann.Rev.Cell Dev.Biol.,* **22,** 23-52.

Torkos, A., Wissel, K., Warnecke, A., Lenarz, T. and Stöver, T., 2008. Technical report: Laser microdissection and pressure catapulting is superior to conventional manual

dissection for isolating pure spiral ganglion fractions from the cochlea. *Hear.Res.,* **235,** 8-14.

Tornabene, S.V., Sato, K., Pham, L., Billings, P. and Keithley, E.M., 2006. Immune cell recruitment following acoustic trauma. *Hear.Res.,* **222,** 115-124.

Trimmer, J.S., Cooperman, S.S., Agnew, W.S. and Mandel, G., 1990. Regulation of muscle sodium channel transcripts during development and in response to denervation. *Dev.Biol.,* **142,** 360-367.

Trimmer, J.S., Cooperman, S.S., Tomiko, S.A., Zhou, J., Crean, S.M., Boyle, M.B., Kalen, R.G., Sheng, Z., Barchi, R.L., Sigworth, F.J., Goodman, R.H., Agnew, W.S. and Mandel, G., 1989. Primary structure and functional expression of a mammalian skeletal muscle sodium channel. *Neuron,* **3,** 33-49.

Turner, J.G., Brozoski, T.J., Bauer, C.A., Parrish, J.L., Myers, K., Hughes, L.F. and Caspary, D.M., 2006. Gap detection deficits in rats with tinnitus: a potential novel screening tool. *Behav.Neurosci.,* **120,** 188-195.

Tzoumaka, E., Tischler, A.C., Sangameswaran, L., Eglen, R.M., Hunter, J.C. and Novakovic, S.D., 2000. Differential distribution of the tetrodotoxin-sensitive rPN4/NaCh6/Scn8a sodium channel in the nervous system. *J.Neurosci.Res.,* **60,** 37-44.

van Looij, M.A.J., Liem, S., van der Burg, H., van der Wees, J., De Zeeuw, C.I. and van Zanten, B.G.A., 2004. Impact of conventional anesthesia on auditory brainstem responses in mice. *Hear.Res.,* **193,** 75-82.

Verma, A.S. and Shapiro, B.H., 2006. Sex-dependent expression of seven housekeeping genes in rat liver. *J.Gastroenterol.Hepatol.,* **21,** 1004-1008.

Wang, L.E., Cao, K.L., Yin, S.K., Wang, Z. and Chen, Z.N., 2006. Cochlear function after selective spiral ganglion cells degeneration induced by ouabain. *Chin.Med.J.,* **119,** 974-979.

Waxman, S.G., Kocsis, J.D. and Black, J.A., 1994. Type III Sodium Channel mRNA is expressed in Embryonic but not Adult Spinal Sensory Neurons, and is Reexpressed following Axotomy. *J.Neurophysiol.,* **72,** 466-470.

Wei, A.D., Gutman, G.A., Aldrich, R., Chandy, K.G., Grissmer, S. and Wulff, H., 2005. International Union of Pharmacology. LII. Nomenclature and molecular relationships of calcium-activated potassium channels. *Pharmacol.Rev.,* **57,** 463-472.

Westenbroek, R.E., Merrick, D.K. and Catterall, W.A., 1989. Differential subcellular localization of the RI and RII Na+ channel subtypes in central neurons. *Neuron,* **3,** 695-704.

Whitaker, W.R., Clare, J.J., Powell, A.J., Chen, Y.H., Faull, R.L. and Emson, P.C., 2000. Distribution of voltage-gated sodium channel alpha-subunit and beta-subunit mRNAs

in human hippocampal formation, cortex, and cerebellum. *J.Comp.Neurol.,* **422,** 123-139.

Whitaker, W.R.J., Faull, R.L.M., Waldvogel, H.J., Plumpton, C.J., Emson, P.C. and Clare, J.J., 2001. Comparative distribution of voltage-gated sodium channel proteins in human brain. *Mol.Brain Res.,* **88,** 37-53.

Whitlon, D.S., Ketels, K.V., Coulson, M.T., Williams, T., Grover, M., Edpao, W. and Richter, C.P., 2006. Survival and morphology of auditory neurons in dissociated cultures of newborn mouse spiral ganglion. *Neuroscience,* **138,** 653-662.

Wilson-Gerwing, T.D., Stucky, C.L., McComb, G.W. and Verge, V.M., 2008. Neurotrophin-3 significantly reduces sodium channel expression linked to neuropathic pain states. *Exp.Neurol.,* **213,** 303-314.

Wooltorton, J.R., Gaboyard, S., Hurley, K.M., Price, S.D., Garcia, J.L., Zhong, M., Lysakowski, A. and Eatock, R.A., 2007. Developmental changes in two voltage-dependent sodium currents in utricular hair cells. *J.Neurophysiol.,* **97,** 1684-1704.

Xie, D., Hu, P., Xiao, Z., Wu, W., Chen, Y. and Xia, K., 2007. Subunits of voltage-gated calcium channels in murine spiral ganglion cells. *Acta Otolaryngol.,* **127,** 8.

Yamada, H., Chen, D., Monstein, H. and Håkanson, R., 1997. Effects of Fasting on the Expression of Gastrin, Cholecystokinin, and Somatostatin Genes and of Various Housekeeping Genes in the Pancreas and Upper Digestive Tract of Rats. *Biochem.Biophys.Res.Commun.,* **231,** 835-838.

Yamasoba, T., Kondo, K., Miyajima, C. and Suzuki, M., 2003. Changes in cell proliferation in rat and guinea pig cochlea after aminoglycoside-induced damage. *Neurosci.Lett.,* **347,** 171-174.

Yang, Y., Wang, Y., Li, S., Xu, Z., Li, H., Ma, L., Fan, J., Bu, D., Liu, B., Fan, Z., Wu, G., Jin, J., Ding, B., Zhu, X. and Shen, Y., 2004. Mutations in SCN9A, encoding a sodium channel alpha subunit, in patients with primary erythermalgia. *J.Med.Genet.,* **41,** 171-174.

Yiangou, Y., Birch, R., Sangameswaran, L., Eglen, R. and Anand, P., 2000. SNS/PN3 and SNS2/NaN sodium channel-like immunoreactivity in human adult and neonate injured sensory nerves. *FEBS Lett.,* **467,** 249-252.

Ylikoski, J., Mrena, R., Makitie, A., Kuokkanen, J., Pirvola, U. and Savolainen, S., 2008. Hyperbaric oxygen therapy seems to enhance recovery from acute acoustic trauma. *Acta Otolaryngol.,* **128,** 1110-1115.

Ylikoski, J., Pirvola, U., Moshnyakov, M., Palgi, J., Arumäe, U. and Saarma, M., 1993. Expression patterns of neurotrophin and their receptor mRNAs in the rat inner ear. *Hear.Res.,* **65,** 69-78.

Yost, W.A., 2000. *Fundamentals of hearing : an introduction.* 4th edition ed. San Diego: Academic Press.

Yu, F.H. and Catterall, W.A., 2003. Overview of the voltage-gated sodium channel family. *Genome Biol.,* **4,** 207-207.7.

Zhang, J.S. and Kaltenbach, J.A., 1998. Increases in spontaneous activity in the dorsal cochlear nucleus of the rat following exposure to high-intensity sound. *Neurosci.Lett.,* **250,** 197-200.

Zhang, Y.H., Chi, X.X. and Nicol, G.D., 2008. Brain-derived neurotrophic factor enhances the excitability of rat sensory neurons through activation of the p75 neurotrophin receptor and the sphingomyelin pathway. *J.Physiol.(Lond.),* **586,** 3113-3127.

Zheng, J., Dai, C., Steyger, P.S., Kim, Y., Vass, Z., Ren, T. and Nuttall, A.L., 2003. Vanilloid Receptors in Hearing: Altered Cochlear Sensitivity by Vanilloids and Expression of TRPV1 in the Organ of Corti. *J.Neurophysiol.,* **90,** 444-455.

Zheng, X.Y., McFadden, S.L. and Henderson, D., 1998. Faster recovery in central than in peripheral auditory system following a reversible cochlear deafferentation.[erratum appears in Neuroscience 1998 Dec;87(4):935]. *Neuroscience,* **85,** 579-586.